Author:
Cobbald, T. J

Title:
The impingement of underexpanded, axisymmetric, rocket motor exhausts and cold jets on flat plates

University of Bristol

Department of Aeronautical Engineering

The Impingement of Underexpanded, Axisymmetric, Rocket Motor Exhausts and Cold Jets on Flat Plates

by

T.J. Cobbald

A Thesis Submitted for the Degree of Doctor of Philosophy in the Faculty of Engineering of the University of Bristol

June 1985

MEMORANDUM

This thesis entitled, "The Impingement of Underexpanded, Axisymmetric, Rocket Motor Exhausts and Cold Jets on Flat Plates", is submitted in support of an application for the Degree of Doctor of Philosophy at the University of Bristol.

No part of the work described in this thesis has been submitted in support of another academic award from either the University of Bristol or any other Institution.

(T.J. Cobbald)

SUMMARY

A programme of experimental work was carried out using hot and cold jets.

The hot jets were produced by a small solid-propellant rocket motor. Nitrogen and air at ambient stagnation temperature were used to produce the cold jets.

All experimental jets were produced with the same convergent axisymtric nozzle which had an exit diameter of 3.12mm.

Pitot pressures were measured along the centrelines of the free jets in the range $0 < Zpt/Re < 50$.

Impingement flowfield pressures were measured at discrete positions across the surface of a flat plate. The measurement positions were arranged in a line across the plate surface. For all tests, the nozzle axis intercepted the line joining the measurement positions on the plate surface.

The plate was perpendicular to the nozzle axis for all tests with cold air. Measurements were made with the plate located in the range $0 < Zp/Re < 50$.

For the tests with rocket exhaust and the nitrogen jets the plate was inclined at 90° and 45° to the jet axis. The nozzle-to-plate separation distances were 5, 10, 20 & 40.

Results are presented from free and impinging air jets for $1 < Pc/Pa < 20$.

Results are presented from free and impinging nitrogen and rocket exhaust jets for $20 < Pc/Pa < 50$.

NOTATION

Ae	–	nozzle exit area
At	–	nozzle throat area
Cp	–	specific heat at constant pressure
Cv	–	specific heat at constant volume
De	–	nozzle exit diameter
L	–	length
M	–	Mach Number
Me	–	Mach Number at nozzle exit plane
P	–	static pressure
Pa	–	ambient pressure
Pc	–	combustion chamber stagnation pressure
Pe	–	static pressure at nozzle exit
Pp	–	pressure at plate surface
Ppt	–	pitot pressure
R	–	electrical resistance
R	–	gas constant
R	–	radial distance
Rb	–	transducer balance circuit resistance
Re	–	nozzle exit radius
Rt	–	transducer bridge resistance
Rs	–	shunt resistance
Sp	–	distance across plate surface from nozzle axis
T	–	static temperature
Tc	–	combustion chamber stagnation temperature
V	–	voltage
V	–	volume
X	–	mole fraction
Z	–	distance along jet axis from nozzle exit
Zmd	–	distance of mach disk from nozzle exit
Zp	–	nozzle-to-plate separation distance
Zpt	–	nozzle-to-probe separation distance
α	–	angle between plate and light beam
γ	–	ratio of specific heats Cp/Cv
θ	–	plate inclination relative to nozzle axis
Ø	–	diameter

CONTENTS

CHAPTER ONE - INTRODUCTION

1.1) GENERAL BACKGROUND

Rocket motors are used to provide propulsive thrust for various types of aerospace vehicle. The thrust is developed by the supersonic jets of hot gas emitted through the rocket motor exhaust nozzles. Usually, for most flight trajectories of rocket-propelled aerospace vehicles the exhaust jets expand freely into the ambient media. There are, however, instances where the exhaust jets impinge on solid obstacles which are either unavoidably or deliberately positioned in the vicinity of the rocket motor exhaust nozzles. Therefore, in these cases, the exhaust jets are deflected from their normal paths. When a rocket exhaust jet is deflected in this manner by a solid obstacle the situation is usually refered to as rocket exhaust impingement.

Examples of situations where rocket exhaust impingement occurs in practice are: rocket vehicle launch, multi-stage or multi-motor rocket vehicle separation, and exploratory extra-terrestial landing. These three examples of impingement will now be examined in greater detail.

Firstly, for rocket vehicle launch, it is normal practice to deflect the exhaust jet away from the launch complex in a controlled manner with a suitably shaped and positioned deflection device. This is done to ensure that delicate components of rocket vehicle, such as flight surfaces, are not accidently exposed to the exhaust which might otherwise occur through the processes of impingement and reflection from an inappropiately positioned obstacle; if delicate parts of the rocket vehicle were exposed to a high velocity and temperature exhaust, then they could be damaged. Additionally, controlled deflection of the exhaust, reduces

the hazards for personnel who may need to be in the vicinity of the launch complex.

Secondly, during the flight of multi-stage and multi-motor rocket vehicles, it is usual practice to discard a stage or motor once the associated propellant supply has been consumed. When separation occurs, the burnt-out stage or motor may then be in the path of the exhaust jets issuing from the remainder of the vehicle which continues flight under power. This powered section of the flight vehicle may therefore be exposed to and damaged by its own exhausts through a process of impingement on, and reflection from, the discarded stage or motor. Usually, this problem can be avoided by altering the trajectory of the discarded section of the flight vehicle. Trajectory modifications are normally effected by operating small auxiliary rocket motors which are incorporated in the discarded section. However, there is now a possibility that the exhausts from the auxiliary motors may impinge directly on the part of the vehicle which continues flight under power, damaging the exposed surfaces and modifying the trajectory.

Finally, for an exploratory extra-terrestial landing, the lander vehicle usually approaches the planet surface at perpendicular incidence. Therefore, if the lander is to remain intact at touchdown, it is necessary to minimise its approach velocity. Control of the approach velocity is normally accomplished by operating a rocket on the lander which is orientated to counteract the gravitational forces (i.e. the jet is directed towards the planet surface). Therefore this can result in the lander vehicle being exposed to, and possibly damaged by the rocket exhaust through the processes of impingement and reflection from the planet surface. Additionally, if the planet surface is friable, then any material blown around by the exhaust may strike and damage the lander. (A similiar situation occurs during VTOL aircraft take-off and landing, although in this case the jet is produced by a gas turbine engine.)

These examples of rocket exhaust impingement show that aerospace vehicles can be jeopardised in a variety of ways by either direct exhaust impingement, or the consequences of the impingement. Therefore, at the design stage of a project, it is important to be able to recognise and minimise any risks which might arise from impingement. To accomplish this, it is necessary to predict the velocities, pressures and temperatures within impingement flows. These predictions thus provide information about the aerodynamic and thermal loading at the surfaces of obstacles. With this loading information, the appropiate design choices can be made to ensure the integrity of structures that will either be exposed to rocket exhausts, or be influenced by a consequence of impingement. Clearly, if such a design strategy is to be sucessful, then reliable and accurate flow prediction methods must be available for rocket exhaust impingement flows. Obviously, these prediction methods can only be devised if rocket exhaust impingement flows are studied and understood.

Inaccurate prediction of rocket exhaust impingement flows, and underestimation of the effects they can cause, have led to projects incurring substantial additional costs and delays. A recent instance of this happening occured with the NASA Space Shuttle. After the launch of the first Shuttle, it was discovered that there was a serious fault in the design of the launch complex (Ref. 1). An analysis of gas pressure recordings, made in the vicinity of the Shuttle tail during the lift-off, revealed the development of pressures four times greater than predicted. It was subsequently determined that the cause of these excess pressures was reflection of the rocket motor exhausts by the launch complex. These pressures jeopardised the Shuttle because they imposed forces on the flight surfaces that were above the designed limits. Modifications to the launch complex to rectify this potentially dangerous design fault cost in the region of $1.5 million. But, even when this had been done, uncertainty persisted until the second Shuttle launch as to whether or not the modifications would have the

required effect. Obviously, if reliable impingement flow prediction methods had been available, then the additional costs and uncertainty would have been avoided.

1.2) CHARACTERISTICS OF ROCKET EXHAUST IMPINGEMENT FLOWS

This section outlines the characteristics of rocket exhausts and impingement flows; this will provide a clearer indication of the type of flows which need to be predicted. In Section 1.3, the various methods of flow prediction are examined.

Rocket motor exhausts are composed of high-temperature chemically-reacting mixtures of gases. The exhausts of some motors may also contain considerable quantities of particulate matter. This particulate matter may be in the liquid phase, the solid phase, or both solid and liquid phases. These gas or gas-particle mixtures are generated by burning either solid or liquid propellants within the combustion chambers of the motors. The stagnation temperatures and pressures developed in the combustion chambers are usually in the ranges 2000-3000°K and 1-20 MN/m^2 respectively. For most rocket exhaust gases, the value of the gas specific heat ratio, Cp/Cv (i.e. 'gamma'), is in the range 1.2 to 1.3.

Most rocket motors are fitted with axisymmetric convergent-divergent exhaust nozzles; typical nozzle exit Mach Numbers, Me, are in the range 2-5. Usually, in most instances of impingement, the exhausts are underexpanded at the nozzle exits, (i.e. Pe > Pa).

Generally, impingement flows formed by rocket exhausts are turbulent three-dimensional mixed supersonic-subsonic flows which contain embedded intersecting shock waves. Free shear layers are formed at the boundaries between the impingement flows and the ambient media, and also at the shock intersections. These basic structural characteristics of impingement flows are identified in Figure 1.1; this shows a schematic of the flowfield formed by the impingement of an underexpanded axisymmetric jet on a planar surface which is perpendicular to the jet axis and also close to the nozzle exit.

In some instances of impingement, the embedded shocks and shear layers interact with the boundary layer formed on the surface of the obstacle causing irregular flow conditions to occur (e.g. stagnation bubbles).

Some impingement flows show significant unsteadiness which occurs in the form of oscillations of their overall structures. The frequency of these oscillations can range from a few Hertz to approximately 20kHz. When unsteadiness occurs, the peak dynamic pressures on the obstacles can exceed the time-averaged pressures by as much as 50%. Unsteadiness is particularly prevalent for impingement on planar surfaces that are perpendicular to the jet axes.

For many rocket motors, chemical reactions amongst different species of the combustion gases are not completed within the combustion chambers, and the reactions continue as the gases pass through the nozzles and the impingement flows. At the free boundaries of impingement flows, mixing - and possibly chemical reaction - occurs between gases in the flows and the gases of the ambient media. If the rates of any of the chemical reactions are comparable with the time taken for the gases to traverse the flows, then the gases will have non-equilibrium chemical compositions. Changes in gas composition usually change the effective physical properties of the gas (e.g. specific heats, viscosity); thus composition changes usually affect the structures of impingement flows.

For multi-phase rocket exhausts, the solid or liquid particles generally have mean maximum dimensions in the range 0.1-10μm, and densities that are several orders of magnitude greater than the gases. Particles with these characteristics cannot follow the very rapid variations in the gas velocities in impingement flows. As a consequence, the particles and gas tend not to be in thermal and kinetic equilibrium; this results in differences between the structures of gas and gas-particle impingement flows.

1.3) PREDICTION OF ROCKET EXHAUST IMPINGEMENT FLOWS

Rocket exhaust impingement flows could be classified as transient chemically-reacting multi-phase three-dimensional mixed supersonic-subsonic multi-shocked turbulent flows. Rigorous theoretical analysis of flows in this class is extremely difficult. At the present time, no general-purpose theoretical method exists which can be used to predict, entirely from first principles, the gas or gas-particle properties in impingement flows for arbitarily chosen nozzle-and-obstacle configurations. The main reason for this is that accurate and reliable computational techniques are not yet available to handle, on a routine basis, all the different flow phenomena present in typical rocket exhaust impingement flows. Many of the computational techniques which are required for handling phenomena such as mixed supersonic-subsonic flows, unsteady shock-boundary layer interactions, etc. are still being researched and developed.

All the purely theoretical methods for modelling impingement flows which have been reported to date rely on various simplifying assumptions, and are only capable of providing flow predictions for physiochemically-stable underexpanded gas-only jets impinging on perpendicular flat plates.

Representative examples of the theoretical methods available for modelling complete impingement flowfields are those which have been reported by Sinha, Zakkay & Erdos (Ref. 2) and Iwamto & Deckker (Ref. 3) who used finite-difference calculation techniques. Other theoreticians have reported the use of the method of integral-relations calculation technique for modelling the segment of the impingement flowfield which is adjacent to the plate surface (e.g. Refs. 4, 5). However, these prediction methods are restricted to impingement situations where the plate is positioned in close proximity to the nozzle exit (i.e. comparable to that shown in Figure 1.1); this is largely because the calculation techniques rely on the simplifying assumption

that the flows are inviscid everywhere except in the shocks. Also, for the method of integral-relations calculation technique there is an additional limitation; this method is only accurate when the jets are uniform or weakly underexpanded. No theoretical methods have been reported, so far, for dealing with impingement situations involving a perpendicular plate which is positioned further away from the nozzle exit where the jets are supersonic and completely turbulent.

Owing to the lack of purely theoretical methods for dealing with all the nozzle-and-obstacle configurations likely to occur in practical impingement situations, it has proved necessary to adopt an empirical or semi-empirical approach to obtain estimates of impingement effects for design purposes.

However, considerations of practicability and cost have restricted the amount of experimental work carried out with actual rocket motors to provide data for developing empirical impingement flow prediction methods. In the case of very large motors, data may have only been obtained by making measurements during flight-vehicle operation (e.g. Refs. 1, 6). The number of studies reported which used laboratory-scale rocket motors are also few in number (e.g. Refs. 7-12). Apart from cost, the main problem is that it is difficult to make reliable measurements within impingement flows produced by rocket motors because of the high temperatures of the exhaust gases or gas-particle mixtures (e.g. see Ref. 13).

Therefore, to simplify experimental investigations of impingement phenomena and minimise costs, air jets are often used to simulate the rocket exhausts. Usually, the air is 'cold' - that is it has a stagnation temperature equivalent to the laboratory ambient temperature as compared with 'hot' gases from real rocket motors.

Numerous experimental studies have been reported which used cold air jets, instead of actual rocket exhausts, for investigating impingement flows. The objectives of the studies have been varied; obstacle types investigated have included planar surfaces (e.g. Refs. 14-41), wedges (e.g. Refs. 42-45), cylinders (e.g. Ref. 46) and cones (e.g. Ref. 47).

The studies with cold air jets have provided a valuable insight into the flow processes occuring in cold jet impingement flows. Also, a considerable amount of pressure, heat-transfer and flow-visualisation data has been obtained, and this has been used to develop a wide variety of empirical and semi-empirical flow prediction methods.

However, uncertainties persist as to the applicability of the empirical flow prediction methods which have been developed from cold jet experimental data to practical impingement situations involving rocket exhaust jets. This is because there are significant physical differences between the cold air jets and the hot rocket exhaust jets. For example, there is certainly a difference between the values of gamma (Cp/Cv) for hot and cold jets, as well as a difference in the densities which results in differences in mixing rates; also, the presence of solid or liquid particles may affect the effective gas properties and the forces on the obstacles.

There is only one previous study, by Piesik & Roberts (Ref. 48), which addresses somewhat indirectly this question of the possible differences between hot and cold jet impingement flows. Piesik & Roberts correlated experimental data obtained from other studies, which used hot and/or cold jets, and developed empirical methods for predicting the impingement pressures and temperatures on a flat surface. This work was restricted in scope. For instance, only impingement on perpendicular surfaces was considered, and the authors concluded that their methods were only valid for

far-field impingement and, furthermore, recommended that they should only be used for preliminary design estimates.

Thus there is a lack of precise correlations between hot and cold jet impingement flow phenomena.

Hunt (Ref. 49) suggested it would be of value to conduct an experimental study to determine the differences between hot and cold jet impingement flows, and to develop a correlation which would allow cold jet pressure data to be applied with confidence to situations involving hot jets. This suggestion by Hunt served as the catalyst for the study of hot and cold jet impingement flows which is reported in this thesis.

1.4) OBJECTIVE OF THIS STUDY

The objective of this study was to measure and correlate the pressure distributions generated on the surface of a flat plate by impinging rocket exhausts and cold jets.

1.5) STRATEGY OF THIS STUDY

In view of the objective outlined, it was necessary to devise an appropiate strategy for tackling this study. Essentially, decisions had to be made on what experimental pressure measurements were required to provide the data on which a correlation could be based. Firstly, this involved identifying the salient test parameters, and then assessing which were important and which could be ignored or kept constant. The results of this assessment were the key decisions to:

- use an actual rocket motor for producing the experimental hot jets

- use ambient-temperature air, or a gas with similiar properties to air (e.g. nitrogen), for the cold jet gas

- use exactly the same test geometries for the experimentation with both the hot and the cold jets

- operate the hot and cold jets at the same jet pressure ratio or ratios (Pc/Pa)

- measure impingement flowfield pressures at discrete positions across the surface of a flat plate

CHAPTER TWO - ROCKET MOTOR

2.1) INTRODUCTION

When the strategy for this study was devised it was decided that the experimental hot jets needed to be produced by an actual rocket motor and not simulated by some other method - see Section 1.5. This meant that a suitable laboratory-scale rocket motor had to be obtained for use in the experimental investigations as there was no motor already available when this study began.

It was decided that the rocket motor needed to be obtained before any other aspect of this study was tackled; this approach was adopted because most other aspects of this study could not be tackled until the characteristics of the motor that was to be used were known.

The rocket motor that was eventually obtained was a small solid-propellant motor which was manufactured by P.A. Hilton Ltd.

The following sections of this chapter describe the design of the Hilton motor and the chemistry of its solid propellant, and outline work that was conducted to assess the performance of the motor and determine the properties of its combustion and exhaust gases.

2.2) MOTOR DESIGN

The Hilton solid propellant rocket motor was designed specifically for laboratory studies (i.e. it was not a component of a flight vehicle). The propellant was supplied in cartridge form by the manufacturer of the motor. A new propellant cartridge was fitted to the motor for each firing.

The external forms of the Hilton motor and a propellant cartridge can be seen in the photograph presented as Figure 2.1.The component parts of the motor are identfied by the two orthographic scale drawings presented as Figure 2.2; one drawing shows a longitudinal section of the motor and the propellant cartridge as fitted for firing, and the other shows an end view of the motor looking towards the nozzle.

As can be seen from Figures 2.2 & 2.3, the main component of the motor was a cylindrical tube which formed the combustion chamber. This tube had an internal length of 162.5mm, an inside diameter of 27.6mm, and a wall thickness that was approximately 3mm. The tube was closed at one end by an exhaust nozzle, and at the other end by a firing-pin-block assembly. The nozzle and firing-pin-block assembly were retained in position by two identical collars. Internal threads on these collars engaged with external threads on the outside of the combustion chamber tube. The firing-pin-block assembly and its retaining collar needed to be removed and then replaced each time the motor was fitted with a new propellant cartridge.

The motor was designed to allow operation with nozzles having different throat areas; this provided a method of obtaining different combustion chamber pressures in the range 3-7 MN/m^2. For axisymmetric nozzles, the throat diameters could be between approximately 3.0 and 3.6mm. (The relationship between the throat area and the chamber pressure will be considered in more detail later - see Section 2.4.)

The motor had a 3mm bore tapping in the wall of the combustion chamber tube. A pressure transducer could be connected to this tapping for monitoring the combustion chamber pressures.

The motor also had a 10mm bore port in the wall of the combustion chamber tube; this port was closed off with a replacable metal diaphragm that was retained in position by a housing with vents. The diaphragm was

designed to rupture if the gas pressure in the combustion chamber exceeded the safe maximum of 17.5 MN/m^2.

With the exception of the firing-pin block and the exhaust nozzles, all parts of the motor were constructed from steel. The firing-pin block was made from Tufnol - a fabric-resin composite material. Tufnol was used for this part because the firing pin needed to be electrically isolated from the main body of the motor - see below. The exhaust nozzles were made from brass. The external surfaces of the steel parts and the nozzles were nickel plated.

As Figure 2.1 shows, the propellant cartridges were cylindrical in shape. The external diameter and length of a cartridge were 26mm and 78mm respectively. The outer shell of each cartridge consisted of a stiff cardboard tube, one end of which was fitted into a brass base, and the other end was closed with a thin disc made of transparent plastic. There was a small raised rim on the brass base of each cartridge; this secured the cartridge in position when it was loaded into the the motor - see Figure 2.2.

Each cartridge contained a main solid propellant grain, housed in the tubular cardboard section, and a much smaller ignition charge, located in the brass base. Combustion of the main propellant grain was initiated by firing the ignition charge.

The ignition charge was fired electrically with a low voltage DC supply (e.g. 12 VDC). This supply needed to be applied between a contact point in the centre of the face of the cartridge base, that was insulated from the main part of the base, and any other point on the brass base. Thus, when a cartridge was loaded in the motor, the ignition charge was fired by connecting the electrical supply between the firing pin and the body of the motor; this formed a circuit through the firing pin, the cartridge contact point, the ignition charge, the cartridge base and the body of the motor.

The main propellant grain in each cartridge was tubular in shape; the length was 60mm, and the external and internal diameters were 20mm and 3mm respectively. The size of the grain was smaller than the cavity available for it in the cardboard section of a cartridge. This arrangement allowed all the surfaces of the grain to burn freely. When combustion of the grain commenced, the protective plastic disc on the end of the cartridge was vapourised by the heat.

When the motor was operating, the unsecured propellant grain was prevented from leaving the cartridge by a blocking bar inside the combustion chamber tube - see Figure 2.2.

2.3) CHEMICAL COMPOSITION OF THE SOLID PROPELLANT

The propellant cartridges used with the Hilton rocket motor were supplied only by the manufacturer of the motor for whom they were produced by Imperial Chemical Industries Ltd.

Two types of propellant cartridge could be supplied; these differed only in the composition of the main propellant grain. The two types of cartridge were designated as follows:

- TYPE 850 cartridge which was fitted with a Mech 1 propellant grain giving a nominal heat release of 3558 J/g (850 cal/g)

- TYPE 670 cartridge which was fitted with a Mech 7 propellant grain giving a nominal heat release of 2805 J/g (670 cal/g)

The technical reference manual supplied with the Hilton motor (Ref. 50), stated that the constituents of both types of propellant grain were as follows:

- nitroglycerine
- nitrocellulose
- ethyl centralite
- di-butyl-phthalate
- potassium nitrate
- mineral jelly

The only other information given about the propellants in the motor manual (Ref. 50) was that the nitroglycerine and nitrocellulose were the major constituents, and that the other constituents were additives present only in small quantities.

Information about the percentages of each constituent in the propellants proved to be unobtainable; also, the significance of the propellant designations Mech 1 and Mech 7 could not be established.

Although no information could be obtained about the precise composition of the solid propellants, it was possible, nevertheless, to determine the propellant type classification from the knowledge of the constituents noted above.

Rocket motor solid propellants are often classified as either double-base or composite propellants (e.g. see Ref. 51). Classification is determined by the main constituents used for a propellant. The main constituents of a double-base propellant are always the organic nitrates nitroglycerine and nitrocellulose. A composite propellant is distinguished by the use of ammonium perchlorate and polymeric hydrocarbons, such as polyurethane, for the main constituents. Consequently, the propellants in the Hilton motor cartridges were judged to be double-base propellants.

2.4) MOTOR PERFORMANCE AND OPERATING CHARACTERISTICS

The only measure of the performance of the Hilton motor that was of major interest to this study was the magnitude of the combustion chamber pressure. This needed to be known for test planning purposes because the intention was to operate the experimental hot and cold jets at the same chamber-to-ambient pressure ratios - see Section 1.5. The magnitude of the chamber pressure will therefore be considered in more detail below. The thrust developed by the motor (approx. 10 Kgf. max.) and other measures of its performance (e.g. specific impulse) were of no great interest to this study and hence these will not be considered.

The pressure in the combustion chamber of the Hilton motor was designed to remain approximately constant when the solid propellant was burning - that is, the pressure-time characteristic was designed to be approximately neutral rather than significantly regressive or progressive. The magnitude of the chamber pressure could be controlled by using exhaust nozzles with different throat areas. It was therefore necessary to know the relationship between the magnitude of the chamber pressure, Pc, and the nozzle throat area, At, for test planning purposes.

When the motor was obtained, however, there was no information available relating Pc and At. Also, the only measurements of the chamber pressure that were available were from tests with nozzles which had the same throat area, and obviously these could not be used to establish the relationship between Pc and At. (The available measurements were in the form of a few recordings of the chamber pressure which were presented, as illustrative examples, in the technical reference manual for the motor (Ref. 50); no other measurements of the chamber pressure appeared to have been published elsewhere.)

Initially, to overcome this difficulty, the possibilities of using theoretical methods for predicting the relationship between Pc and At were investigated. Unfortunately, it was found that the available prediction methods (e.g. see Refs. 51, 52.) could not be used in this instance. The main problem was with several coefficients in an empirical equation that was used for modelling the combustion of the solid propellant; values for these coefficients were not available for the propellants incorporated in the Hilton motor cartridges.

Therefore, as the combustion chamber pressures could not be predicted, the only tractable way to determine the variation of Pc with At was by experiment. Consequently, a series of test firings conducted with different nozzles fitted to the motor and the associated chamber pressures measured. These tests will now be outlined as they provide a convenient opportunity to comment on the operating characteristics of the motor.
if only qualitatively

The experimental arrangement used for the test firings was as follows. The motor was bolted to a bracket which was attached to the steel framework of the laboratory fire escape; an outdoor location was used in order to avoid polluting the laboratory with the motor exhaust gases. The combustion chamber pressures were monitored with a piezo-electric pressure transducer (AVL 6QP) which was mounted within a water-cooled housing. The electrical signals from the transducer were conditioned with a charge amplifier (AVL Type TA-1/B), and recorded with a UV oscillograph (SE Labs Type 3006/DL fitted with a B420 galvanometer).

Test firings were conducted with convergent axisymmetric nozzles fitted to the motor. A total of five nozzles were used, and these had exit/throat diameters, De, of 3.0, 3.23, 3.51, 3.63 & 3.74mm. TYPE 670 propellant cartridges were used for all test firings. It was not possible to conduct series of tests with both TYPE 670 & 850 propellant cartridges because of cost constraints; (ultimately, TYPE 670 cartridges were also used for all subsequent series of tests with the Hilton motor which were conducted in the course of this study).

Observations made during the series of tests were as follows. Each time the motor was fired, by completing the electrical ignition circuit, the ignition charge in the propellant cartridge was heard to detonate immediately; but then a delay of between 1.5 and 2.5 seconds occured before combustion of the main propellant grain commenced. Hilton (Ref.50) stated that this delay occurred as a consequence of safety considerations in the propellant cartridge design.

Two forms of main propellant grain combustion were heard in the course of the test firings; these will be classified here as 'stable' and 'unstable' combustion. For the stable combustion, the propellant was consumed in one sustained burn of appproximately one second duration. When unstable combustion occured, the propellant was consumed by three to five discrete burns that were 100-300 milliseconds in duration and separated by

approximately one second intervals. It was found that firings with the De=3.0, 3.23, 3.51 & 3.63mm nozzles always resulted in stable combustion, and that unstable combustion always ocurred when the De=3.74mm nozzle was used.

Visually, the exhaust jets appeared luminous in the vicinity of the nozzle exit but black elsewhere; this suggested that significant quantities of soot (i.e. carbonaceous particulate matter) were present in the exhaust gases.

When the motor was dismantled after each firing, deposits of soot were found on the walls of the combustion chamber and the nozzle. The soot deposition on the chamber wall was approximately 0.5mm thick. This deposition was in the form of a finely divided powder and was easily removed with a rag. In contrast, the soot deposited on the nozzle wall was like a very thin, hard, layer of paint; its removal was only possible with the aid of a solvent (e.g. acetone). Attempts were made to determine the thickness of the soot deposition at the throat of a nozzle by measuring the throat diameters before and after test firings. Although a travelling microscope was used for these measurements, no differences in the diameters could be detected.

The measurements of the combustion chamber pressures will now be considered. Sample pressure-time recordings from test firings with the De=3.00, 3.23, 3.51 & 3.63mm nozzles are presented in Figure 2.3; a recording from a test with the De=3.74mm nozzle is presented separately in Figure 2.4.

It can be seen from Figures 2.3 & 2.4 that the variations in the chamber pressure with time were significantly different for the stable and unstable forms of propellant combustion. When stable propellant combustion occured, the chamber pressure first increased rapidly above ambient pressure, then remained approximately constant for a time period of between 0.5 and 1.0 seconds, and then finally decreased rapidly back to ambient pressure. When unstable combustion occured, the chamber pressure-time variation was characterised by a series of pressure pulses (i.e. rapid increases of the chamber pressure above ambient pressure followed by immediate decreases back to ambient pressure) which had a pulse-to-pulse time period of approximately one second.

Of the two forms of chamber pressure-time variation which were produced by the Hilton motor, only that associated with stable propellant

combustion was considered to be of use for the planned experimental investigations of rocket exhausts impinging on a flat plate. The reason for this was that there was a much better prospect of making accurate measurements of the pressures at the plate surface if the pressure ratio of the exhaust jet remained reasonably constant for a period of time during each test rather than if it fluctuated rapidly. Therefore, the pressure-time characteristic associated with the unstable form of propellant combustion will not be considered further.

Concerning the relationship between the magnitude of the chamber pressure attained during stable propellant combustion and the nozzle throat area: the recordings presented in Figure 2.3 show that when the nozzle throat diameter was increased from 3.0 to 3.63mm the mean chamber pressure decreased from approximately 6.5 to 3 MN/m^2. A correlation of these mean pressures with the corresponding nozzle throat areas revealed that Pc was almost exactly inversely proportional to At.

2.5) SOLID PROPELLANT COMBUSTION PRODUCTS

In view of the objective of this study it was obviously important to have information on the chemical and physical properties of the combustion products generated by the solid propellant used with the Hilton rocket motor. Normally, this type of information would be obtained by using theoretical methods to analyse the solid propellant combustion processes; experimental measurements might also be made to verify the theoretical predictions. In the case of this study, however, it was not possible to analyse the propellant combustion processes using theoretical methods; this was because the precise composition of the solid propellant was unknown - see Section 2.3. Also, it was only possible to measure one property of the combustion products by experiment - this was the pressure (see previous section); it was not feasible to attempt to measure other properties (e.g. composition, temperature, etc.) because suitable instrumentation was not readily available. Therefore, to circumvent these difficulties, it was necessary to look elsewhere for information on the solid propellant combustion products. In the event, sets of data on the properties of the combustion products were obtained from Hilton , ICI and PERME , and these are reproduced in Tables 1, 2 and 3, respectively.

On referring to Tables 1, 2 & 3, it will be seen that the sets of data provide information on the combustion products generated by the TYPE 670 propellant and not both the TYPE 670 and TYPE 850 propellants. Cartridges containing TYPE 850 propellant were not used with the Hilton motor at any stage during this study, and hence the combustion products generated by the TYPE 850 propellant were of no interest.

Each set of data includes information on the chemical composition and various physical properties of the gas-phase combustion products in the motor combustion chamber and at various locations in different exhaust nozzles; the tables do not include any information on solid-phase combustion products (e.g. soot) because none was supplied by Hilton, ICI or PERME.

Although it was established that these data were all calculated values and not derived from experimental measurements, no information was available on how these results were calculated. Therefore their reliability is uncertain, especially since as mentioned above apparently no account was taken of the influence of solid matter present in the rocket exhaust. This would reduce the value of γ by a small amount. Thus there will be an effective value of γ which differs from the calculated "gas only" value.

The three sets of data in Tables 1 - 3 show variations in γ of between 1·265 and 1·29, but of course the different values are given for different nozzles and for different locations in a particular nozzle, where different temperatures clearly pertain. An unexplained feature of the PERME data is that the value of γ goes down from the throat to the nozzle exit. Note that ICI provided data on the combustion products at two different chamber pressures (Tables 2a and 2b), and although PERME also quoted the chamber pressure for their data (Table 3), no information on chamber pressure was supplied by Hilton in the data of Table 1. However, a comparison of Tables 2a and 2b indicates that pressure has a negligible influence on the predicted combustion chamber gas compositions and therefore the lack of a value for chamber pressure in the Hilton data is not considered to be important.

The tables show that the major species were predicted to be CO, CO_2, H_2, H_2O and N_2. It is only possible to make a direct comparison of the three sets of data on the concentration of these species in the combustion chamber and this is done in Fig. 2.5. Note that the exhaust gas composition and properties change as the gases flow through the nozzle and thus as the temperature changes. The effect of temperature on the values of γ for the five species is shown in Fig. 2.6, and an evaluation of the effect of temperature on the TYPE 670 propellant gas specific heat ratio as obtained from the three sets of gas composition data is shown in Fig. 2.7.

2.6) CONCLUDING REMARKS

In summary therefore it is not possible to define accurately the value of γ, and therefore to define the true conditions in the exhaust plane of the rocket motor nozzle, so it is not possible to use simple one-dimensional flow analysis.

As a result of these considerations, it was decided to use only sonic nozzles so that the exit Mach number was always unity irrespective of the exhaust gas composition and therefore of the value of γ.

CHAPTER THREE - PREDICTION OF FREE JET FLOWS

3.1) INTRODUCTION

Need approximate prediction of differences between hot and cold jets to design test rig.

In general the jet structure is governed by the following set of variables:

nozzle exit mach number
nozzle exit wall angle
jet pressure ratio
properties of gases (i.e. gamma etc.)

But, for this study axisymetric sonic nozzles were used. Therefore:

nozzle exit mach no=1 always
nozzle exit wall angle=0 always

This leaves jet pressure ratio and gas properties as key variables.

For a constant gamma gas such as air the effect of the jet pressure ratio on the jet structure is as sketched in Figure 3.1.

Essentially, for this work we are interested in effect of gamma on jet structures i.e. locations of the jet boundary, jet shock and mach disk.

The boundary and jet shock were predicted with a MOC program that was already available.

Mach disk location was predicted using a (published) empirical correlation.

3.2) METHOD OF CHARACTERISTICS ANALYSIS

A method of characteristics computer program was used for assessing the influence of gamma on the free jet structures. The program that was used was coded by Gummer (Ref 22) and based on a calculation scheme devised by Vick et. al. (Ref. 53).

The results obtained are presented in Figures 3.2 and 3.3.

Figure 3.2 shows that as the value of gamma decreases the radial distance of the jet boundary and jet shock from the jet centreline increase.

Figure 3.4 shows the predicted variations of key flow variables along the jet centreline downstream of the nozzle exit. Variations of gamma have a significant influence on the Mach number distributions, but virtually no effect on the stagnation pressure ratio (i.e. pitot pressure).

3.3) MACH DISK LOCATION

The influence of gamma on the Mach disk location was predicted using Lewis and Carlson's (Ref.54) empirical correlation. The results obtained are presented in Figure 3.4 together with the empirical correlation equation.

3.4 CONCLUDING REMARKS

Essentially it appears that reducing the value of gamma causes the jet to widen and shorten. However, the magnitudes of the changes for the jets of the pressure ratio considered are small.

Most interesting and significant result to emerge was that the jet centreline pitot pressure distribution between the nozzle exit and the first mach disk appears to be virtually uninfluenced by changes in gamma; (it is also unaffected by changes in the jet pressure ratio, but this is cannot be seen from the results since only one pressure ratio was considered)

CHAPTER FOUR - EXPERIMENTAL TEST RIG

4.1) INTRODUCTION

Having obtained and evaluated the Hilton motor, and carried out the theoretical studies to predict the likely magnitude of the differences between the hot and cold free jets, it was then feasible to tackle the design and construction of the test rig that was to be used for the main program of experimental work of this project. The principal aim was to obtain pressure data from hot and cold jets impinging on perpendicular and inclined flat plates for comparison and correlation. A subsidiary aim was to obtain free jet axial pitot pressure data for comparison with the theoretical predictions.

At the outset, there did not appear to be any fundamental problems that would prevent the acquisition of the required cold jet data. However, for the hot jet impingement testing there was some concern about the possible consequences of the high levels of soot in the Hilton motor exhaust gases. The small size of the exhaust jets meant that the flat plate pressure tappings, and the pitot probes, would need to have extremely small diameters to ensure adequate resolution of the rapidly changing pressure distributions which were expected. Thus there was a possibility that the soot might block the flat plate pressure tappings and the pitot probes. Therefore, it was considered to be essential to demonstrate that the soot would not be a problem by verifying that sensible impingement and pitot pressures could be measured before embarking on the design and construction of the test rig for the main program of experimental work.

A simple test rig was therefore built for a set of trial impingement and free jet tests using the Hilton motor only. This simple rig comprised of a space frame which was used to retain the motor and either a perpendicular flat plate or a

pitot probe. The test instrumentation consisted of two pressure transducers, two transducer signal conditioning amplifiers, and a UV oscillograph for signal recording. One of the transducers was used for monitoring the motor combustion chamber pressure, and the other was connected to either a pitot probe or a tapping in the flat plate. Using sonic nozzles, a set of tests were conducted to monitor the pitot pressure on the axis of a free jet, and the static pressure at the surface of the flat plate for an impinging jet.

The initial trial tests were not encouraging; in nearly every case the soot caused either complete or partial blockage of the pitot probe or the plate tapping. Also, on some occasions the high temperature and velocity exhaust jet destroyed the pitot probes completely. However, after several stages of modifications to the designs of the pitot probe and flat plate pressure tapping, and development of the test techniques, it was found that sensible and repeatable pressure measurements could be made despite the soot.

Therefore, having demonstrated that it was practicable to use the Hilton motor for hot jet testing, it was then possible to proceed more confidently with the design and construction of the test rig required for the main program of experimental work. The following sections of this chapter are concerned with the design specification, general arrangement and parts description for the rig that was built.

4.2) DESIGN SPECIFICATION

The set of general specifications formulated for the overall design of the test rig were as follows:

- The same nozzle, flat plate and pitot probe to be used for both hot and cold jet tests to permit direct comparison of the pressure data.

- The plate or pitot probe to remain in a fixed position relative to the nozzle for the duration of any one test (i.e. static test geometry).

- The range of nozzle-to-plate and nozzle-to-probe separation distances to be 0-50 nozzle-exit radii.

- The range of flat plate inclinations, relative to the jet axis, to be 90°-30°.

- The rig to be designed to use the Hilton motor for generating the hot jets in the first instance, and then if unforeseen problems occured with the Hilton motor, allow the substitution of a different motor.

- The Hilton motor combustion chamber to act as the settling chamber for the cold jet test configurations; (the design of the motor was such that this could be achieved quite easily).

- The cold jet gas to be either air or some other inexpensive, non-hazardous gas having a specific heat ratio, Cp/Cv, similiar to air (e.g. nitrogen)

- The range of cold jet settling chamber pressures to be similiar to the range of Hilton motor combustion chamber pressures (i.e. approx. 3-7 MN/m^2).

- The operating duration of the cold jet to be similiar to, or greater than, the duration of the Hilton motor

(i.e. => 1 sec.).

- The rig to be designed in a way that would allow unobstructed views of the free and impinging jets for flow visualisation.

- The rig to be situated indoors; all the earlier test firings of the Hilton motor had been conducted out of doors to avoid polluting the laboratory atmosphere with the soot laden exhaust gases, but this had proved to be inconvenient.

- The same gas pressure monitoring instrumentation and data acquisition system to be used for both hot and cold jet testing.

- The gas pressures to be monitored with electrical pressure transducers, and the transducer signals to be recorded in machine readable form to allow direct transfer of data to a computer for processing.

4.3) GENERAL ARRANGEMENT

The test rig was located in the Gas Dynamics Laboratory of the Department of Aeronautical Engineering at the University of Bristol. It consisted of the following major component parts:

- universal test stand
- ventilation system
- cold gas supply system
- shadowgraph/schlieren system
- data acquisition system

The universal test stand was a piece of apparatus which was designed to accomodate all the required impingement and free jet test configurations using hot and cold jets. The function of the ventilation system was to remove the rocket motor exhaust gases from the laboratory during hot jet tests. Gas supplies for the cold jets were provided by the cold gas supply system. If required, flow visualization of the cold jets could be accomplished with the shadowgraph/schlieren system. A computer-based data acquisition system was used to control the rig, and obtain and process the required gas pressure data from hot and cold jets.

Figure 4.1 shows a plan view of the layout of these major component parts of the test rig in the laboratory.

The major component parts of the rig will be described separately in greater detail in later sections of this chapter. Before then, it will be convenient to examine three small important component parts of the rig. These parts are the nozzle that was used for producing the jets, the pressure tapped flat plate that was used to obtain the impingement pressure data, and the pitot probe assembly that was used for pitot pressure measurements in the free jets.

4.4) NOZZLE

It was decided that in this study the hot and cold jet pressure data would be obtained and compared for identical test geometries - see Section 1.4. Therefore, as far as the nozzles were concerned, the simplest method of achieving this aim was to use the same nozzle for producing both the hot and the cold jets for any given test geometry.

In terms of basic design, the nozzles required for the experimental investigation needed to:

- have convergent internal wall profiles
- have axisymmetric internal wall profiles
- have a range of different throat diameters to allow hot jets with different pressure ratios to be produced
- permit close range inclined impingement tests to be conducted without mechanical interference occuring between the plate and either the nozzle or the nozzle retaining collar of the motor
- retain the same wall profile after being used for a large number of firings with the rocket motor (i.e. withstand abalative effects of motor combustion gases)

The set of convergent nozzles that were supplied with the Hilton motor, and used for the trial test firings, could not meet these requirements for two reasons. Firstly, the axial dimensions of the nozzles were too small to permit the required inclined impingement tests to be conducted - see Figure 2.2. Secondly, the internal walls of the nozzles were neither free of major imperfections nor absolutely axisymmetric. Some of the imperfections were present when the nozzles were new, but most were introduced during the trial test firings. In this respect, the choice of brass

for the nozzle material seemed inappropiate - see Section 2.3.

Therefore, a new set of axisymmetric convergent nozzles were designed and manufactured to satisfy the requirements of this study. These nozzles were made from EN 58J stainless steel (AISI 316) and had different exit diameters, generic internal wall profiles, and the same external forms. Three of the nozzles can be seen in the photograph presented as Figure 4.2.

Ultimately, only one of the new nozzles was used for producing all the hot and cold jets in the main program of experimental tests; this was due to limitations in the amount of time that was eventually available for testing. A dimensioned scale drawing of this particular nozzle is shown in Figure 4.3. The mean diameter and circularity of the nozzle exit were determined by examining the end of the nozzle at x50 magnification. The mean exit diameter of the nozzle was found to be 3.12mm. The deviations of the nozzle lip circumference from true circularity were assessed to be +/-0.01mm.

A three-stage manufacturing process was used to make the new nozzles. First, the external form of a nozzle was turned from a piece of EN 58J round bar. Secondly, using a boring bar, the inside of a nozzle was rough machined to within approximately 0.25mm of the required profile. Finally, electro discharge machining (EDM) was used to produce the finished internal profile. A satisfactory internal nozzle surface could not be obtained by boring because of excessive tool chatter, hence the use of EDM. Axisymmetric brass electrodes were used in the EDM process. The profiles of the electrodes were the same as the required nozzle profiles, but the radial dimensions were made 0.010mm smaller. The electrodes were rotated during the discharge machining and this ensured that the final nozzle profiles were axisymmetric. A problem that emerged with the EDM process was poor control of the absolute machining

tolerances. This made it difficult to produce a nozzle with an exit diameter that was exactly as specified. For example, the final exit diameter of the nozzle used for this study was 3.12mm, but this had been specified as 3.00mm.

4.5) FLAT PLATE

One pressure-tapped flat plate was manufactured for use with the test rig. The plate was 150mm square; this size was considered to be large enough for any flow transitions at the plate edges to have a neglible influence on the measured pressure distributions.

The plate was manufactured from a piece of 12mm thick mild steel plate which had not been subjected to any special conditioning or treatment (e.g. surface hardening). The faces of the plate were surface ground.

The plate incorporated fifteen pressure tappings which were arranged in a linear array. Each tapping was connected to a pressure transducer with a short length of flexible nylon tubing; (further details on the transducers will be given later - see Section 4.11). The middle tapping in the array was located at the geometrical centre of the plate. The pitch of the tappings was specified to be 3.175mm. The precise distances between the tappings were measured after the plate had been manufactured. These measurements were made by examining the plate surface at x50 magnification; (values for the tapping-to-tapping distances will be given later - see Section 5.3).

Dimensioned orthographic line drawings of the plate and a cross-section of a pressure tapping are presented in Figure 4.4.

Refering to Figure 4.4 it will be seen that each tapping orifice, in the face of the plate that was exposed to the jet, was 0.35mm in diameter. This diameter was used for the orifice simply because 0.35mm twist drills were the smallest that could be obtained for drilling these holes. Hence, the resolution of the pressure distributions in the impingement flowfields was the best that could be obtained.

The plate was attached to its support structure with four bolts. These bolts screwed into blind tapped holes located in the rear face of the plate, that is the face not exposed to the jets.

4.6) PITOT PROBE

The pitot pressures in the free jets were monitored with disposable probe assemblies. These probes were held in position in the jets with a probe holder. Photographs of a probe and the holder are presented as Figures 4.5 & 4.6 respectively. Dimensioned orthographic scale drawings of the same items are shown in Figure 4.7.

The designs of the probe and the probe holder were developed in the course of the trial experiments to monitor the pitot pressures in the Hilton motor exhaust jet - see Section 4.1. In those tests it was found that the small bore pitot probes became susceptible to blockage by the soot in the motor exhaust if they were used for more than one test firing. Using a new probe for each test firing was therefore the only way to obtain reliable pressure measurements; hence the development of the disposable probe arrangement.

Refering to the drawings in Figure 4.7 , the important features to note about the designs of the probe and holder are as follows. Firstly, the temperature sensitive parts of the probe assembly (i.e solder joints and nylon tube connection to the pressure transducer) were shielded from the rocket exhaust jet by the holder. Secondly, the stainless steel tube part of the probe assembly was fitted tightly in the conical cap of the holder; this was designed to minimise any oscillation of the probe tip when monitoring pressures in the jets. Finally, the base plate of the probe holder had the same dimensions as the pressure tapped flat plate; this allowed the use of a common support structure for the probe holder and flat plate.

4.7) UNIVERSAL TEST STAND

The universal test stand was a piece of apparatus that was designed to accomodate all the required experimental test configurations with free and impinging, hot and cold jets. In this arrangement, the rocket motor combustion chamber acted as the cold jet settling chamber, and the flat plate and pitot probe holder shared the same mounting. This allowed different test configurations to be set easily without major rearrangement of the rig hardware and pressure monitoring instrumentation.

The test stand consisted of a substantial chassis which supported separate mounting modules for the rocket motor/cold jet settling chamber, and the flat plate/pitot probe holder. These modules can be seen in Figure 4.8 which shows a photograph of the test stand configured for a cold jet impingement test with an inclined plate. An annotated scale drawing of the same test stand configuration is presented as Figure 4.9.

The motor and plate mounting modules could be bolted at several discrete positions on the top of the chassis, and this allowed coarse adjustment of the nozzle-to-plate separation distance. Fine adjustment of the position of the nozzle in the horizontal plane was achieved by operating the two-axis machine table incorporated into the rocket motor mounting module. The vertical position of the rocket motor was fixed, and the axis of the exhaust nozzle was 0.72m above floor level.

The flat plate mounting module incorporated a hinged traversing assembly; this allowed the plate to be set at inclinations between 0° and 90° relative to the nozzle axis (i.e. projected nozzle axis). The axis of rotation of the hinge was horizontal, but offset from the plate surface; consequently the point of intersection of the nozzle axis with the plate surface changed when the plate inclination was changed. Alignment, or re-alignment, of the nozzle axis

with a specific point on the plate, (e.g. the pressure tapping at the plate centre), was achieved by adjusting the vertical position of the hinge assembly. Photographs of the plate traversing assembly can be seen in Figure 4.10. The drawings in Figure 4.11 show the positions of the plate traversing mechanism for three different plate inclinations and the nozzle axis aligned with the plate centre.

Figure 4.12 is a scale drawing of the test stand configured for a test to measure the pitot pressure in the rocket motor exhaust. When hot jet tests were conducted, the final segment of the cold gas supply pipe was removed from the test stand, as shown in Figure 4.12. The orientation of the pitot probe holder shown in Figure 4.12 was also used for cold jet pitot tests.

4.8) VENTILATION SYSTEM

Visually, the exhaust from the Hilton motor appeared as black smoke; this was due to the soot particles in the combustion gases. The volume of smoke generated during a single firing of the motor was too great for it to be discharged into the laboratory where the test rig was situated. Therefore, the test rig needed a ventilation system that would capture the rocket exhaust, and convey it to the atmosphere outside the laboratory.

The ventilation system that was designed and built can be seen in two photographs presented as Figure 4.13; the flow direction and component parts of the system are identified in Figure 4.1. It can been seen from these figures that the system consisted of a fan unit and sections of ducting, and that it had two modes of operation. During a hot jet test, the rocket exhaust was captured by the section of ducting placed around the universal test stand. This section of ducting was removed between tests to allow the test stand to be configured or adjusted. All the other sections of ducting were permanently fixed in position.

The ventilation system was designed so that its volumetric flow rate was slightly greater than the volumetric flow rate of the fully expanded rocket exhaust gases. Thus only a small amount of air was drawn around the universal test stand whilst the rocket motor was operating. The velocity of the airstream was kept low (estimated to be in the order of 1-2 m/sec) by making the cross-sectional area of the duct around the test stand large; thus this ensured that the ventilation system had a neglible influence of the impingement and free jet flowfields.

4.9) COLD JET GAS SUPPLY SYSTEM

It was decided that for this study the impingement and free jet pressure data would be obtained using hot and cold jets which had the same pressure ratios - see Section 1.4. Therefore, a cold jet gas supply system was required for delivering gas, to the cold jet settling chamber, at a range of stagnation pressures similiar to the range of pressures that could be developed by burning solid propellants in the Hilton rocket motor combustion chamber, that is approximately 3-7 MN/m^2.

The source of gas was the first issue which had to be considered when devising the supply system. The existing compressed air supply facilty in the laboratory was, unfortunately, only capable of delivering air at a maximum pressure of 2.75 MN/m^2. Another source of gas therefore had to be found. Eventually, it was decided that the supply would be obtained from cylinders of commercially available compressed nitrogen gas (BOC N_2 with O_2 removed) that were filled to an initial pressure of 17.75 MN/m^2. It was estimated that with one of these cylinders of nitrogen, a 20 second duration cold jet could be produced at the maximum pressure ratio required (i.e. worst case duration).

Although the compressed air supply facility mentioned above was not able to deliver air at the required pressures, it could in principal deliver an almost continuous supply of air, at pressures up to 2.75 MN/m^2, through the size of nozzles being used for this study. The continuous nature of this supply offered an easy way of checking that the rig was functioning correctly before conducting short duration tests with the nitrogen gas and the rocket motor. It was therefore decided that the cold gas supply system would be designed so that jets could be generated with either the compressed air or the nitrogen.

A schematic diagram of the cold jet gas supply system that was designed and built is presented as Figure 4.14. The

system utilised four cylinders of nitrogen. This number of cylinders was calculated to be the minimum necessary to deliver the required amount of gas without unacceptable pressure losses occuring in the cylinder outlet valves. The air supply was obtained from the compressed air main that terminated in the vicinity of the rig. Since the air main was contaminated with particulate matter, the air was drawn through an in-line filter (Micro-Filtrex MFL-3-2).

The nitrogen or air were selected as the cold jet gas by means of manually-operated interlocking stop valves (Dynaquip VC8FCOF), as shown in Figure 4.14. These valves permitted either the nitrogen supply or the air supply, but not both, to be connected to the rest of the cold jet supply system. The arrangement of the interlocking valves was designed so that it was impossible to connect the two sources of gas together.

The selected gas passed through a manually-adjustable pressure regulator (Hale Hamilton G20) and a fast-acting flow-control valve (Hale Hamilton QA1) before it reached the cold jet settling chamber. The bore of the interconnecting piping was 10mm (Ermeto 02/524/01). The flow-control valve was essentially a stop valve that was used to switch the cold jet gas supply on and off quickly. Before operating the flow-control valve, the required settling chamber pressure was preset by adjusting the regulator outlet pressure. In practice, the regulator output pressure needed to be set to a higher value than the required settling chamber pressure; this was necessary to compensate for frictional pressure losses that occured in the flow-control valve and connecting piping. The correlation between the regulator outlet pressure, obtained with the flow-control valve closed, and the settling chamber pressure, obtained when the flow-control valve was fully open, was determined by experiment.

Visual indication of the regulator inlet and outlet pressures was provided by dial-type pressure gauges

(Budenberg Standard Test Gauges). The gauges were isolated, after adjustment of the regulator, by closing the stop valves in their connecting pipes; this prevented pressure transients, caused by flow-control valve operation, from damaging the delicate bourdon tube mechanisms in the gauges.

The flow-control valve was actuated by a pneumatic ram (Schrader 350-12010-25). A photograph and schematic diagram of the ram and valve assembly are presented as Figure 4.15. Control of the ram was performed by the system that is illustrated schematically in Figure 4.16. Regulated low pressure air was supplied to and released from the ram by a solenoid actuated spool valve (Schrader 5301ETA-12V). The energising current for the spool valve solenoid was switched on and off by the same microcomputer system that was used for data acquisition - see Section 4.11; this allowed jet control and data acquisition to be synchronised.

Figure 4.15 shows that a rubber damper was positioned between the shaft of the pneumatic ram and the shaft of the flow-control valve. The flow-control valve could be operated either with or without this damper. Without the damper, the flow-control valve was always opened completely by the ram; thus, this produced a constant settling chamber pressure. With the damper, the flow-control valve would be opened completely the instant ram was pressurised, but thereafter the flow-control valve would gradually close with the ram still pressurised; the settling chamber pressure therefore decreased gradually from a peak initial value. This effect occured because the rubber damper was visco-elastic. The rate of change of the chamber pressure depended on the thickness and hardness of the block of rubber used for the damper. The benefit of the changing chamber pressure was that it allowed quasi-steady pressure data to be obtained for a range of jet pressure ratios during a single test run.

The pressure gauges and most of the valves of the cold jet supply system were mounted on a control panel. The bank of

nitrogen cylinders were held in a rack that was located next to the control panel. A photograph of the control panel and the cylinder rack is presented as Figure 4.17. The pipeline connecting the flow-control valve to the settling chamber incorporated a flexible segment of pipe (HIFLEX HI-98); this can be seen in Figures 4.8 & 4.9.

It was decided that the body of the Hilton motor would function as the cold jet settling chamber; this was to ensure that the chamber flow conditions were similiar for the hot and cold jets. When the motor was configured as a settling chamber, the firing pin block - see Figure 2.2 - was removed and replaced with aninlet diffuser for the cold gas supply. The diffuser was conical and had a half-angle of 30°. No flow stabilisation gauzes were used in the chamber.

4.10) SHADOWGRAPH AND SCHLIEREN SYSTEM

A system for shadowgraph and schlieren flow visualisation was available when this study commenced; originally, this system had been designed and used by Carling (Ref.31) for an earlier study of air jet impingement at Bristol. It was considered that this system would be of use when investigating the cold jet flows in the present study; therefore the test rig was designed in a way which allowed it to be utilised.

The system was a conventional single-pass arrangement which used a pair of concave mirrors rather than lenses. The components of the system were built into, or supported by, a set of five free-standing units. These units were designated as follows:

- source light train unit
- primary mirror unit
- secondary mirror unit
- camera/screen unit
- knife edge cut-off unit (schlieren only)

With the system configured for shadowgraph flow visualisation photography, the positions of the relevant units in relation to the other parts of the test rig would be as shown in Figures 4.1 & 4.18. A schematic diagram of the system is presented as Figure 4.19.

4.11) DATA ACQUISITION SYSTEM

A distributed computer system was used to obtain and process the required experimental pressure data. This system is shown in schematic form in Figure 4.20. Essentially, the system consisted of two computers that were linked together for interactive transaction processing and data file transfer through an automatic computer communications exchange. One of the computers, a microcomputer, was located in the laboratory along with the other parts of the test rig; the second computer was a multi-user minicomputer that was situated in another part of the building. During a test, the microcomputer controlled the test rig when appropriate, and obtained the experimental pressure data. After a test, the data were transmitted from the microcomputer to the minicomputer. The minicomputer was used for processing the test data, and producing hardcopy test results in graphical formats.

The laboratory based part of the system shown in Figure 4.20 - the part used for rig control and data acquisition - was specifically configured for this study and will be described in more detail below. The other parts of the system were already installed and therefore these will not be described further.

A photograph of the laboratory based rig control and data acquisition system, and a schematic diagram identifying the components of the system visible in the photograph, are presented as Figure 4.21. The positions of the components of the system in the laboratory are shown in Figure 4.1.

The microcomputer (Cromemco Z2D) was the main component of the rig control and data acquisition system. This incorporated a microprocessor (Zilog Z80A), 64 kbytes of semiconductor memory, two 171 kbyte floppy disk drives, three serial data ports, a parallel data port, 16 analogue-to-digital input channels, and two digital-to-analogue output channels. (Note that 1 kbyte = 1024 bytes). A

schematic diagram, presented as Figure 4.22, illustrates the internal configuration of the microcomputer and also indicates how it was connected to the other components of the system.

The microcomputer was programmed to respond to a set of commands which were entered on the keyboard of the VDU (Televideo 920) connected to one of the serial data ports. The VDU also received and displayed status information from the microcomputer. Details of the programs used with the microcomputer will be covered in the next section of this chapter.

When cold jet tests were conducted, the microcomputer switched the cold jet gas supply on and off by controlling the electrical current to the solenoid spool valve of the cold jet gas supply system - see Figure 4.16. Control was effected through a solenoid drive interface; this purpose-built unit was connected between the microcomputer parallel data port and the spool valve. The interface enabled a logic signal (i.e. a TTL signal), sent from the microcomputer port, to switch the heavier current required to actuate the spool valve. Details of the interface circuit are shown in Figure 4.23.

A multi-channel pressure monitoring subsystem was connected to the microcomputer; this was used to obtain the experimental pressure data. Essentially, this subsystem consisted of 16 pressure transducers and a 16-channel differential amplifier unit. The electrical signals generated by the transducers were amplified and fed into the 16 analogue input channels of the microcomputer. During a test, the microcomputer performed real-time digitisation of the analogue signals and stored the resulting data values in its semiconductor memory. The components of the pressure monitoring subsystem will now be examined in more detail.

The pressure transducers were configured differently for the different types of test. The configuration used for hot jet

impingement tests is shown in schematic form in Figure 4.24. The transducer which was connected to the rocket motor combustion chamber had a pressure range of 0-13.8 MN/m² and was manufactured by Precise Sensors Inc. (type no. 111-2-2000-G-34-10P). The pressure sensing element of this particular transducer was watercooled. The other fifteen transducers - connected to the flat plate tappings - were manufactured by Microgage Inc. (type no. P102-1000-G); these were all rated for a pressure range of 0-6.9 MN/m². The same arrangement of transducers was used for cold jet impingement tests when the Hilton motor served as the cold jet settling chamber.

When tests were conducted to monitor the pitot pressures in free jets, only two of the transducers were used. For these tests, the Precise Sensors transducer was connected to the tapping in the combustion chamber of the rocket motor and one of the Microgage transducers was connected to the pitot probe; the other 14 Microgage transducers were not used. This configuration of the transducers was used for both the hot and the cold free jet tests.

All the pressure transducers were mounted on the universal test stand; the positions are identified in Figures 4.9 & 4.12. These figures also show the cooling water pipes that were connected to the Precise Sensors transducer. The cooling water was drawn directly from the mains supply in the laboratory.

Information on the the cavity volumes of the pressure transducers, and the geometries of the associated connecting tubes, can be found in Figure 4.25.

All the pressure transducers were strain gauge type transducers (i.e. variable resistance type). Each transducer incorporated four strain gauges which were connected together as a conventional four-arm bridge circuit. The electrical cable from each transducer bridge contained two power and two signal leads; these were plugged

into the amplifier unit. All the transducer bridges were powered from the same 10 Volt DC power supply unit; this supply unit was connected to the amplifier unit as shown in Figure 4.24. The amplifier unit also included separate balance (i.e. null adjust) and shunt calibration circuits for each transducer bridge.

The same wiring arrangement was used for all transducer bridge, balance, and shunt circuits; this arrangement can be seen in the schematic circuit diagram presented as Figure 4.26. The values of resistances Rt, Rb, and Rs are omitted from Figure 4.26 because they were different for each transducer. The nominal values of the bridge resistances, Rt, were 320 and 450 Ohms for the Precise Sensors and the Microgage transducers respectively. The resistance in the balance circuit, Rb, was chosen to suit the initial amount of unbalance in the transducer bridge. The shunt resistance, Rs, was selected when the transducer was calibrated by application of known pressures.

The amplitudes of the electrical signals generated by the transducers were too small to be fed straight to the analogue input channels of the microcomputer; hence the need for the amplifiers. The 16-channel amplifier unit was specifically designed and built for this study. Each amplifier channel incorporated three operational amplifier integrated circuits which were arranged in a differential input single-ended output configuration. A simplified schematic diagram of an amplifier circuit is shown in Figure 4.27.

The 16-channel analogue input circuitry in the microcomputer was based on a multi-function integrated circuit (Burr Brown SDM-856-KG). This integrated circuit incorporated a 16-to-1 multiplexer (MUX), a sample-and-hold unit (S&H) with an aperture time of 100 nanoseconds, and an analogue-to-digital converter (ADC) with a resolution of 12 bits. The input signals were scanned sequentially by the MUX and fed to the S&H, which sampled the voltages of the signals, and fed

these to the ADC. The ADC converted the sampled voltages into 12-bit digital values. The operation of this integrated circuit was controlled by instructions sent from the microprocessor, which also read the data values from the ADC and stored them in the semiconductor memory of the microcomputer. The time required to address a specific input channel, convert the sampled input voltage to a digital value, and store the value in memory was 61 μs. Therefore, a scan of all 16 channels required a time of 976 μs (i.e. 16 x 61 μs); when fewer channels were scanned, the time was proportionally reduced. A scan cycle was initiated when the microprocessor received an interupt from a hardware interval timer (i.e. real-time clock) which was incorporated in the microcomputer. This programmable timer generated interupts at regular intervals, and thus functioned as the master time-base for the data acquisition process. The interupt time interval was programmed in units of 1 millisecond; the shortest and longest intervals were 2 and 32767 milliseconds respectively. Thus the maximum rate at which data could be obtained and stored was 500 values/channel/second (i.e. a total of 500, 1000, ... 8000 values/sec from 1,2, ... 16 channels respectively).

Of the 64 kbytes of semiconductor memory in the microcomputer, 19 kbytes were used for code storage (i.e. microprocessor instructions); this left 45 kbytes for data storage. Two bytes of memory were used for storing each data value generated by the ADC. Therefore, the upper limit to the total number of data values that could be stored in the course of one test was 23040 (i.e. 1024 x 45/2). Thus, when 16 analogue input channels were in use, 1440 data values (i.e. 23040/16) could be stored per channel; when fewer channels were used, the number of data values that could be stored per channel was proportionately greater.

As indicated in Figure 4.22, the two digital-to-analogue output channels of the microcomputer were connected to the X and Y inputs of an oscilloscope (Advance OS-4000); this oscilloscope was fitted with a standard short-persistence

phosphor CRT. Each analogue output channel was based on a 12-bit digital to analogue converter (DAC) integrated circuit (Burr Brown DAC-80-CBI-V). When required, the DAC's repeatedly converted specified sequences of digital values into analogue signals, and these were displayed as a trace on the oscilloscope screen. Thus this arrangement functioned as a refreshed vector graphics display. The vector plotting rate was approximately 20000 vectors/sec. A maximum of 512 vectors could be displayed simultaneously. This graphics display was used for monitoring the data values obtained from the ADC.

After conducting a test, satisfactory data were transfered from the microcomputer semiconductor memory to a floppy disk (i.e. removable magnetic media used in the microcomputer disk drives for program and data storage). The data were converted to ASCII (American Standard Code for Information Interchange) format as they were transfered from memory to disk. In ASCII format, each data value required 5 bytes of disk storage. The capacity of a disk was 171 kbytes; thus it was possible to store the data from more than one test on a single disk. The test data needed to be temporarily stored on floppy disk, in a sequential-access ASCII data file, before it could be transfered to the minicomputer for processing.

Data files were transfered to the minicomputer through the FACX, as shown in Figure 4.20. One of the microcomputer serial ports was connected to the FACX for this purpose - see Figure 4.22. Once communications were established between the two computers, the FACX was effectively transparent to the flow of data. The data transmission rate was approximately 120 bytes/sec.

4.12) MICROCOMPUTER SOFTWARE

Applications software was required for the microcomputer (Cromemco Z2D) which would first capture the experimental pressure data and then transfer it to the minicomputer (GEC 4090). This software requirement was met by two programs. One program was used for data capture, and the other for data file transfer. The data capture program (DCP) was written specifically for this study; the data file transfer program (FTP) was already available. Both programs operated in conjunction with, but not concurrently with, the microcomputer operating system (Cromemco Disk Operating System - CDOS).

The DCP was an interactive command-driven program which provided the following facilities:

- 1 to 16 active analogue input channels
- real-time textual display of data without capture
- real-time graphical display of data without capture
- capture of zero-offset signal datasets
- capture of calibration signal datasets
- capture of transient signal datasets
- variable data capture rates
- conditional software triggering for data capture
- variable amounts of pretrigger for transient datasets
- selective graphical display of captured datasets
- storage of captured datasets on floppy disk
- retrieval of datasets from floppy disk (for display)
- configurable rig control sequences
- synchronised rig control and data capture

The DCP was written in Z80 assembly language (Cromemco Z80 Macro Assembler). It was necessary to use assembly language in order to obtain an acceptable program execution rate; higher level languages, such as FORTRAN, would have been too slow.

input-output subprogram; this subprogram could also transfer a data file back into the microcomputer semiconductor memory, and this allowed the graphical display of previously captured datasets.

The microcomputer incorporated a total of 64 kbytes of semiconductor memory. When the assembled DCP object code was loaded into the microcomputer for execution it occupied approximately 8 kbytes of the available memory. It was necessary for CDOS to be co-resident in memory during DCP execution. CDOS required 11 kbytes of memory, and therefore 45 kbytes were left for data storage. The entire 45 kbyte data storage space was utilised by the DCP. The DCP segmented the data space into four variable-sized regions. One region was used as program work-space; the others were used for storing the zero-offset, calibration, and transient signal datasets. Memory allocation maps for the system and DCP address spaces are shown in Figure 4.29.

Simplified flow charts for each of the six DCP code modules are presented as Figures 4.30 to 4.35.

The file transfer program (FTP) will now be considered. This program was obtained from the Rutherford and Appleton Laboratory . The FTP was designed to communicate with a similiar program which operated on the minicomputer. When the FTP was operated, the data in a specified file on a microcomputer disk was transmitted and copied to an equivalent file on one of the minicomputer disks.

The FTP used an asynchronous block-orientated communications protocol. This protocol incorporated an error detection procedure. Some types of errors were corrected automatically and this allowed the file transmission to continue; others terminated the communications process. For example, if an error was detected in a transmitted data block, then the block was retransmitted; if too many attempts were made to retransmit the same block, a line fault was assumed and the FTP terminated.

The DCP source code consisted of approximately 3000 assembly language statements. The code was structured as six modules; these modules were designated as follows:

- main program
- configuration subprogram
- zero and calibration subprogram
- transient signal capture and rig control subprogram
- graphics display subprogram
- disk input-output subprogram

When the DCP began operating, the main program assigned default values to the program variables, and then entered a command interpretation mode whilst waiting for commands to be typed on the VDU keyboard. One command caused the program to terminate; others allowed random selection of the facilities provided by the subprograms. The subprograms requested or allowed subsidiary commands to be typed on the VDU. Main program command interpretation mode was regained when execution of the subprograms terminated. The operating inter-relationship between the main program and the subprograms is illustrated schematically by the state transition diagram shown as Figure 4.28. For completeness, this diagram also indicates state transitions from system reset.

The configuration subprogram allowed the default values of the program variables to be altered (e.g. number of analogue input channels, data capture rate, rig control sequences, etc.). The zero and calibration subprogram provided the real-time displays of the data obtained from the analogue input channels, and captured the zero-offset and calibration signal datasets. Concurrent rig control and capture of transient signal datasets were achieved by the rig control and transient signal capture subprogram. The graphics display subprogram allowed display of one channel of captured transient signal data at one time, and provided incremental pan and zoom facilities. The captured datasets and program variables were filed on floppy disk by the disk

CHAPTER FIVE - EXPERIMENTAL PROCEDURES

5.1) INTRODUCTION

The experimental rig described in the previous chapter was utilised for series of tests with rocket, nitrogen and air jets. Essentially, the tests involved the measurement of pitot pressures in the free jets, the measurement of flat plate pressure distributions for impinging jets, and some complementary flow visualisation photography.

The tests with the rocket and nitrogen jets were conducted to provide the hot and cold jet pressure data which were required for comparison and possible correlation.

Originally, the intention had been to use the air jets only for verifying that the experimental rig was functioning correctly before conducting tests with the short-duration rocket and nitrogen jets. Subsequently, however, the original study objective was revised to include the systematic acquisition of air jet pressure data, prior to conducting the tests with the rocket and nitrogen jets. Significant trends were perceivable in the air jet data, and these allowed a refinement of the test strategy with the rocket and nitrogen jets. This approach to the experimental investigation enabled more cost-effective utilisation of the limited quantities of rocket propellant and nitrogen gas that were available for this study.

The following sections of this chapter document the test configurations that were investigated, describe various aspects of the test rig operation, explain the procedures that were used to obtain and process the experimental pressure data, and outline the flow visualisation techniques.

5.2) FREE JET TEST CONFIGURATIONS

Tests were conducted to measure pitot pressures at positions along the centrelines of the free air, nitrogen, and rocket jets. The salient geometrical variables associated with these tests are identified in the schematic diagram presented as Figure 5.1. All the jets were produced by the convergent nozzle with a 3.12mm diameter throat (Re=1.56mm) - see Figure 4.3. The non-dimensional nozzle-to-probe separation distances, Zpt/Re, for the tests were as shown in Table 4.

5.3) IMPINGING JET TEST CONFIGURATIONS

Impingement tests were conducted with the air, nitrogen, and rocket jets. The salient geometrical variables associated with these tests are identified in the schematic diagram presented as Figure 5.1. All the jets were produced by the convergent nozzle with a 3.12mm diameter throat. The non-dimensional nozzle-to-plate separation distances, Zp/Re, and plate angles, θ, for the tests were as shown in Table 5.

All the impingement tests were conducted with the nozzle axis intersecting the line joining the linear array of plate pressure tappings. Also, for all tests, the plate was orientated so that the line of tappings was perpendicular to the axis of the hinge of the plate traversing assembly, (i.e. when θ=90°, the line of tappings was vertical and not horizontal).

The pitch of the array of the fifteen plate pressure tappings (nominally 3.125mm) was too large to provide satisfactory resolution of the variations of the impingement flowfield pressure distributions across the plate surface. Therefore, to improve the resolution, multiple tests were conducted for each nozzle/plate configuration with the plate displaced to different positions in its own plane. The displacements were fractions of the tapping pitch in a direction parallel to the line of the tappings. Initially, three tests were conducted, for each nozzle/plate configuration, to give a combined total of 45 measurement locations. For the first test, the plate was positioned so that the pressure tapping at the middle of the array was in line with the nozzle axis. For the second and third tests, the plate was positioned so that the nozzle axis intersected the plate surface at distances of 1.0 and 2.0mm from the middle tapping respectively. When severe gradients were observed in the pressure distributions, a further three tests were conducted to give a combined total of 90 measurement locations. For these three additional tests, the plate was positioned so that the nozzle axis intersected

the plate surface at distances of 0.5, 1.5 & 2.5mm from the middle tapping respectively. Table 6 gives the precise locations of the tappings - relative to the point of intersection between the nozzle axis and the plate surface - for the six plate positions described. Table 7 shows which plate positions were used for the various test configurations investigated.

5.4) TEST STAND ADJUSTMENT

The universal test stand incorporated various positioning mechanisms for adjusting the locations of the rocket motor, pressure-tapped flat plate and pitot probe. The adjustment procedure used when setting the test configurations which were mentioned in the two preceeding sections was as follows.

Firstly, the orientation of the nozzle axis was checked to ensure that it was parallel to the axis of the lead screw - incorporated in the machine table of the motor mounting module - which was used for adjusting the nozzle-to-plate and nozzle-to-probe separation distances. If these axes were not parallel, then the point that the nozzle axis intercepted the plate or probe would have changed when the separation distances were set during the final adjustment operation -see below. The orientation of the nozzle axis was checked using a dial-type displacement gauge and a special-purpose alignment device. The alignment device was fitted to the motor in place of the nozzle and provided a flat surface which was parallel to the nozzle axis (for the stylus of the dial gauge to rest against). A photograph of the alignment device is presented as Figure 5.3(a). Misalignment of the axes was corrected by adjusting the bolting position of the motor on its support bracket and/or the bolting position of the support bracket on the machine table. When the nozzle was refitted to the motor, after checking the orientation of the axis, it was always set at the same 'roll angle' relative to the combustion chamber tube; thus, the nozzle was set at the same 'roll angle' for all tests.

The surface of the plate or the axis of pitot probe was then set at the required orientation relative to the nozzle axis by adjusting the inclination of the hinged part of the plate/probe holder mounting assembly. This adjustment was accomplished with the aid of an adjustable set square and another special-purpose alignment device. The alignment

device fitted over the external cylindrical surface of the nozzle and provided a plane surface that was perpendicular to the nozzle axis; a photograph of this device is presented as Figure 5.3(b). The set square was used for monitoring the angle between the surface of the alignment device and either the surface of the pressure tapped flat plate or the base plate of the pitot probe holder.

The nozzle axis was then aligned with the required point on the surface of the flat plate or with the axis of the pitot probe. This was accomplished by traversing the motor laterally and/or the plate/probe mounting vertically. When these adjustments were made, the position of the nozzle axis was tracked with a third special-purpose alignment device; a photograph of this device is presented in Figure 5.3(c). This device fitted over the external cylindrical surface of the nozzle and provided a solid representation of the nozzle axis which terminated in a point.

Finally, the required nozzle-to-plate or nozzle-to-probe separation distance was then set by adjusting the location of the rocket motor. Slip gauges were used for verifying that the separation distances were set correctly.

5.5) ROCKET MOTOR OPERATION

The Type 670 propellant cartridges were used for all tests with the Hilton rocket motor. The combination of this propellant and the stainless steel nozzle with a 3.12mm diameter throat produced approximately the same variation of chamber pressure with time for all test firings. A sample recording of the rocket motor chamber pressure is presented as Figure 5.4.

Figure 5.4 shows that there was a significant reduction of the chamber pressure, from the peak inital value, during the test firing. This regressive pressure-time behaviour permitted pressure data to be obtained for a range of chamber pressures in a single test.

The pressure-time recording shown in Figure 5.4 differed from those obtained during the tests to determine the performance of the Hilton motor. Two recordings from the earlier tests, presented in Figures 2.3(a) & 2.3(b), show that the chamber pressures remained nearly constant during the motor firings with the Hilton nozzles of throat diameters of 3.00 and 3.23mm. The differences in the variations of the chamber pressure with time probably resulted from differences in the thermal expansion characteristics of the two types of nozzle following exposure to the high temperature combustion gases at the start of the motor firings.

In the case of the stainless steel nozzle, transient thermal expansion probably caused a small but significant increase in the nozzle throat area, and therefore the chamber pressure decreased as a consequence. (See Section 2.5 for further details of the relationship between the nozzle throat area and the combustion chamber pressures.) In the case of the tests with the Hilton nozzles, the changes in the throat areas were probably neglible; hence the nearly constant chamber pressure during the test firings.

The differences in the magnitudes of the thermal expansions can be accounted for by the differences in the designs of the nozzles and, in particular, the differences in the wall thicknesses in vicinity of the throats - see Figures 2.2 & 4.3.

5.6) COLD JET GAS SUPPLY SYSTEM OPERATION

For all tests involving pressure measurements with cold jets, the cold jet gas supply system was operated with a rubber damper in the flow-control valve actuation mechanism - see Figure 4.15. The visco-elasticity of the damper caused the cold jet settling chamber pressure to decrease gradually from a peak initial value - see Section 4.9; this allowed pressure data to be obtained for a range of chamber pressures during a single test, as was also the case for the hot jet tests.

The variation of the settling chamber pressure with time was approximately the same for all nitrogen jet tests; a sample recording of the chamber pressure is presented as Figure 5.5. Likewise, for the experimentation with air jets, the variation of the chamber pressure with time was approximately the same for all tests; a sample recording is shown in Figure 5.6

The flow-control valve was fitted with different dampers for the nitrogen and air jet testing. The dimensions and viscoelastic properties of these dampers were chosen by experiment.

5.7) PRESSURE MONITORING SUBSYSTEM CALIBRATION

Before testing commenced, the pressure monitoring subsystem of the data acquisition system was calibrated by applying known pressures to the transducers and monitoring the corresponding signals which were generated by the amplifier unit. Dead weight testers (Budenburg) were used for producing known gauge pressures in the range 0-7 MN/m^2. The microcomputer and the data capture program (DCP) were used for monitoring the output signals from the amplifiers.

The initial calibration established that the pressure-voltage characteristics of all channels of the pressure monitoring subsystem were linear and free from hysteresis.

The drawback to the conventional method of calibration was that it took a long time to complete. Therefore, during testing, the transducer shunt calibration circuits were used instead for calibrating the pressure monitoring subsystem.

A schematic diagram of a shunt circuit can be seen in Figure 4.26. When the switch in a shunt circuit was closed, the shunt resistor altered the effective resistance of one arm of the transducer bridge and thus simulated the application of a calibration pressure to the transducer. The exact pressures simulated by the shunt resistors were determined by reference to calibrations made using the dead weight testers.

5.8) PRESSURE DATA ACQUISITION

The same procedure was used when operating the data acquisition system to obtain pressure data for all tests with the hot and cold, free and impinging jets. This procedure was as follows.

Firstly, the microcomputer data capture program (DCP) was configured to suit the test. This was accomplished by supplying the following information to the DCP:

- number of active input channels
- number of zero-offset signal data values/channel
- number of calibration signal data values/channel
- number of transient signal data values/channel
- data capture rate
- trigger channel
- trigger signal level
- number of pretrigger transient signal data values
- rig control sequencing data

The signal transfer characteristics of the pressure monitoring subsystem were then adjusted to suit the test. The microcomputer real-time display was used for monitoring the signals generated by the subsystem when the adjustments were made.

The zero-offset and calibration signal datasets were then captured; usually, 50 data values/channel were obtained for both datasets. The zero-offset signals corresponded to ambient pressure on the transducers; the laboratory barograph (Cassella) was used for monitoring the ambient pressure during the testing. The calibration signals were generated by closing the switches of the transducer shunt circuits; these circuits simulated the application of a known calibration pressure to each of the transducers.

The jet was then operated and the associated transient signal dataset captured. Usually, 1000 data values/channel were obtained for the transient signal dataset.

The captured transient signal data were then inspected using the graphics display of the microcomputer system.

The data stored in the microcomputer semiconductor memory were then transfered to a floppy disk data file. The data file incorporated the following datasets:

- DCP configuration dataset (i.e. number of active channels, etc.)
- zero-offset signal dataset
- calibration signal dataset
- transient signal dataset

The data file was then transmitted to the minicomputer for processing; this was accomplished using the file transfer program (FTP).

5.9) PRESSURE DATA PROCESSING

The minicomputer system - see Figure 4.20 - was used for processing the files of experimental data, which were sent from the microcomputer, and for producing hardcopy of the results in various graphical formats. The associated applications software was written specifically to suit the requirements of this study and was composed of a set of programs which were coded in FORTRAN.

Essentially, the same procedure was used for processing the data files from all types of test, (i.e. tests with hot and cold, free and impinging jets); this processing procedure was as follows.

Firstly, each data file was appended to another file which had been created on the minicomputer; this other file contained coded details of the associated test configuration (e.g. type of test, ambient pressure, nozzle/plate/probe geometry, etc.). The details of the test configuration were coded as one dataset. Thus, the file for each test then contained five datasets; viz:

- test configuration dataset (TCD)
- DCP configuration dataset (DCD)
- zero-offset signal dataset (ZSD)
- calibration signal dataset (CSD)
- transient signal dataset (TSD)

The incorporation of the TCD in each data file allowed the file to be processed in batch mode; it also allowed the origin of the other datasets to be tracked during processing. The processing programs accessed the DCD for details of the structures of the ZSD, CSD & TSD. These signal datasets were structured as two-dimensional arrays of values. The processing programs referenced the values in the these arrays either individually, or as scan-records, or as channel-records. A scan-record was a subset of values which were obtained during a single cycle of the data

acquisition system multiplexer (i.e. one value from each active channel). A channel-record was a subset of values from one of the active channels.

In the next processing operation on each file, the values stored in the ZSD, CSD and TSD were converted from integer to floating-point numbers. The floating-point number format provided six significant decimal digits for the mantissa, and allowed the exponent to range from -76 to +76; (the associated FORTRAN data type was REAL*4). This number format was maintained for all subsequent computational operations.

The TSD values of each file were then transformed from voltage values to absolute pressure values. The transformations were made using linear pressure-voltage transformation functions; (the pressure monitoring subsystem exhibited linear response characteristics - see Section 5.7). A separate transformation function was used for each TSD channel-record. Each transformation function was defined by a pair of voltage and pressure values; these were the arithmetic means of the zero-offset and calibration voltage values, which were evaluated from the related ZSD and CSD channel-records, and the corresponding known pressure values, which were extracted from the TCD (i.e. the ambient pressure, and the pressure simulated by the transducer shunt circuit). A rule-based data-verification routine was incorporated in the program which evaluated the means of the zero-offset and calibration voltages; this routine detected and excluded any irregular values (e.g. those associated with noise spikes) from the averaging process. For consistency in the dataset naming conventions, the transformed TSD will be refered to from now on as the transient pressure dataset (TPD).

At this stage of the processing sequence, the TPD channel-records of each file were plotted for inspection. An example plot is presented as Figure 5.7; this shows the 16 channel-records from a hot jet impingement test. The time

axis coordinates for the plots were calculated from the value of the data capture rate which was stored in the DCD.

The 61μs time-offset between each value in each TPD scan-record was then eliminated; this time-offset was caused by the data acquisition system multiplexer - see Section 4.11. The time-offsets were eliminated by evaluating new values for each scan-record; the new values were obtained by linear interpolation of the existing channel-record values with respect to time. The new values in the TPD scan-records were then equivalent to those which would have been obtained if the signals from all the active channels of the pressure monitoring subsystem had been sampled at the same instants in time (i.e. in parallel).

The TPD values were then non-dimensionalised by evaluating various pressure ratios. The pitot or plate pressure values in each scan-record were divided by the chamber pressure value from the same scan-record - hence the elimination of the time-offsets above; this computation yielded the pitot or plate pressure ratios, Fpt/Fc or Fp/Fc. The chamber pressure value in each scan-record was divided by the ambient pressure value; this yielded the jet pressure ratio, Fc/Fa. The non-dimensionalised TPD will refered to henceforth as the transient pressure ratio dataset (TPRD).

A sequence of processing operations was then performed to generate a standard set of pressure ratio scan-records from the TPRD. This standard set of scan-records allowed the pressure ratio data from different tests to be merged and/or compared without further processing. The sequence of operations was as follows.

Firstly, the TPRD was analysed to determine the times during the test when the jet pressure ratio, Fc/Fa, was equal to specified values. The specified values of Fc/Fa were in the form of a series which started at 1.00 and then increased by increments of 0.25 (i.e 1.00, 1.25, 1.50, 1.75, ... etc.). The last value of Fc/Fa in the series was equivalent to the

maximum for the test; this was between 20 and 22 for the tests with air jets, and between 50 and 55 for the tests with rocket and nitrogen jets. The required times were found by linear interpolation of the TPRD channel-record of Pc/Pa values with respect to time. Each value of time obtained was paired with the associated value of jet pressure ratio and these were stored together, as a record, in an index dataset (ID).

Normally, the ID contained at least two records for each specified value of Pc/Pa because the jet pressure ratio first increased and then decreased during every test. If the jet pressure ratio fluctuated about a specified value during a test, then the ID contained more than two records with this value of Pc/Pa.

A third value was then added to each ID record; this was the rate of change of the jet pressure ratio with time, $\delta(Pc/Pa)/\delta t$, which occured at the instant in time specified by the value of time stored in the same record. These rate values were obtained by differential analysis of the TPRD channel-record containing the values of Pc/Pa.

The order of the ID records was then rearranged so that the magnitudes of the Pc/Pa values were in ascending order relative to the start of the dataset. This rearrangement therefore grouped together records with the same value of Pc/Pa. Each group will be refered to as an index dataset group (IDG). The order of the records in each IDG was then rearranged so that the absolute magnitudes of the $\delta(Pc/Pa)/\delta t$ values were in ascending order relative to the start of each group. The first record of each IDG - the one with the lowest absolute $\delta(Pc/Pa)/\delta t$ value - was then retained in the ID and the other records were deleted.

The ID time values were then used as pointers for generating the standard set of pressure ratio scan-records from the TPRD. Each new scan-record was formed by simultaneous linear interpolation of all TPRD channel-records with

respect to time. The standard set of scan-records were stored in a new dataset - this will be termed the pressure ratio dataset (PRD).

The TCD and PRD were then retained in each data file and the other datasets were deleted. This was the last processing operation performed on each separate data file.

Subsequently, the separate data files from series of tests were concatenated after they had been processed. Thus, this operation linked together all the TCD-PRD pairs from each series of tests in one file - this type of file will be refered to as a test series data file (TSDF). A separate TSDF was created for the series of:

- free air jet tests
- free nitrogen jet tests
- free rocket jet tests
- impinging air jet tests
- impinging nitrogen jet tests
- impinging rocket jet tests

Finally, sets of data were then extracted from each TSDF and plotted. Initially, isometric and contour plots were produced that illustrated the variations of the pitot pressure ratio along the jet axes and the variations of the plate pressure ratio across the surface of the flat plate for ranges of jet pressure ratios. Subsequently, two-axis plots were produced that illustrated the distributions of the pitot and plate pressure ratios for various discrete jet pressure ratios. The plots that were produced will be presented and discussed in the next chapter.

5.10) HOT JET FLOW VISUALISATION

When hot jet impingement tests were conducted, some of the soot in the rocket motor exhausts was deposited on the pressure-tapped flat plate. The soot was usually deposited in a thin layer over the entire surface of the plate.

Surface flow patterns were observed in the soot depositions. These patterns were visible only when the depositions were illuminated by a beam of light; the patterns were not apparent in diffuse lighting conditions. Also, different features of the patterns tended to be emphasised when the angle between the incident light beam and the surface of the plate was varied.

It was considered that the soot patterns provided useful information about the flow conditions which occured at the surface of the flat plate during hot jet impingement. Therefore, after every hot jet impingement test, the soot depositions were photographed before they were cleaned off the plate.

The soot depositions were photographed using a single-lens-reflex camera (Asahi Pentax SP-1000), which was equipped with a lens of 55mm focal length. The camera was loaded with monochrome film rated at 400 ASA (Kodak Tri-X Pan). A photographic slide projector lamp (250 Watt) was used for the light source.

All photographs of the soot depositions were taken with the axis of the camera aligned perpendicular to the plate surface. Sets of photographs were taken with the projector lamp oriented in two different positions. For these projector positions, the angles between the light beams and the surface of the plate, α, were approximately 30° and 45°.

The films were developed in accordance with the manufacturer's standard recommendations. Prints of approximately equal size were produced that showed the

depositions for the whole of the plate and for the central region around the pressure tappings.

No other forms of flow visualisation were used during the tests with the Hilton rocket motor.

5.11) COLD JET FLOW VISUALISATION

The shadowgraph/schlieren system was used for observing the structures of the cold jet flows.

The procedures employed for aligning and operating the shadowgraph/schlieren system were exactly the same those described by Carling (Ref.31), and therefore these procedures will not be reiterated here. (Note that this shadowgraph/schlieren system was originally designed and used by Carling - see Section 4.10.)

No shadowgraph or schlieren photographs of the cold jet flows were made in the course of the test program; this was due to constraints on the amount of time available for this study.

CHAPTER SIX - PRESENTATION AND DISCUSSION OF RESULTS

6.1) INTRODUCTION

The experimental results obtained from the series of free and impinging jet tests with air, nitrogen and rocket jets are presented and discussed in this chapter. The nozzle-and-probe and nozzle-and-plate test configurations were described previously in Sections 5.2 & 5.3 respectively.

For all series of tests, results are presented in the form of pressure distributions. In the case of the rocket jet impingement tests, photographs of the soot depositions on the surface of the plate are also presented.

When examining the results, it should be remembered that the pressure ratio of all experimental jets varied with time. The variations Pc/Pa with time for the rocket, nitrogen and air jets can be seen in the sample recordings which were presented earlier as Figures 5.4, 5.5, & 5.6 respectively.

In the following sections of this chapter, the results from the free jet tests will be considered before those from the impingement tests; also, for both types of test, the results from air jet tests will be considered before those from the rocket and nitrogen tests.

6.2) FREE AIR JET

Results from the series of tests with free air jets are presented in Figures 6.1 to 6.4 inclusive.

Figure 6.1 is an isometric plot which shows how the jet centreline pitot pressure distribution, Ppt/Pc versus Zpt/Re, varies with jet pressure ratio, Pc/Pa. The data plotted in Figure 6.1 are also shown in contour format in Figure 6.2; (note that the values marked on the contour lines are values of Ppt/Pc).

Figure 6.3 is a two-axis plot which shows the jet centreline pitot pressure distributions, Ppt/Pc versus Zpt/Re, for the discrete jet pressure ratios, Pc/Pa, of 5, 10, 15 & 20; the individual data points are also shown in this figure for each pressure distribution.

Figure 6.4 is a two-axis plot which compares the jet centreline pitot pressure distribution for Pc/Pa=6.758 obtained in this study with that obtained by Donaldson & Snedeker (Ref25).

The non-dimensional nozzle-to-probe separation distances, Zpt/Re, have been used for the jet axis coordinate data in Figures 6.1 to 6.4. Therefore, the distance between the tip of the pitot probe and the detached probe bow shock has not been taken into account for those measurement positions on the jet axis where the flow was supersonic.

6.3) FREE ROCKET AND NITROGEN JET

Results from the series of tests with free rocket and nitrogen jets are presented in Figures 6.5 to 6.10 inclusive.

Figures 6.5 & 6.6 are isometric plots which show for the nitrogen and rocket jets how the pitot pressure distributions along the jet axes, Ppt/Pc versus Zpt/Re, vary with jet pressure ratio, Pc/Pa. The data plotted in these figures are also shown in contour format in Figures 6.7 & 6.8; (note that the values marked on the contour lines are values of Ppt/Pc).

Figures 6.9 & 6.10 are two-axis plots which show comparisons between pitot pressure distributions along the axes of the rocket and nitrogen jets for the case when the pressure ratio of both jets is 40.

The non-dimensional nozzle-to-probe separation distances, Zpt/Re, have been used for the jet axis coordinate data in Figures 6.5 to 6.10. Therefore, the distance between the tip of the pitot probe and the detached probe bow shock has not been taken into account for those measurement positions on the jet axis where the flow was supersonic.

6.4) AIR JET IMPINGEMENT ON A PERPENDICULAR PLATE

Results from the series of tests with air jets impinging on a flat plate set perpendicular to the jet axis are presented in Figures 6.11 to 6.29 inclusive.

Figures 6.11, 6.12, 6.13 & 6.14 are isometric plots which show how the plate pressure distribution, Pp/Pc versus Sp/Re, varies with plate position, Zp/Re, for jet pressure ratios, Pc/Pa, of 5, 10, 15 & 20 respectively. The data plotted in these figures are also shown in contour format in Figures 6.15 to 6.18; (note that the values marked on the contour lines are values of Pp/Pc).

Figures 6.19, 6.20, 6.21 & 6.22 are isometric plots which show how the plate pressure distribution, Pp/Pc versus Sp/Re, varies with jet pressure ratio, Pc/Pa, for plate positions, Zp/Re, equal to 5, 10, 20 & 40 respectively. The data plotted in these figures are also shown in contour format in Figures 6.23 to 6.26; (note that the values marked on the contour lines are values of Pp/Pc).

Figures 6.27, 6.28 & 6.29 contain five, two-axis plots; these show how selected plate pressure distributions obtained in this study compare with those obtained by other investigators.

6.5) ROCKET & NITROGEN JET IMPINGEMENT ON A PERPENDICULAR PLATE

Results from the series of tests with rocket and nitrogen jets impinging on a flat plate set perpendicular to the jet axis are presented in Figures 6.30 to 6.53 inclusive.

Figures 6.30, 6.31, 6.32 & 6.33 are isometric plots which show for the nitrogen jet how the plate pressure distribution, Pp/Pc versus Sp/Re, varies with jet pressure ratio, Pc/Pa, for plate positions, Zp/Re, equal to 5, 10, 20 & 40 respectively. The data plotted in these figures are also shown in contour format in Figures 6.34 to 6.37; (note that the values marked on the contour lines are values of Pp/Pc). A comparable set of isometric and contour plots of the rocket jet plate pressure distributions are shown in Figures 6.38 to 6.45.

Figures 6.46, 6.47, 6.48 & 6.49 contain photographs of the soot depositions which were formed on the plate during the rocket jet impingement tests with Zp/Re equal to 5, 10, 20 & 40 respectively.

Figures 6.50, 6.51, 6.52 & 6.53 are two-axis plots which show, for rocket and nitrogen jets with pressure ratios of 40, comparisons between the plate pressure distributions for plate positions, Zp/Re, equal to 5, 10, 20 & 50 respectively.

6.6) ROCKET & NITROGEN JET IMPINGEMENT ON AN INCLINED PLATE

Results from the series of tests with rocket and nitrogen jets impinging on a flat plate inclined at an angle of 45° to the jet axis are presented in Figures 6.54 to 6.77 inclusive. The format of the results presented in this set of figures is exactly the same as that which was used in the previous section for the results from the perpendicular impingement tests.

CHAPTER SEVEN - CONCLUSIONS

Figures 6.50 to 6.53 show a comparison of pressure distributions for the rocket and nitrogen jets impinging on a normal flat plate and Figures 6.74 and 6.77 compare the pressure distributions for the 45^{o} inclined flat plate.

For the normal flat plate the agreement is quite close, but in all cases the rocket jet impingement produces somewhat lower pressures.

For the inclined plate the agreement is not quite so close, but nevertheless the pressures produced by the rocket jet are lower than those produced by the nitrogen jet.

Thus for the set of nozzle-and-plate configurations and jet conditions investigated, there are only small differences between the hot and cold jet impingement pressures formed at the plate surface.

The main conclusion of this study is therefore that the differences between rocket exhaust and cold gases do not significantly affect impingement pressures formed at the surface of a flat plate.

Accordingly, empirical methods for predicting impingement pressures which are based on cold jet experimental data can be used with more confidence for impingement situations involving hot jets.

LIST OF REFERENCES

1 - LEWIS, R.S.
"Shaking Space Shuttle Came Close to Disaster".
New Scientist, Vol. ?, pp. 776, Sept 1981

2 - SINHA, R.; ZAKKAY, V.; & ERDOS, J.
"Flowfield Analysis of Plumes of Two-Dimensional Underexpanded Jets by a Time-Dependent Method".
AIAA Jnl., Vol. 9, No. 12, pp. 2363-2369, Dec 1971

3 - IWAMTO, J.; DECKKER, B.E.
"Development of Flow Field when a Symmetrical Underexpanded Sonic Jet Impinges on a Flat Plate".
Jnl. Fluid Mech., Vol. 113, pp. 299-313, 1981

4 - BELOV, I.A.; GINZBURG, I.P.; & SHUB, L.
"Supersonic Underexpanded Jet Impingement Upon a Flat Plate".
Int. Jnl. of Heat & Mass Transfer, Vol. 16, pp. 2067-2076, 1973

5 - KALGHATGI, G.T.; & HUNT, B.L.
"Method of Integral Relations and Triple Point Location in Impinging Jets".
Jnl. Spacecraft, Vol. 13, No. 12, pp. 763-765, 1976

6 - JEPPS, G.; & ROBINSON, M.L.
"Convective Heating at the Deflecting Surface of a Rocket Launch Pad".
Jnl. RAeSoc., Vol. 71, pp. 469-475, 1967

7 - BRESSETTE, W.E.; & LEISS, A.
"Effects on Adjacent Surfaces from the Firing of Rocket Jets".
NACA, RM L57 D19a, Mar 1957

8 - PIESIK, E.T.; KOPPANG, R.R.; & SIMKIN, D.J
"Rocket Exhaust Impingement on a Flat Plate at High Vacuum".
Jnl. Spacecraft, Vol. 3, No. 11, pp. 1650-1657, Nov 1966

9 - GINZBURG, I.P.; BELOV, I.A.; ZAZIMKO, V.A.; & TERPIGOREV, V.S.
"On the Effect of Jet Turbulence on the Heat Flux to a Perpendicular Flat Plate".
Heat & Mass Transfer, Minsk, Vol. 1, pp. 381-393, 1968

10 - ROCHELLE, W.C.; & KOOKER, D.E.
"Heat Transfer and Pressure Analysis of Rocket Exhaust Impingement on Flat Plates and Curved Panels".
Jnl. Spacecraft, Vol. 6, No. 3, pp. 248-256, Mar 1969

11 - LENG, J.; OSONITSCH, C.W.; & LACINSKI, I.M.
"Effects of Oblique Shock Waves in the Near Field of Rocket Plumes".
Jnl. Spacecraft, Vol. 6, No. 11, pp. 1316-1319, Nov 1969

12 - CLARK, L.V.
"Experimental Investigation of Close-Range Rocket Exhaust Impingement on Surfaces in a Vacuum".
NASA, TN D-5895, 1970

13 - McGREGOR, W.
"Some Problems with Gas/Particle Diagnostics in Solid Propellant Combustion".
AIAA Paper, No. 79-0084, Jan 1979

14 - STITT, L.E.
"Interaction of Highly Underexpanded Jets with Simulated Lunar Surfaces".
NASA TN D-1095, 1961

15 - STITT, L.E.; & LATTO, W.T.
"Highly Underexpanded Exhaust Jets Against Adjacent Surfaces".
Astro. & Aero. Eng., Vol. 1, No. 1, pp. 107-110, 1963

16 - EASTMAN, D.W.; & RADTKE, L.P.
Flow Field of an Exhaust Plume Impinging on a Simulated Lunar Surface".
AIAA Jnl., Vol. 1, No. 6, pp. 1430-1431, 1963

17 - VICK, A.R.; & ANDREWS, E.H.
"An Investigation of Highly Underexpanded Free Jets Impinging upon a Parallel Flat Surface".
NASA, TN D-2326, 1964

18 - LAND, N.S.; & CLARK, L.V.
"Experimental Investigation of Jet Impingement on Surfaces of Fine Particles in a Vacuum Environment".
NASA, TN D-2633, 1965

19 - VICK, A.R.; & ANDREWS, E.H.
"An Investigation of Highly Underexpanded Exhaust Plumes Impinging upon a Perpendicular Flat Surface".
NASA, TN D-3269, 1966

20 - JANOS, J.J.; & HOFFMAN, S.
"Forces and Moments Due to Air Jets Exhausting Parallel to Large Flat Surfaces in a Near Vacuum".
NASA, TN D-5147, 1966

21 - HENDERSON, L.F.
"Experiments on the Impingement of a Supersonic Jet on a Flat Plate".
Z. Agnew. Math. Phys., Vol. 17, pp. 953-969, 1966

22 - GUMMER, J.H.
"Interaction of a Supersonic Jet with a Flat Plate".
University of Bristol, Dept. Aero. Eng., MSc Thesis, 1968

23 - GREENWOOD, R.N.
"The Measurement of Recovery Temperature in the Region of the Interaction of a Supersonic Jet with a Flat Plate".
University of Bristol, Dept. Aero. Eng., MSc Thesis, 1969

24 - GINZBURG, I.P.; SEMILETENKO, B.G.; TERPIGOREV, V.S.; & USKOV, V.N.
"Some Peculiarities of Interaction Between Supersonic Underexpanded Jet with a Flat Plate".
Jnl. Eng. Phys., Vol. 19, No. 3, pp. 412-417, 1970

25 - DONALDSON, C.DuP.; & SNEDEKER, R.S.
"A Study of Free Jet Impingement, PART 1, Mean Properties of Free and Impinging Jets".
Jnl. Fluid Mech., Vol. 45, No. 2, pp. 281-319, 1971

26 - GUMMER, J.H; & HUNT, B.L.
"The Impingement of a Uniform, Axisymmetric, Jet on a Perpendicular Flat Plate".
Aero. Quart., Vol. 22, pp. 403-420, 1971

27 - GUBANOVA, O.I.; LUNEV, V.V.; & PLASTININA, L.I.
"On the Central Stalling Region at Interaction of a Underexpanded Supersonic Jet with a Plate".
Fluid Dynamics, Vol. 6, No. 2, pp. 135-138, 1971

28 - MORRIS, P.E.
"A Photographic Survey of Supersonic Jet Impingement on a Flat Plate Using Uniform Flow Nozzles Run at Various Pressure Ratios".
University of Bristol, Dept. Aero. Eng., MSc Thesis, 1972

29 - HOFFMAN, S.
"Normal Impingement Loads Due to Small Air Jets Issuing from a Base Plate and Reflecting off a Platform for Various Jet Mach Numbers, Separation Distances and Ambient Pressures".
NASA, TN D-6817, 1972

30 - BELOV, I.A.; GINZBURG, I.P.; GORSHKOV, G.F.; KOMAROV, V.S.; & TERPIGOREV, V.S.
"Heat Transfer of Jets Impinging on Bluff Bodies"
Heat and Mass Transfer, Minsk, Vol. 1, No. 2, pp. 271-281, 1972

31 - CARLING, J.C.
"The Impingement of Uniform, Axisymmetric, Supersonic Jets of Air on Plane Perpendicular Surfaces".
University of Bristol, Dept. Aero. Eng., PhD Thesis, 1974

32 - GUMMER, J.H; & HUNT, B.L.
"The Impingement of Non-Uniform, Axisymmetric, Supersonic Jets on a Perpendicular Flat Plate".
Israel Jnl. Tech., Vol. 12, pp. 221-235, 1974

33 - CARLING, J.C.; & HUNT, B.L.
"The Near Wall Jet of a Normally Impinging, Uniform, Axisymmetric, Supersonic Jet".
Jnl. Fluid Mech., Vol. 66, pp. 159-176, 1974

34 - KALGHATGI, G.T.
"Some Aspects of Supersonic Jet Impingement on Plane Perpendicular Surfaces".
University of Bristol, Dept. Aero. Eng., PhD Thesis, 1975

35 - KALGHATGI, G.T.; & HUNT, B.L.
"The Three Shock Confluence Problem for Normally Impinging, Overexpanded Jets"
Aero. Quart., Vol. 26, pp. 117-132, May 1975

36 - KALGHATGI, G.T.; & HUNT, B.L.
"The Occurence of Stagnation Bubbles in Supersonic Jet Impingement Flows".
Aero. Quart., Vol. 27, pp. 169-185, 1976

37 - BACK, L.H.; & SAROHIA, V.
"Pressure Pulsations on a Flat Plate Normal to Underexpanded Supersonic Jet".
AIAA Jnl., Vol. 16, No. ?, pp. 634-636, 1978

38 - LAMONT, P.J.; & HUNT, B.L.
"The Impingement of Underexpanded, Axisymmetric Jets on Normal and Inclined Flat Plates"
University of Bristol, Dept. Aero. Eng., Report No. PJL/BLH 7901 , 1979

39 - LAMONT, P.J.; & HUNT, B.L.
"The Impingement of Underexpanded, Axisymmetric Jets on Perpendicular and Inclined Flat Plates"
Jnl. Fluid Mech., Vol. 100, pp. 471-511, 1980

40 - KUPTSOV, V.M.; SYRCHIN, A.F.; FILIPPOV, K.N.; & KHARKOV, V.D.
"Pressure Pulsations on an Obstacle in a Jet".
Fluid Dynamics, Vol. 15, No. 1, pp. 132-136, 1980

41 - PORTER, R.
"The Heat Transfer between Impinging, Axisymmetric, Underexpanded Jets and Perpendicular and Inclined Flat Plates"
University of Bristol, Dept. Aero. Eng., PhD Thesis, 1983

42 - GLISTER, M.J.; & FOREMAN, T.J.
"An Investigation of Loads on Wedges Placed in Supersonic Jets".
University of Bristol, Dept. Aero. Eng., BSc Thesis (Report No. 198), 1975/1976?

43 - LAMONT, P.J.; & HUNT, B.L.
"The Impingement of Underexpanded, Axisymmetric Jets on Wedges".
Jnl. Fluid Mech., Vol. 76, No. 2, pp. 307-336, 1976

44 - MONK, B.; & WETHERILL, K.
"An Investigation of Loads on Wedges Placed in Supersonic Jets".
University of Bristol, Dept. Aero. Eng., BSc Thesis (Report No. 235), 1979

45 - HUNT, B.L.
"Loads Due to Underexpanded Jets Impinging on Wedges".
Aero. Quarterly, Loads and pressures due to underexpanded jets impinging on surfaces vol. 34, pp 76-98 May 1983.

46 - MADDOX, A.R.
"Impingement of Underexpanded Plumes On Adjacent Surface".
"Jnl. Spacecraft, Vol. 5, No. 6, pp. 718-724, Jun 1968

47 - JENNIONS, I.K.; & HUNT, B.L.
"The Axisymmetric Impingement of Air Jets on Cones"
Aero. Quart., Vol. 31, pp. 26-41, 1980

48 - PIESIK, E.T.; & ROBERTS, D.J.
"A Method to Define Low Altitude Rocket Exhaust Characteristics and Impingement Effects".
Jnl. Spacecraft, Vol. 7, No. 4, pp. 446-451, Apr 1970

49 - HUNT, B.L.
Private Communication.
University of Bristol, Dept. Aero. Eng.

50 - HILTON, P.A.
"Solid Propellant Test Rig - Operating Instructions"
P.A. Hilton Ltd, Kings Somborne, Hants, U.K.

51 - WILLIAMS, F.A.; BARRERE, M. and HUANG, N.C.
"Fundamental Aspects of Solid Propellant Rockets"
AGARD 116, pp. 185-252, 1969.

52 - MILLER, W.H. and BARRINGTON, D.K.
"A Review of Contemporary Solid Rocket Motor Performance Prediction Techniques"
Jul. Spacecraft, vol. 7, no. 3, pp. 225-237, March 1970.

53 - VICK, A.R., CUBBAGE, J.M. and ANDREWS, E.H.
"Rocket Plume Problems and Some Recent Related Research"
AGARD 87, vol. 2, pp. 129-180, 1964.

54 - LEWIS, C.H. and CARLSON, D.J.
"Normal Shock Location in Underexpanded Gas and Gas-Particle Jets"
AIAA Jnl., vol. 2, no. 4, pp. 776-7, April 1964.

55 - STULL, D.R. *et al*
"Thermochemical Tables" 2nd edition
NSRDS - NBS 37, 1971.

LIST OF TABLES

TABLE 1 HILTON COMBUSTION GAS DATA

Propellant	-	TYPE 670	
Nozzle	-	Not Specified	
Pressures	-	None Specified	
Temperature (°K)	-	Flame Temperature	= 2240
	-	Freezing Out Temp.	= 1600
Sp. Heat Ratio	-	@ 2240 °K	= 1.27
	-	@ 1600 °K	= 1.29

Gas Composition	Concentrations (Mole Fraction)	
Constituent	@ 2240 °K	@ 1600 °K
CO	0.4629	0.4413
CO_2	0.0733	0.0948
H_2	0.1938	0.2158
H_2O	0.1667	0.1448
N_2	0.1033	0.1033

TABLE 2a ICI COMBUSTION GAS DATA

Propellant	-	TYPE 670		
Nozzle	-	Area Ratio, Ae/At	=	4.718
Pressure (Mn/m^2)	-	Combustion Chamber	=	3.4475
	-	Nozzle Throat	=	1.9033
	-	Nozzle Exit	=	0.1013
Temperature (^oK)	-	Flame	=	2179
	-	Nozzle Throat (Froz. Flow)	=	1926
	-	Nozzle Exit (Froz. Flow)	=	1012
	-	Nozzle Exit (Equil. Flow)	=	1060
Velocity (m/sec)	-	Nozzle Exit	=	2001.15
Molecular Wt. (g/Mol)			=	22.32
Sp. Heat Ratio			=	1.2652

Gas Composition	Concentration (Mole Fraction)	
Constituent	Combustion Chamber	Nozzle Exit (Equil. Flow)
CO	0.46075 E+00	0.38936 E+00
CO_2	0.70842 E-01	0.14234 E+00
H_2	0.20123 E+00	0.27293 E+00
H_2O	0.15878 E+00	0.87375 E-01
N_2	0.10796 E+00	0.10798 E+00
C	0.40674 E-13	0.16375 E-27
H	0.38198 E-03	0.54005 E-08
O	0.39007 E-07	0.13307 E-18
N	0.33992 E-09	0.25259 E-20
NO	0.13894 E-05	0.80098 E-14
OH	0.40769 E-04	0.58463 E-11
O_2	0.26314 E-07	0.23027 E-19

TABLE 2b ICI COMBUSTION GAS DATA

Propellant	-	TYPE 670		
Nozzle	-	Area Ratio, Ae/At	=	7.559
Pressure (Mn/m^2)	-	Combustion Chamber	=	6.8950
	-	Nozzle Throat	=	3.8065
	-	Nozzle Exit	=	0.1013
Temperature (°K)	-	Flame	=	2179
	-	Nozzle Throat (Froz. Flow)	=	1926
	-	Nozzle Exit (Froz. Flow)	=	864
	-	Nozzle Exit (Equil. Flow)	=	923
Velocity (m/sec)	-	Nozzle Exit	=	2113.27
Molecular Wt. (g/Mol)			=	22.32
Sp. Heat Ratio			=	1.2652

Gas Composition	Concentration (Mole Fraction)	
Constituent	Combustion Chamber	Nozzle Exit (Equil. Flow)
CO	0.46078 E+00	0.36680 E+00
CO_2	0.70839 E-01	0.16490 E+00
H_2	0.20128 E+00	0.29548 E+00
H_2O	0.15881 E+00	0.64819 E-01
N_2	0.10796 E+00	0.10798 E+00
C	0.40681 E-13	0.12609 E-31
H	0.27013 E-03	0.13519 E-09
O	0.27201 E-07	0.20579 E-22
N	0.38297 E-09	0.85307 E-24
NO	0.98246 E-06	0.18837 E-16
OH	0.28830 E-04	0.34063 E-13
O_2	0.91741 E-08	0.26476 E-23

TABLE 3 PERME COMBUSTION GAS DATA

Propellant	-	TYPE 670	
Nozzle	-	Area Ratio, Ae/At	= 5.3106

Flow Parameter	Combustion Chamber	Nozzle Throat	Nozzle Exit
Pressure (MN/m^2)	6.8884	3.7850	0.1719
Temperature (K)	1768.8	1552.8	796.5
Density (kg/m^3)	9.6786	6.0582	0.5365
Enthalpy (kJ/Mol)	-46.618	-54.880	-83.975
Entropy (J/Mol K)	10.201	10.201	10.201
Velocity (m/sec)	0.0	888.4	1889.1
Mach Number	0.000	1.000	2.975
Molecular Wt. (g/Mol)	20.939	20.940	20.943
Specific Heat (J/kg K)	1781.8	1759.2	1628.3
Specific Heat Ratio	-	1.2782	1.2758

Gas Composition	Concentration (Mole Fraction)		
Constituent	Combustion Chamber	Nozzle Throat	Nozzle Exit
CO	0.48996 E+00	0.48239 E+00	0.41706 E+00
CO_2	0.48325 E-01	0.55916 E-01	0.12134 E+00
H_2	0.26628 E+00	0.27393 E+00	0.33956 E+00
H_2O	0.96126 E-01	0.88546 E-01	0.22721 E-01
N_2	0.97225 E-01	0.97230 E-01	0.97246 E-01
C	0.54811 E-16	0.24577 E-16	0.26621 E-36
H	0.17061 E-04	0.27650 E-05	0.11124 E-11
K	0.46930 E-03	0.38205 E-03	0.44121 E-04
O	0.18925 E-10	0.25863 E-12	0.11563 E-27
CHO	0.35329 E-06	0.62182 E-07	0.18589 E-12
HO_2	0.99022 E-14	0.80659 E-16	0.69801 E-33
KO_2	0.44932 E-10	0.28403 E-11	0.27048 E-21
KOH	0.16030 E-02	0.16903 E-02	0.20286 E-02
OH	0.39217 E-06	0.31488 E-07	0.24282 E-16
O_2	0.30453 E-11	0.38577 E-13	0.50353 E-29

TABLE 4 FREE JET TEST CONFIGURATIONS

Jet	Nozzle-to-Probe Distances Zpt/Re
Air	0, 1, 2, ... 49, 50
Nitrogen	0, 1, 2, ... 10, 11 12, 14, 16, ... 38, 40 50
Rocket	2, 4, 5, 6, 7, 8, 9, 10 12, 14, 16, ... 38, 40 50

TABLE 5 IMPINGING JET TEST CONFIGURATIONS

Jet	Nozzle-to-Plate Distances, Zp/Re	Plate Angles θ
Air	1, 2, 3, ... 49, 50 3.92, 14.64	90°
Nitrogen	5, 10, 20, 40	90°
	5, 10, 20, 40	45°
Rocket	5, 10, 20, 40	90°
	5, 10, 20, 40	45°

TABLE 6 FLAT PLATE PRESSURE TAPPING LOCATIONS

Non-Dimensional distances across the plate surface between the nozzle axis and the pressure tappings, (i.e. Sp/Re where Re=1.56). Refer to Section 5.3 of text for an explanation of the six plate positions.

Tapping Number \ Plate Position	1	2	3	4	5	6
1	-14.292	-13.651	-13.010	-13.971	-13.330	-12.689
2	-12.240	-11.599	-10.958	-11.920	-11.279	-10.638
3	-10.221	-9.580	-8.939	-9.901	-9.260	-8.619
4	-8.170	-7.529	-6.888	-7.849	-7.208	-6.567
5	-6.151	-5.510	-4.869	-5.830	-5.189	-4.548
6	-4.115	-3.474	-2.833	-3.795	-3.154	-2.513
7	-2.051	-1.410	-0.769	-1.731	-1.090	-0.449
8	0.000	0.641	1.282	0.321	0.962	1.603
9	2.038	2.679	3.321	2.359	3.000	3.641
10	4.058	4.699	5.340	4.378	5.019	5.660
11	6.071	6.712	7.353	6.391	7.032	7.673
12	8.106	8.747	9.388	8.426	9.067	9.708
13	10.141	10.782	11.423	10.462	11.103	11.744
14	12.167	12.808	13.449	12.487	13.128	13.769
15	14.170	14.811	15.452	14.490	15.131	15.772

TABLE 7 IMPINGEMENT TESTS PLATE POSITIONS

Air Jet Impingement Tests
Plate Positions 1, 2 & 3 used for all tests

Nitrogen and Rocket Jet Impingement Tests		
Zp/Re	Plate Positions	
	Θ = 90°	Θ = 45°
5	1, 2, 3	1, 2, 3, 4, 5, 6
10	1, 2, 3	1, 2, 3, 4, 5, 6
20	1, 2, 3	1, 2, 3
40	1, 2, 3	1, 2, 3

LIST OF FIGURES

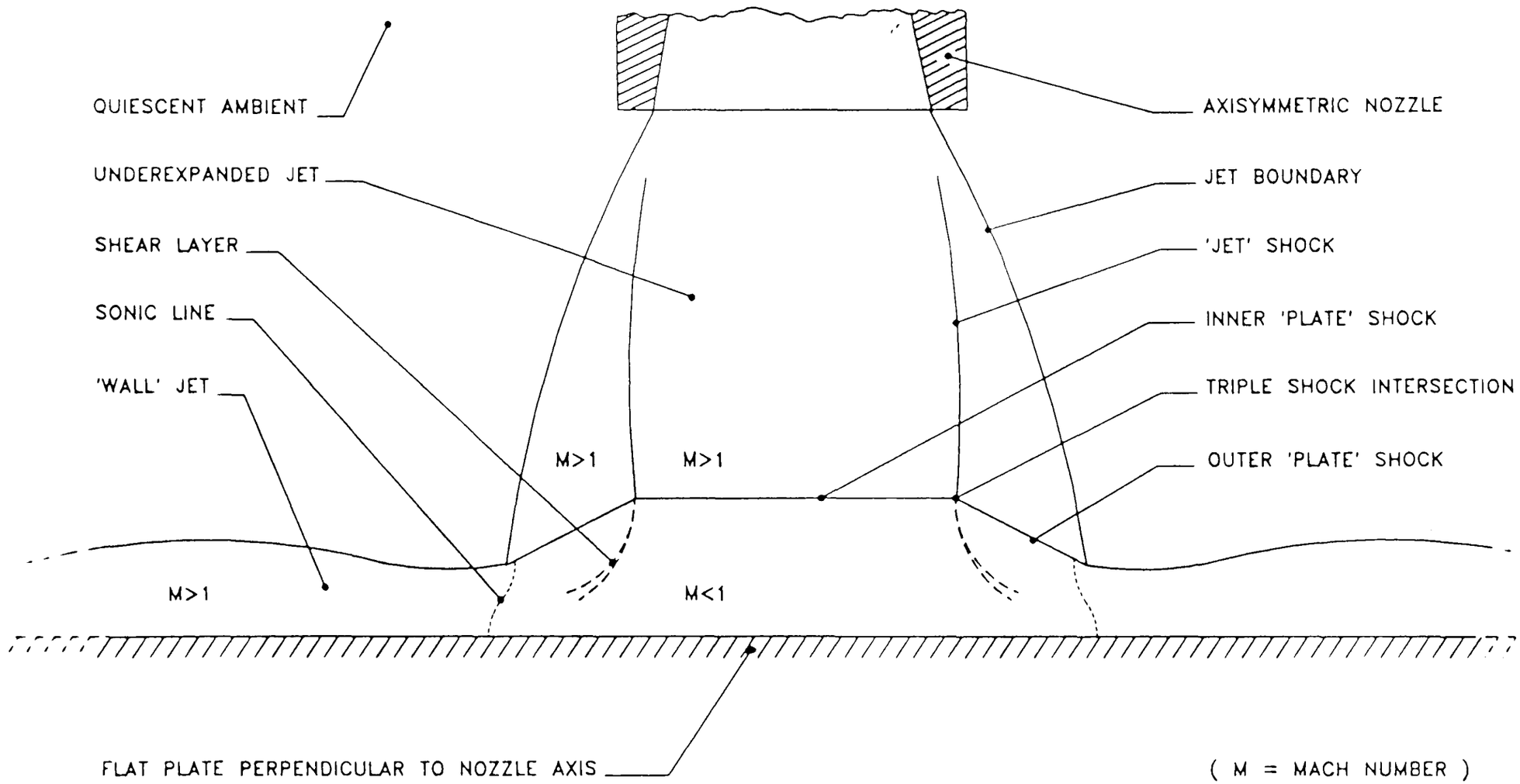

FIGURE 1.1 ANNOTATED SCHEMATIC DIAGRAM OF A SIMPLE JET IMPINGEMENT FLOWFIELD

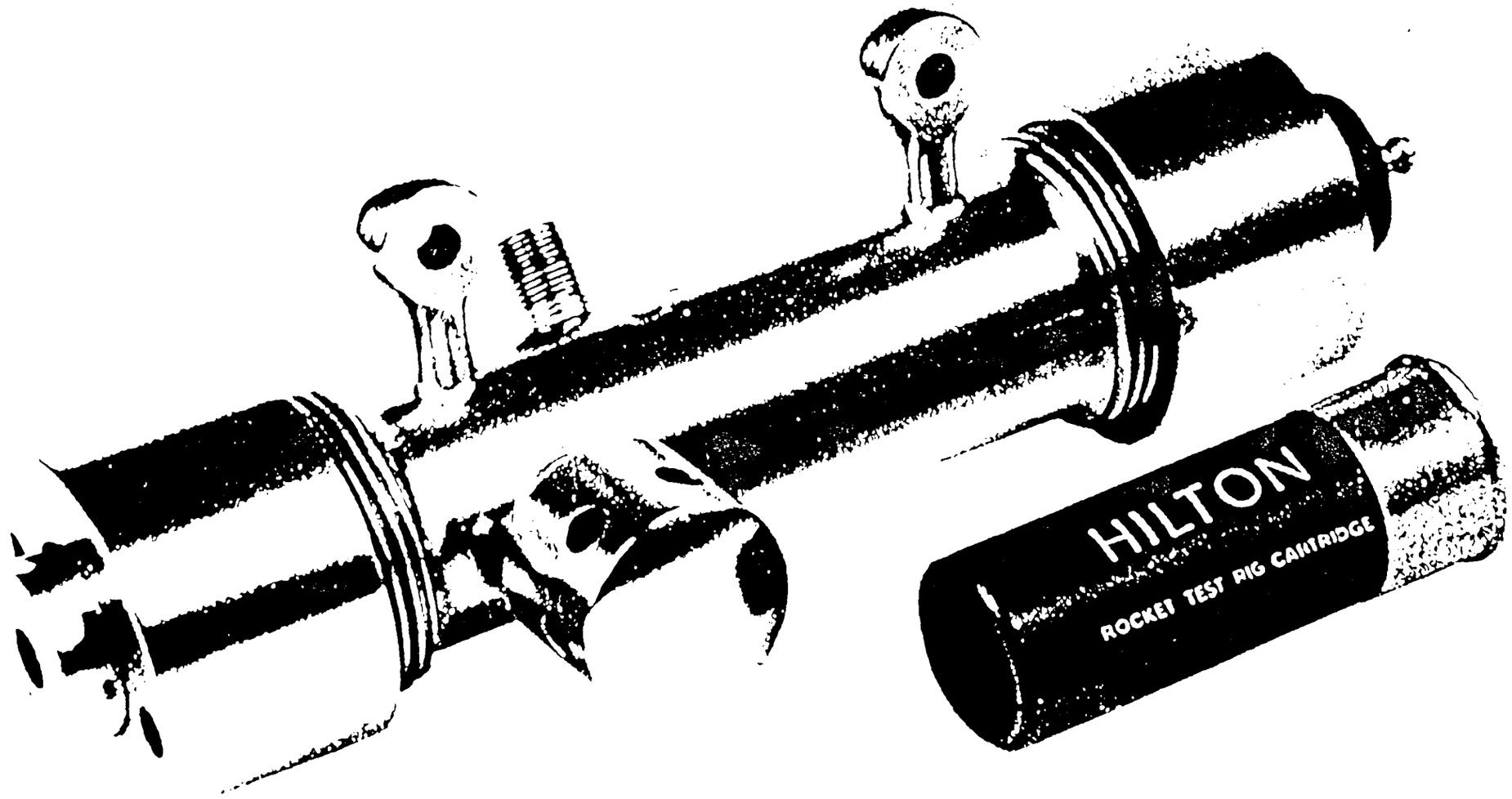

FIGURE 2.1 VIEW OF THE HILTON ROCKET MOTOR AND A PROPELLANT CARTRIDGE

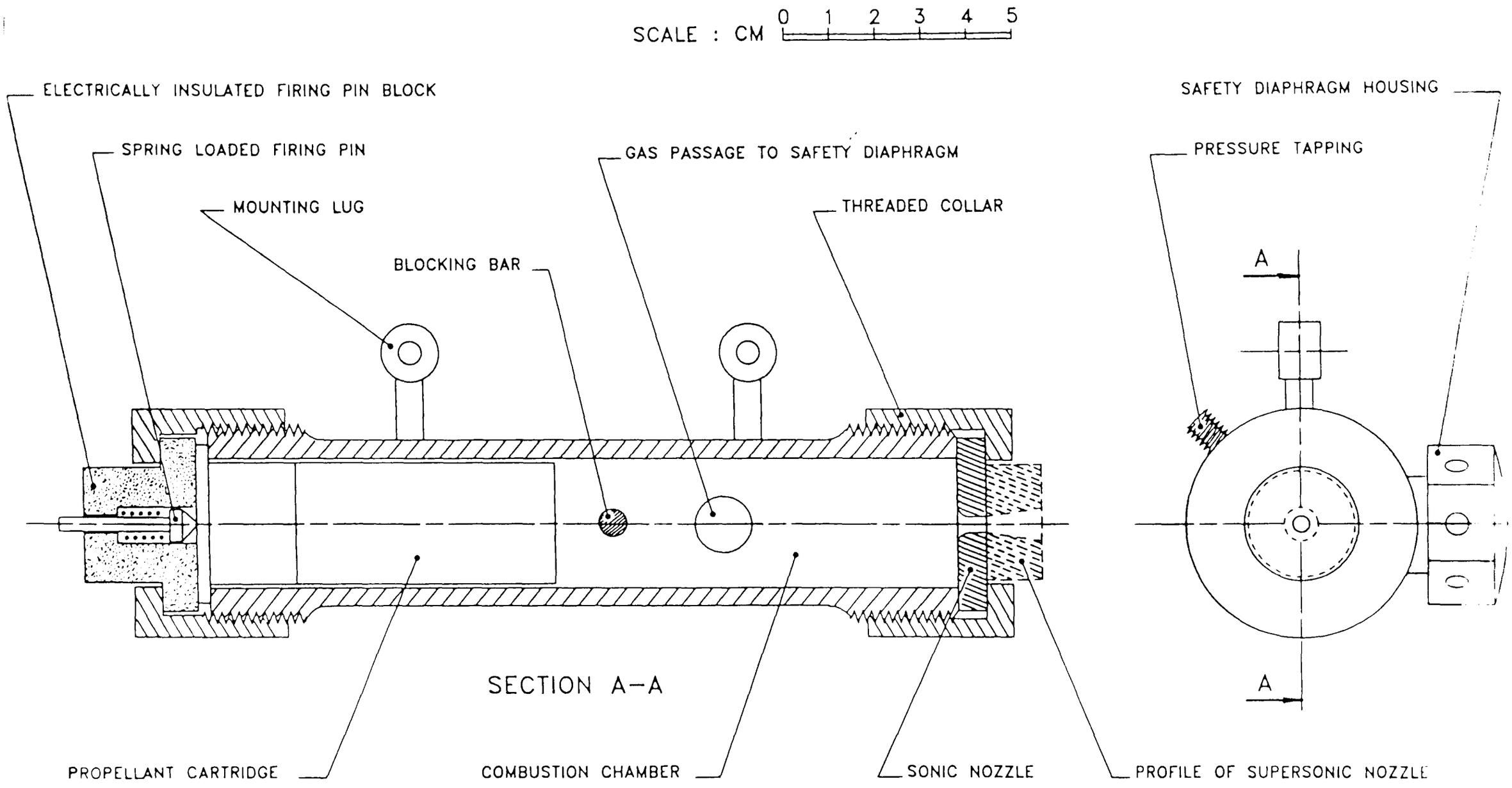

FIGURE 2.2 SECTIONED DRAWING OF THE HILTON SOLID PROPELLANT ROCKET MOTOR

NOTES: 1) PRESSURES ARE ABSOLUTE VALUES 2) ALL TESTS WITH TYPE 670 PROPELLANT CARTRIDGE

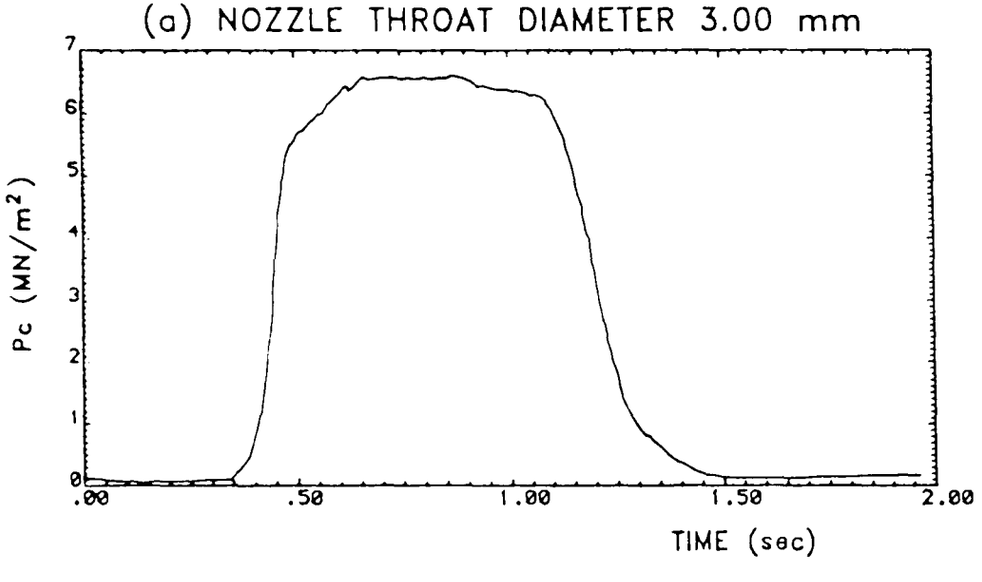

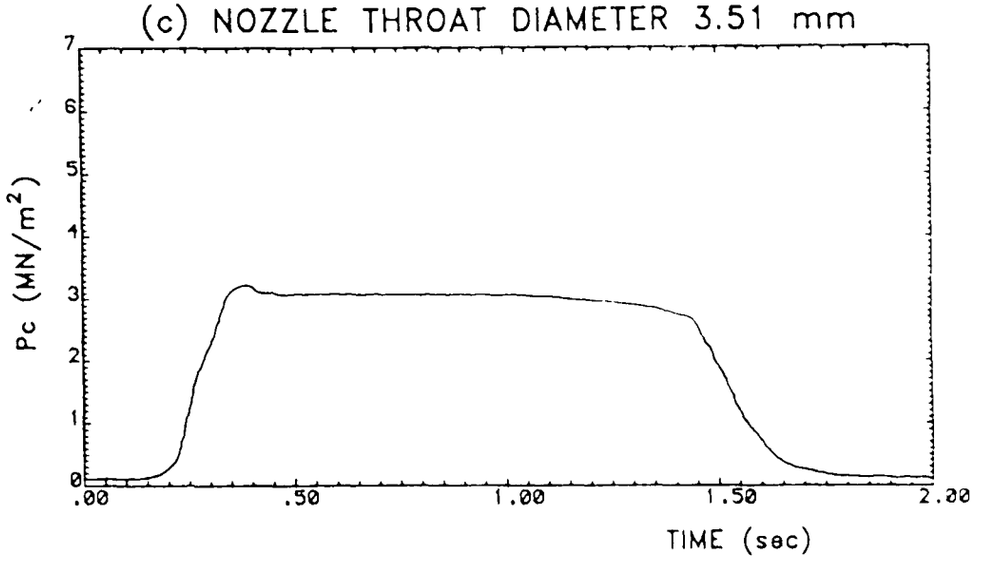

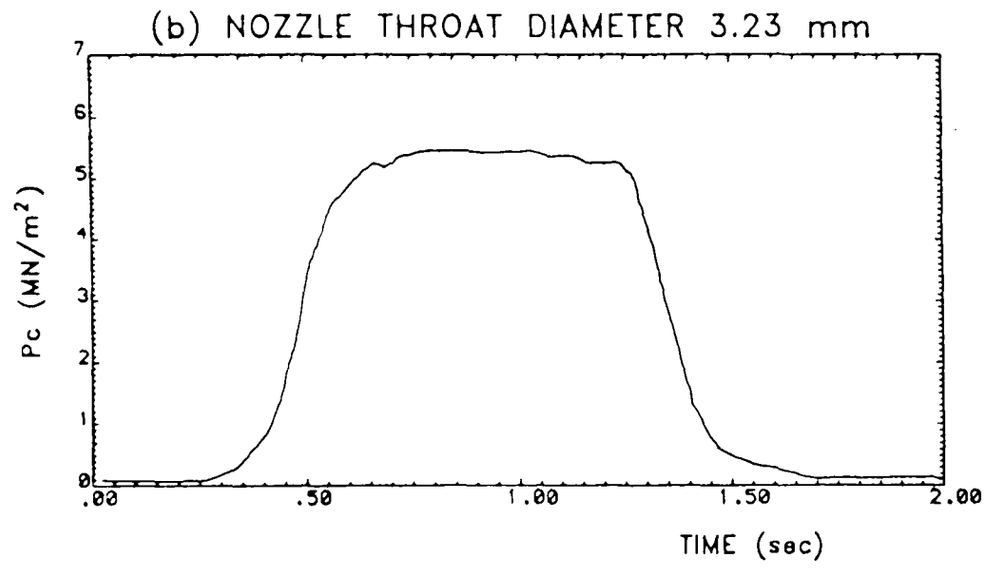

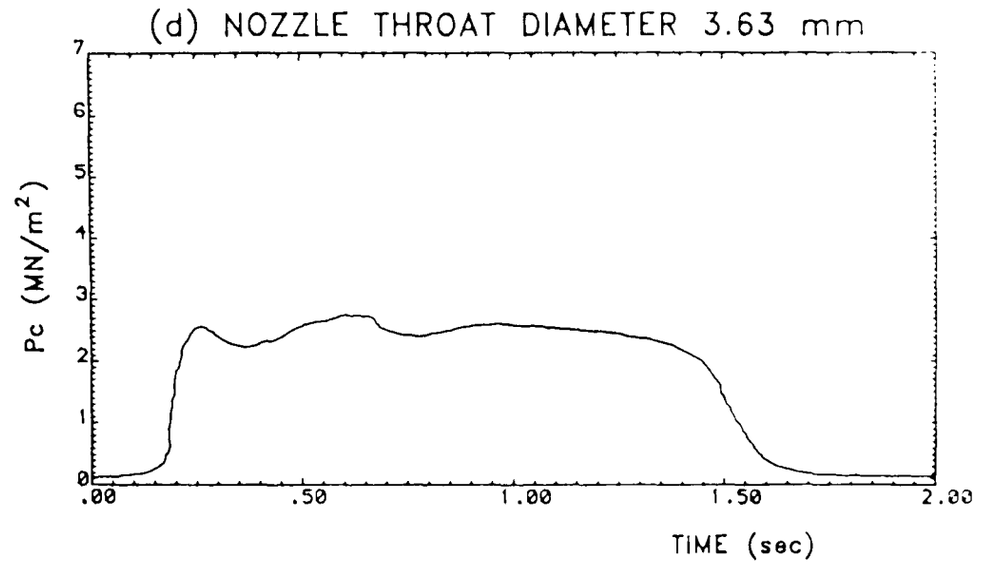

FIGURE 2.3 RECORDINGS OF THE HILTON MOTOR CHAMBER PRESSURE – STABLE PROPELLANT COMBUSTION

NOTES:

1) NOZZLE THROAT DIAMETER = 3.74 mm

2) PRESSURES ARE ABSOLÚTE VALUES

3) TEST WITH TYPE 670 PROPELLANT CARTRIDGE

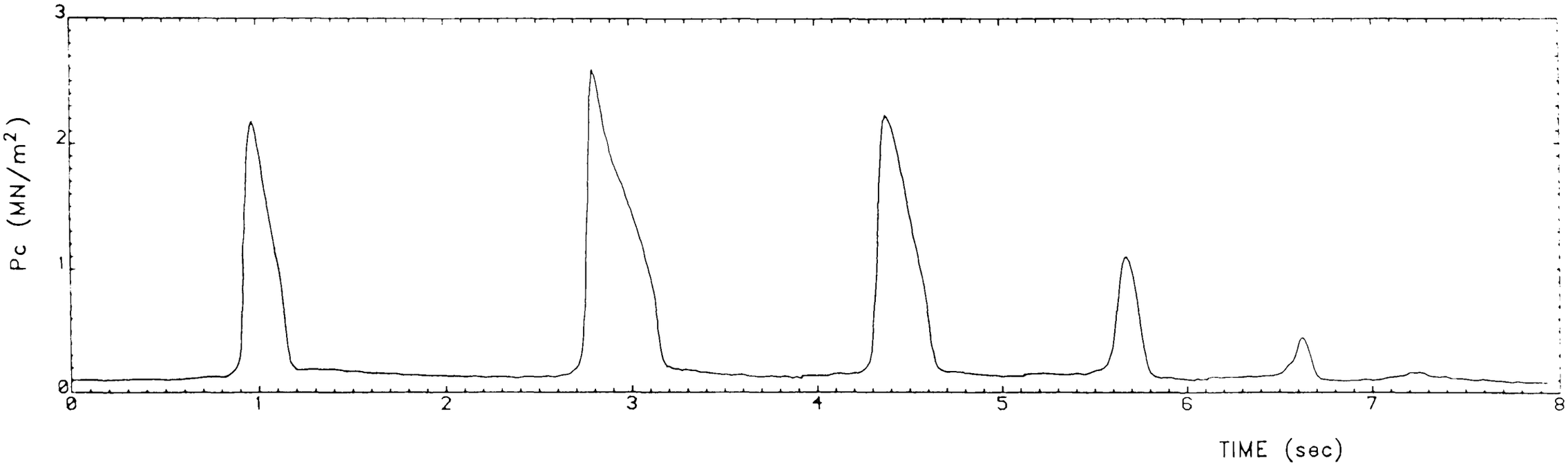

FIGURE 2.4 RECORDING OF THE HILTON MOTOR CHAMBER PRESSURE – UNSTABLE PROPELLANT COMBUSTION

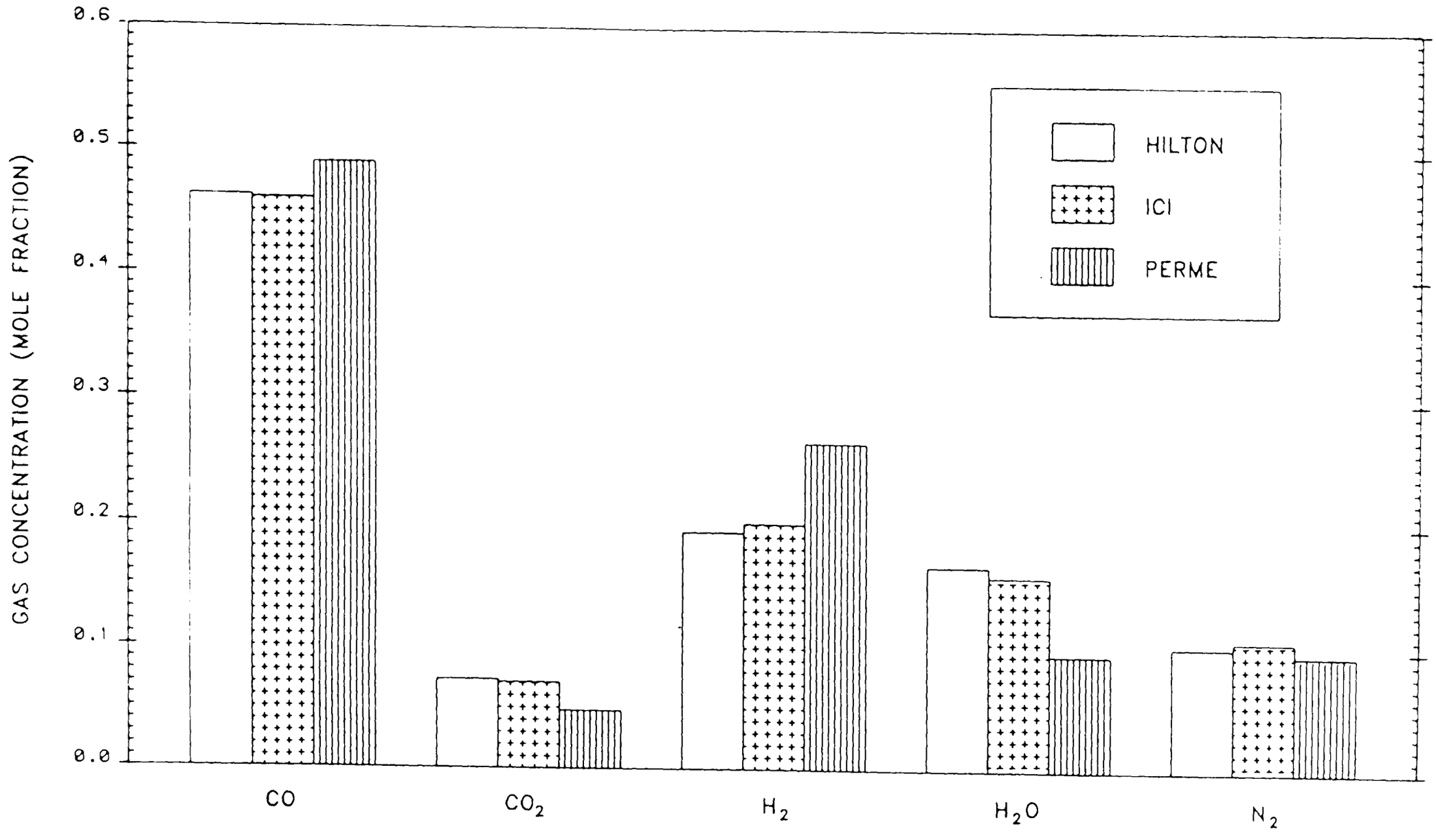

FIGURE 2.5 COMPARISON OF THE HILTON, ICI, AND PERME TYPE 670 PROPELLANT DATA ON THE CONCENTRATIONS OF THE FIVE MAJOR GAS SPECIES FOUND WITHIN THE HILTON ROCKET MOTOR COMBUSTION CHAMBER

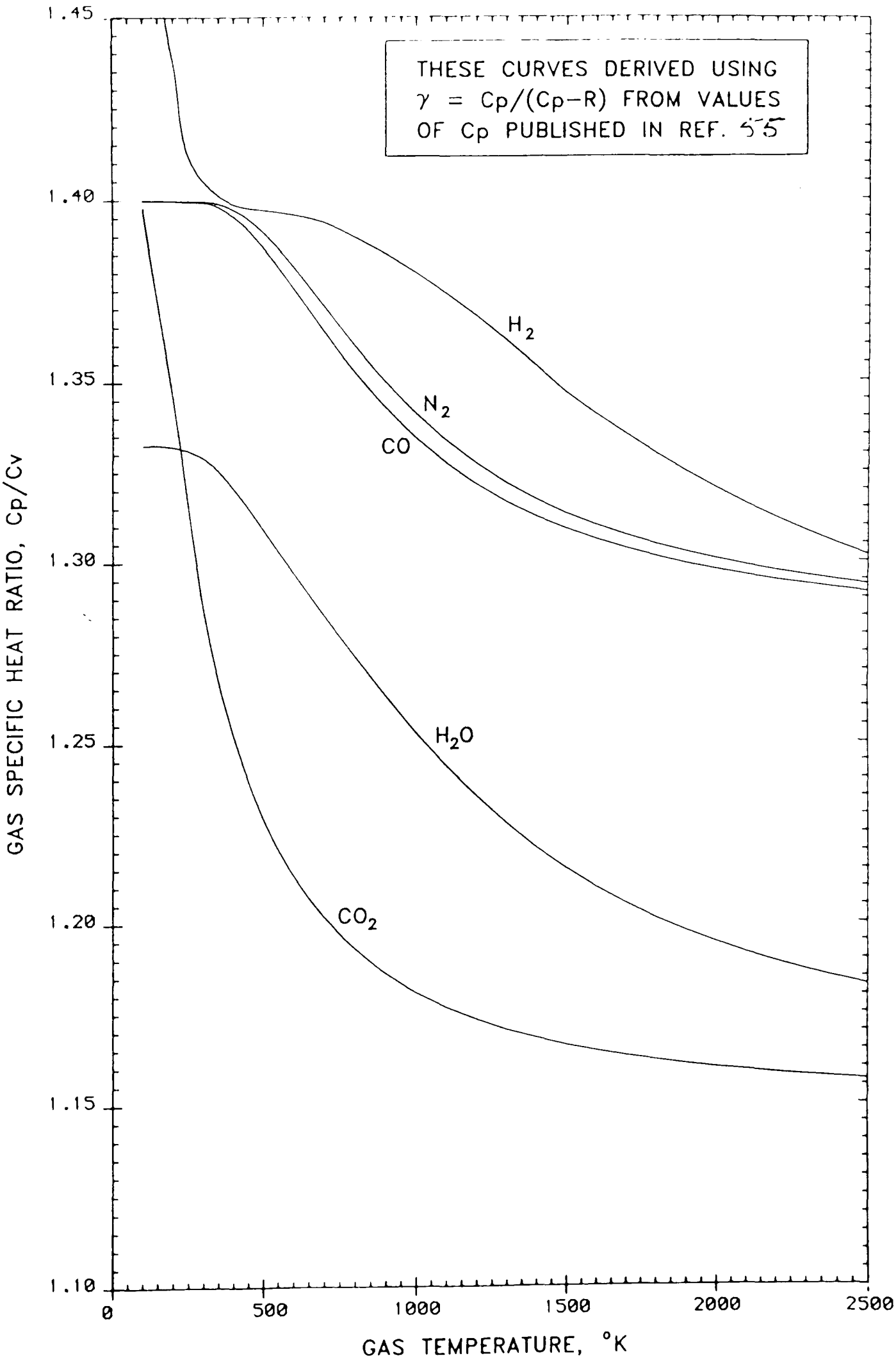

FIGURE 2.6 EFFECT OF TEMPERATURE ON THE SPECIFIC HEAT RATIOS (Cp/Cv) OF CO, CO_2, H_2, H_2O, AND N_2

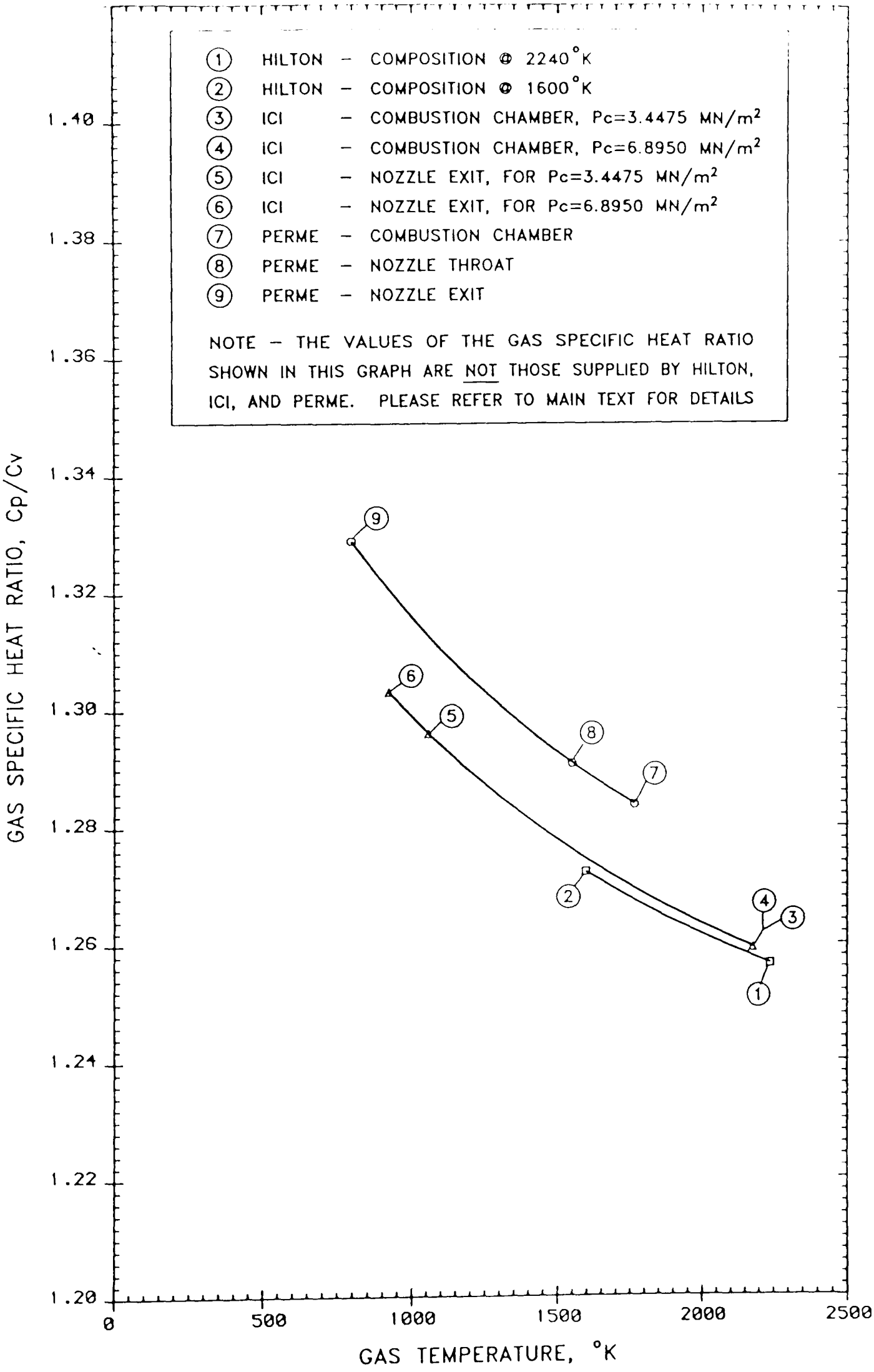

FIGURE 2.7 EFFECT OF TEMPERATURE ON TYPE 670 PROPELLANT GAS SPECIFIC HEAT RATIO AS EVALUATED FROM THE HILTON, ICI, & PERME GAS COMPOSITION DATA

INCREASING JET PRESSURE RATIO (Pc/Pa)

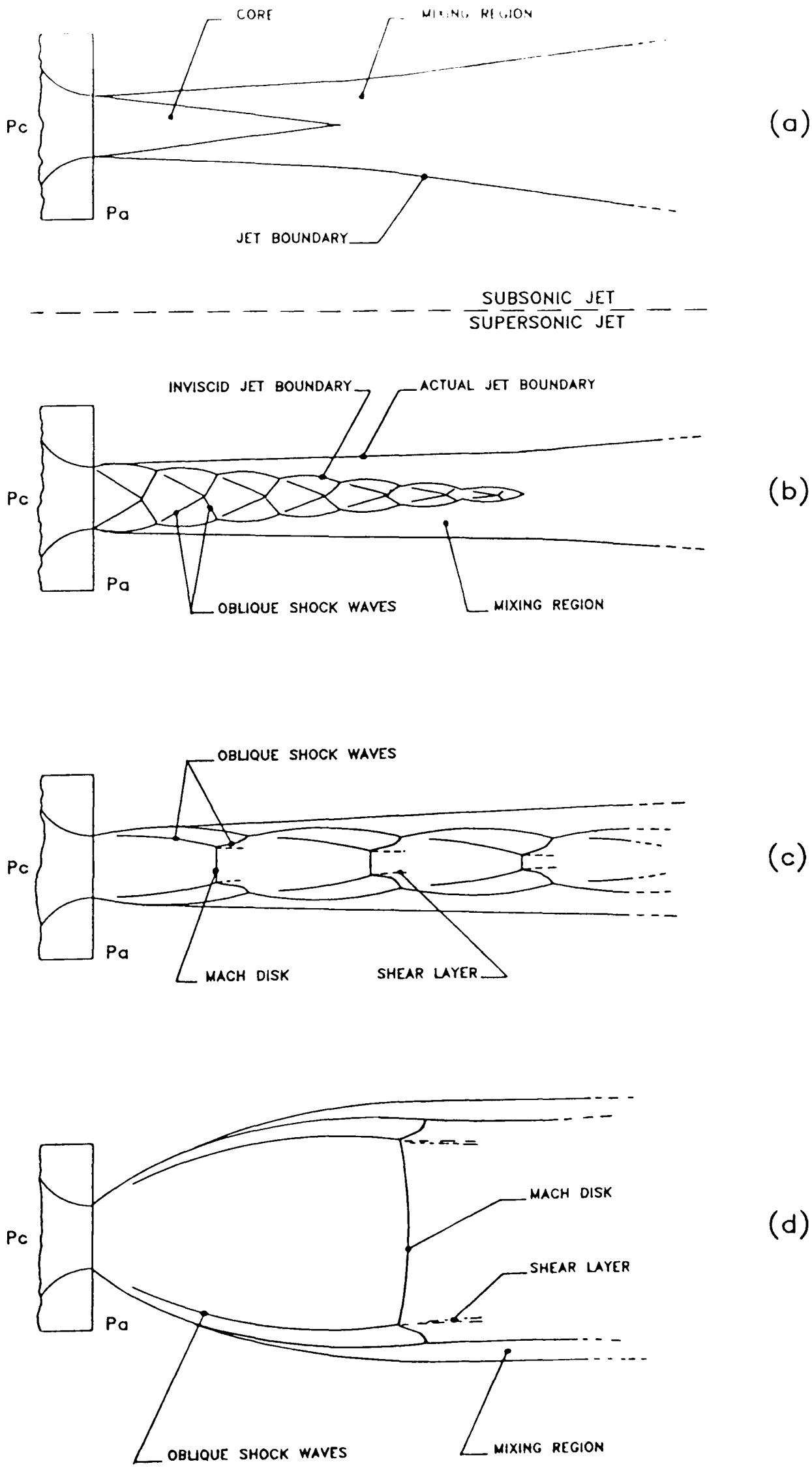

FIGURE 3.1 SCHEMATIC DIAGRAMS SHOWING STAGES IN UNDEREXPANDED FREE JET DEVELOPMENT

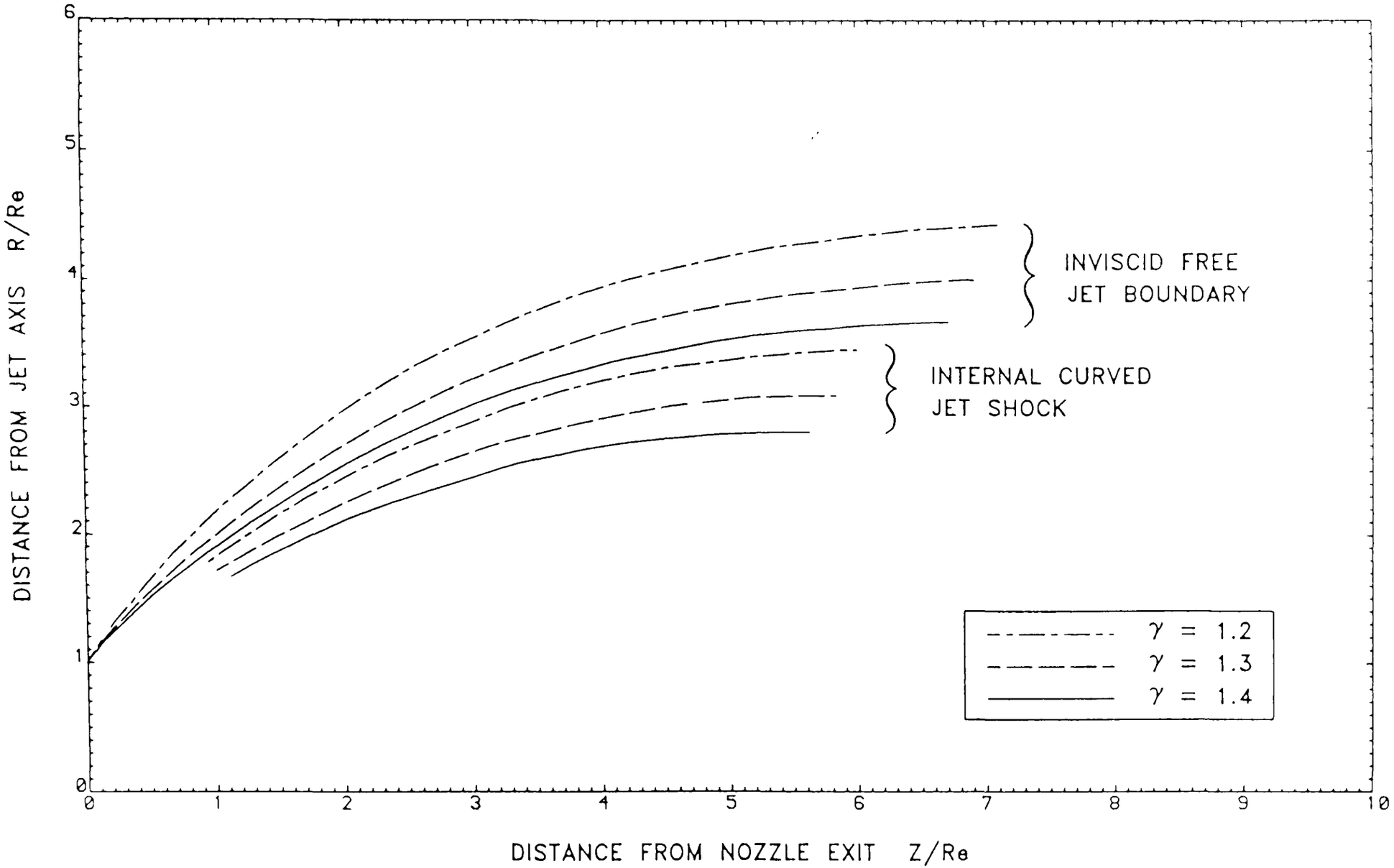

FIGURE 3.2 EFFECT OF THE GAS SPECIFIC HEAT RATIO ON THE STRUCTURE OF THE FREE JET NEAR FIELD AS PREDICTED BY THE METHOD OF CHARACTERISTICS ANALYSIS FOR: Me=1.0, Pc/Pa=40.0

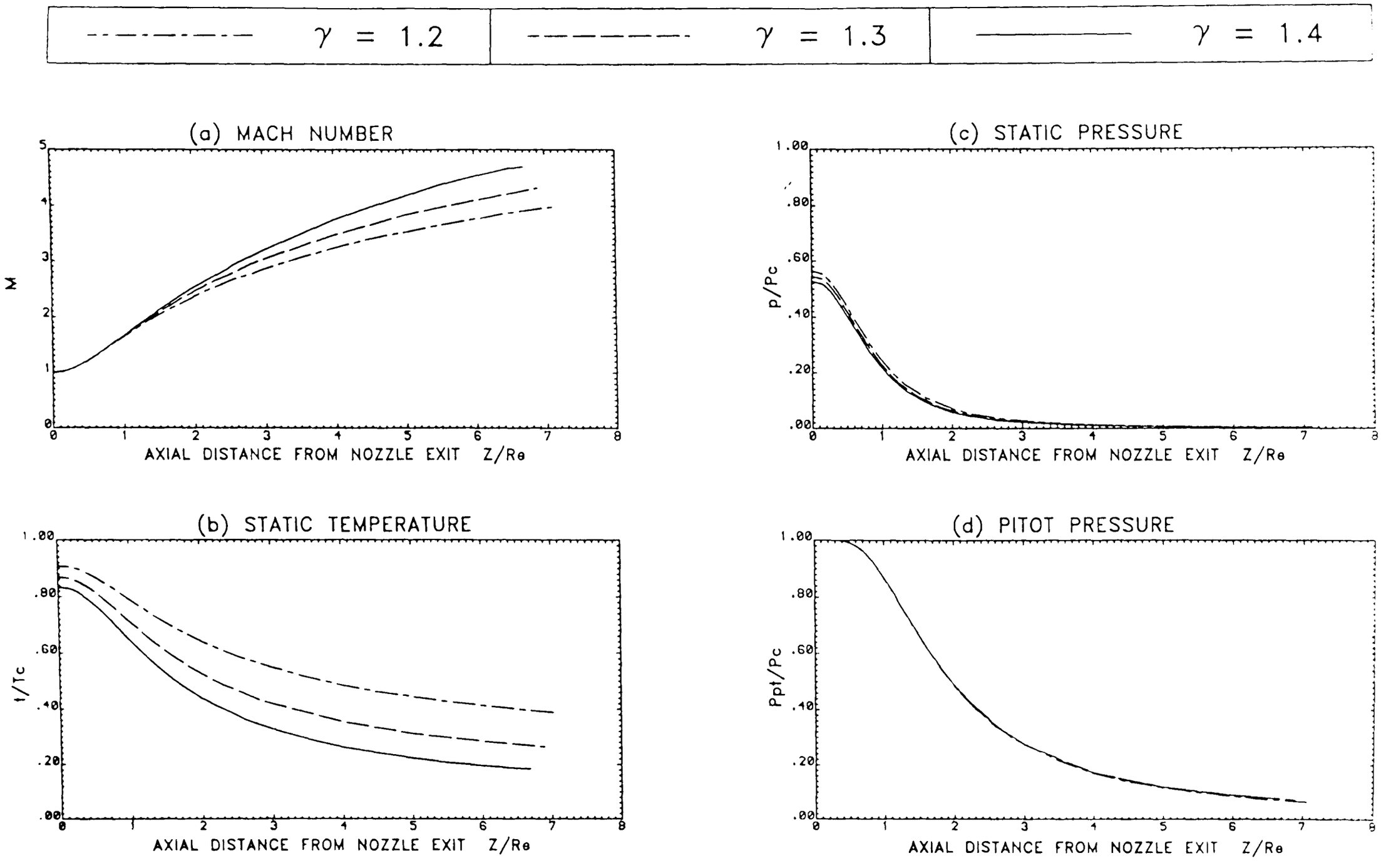

FIGURE 3.3 EFFECT OF THE GAS SPECIFIC HEAT RATIO ON FOUR FREE JET AXIAL FLOW PARAMETERS AS PREDICTED BY THE 'MOC' ANALYSIS FOR: Me=1.0, Pc/Pa=40.0

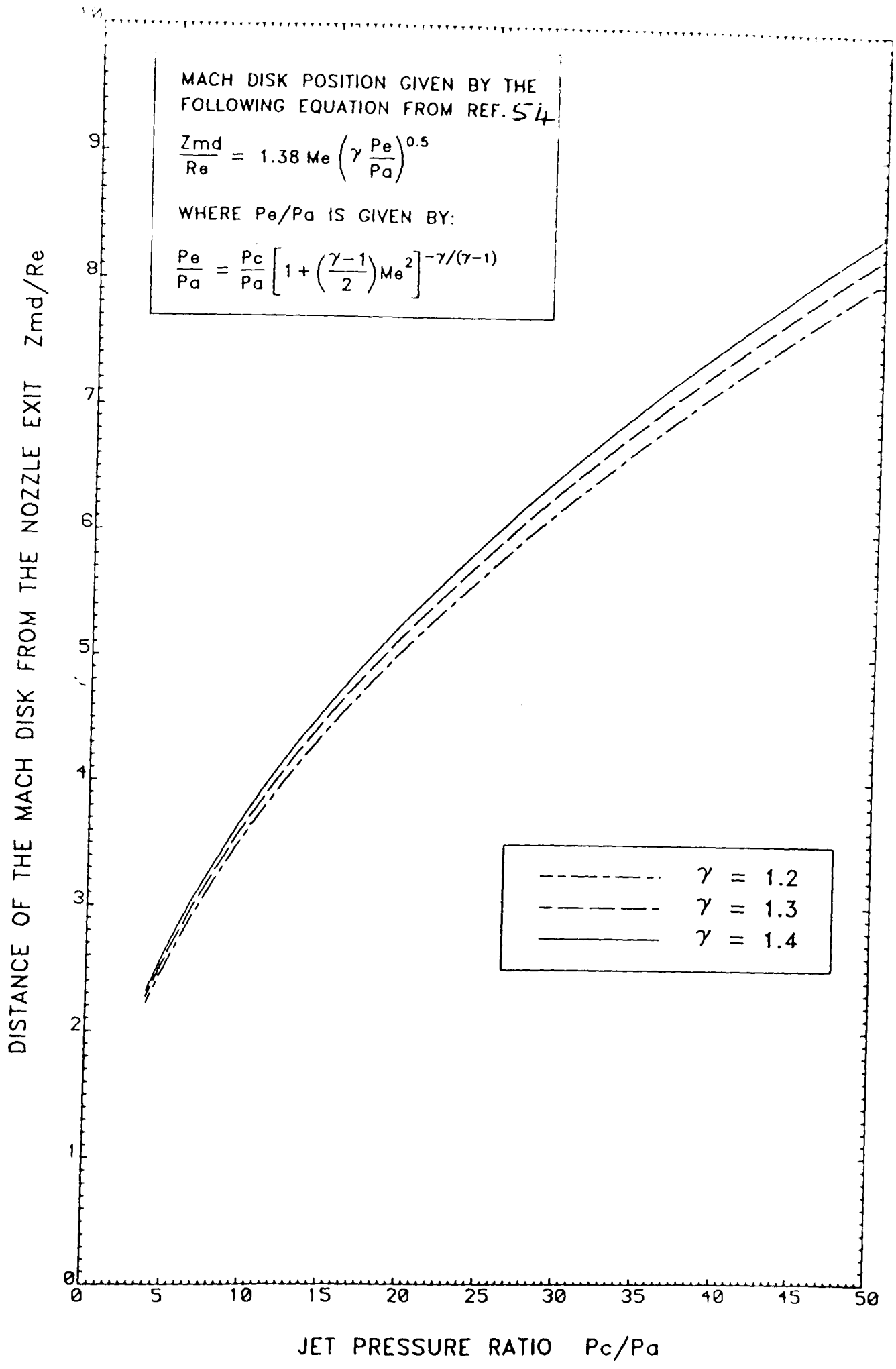

FIGURE 3.4 INFLUENCE OF THE JET PRESSURE RATIO ON THE POSITION OF THE FIRST FREE JET MACH DISK AS PREDICTED BY LEWIS AND CARLSON'S CORRELATION EQUATION FOR : Me = 1.0 ; γ = 1.2, 1.3, 1.4

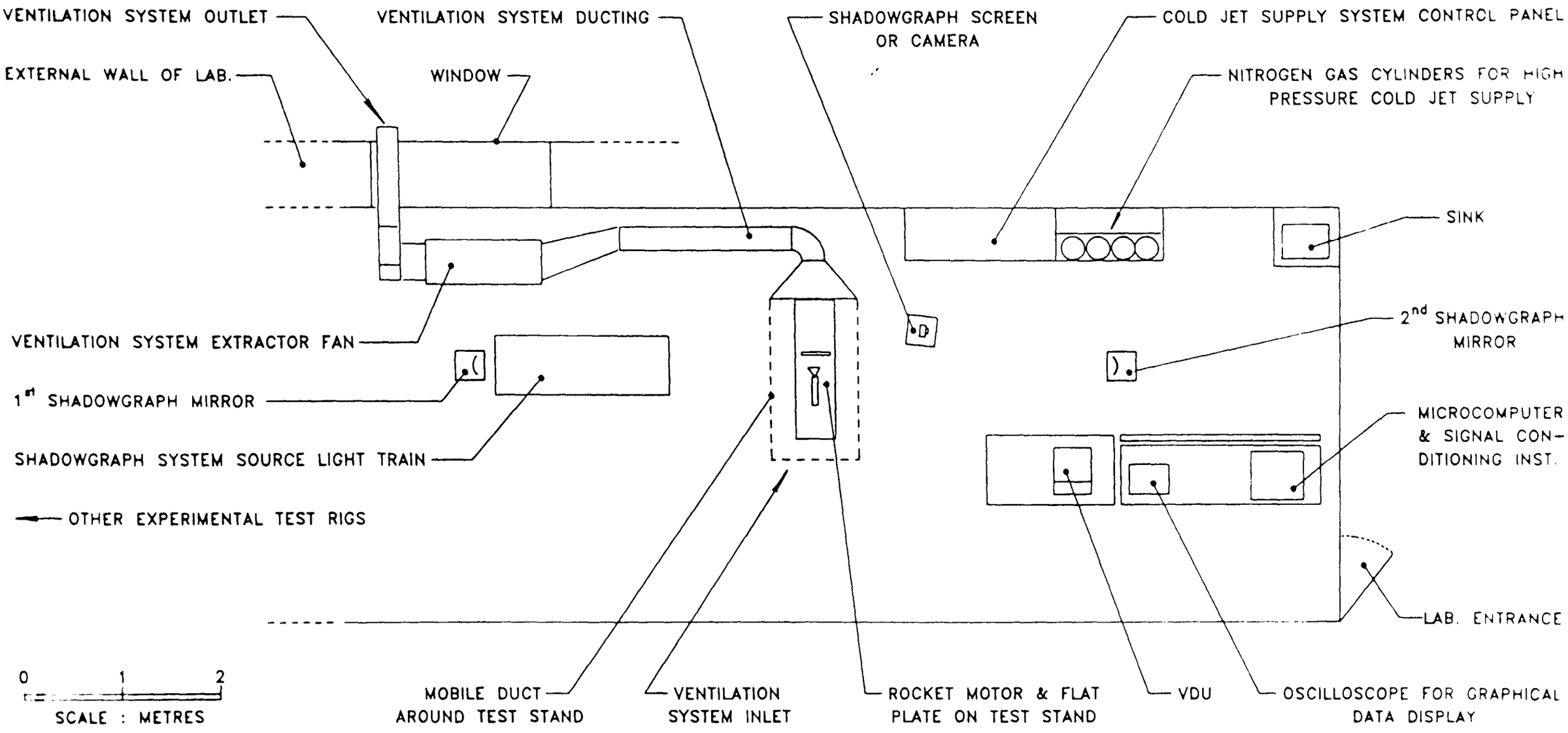

FIGURE 4.1 PLAN OF THE LAYOUT OF THE TEST RIG IN THE GAS DYNAMICS LABORATORY

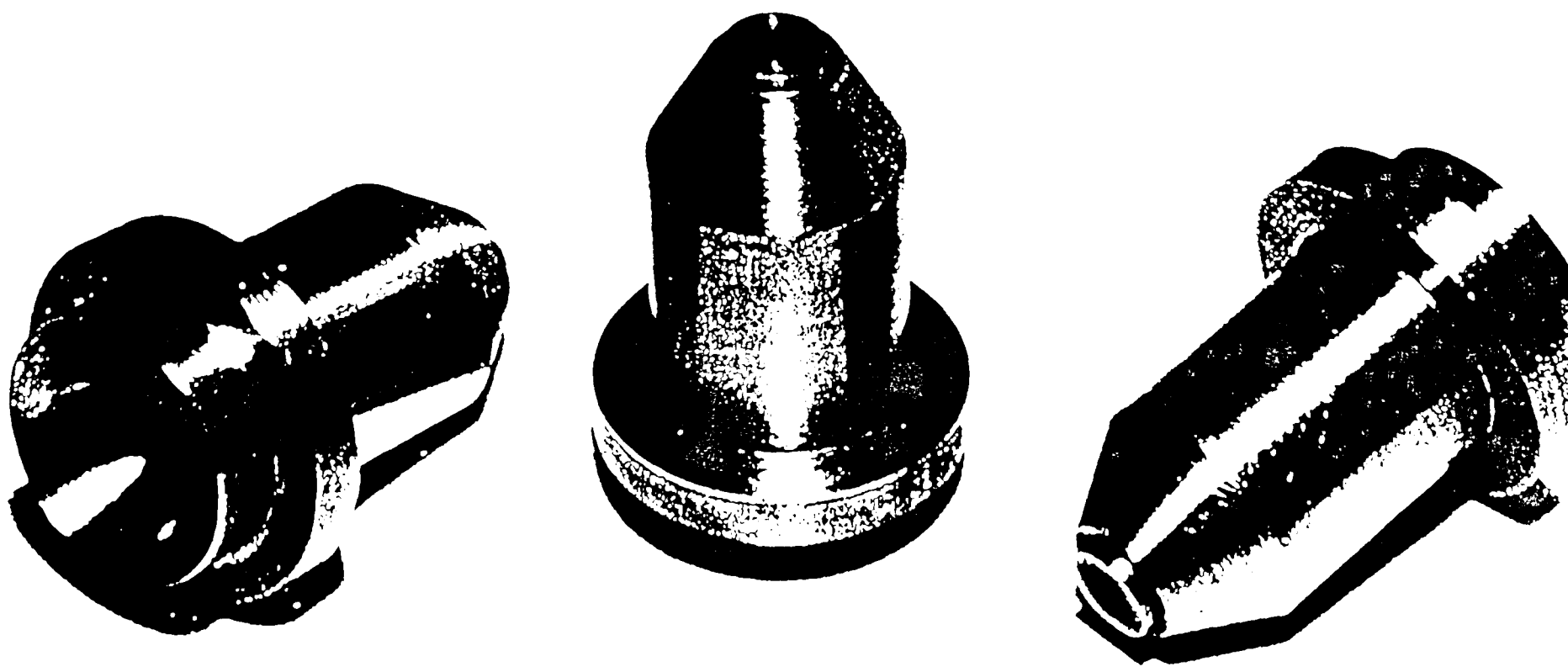

FIGURE 4.2 VIEW OF THE CONVERGENT STAINLESS STEEL NOZZLES

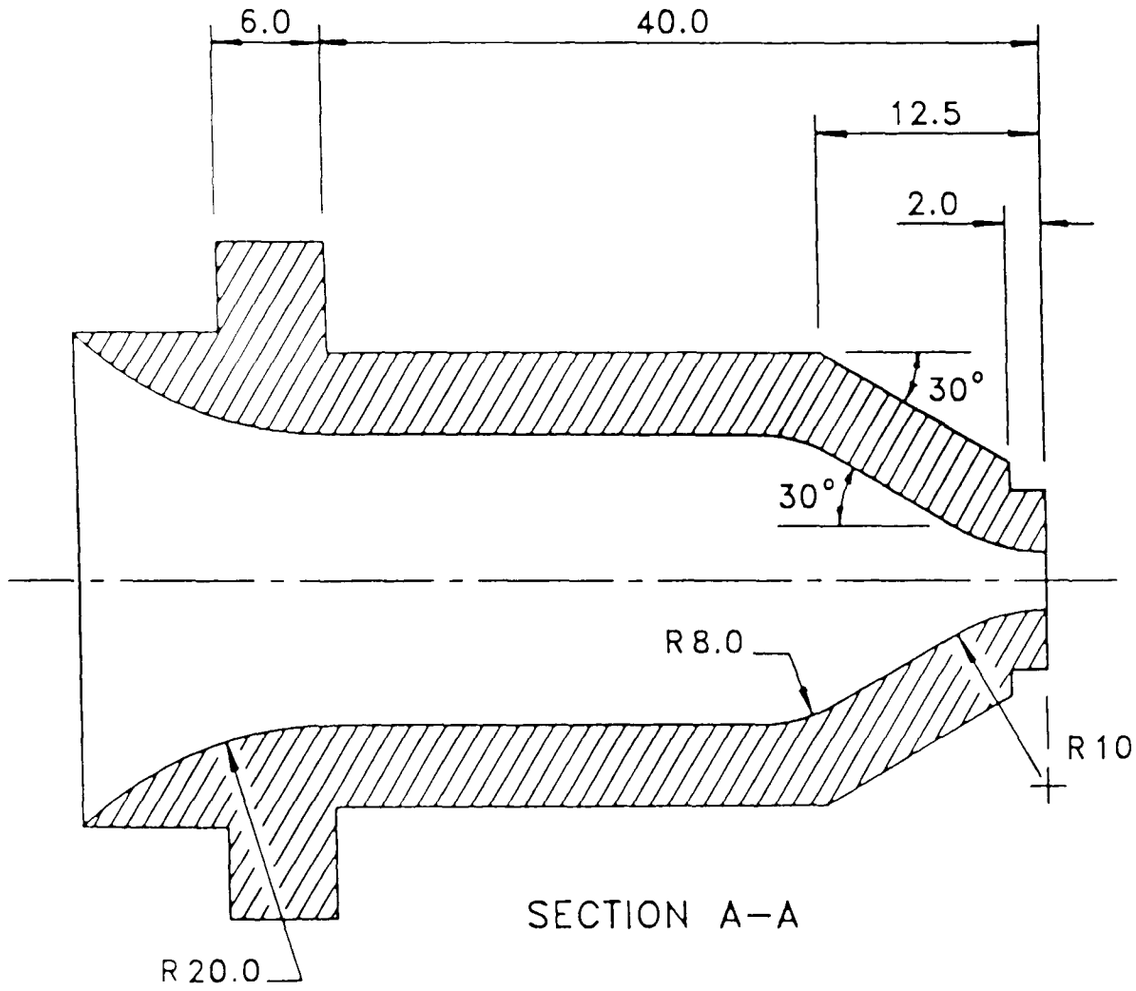

SECTION A–A

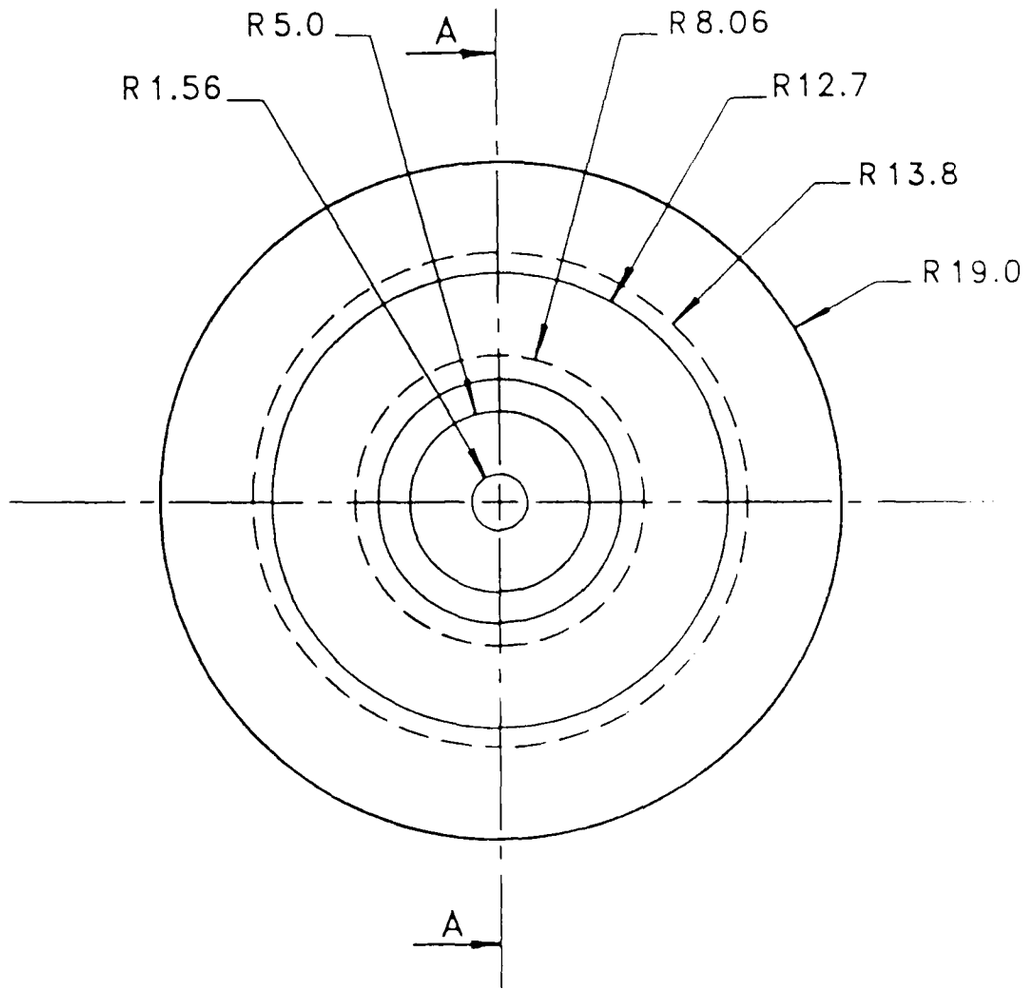

SCALE	–	2x FULL SIZE
DIMENSIONS	–	MILLIMETRES
MATERIAL	–	EN58J (AISI 316)

FIGURE 4.3 THE CONVERGENT NOZZLE WITH A 3.12mm DIAMETER THROAT

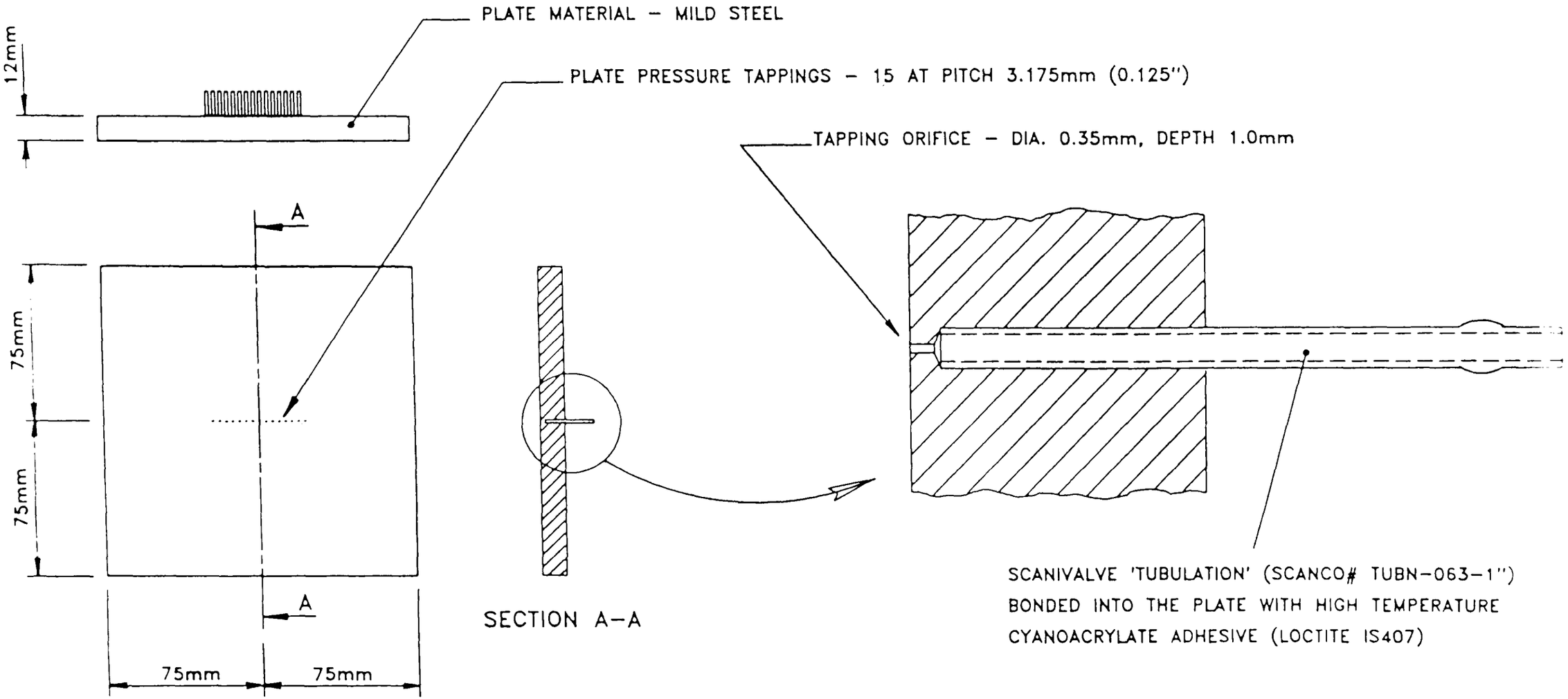

a) DRAWING OF PLATE SHOWING TAPPING ARRANGEMENT

b) ENLARGED DRAWING OF A PLATE PRESSURE TAPPING

FIGURE 4.4 THE PRESSURE TAPPED FLAT PLATE

FIGURE 4.5 VIEW OF A DISPOSABLE PITOT PROBE

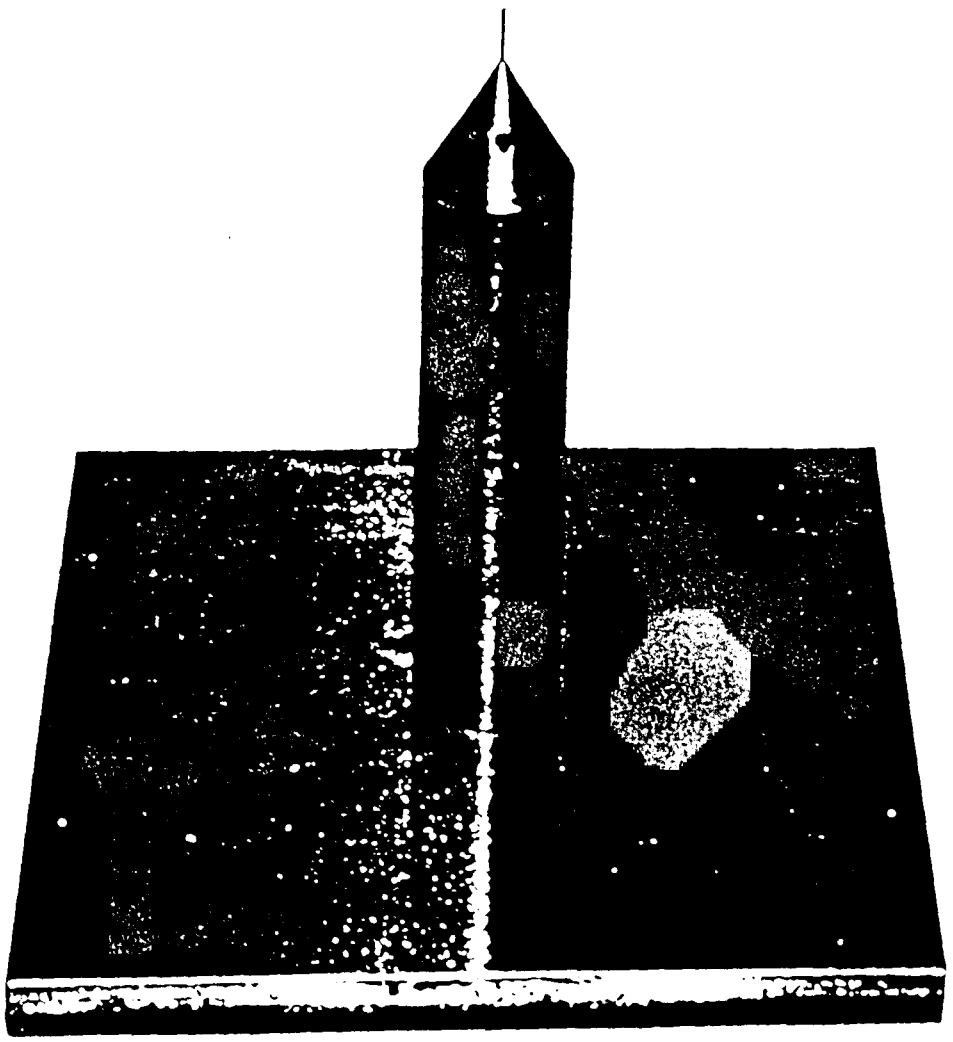

~~FIGURE 4.6~~ VIEW OF THE PITOT PROBE HOLDER

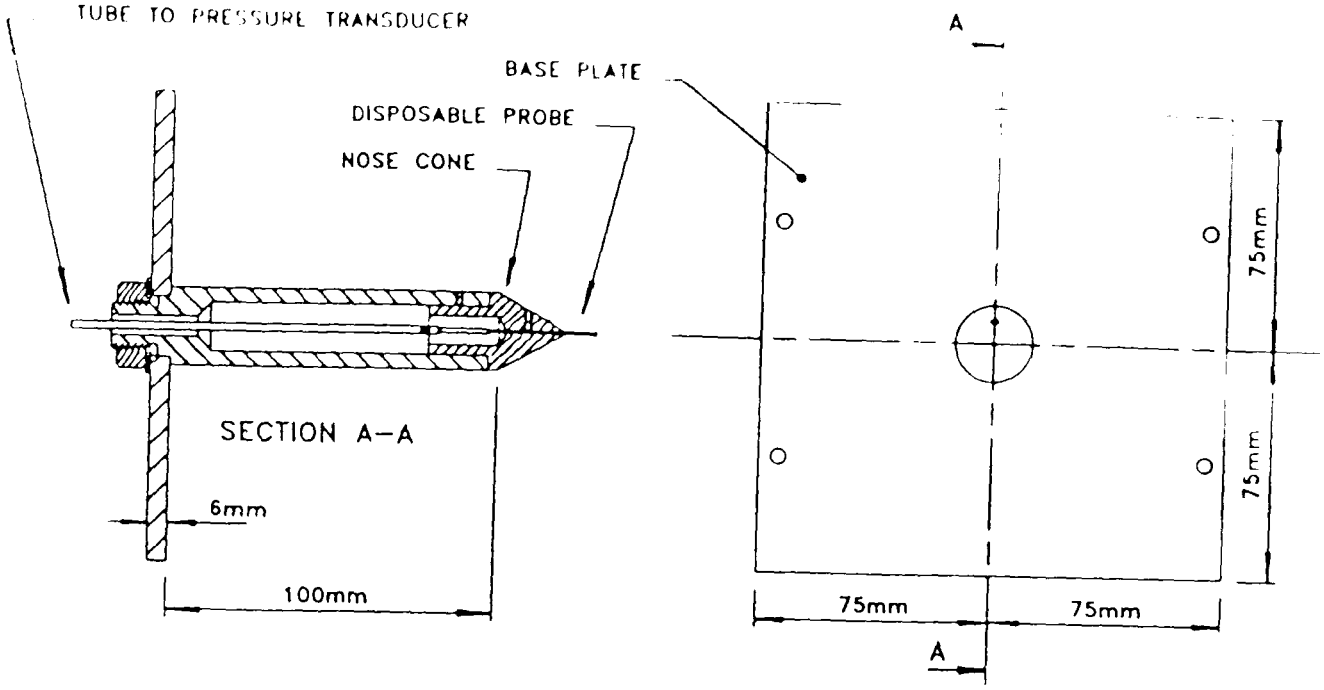

a) PROBE HOLDER GENERAL ASSEMBLY (SCALE 1/3 x FULL SIZE)

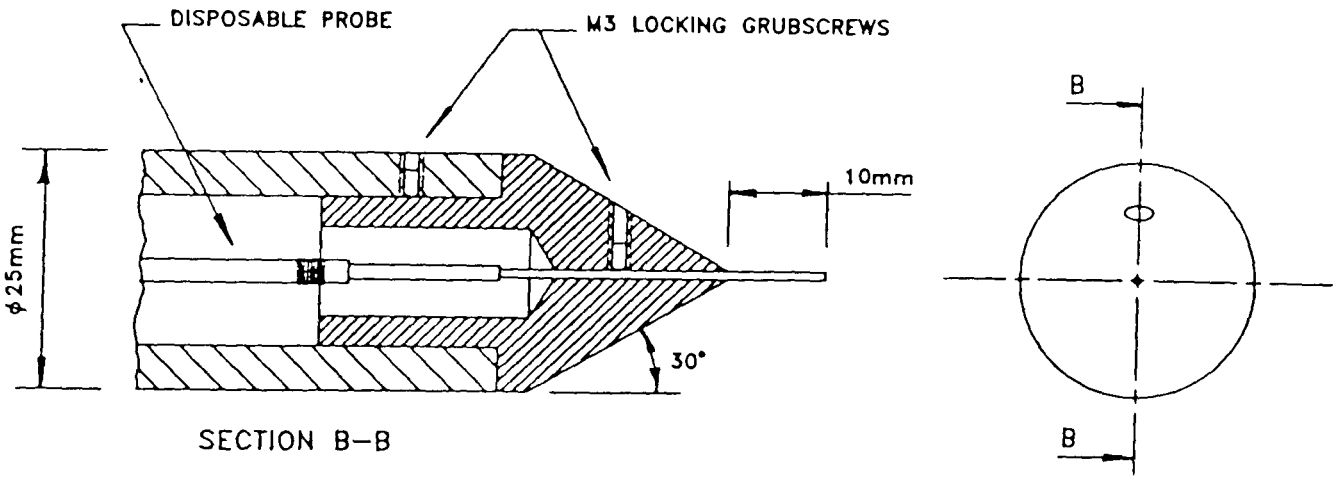

b) PROBE HOLDER NOSE CONE DETAIL (SCALE FULL SIZE)

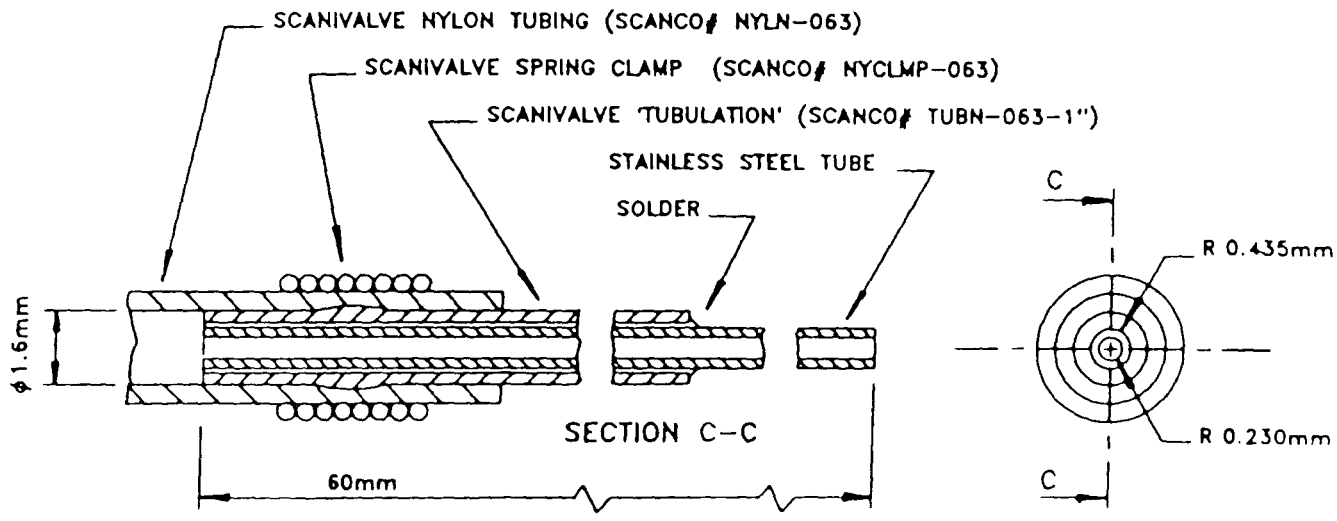

c) DISPOSABLE PROBE DETAIL (SCALE 5x FULL SIZE)

FIGURE 4.7 DRAWINGS OF THE PITOT PROBE AND HOLDER

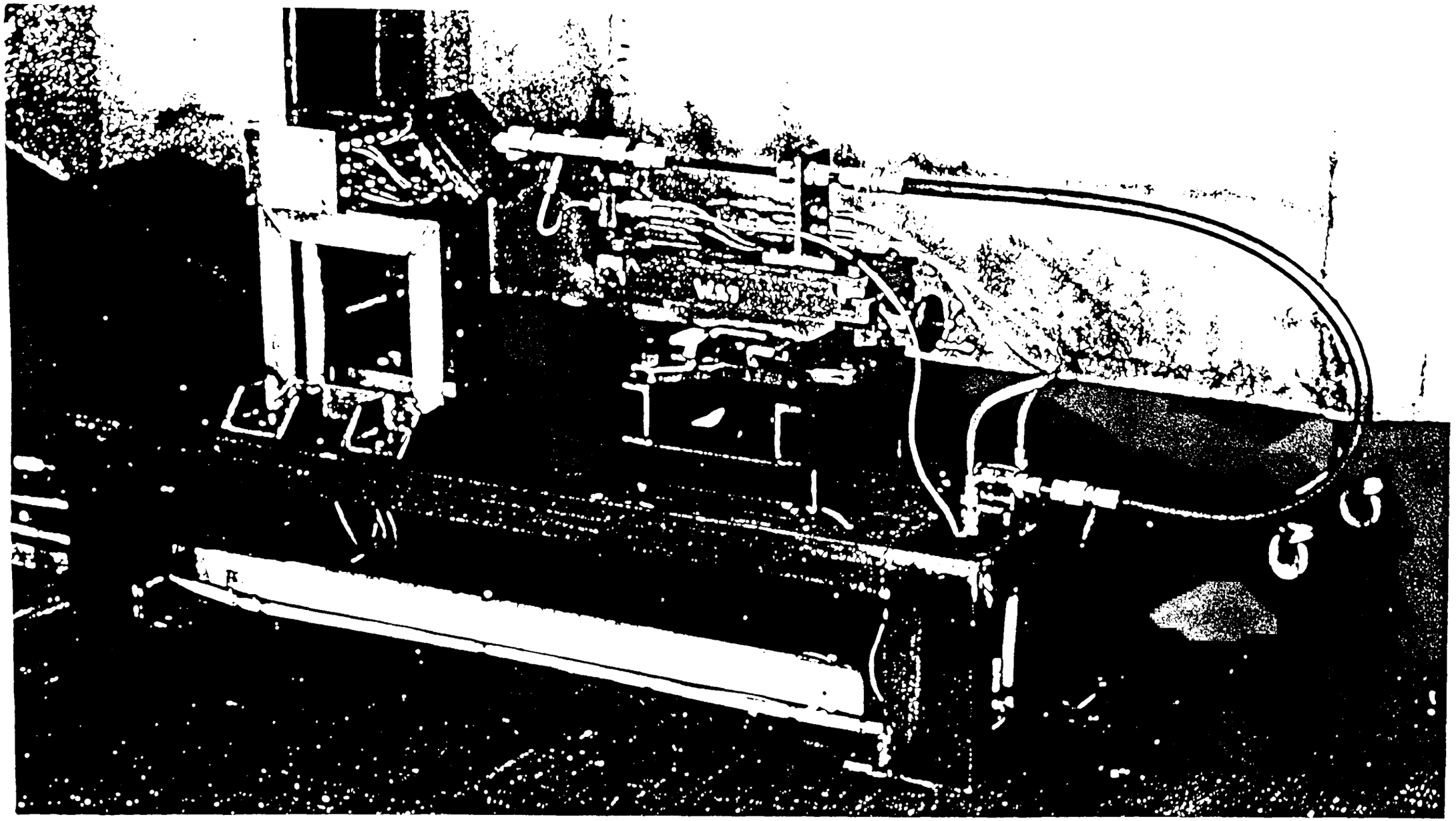

FIGURE 4.8 VIEW OF THE UNIVERSAL TEST STAND SHOWING THE CONFIGURATION FOR A COLD JET IMPINGEMENT TEST WITH A PLATE INCLINATION OF 45°

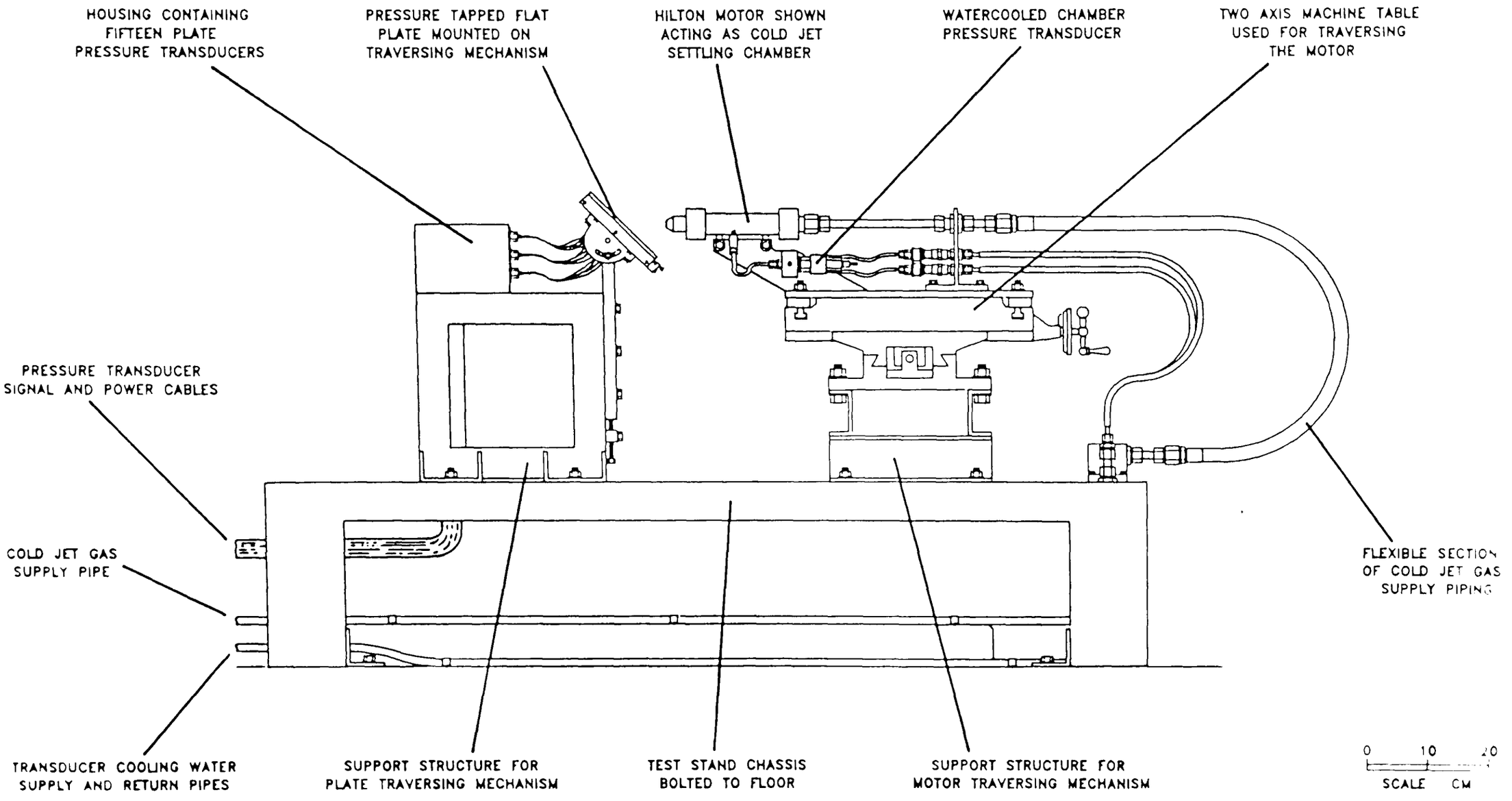

FIGURE 4.9 DRAWING OF THE UNIVERSAL TEST STAND SHOWING THE CONFIGURATION FOR A COLD JET IMPINGEMENT TEST WITH A PLATE INCLINATION OF 45°

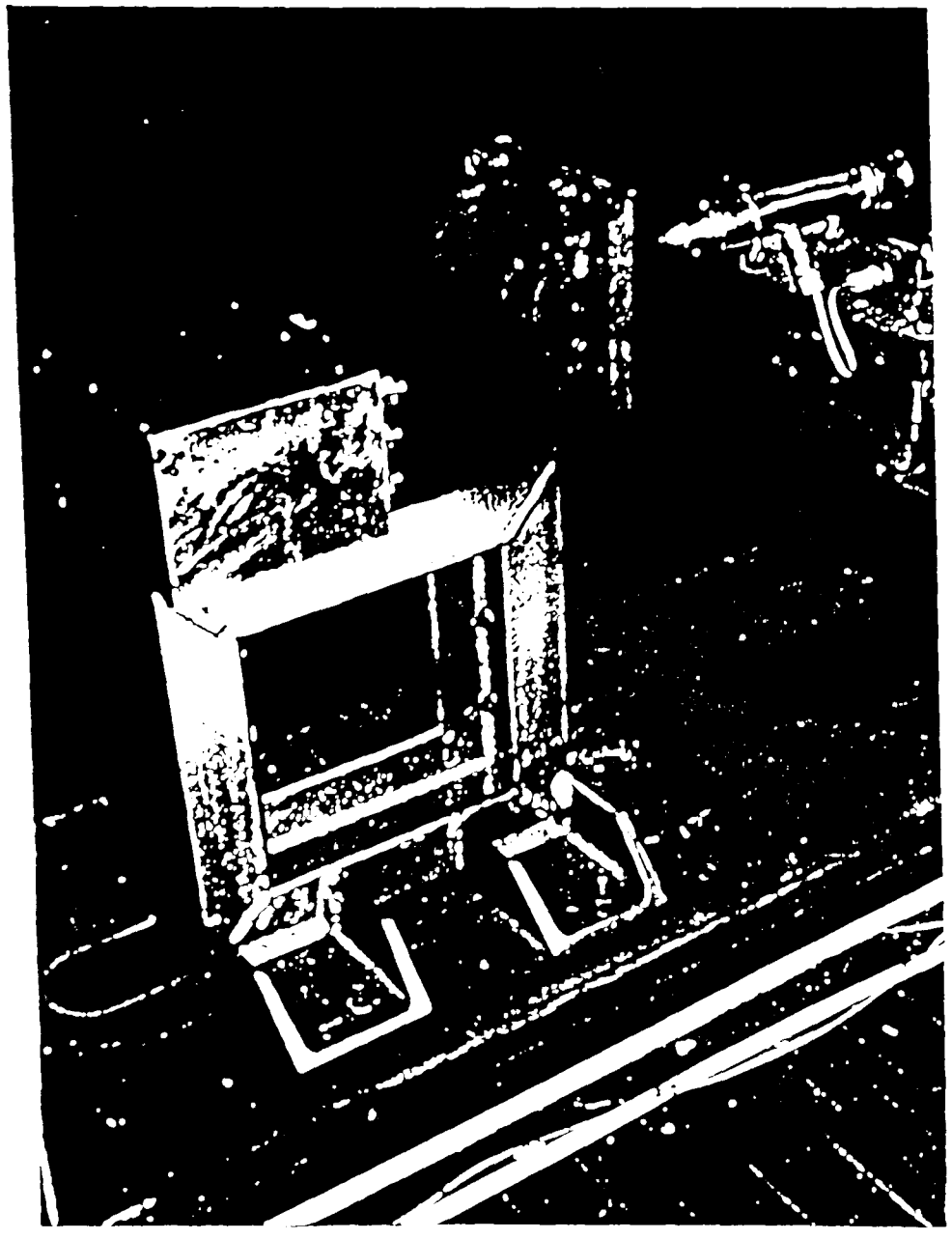

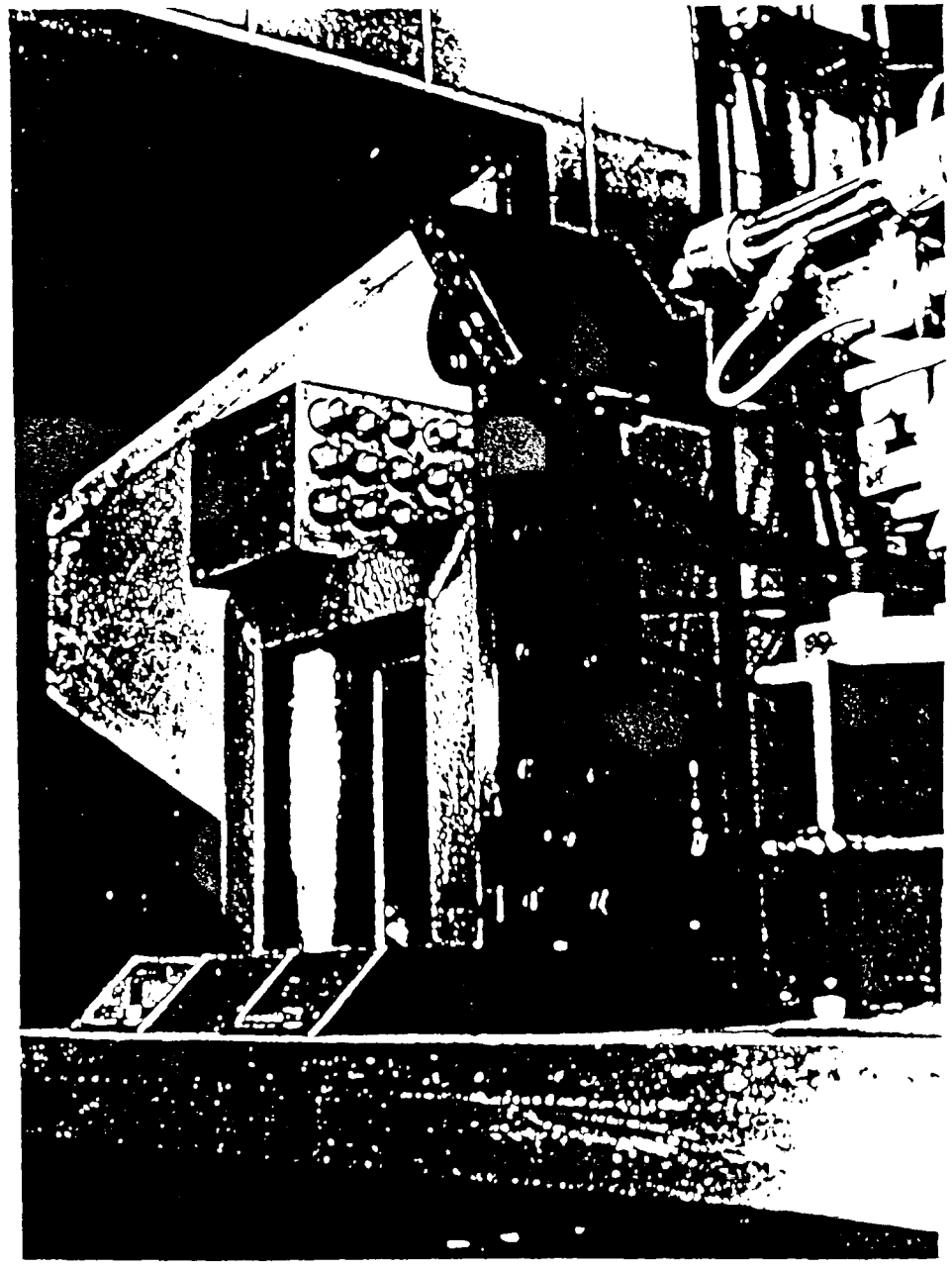

FIGURE 4.10 VIEWS OF THE FLAT PLATE TRAVERSING ASSEMBLY

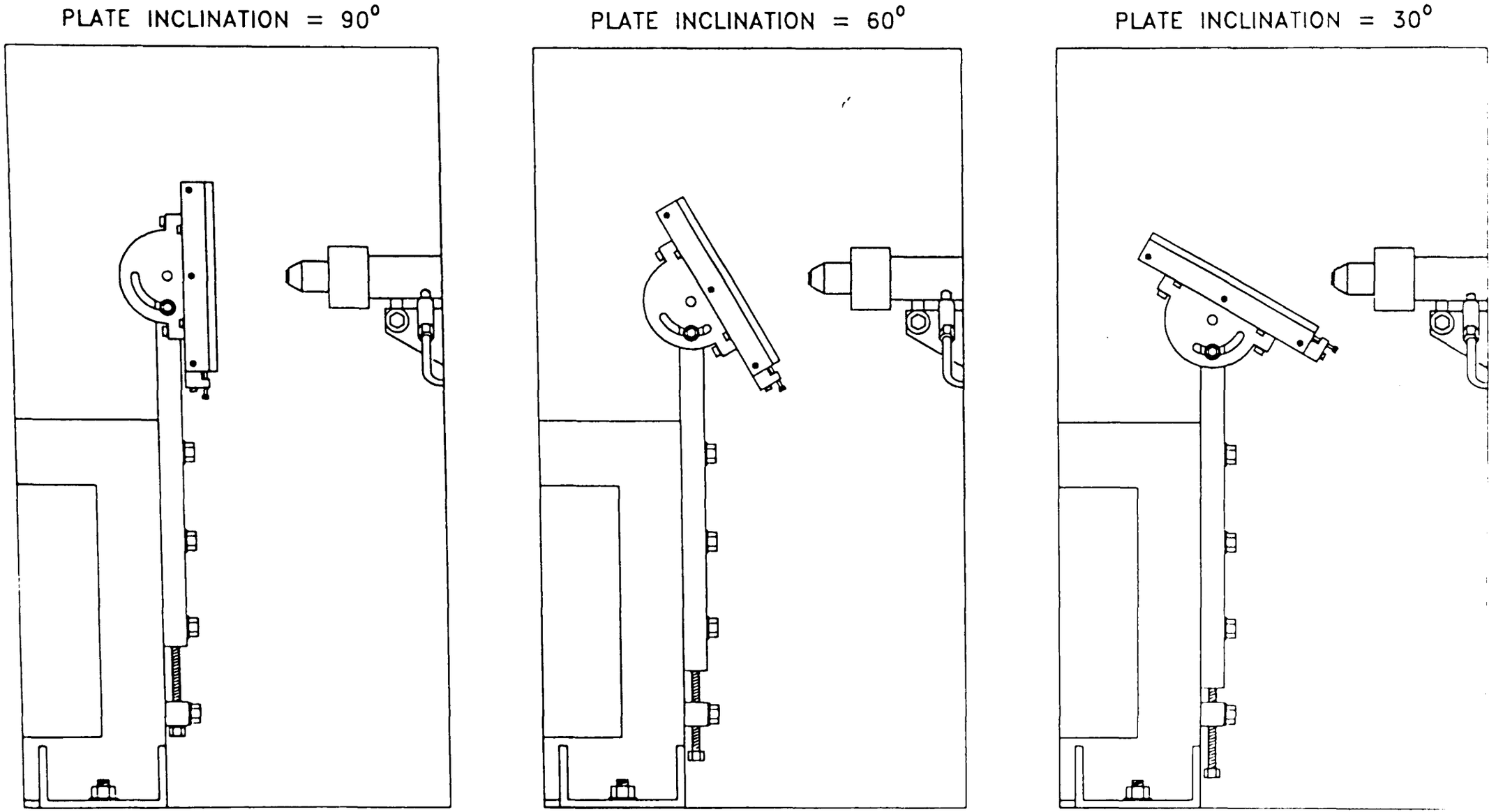

FIGURE 4.11 SIDE ELEVATION DRAWINGS OF THE FLAT PLATE TRAVERSING ASSEMBLY

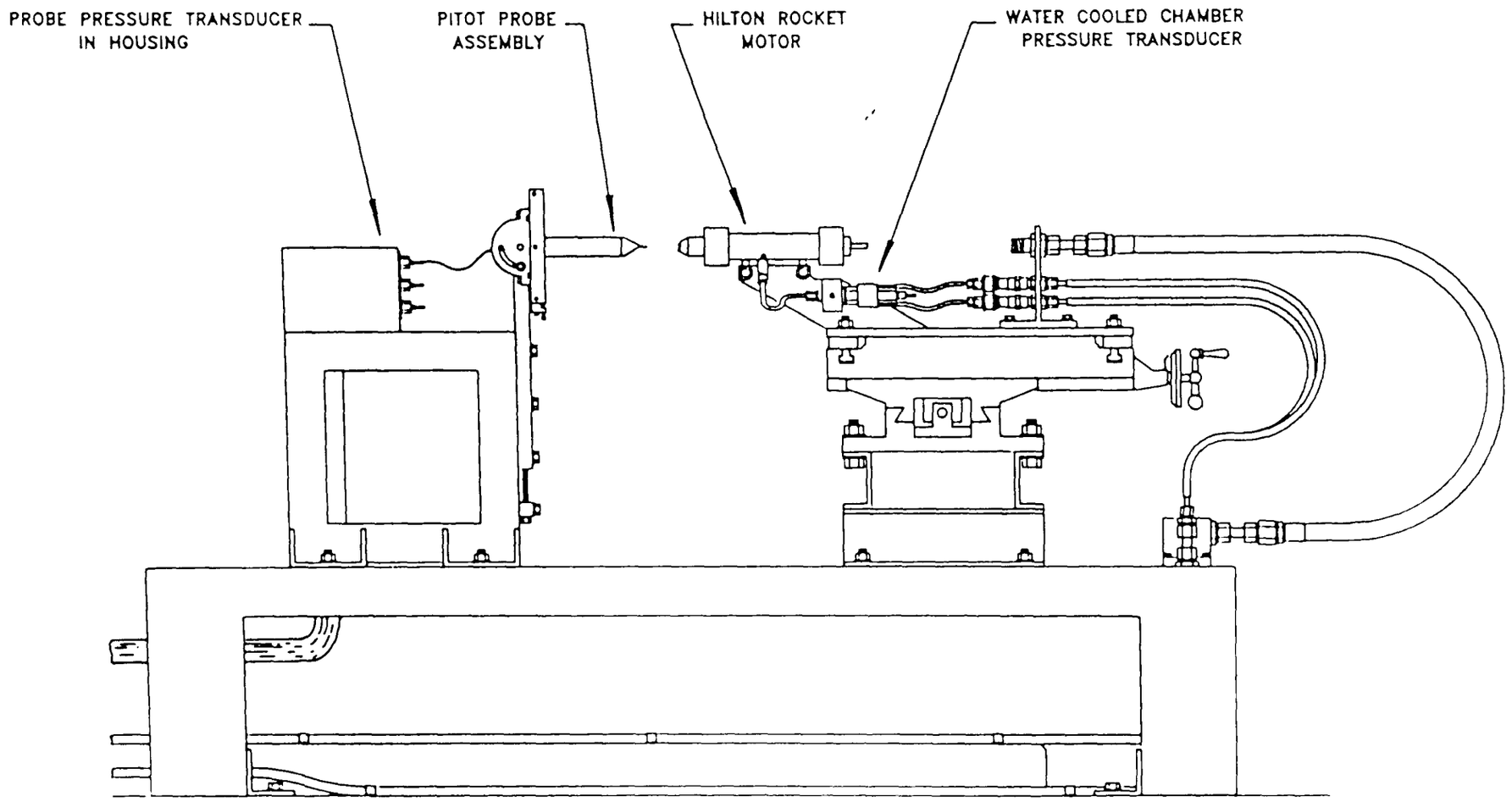

NOTE SEE FIGURE 4.9 FOR ADDITIONAL DETAILS

FIGURE 4.12 DRAWING OF THE UNIVERSAL TEST STAND SHOWING THE CONFIGURATION FOR A TEST TO MEASURE THE PITOT PRESSURE IN THE ROCKET EXHAUST

a) RUN MODE – MOBILE DUCT IN POSITION

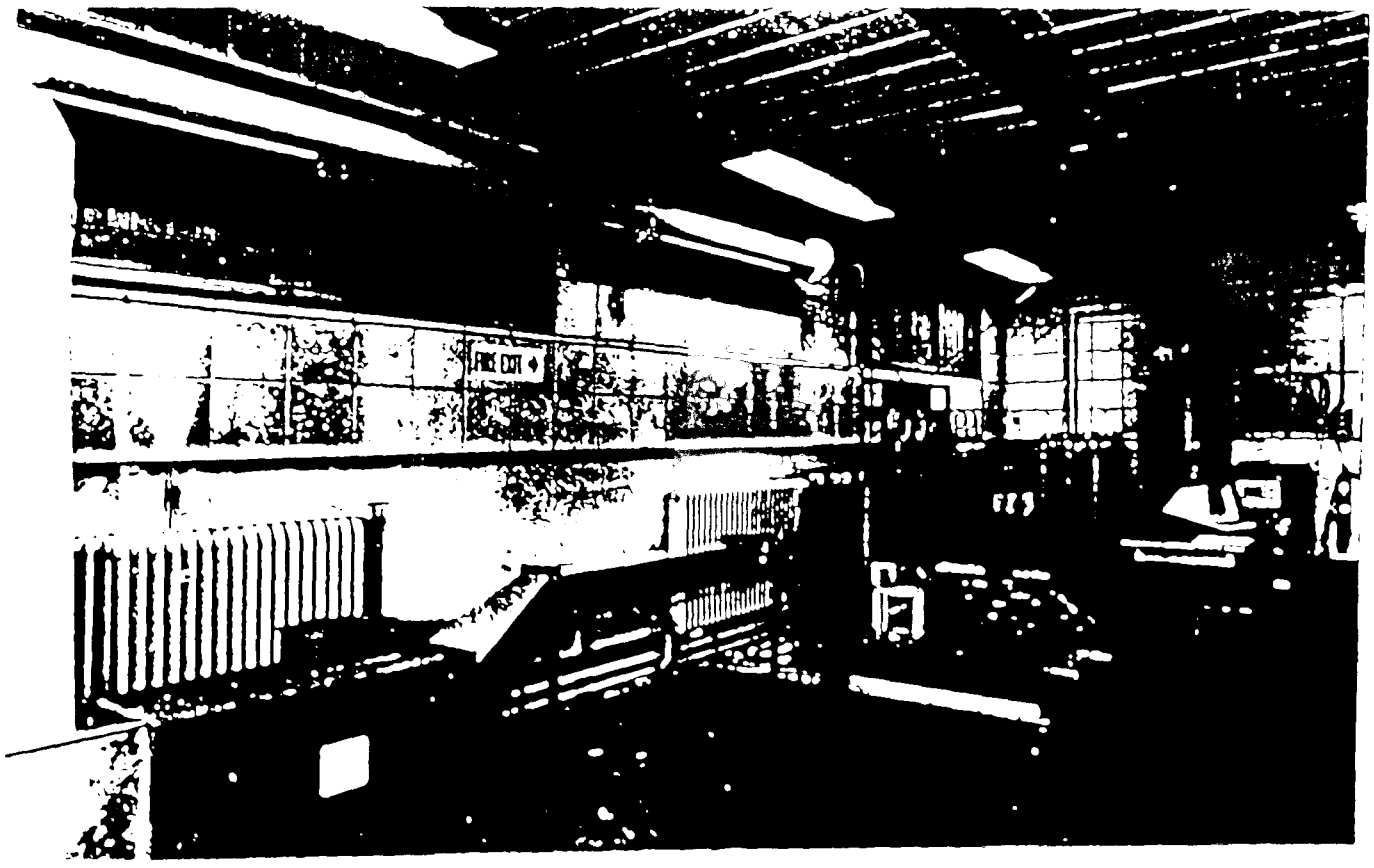

b) ADJUST MODE – MOBILE DUCT REMOVED

FIGURE 4-13 VIEWS OF THE VENTILATION SYSTEM

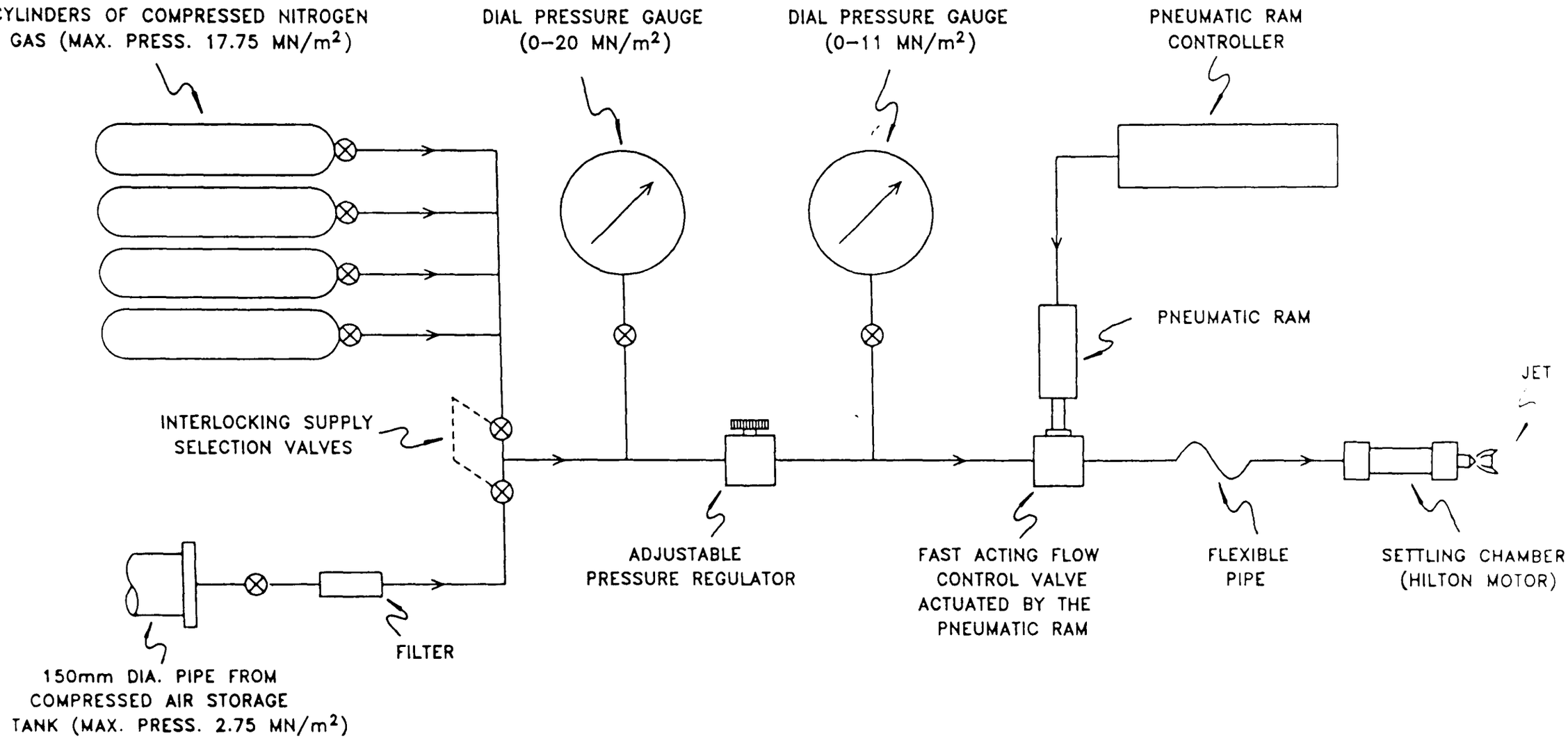

GAS SUPPLIES → SUPPLY SELECTION → REGULATION → FLOW CONTROL → COLD JETS

FIGURE 4.14 SCHEMATIC DIAGRAM OF THE COLD JET SUPPLY SYSTEM

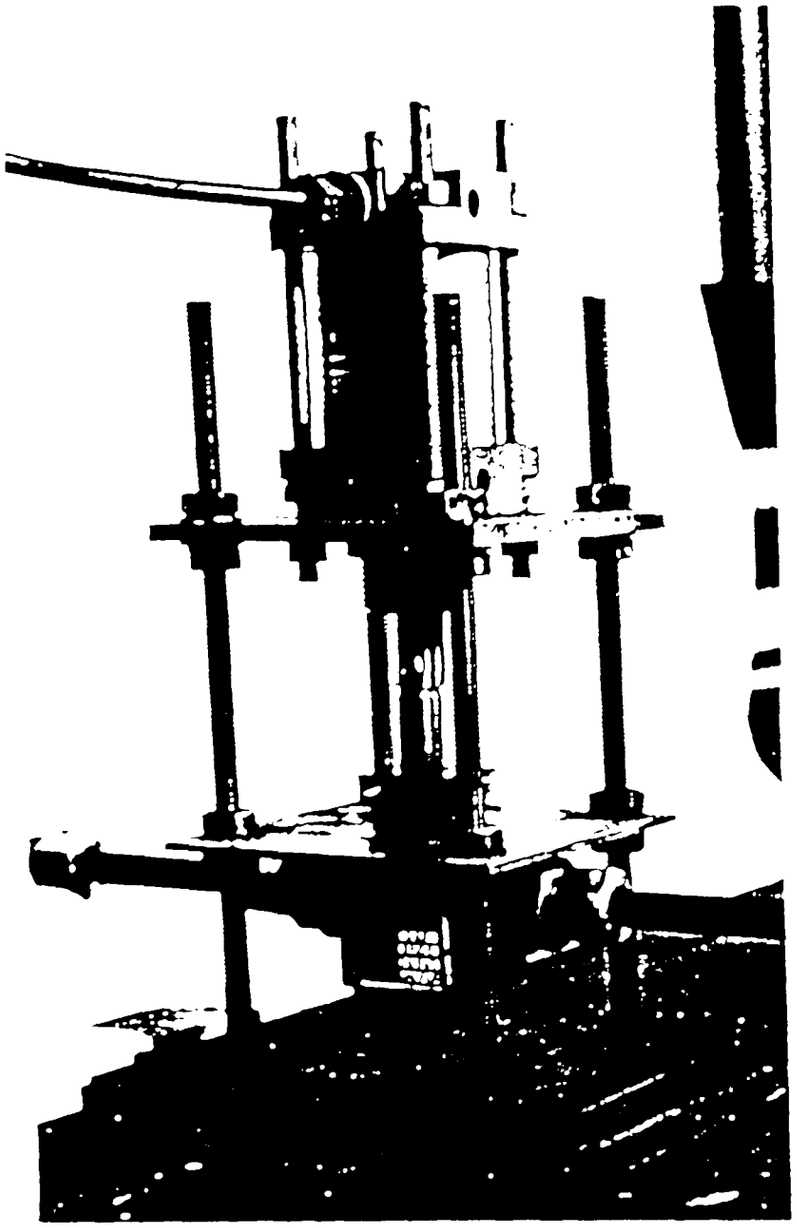

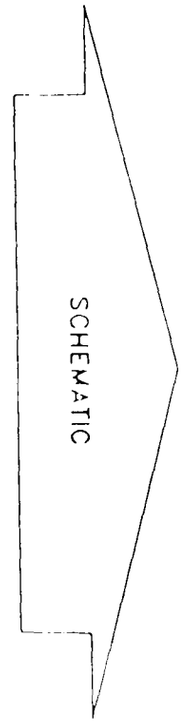

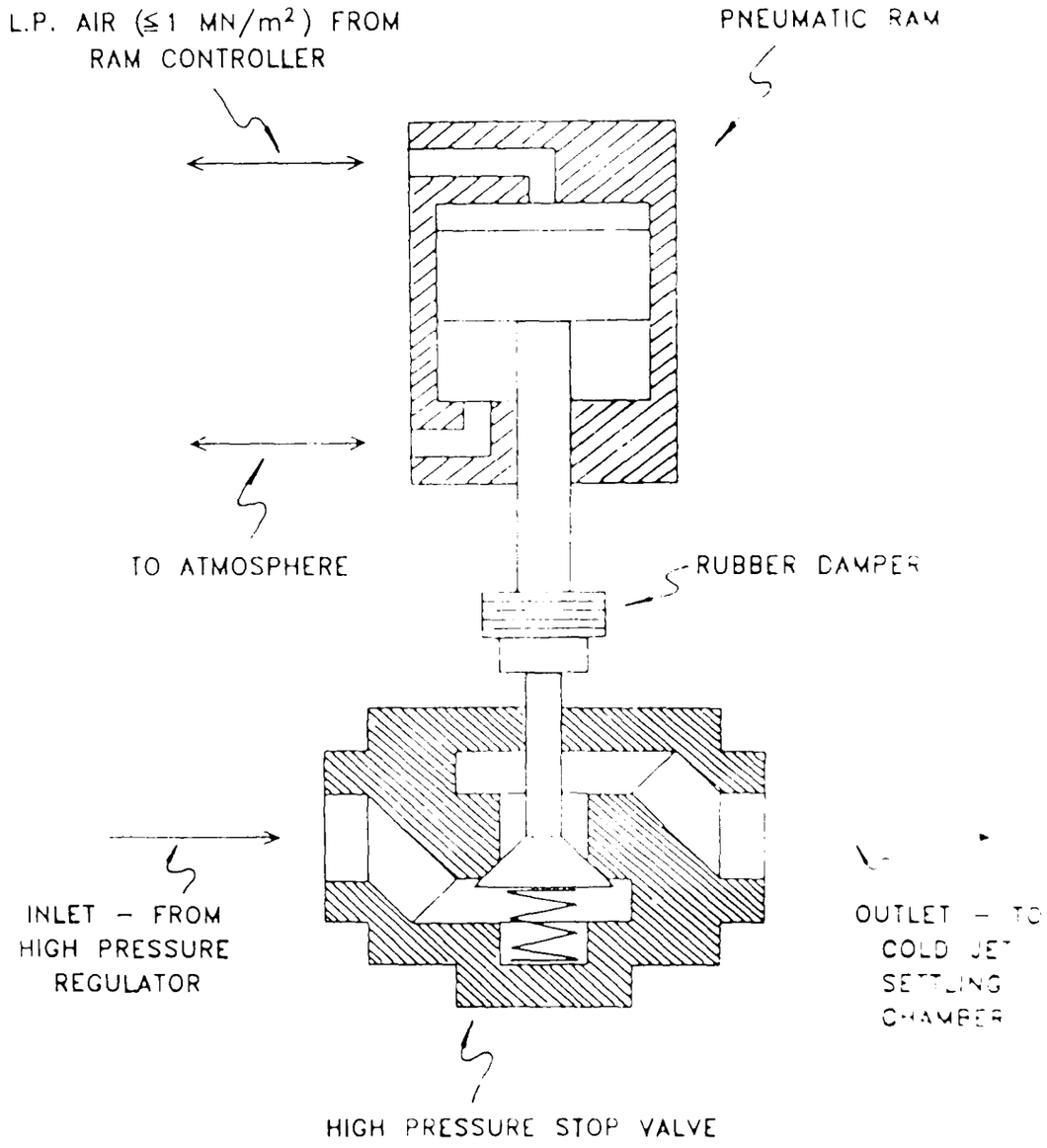

FIGURE 4.15 FAST ACTING FLOW CONTROL VALVE ASSEMBLY

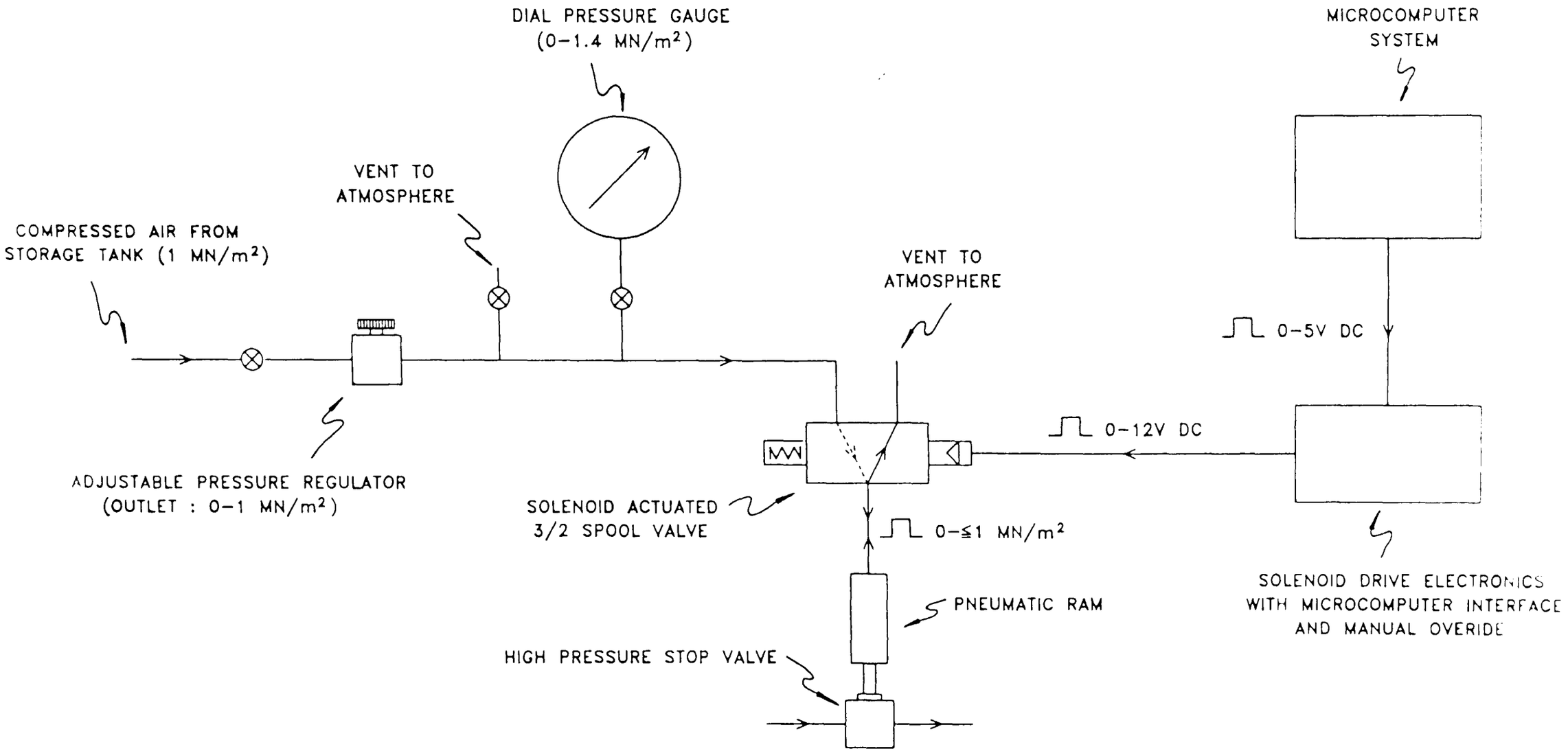

FIGURE 4.16 SCHEMATIC DIAGRAM OF THE PNEUMATIC RAM CONTROLLER

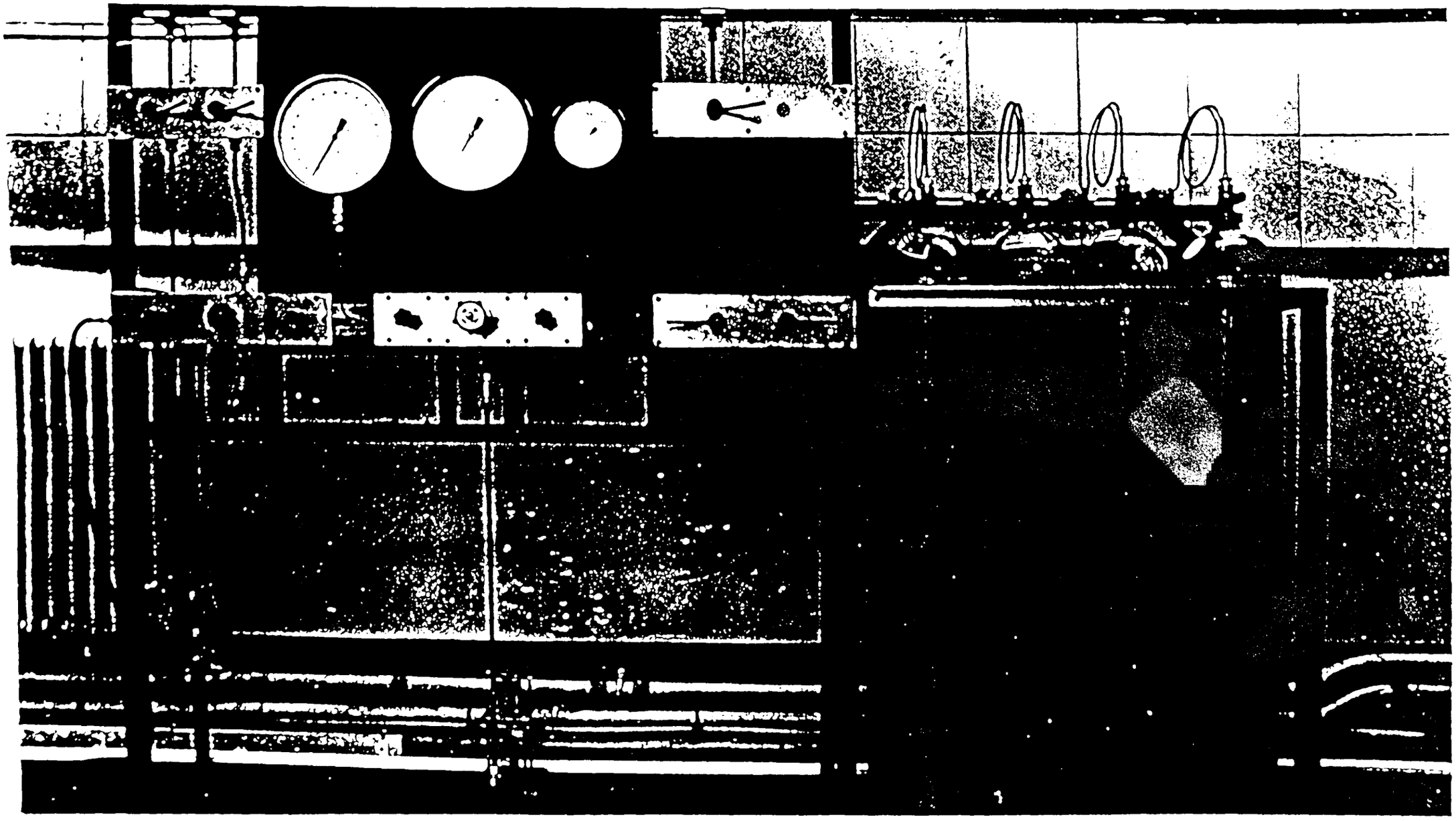

FIGURE 4.17 VIEW OF THE COLD JET SUPPLY SYSTEM CONTROL PANEL AND THE HIGH PRESSURE NITROGEN GAS CYLINDERS

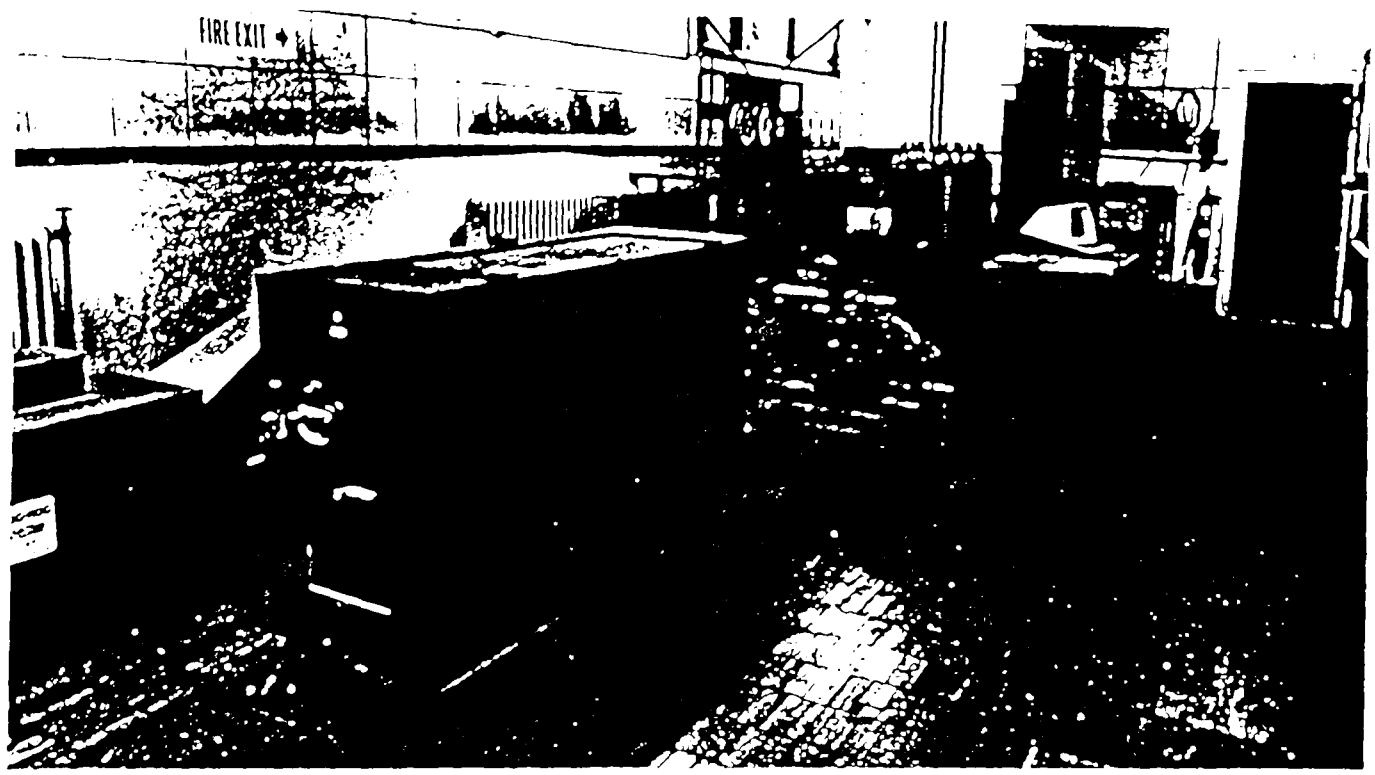

FIGURE 4.18 VIEWS OF THE SHADOWGRAPH SYSTEM

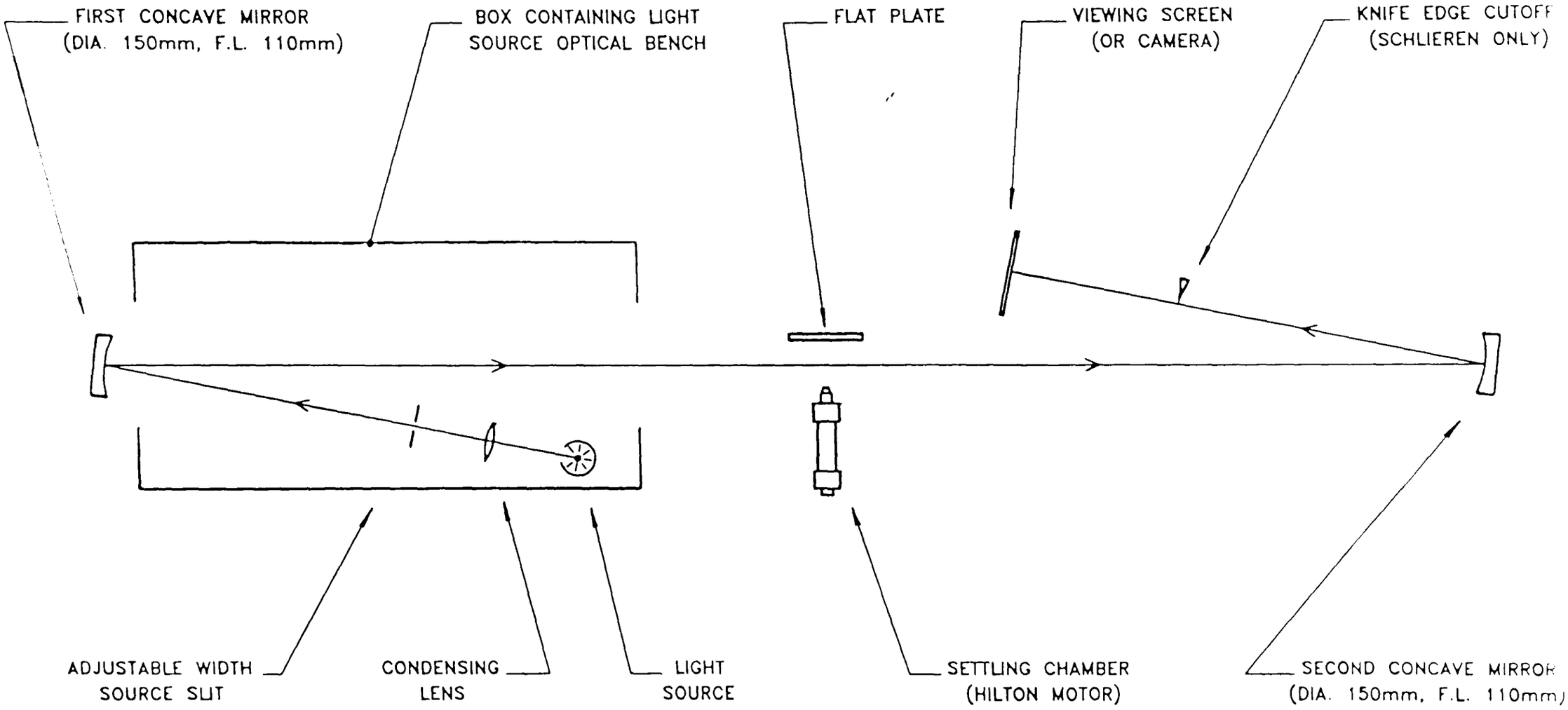

FIGURE 4.19 SCHEMATIC DIAGRAM OF THE SHADOWGRAPH/SCHLIEREN SYSTEM

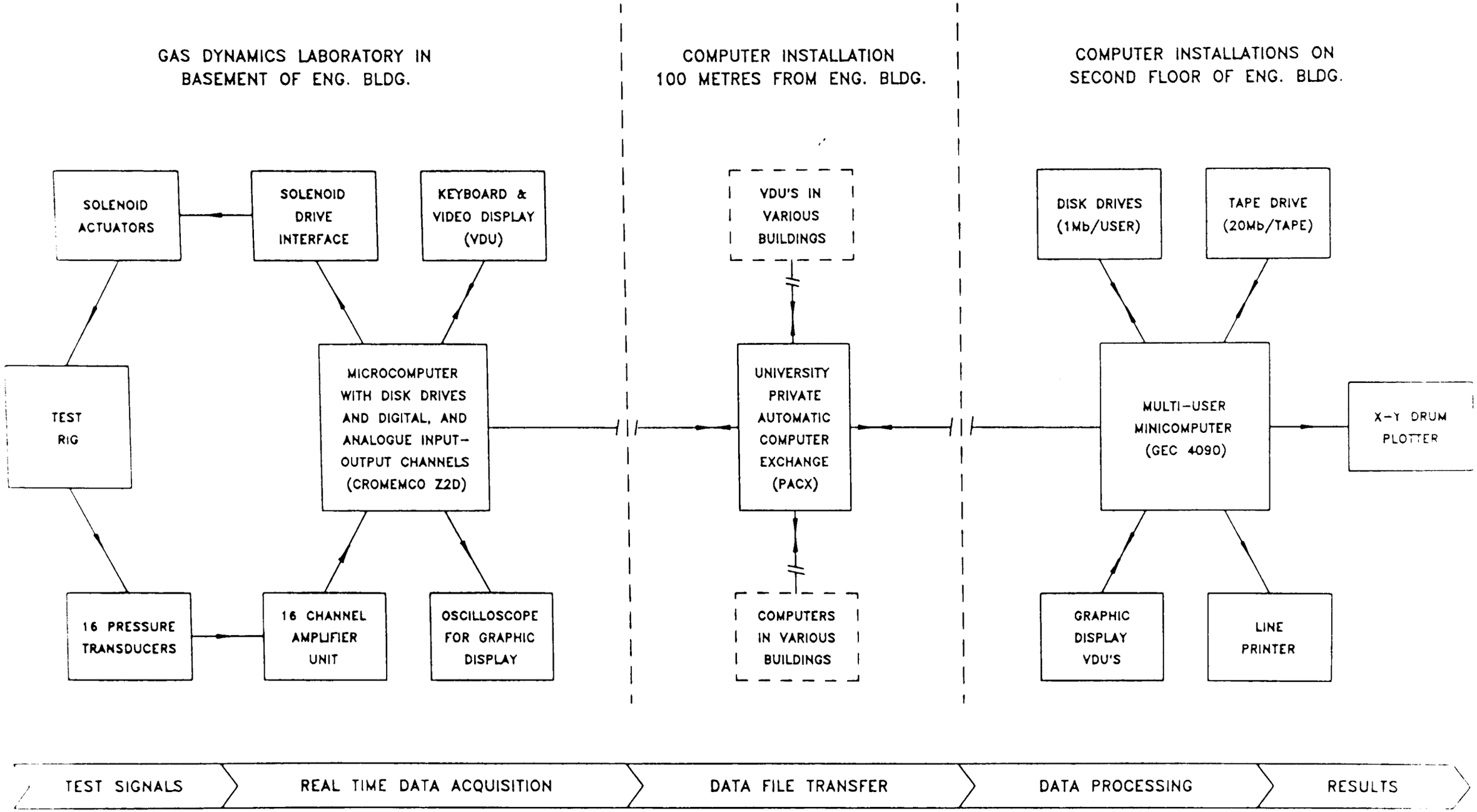

FIGURE 4.20 SCHEMATIC OF THE SYSTEM USED FOR OBTAINING AND PROCESSING PRESSURE DATA

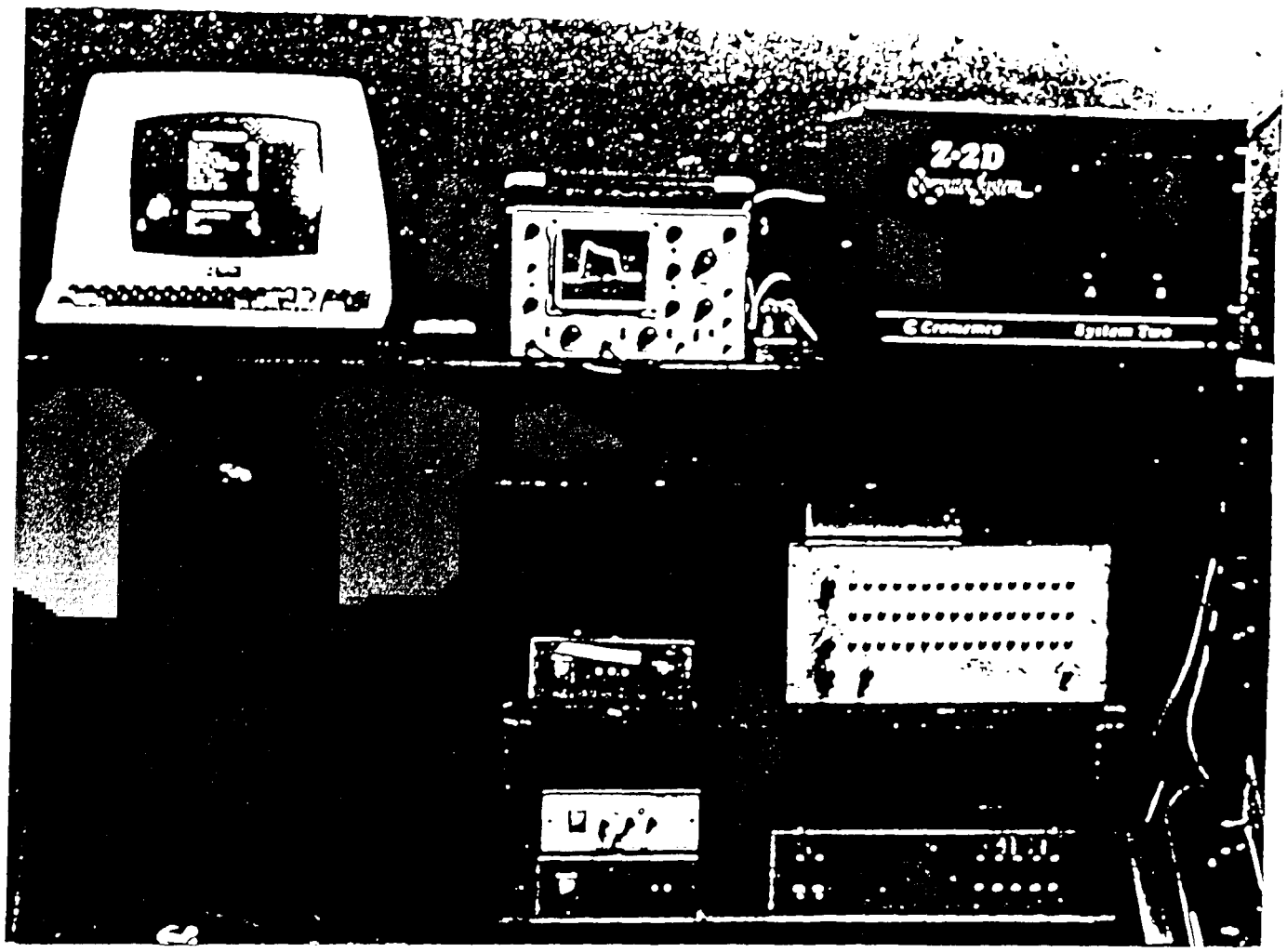

FIGURE 4.21 VIEW OF THE LABORATORY BASED DATA ACQUISITION AND RIG CONTROL SYSTEM

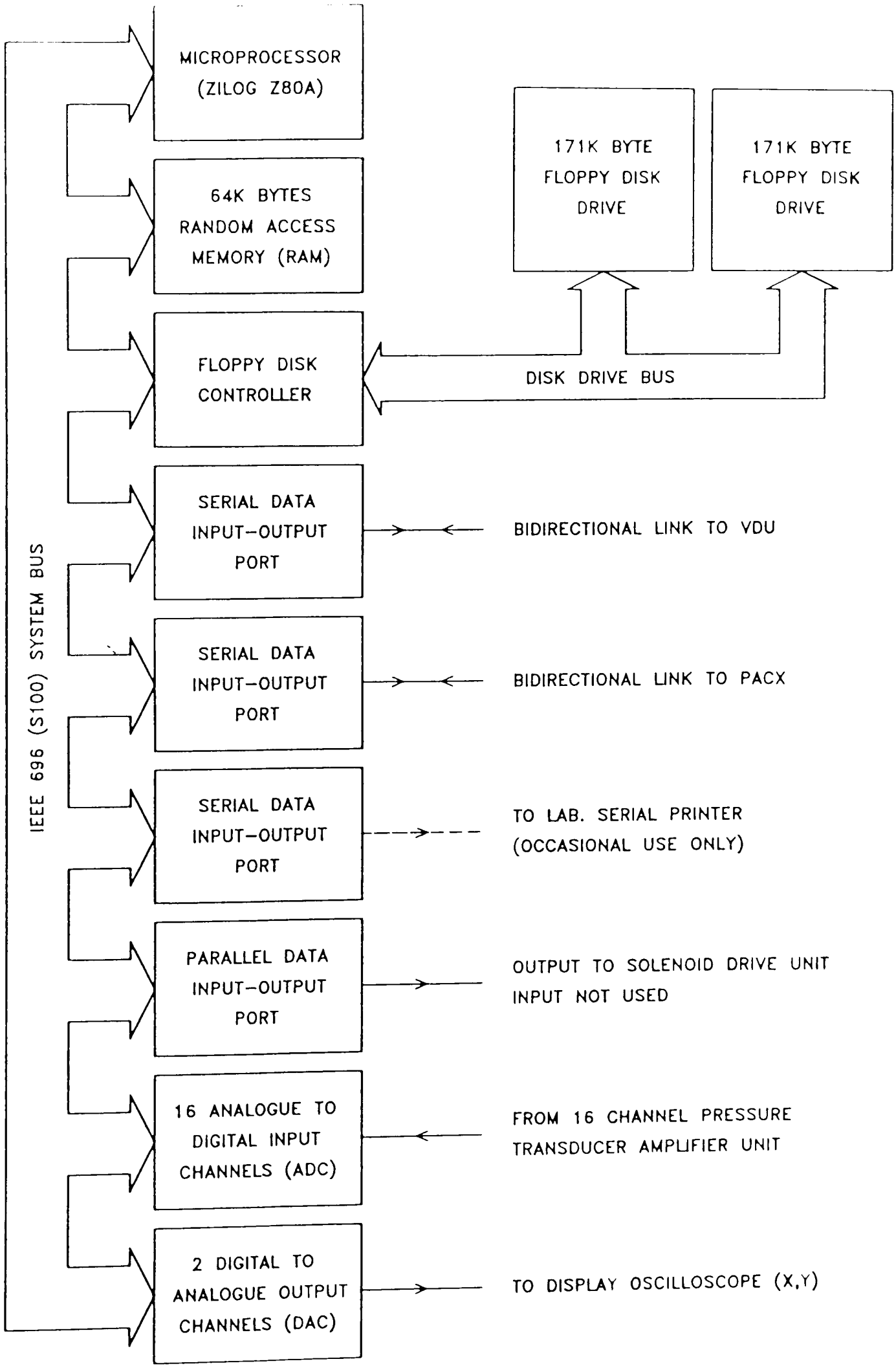

FIGURE 4.22 SCHEMATIC DIAGRAM OF THE MICROCOMPUTER

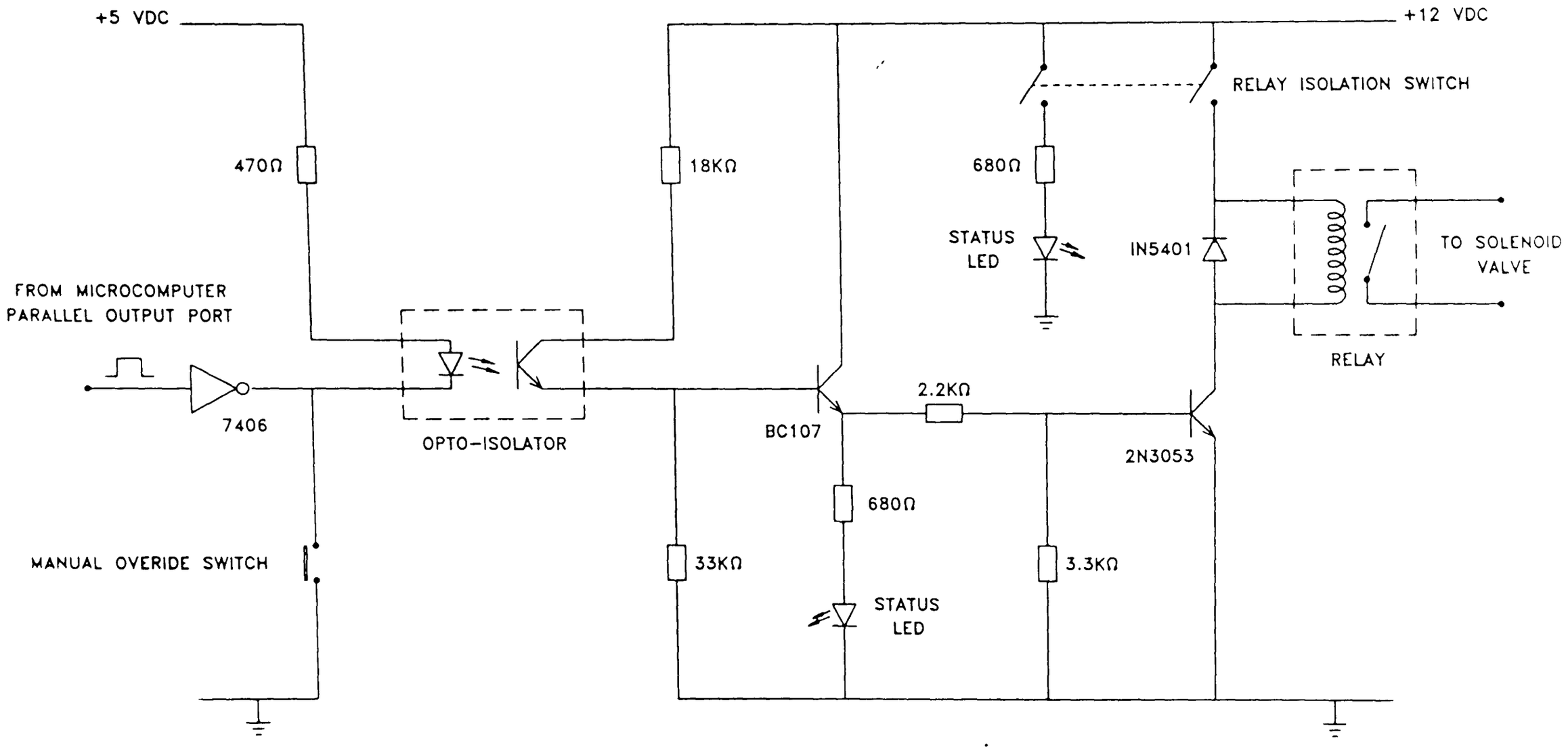

FIGURE 4.23 SCHEMATIC DIAGRAM OF THE SOLENOID VALVE INTERFACE CIRCUIT

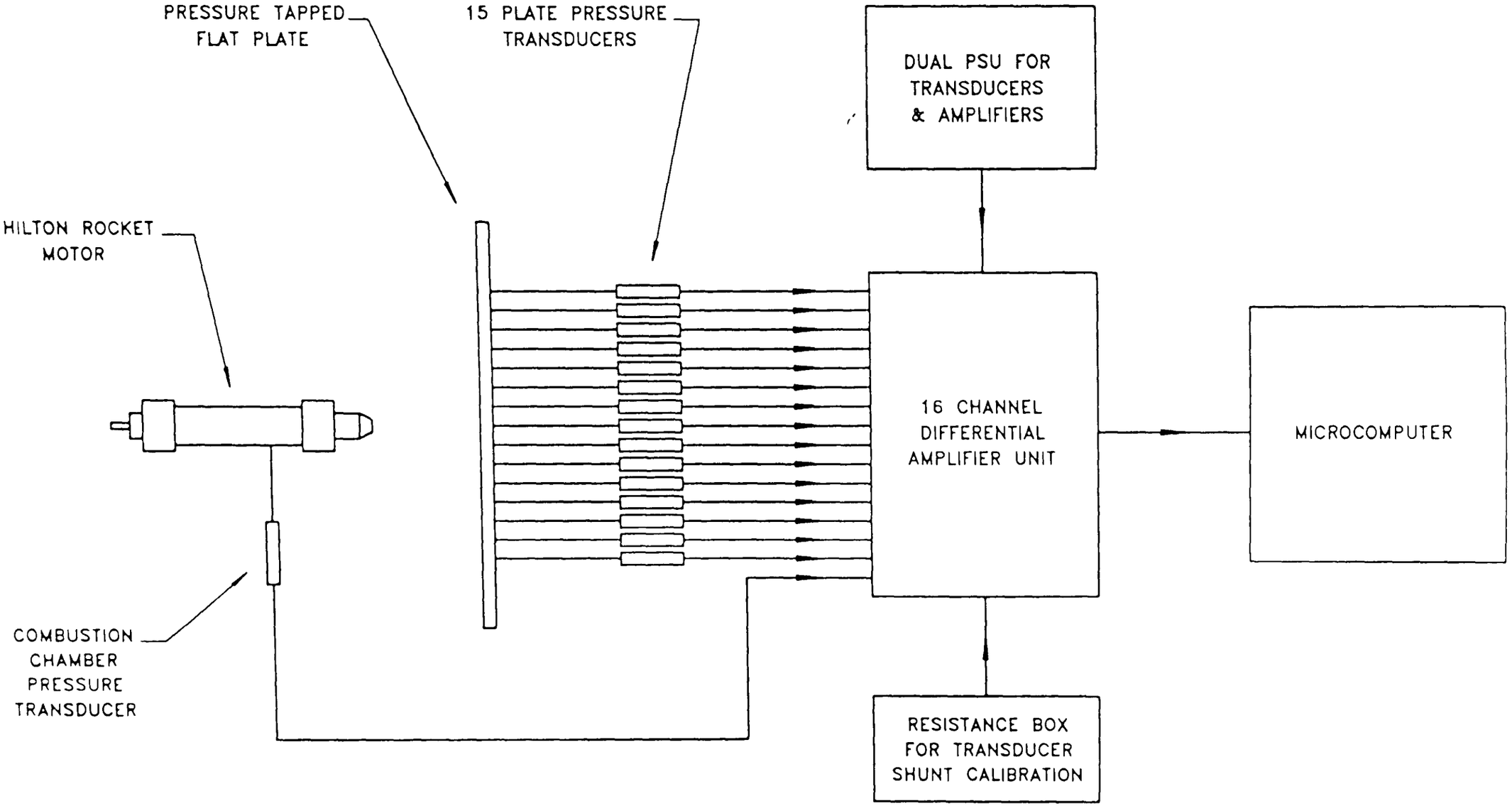

FIGURE 4.24 SCHEMATIC DIAGRAM OF THE PRESSURE MONITORING SUBSYSTEM

NOTE ON DIMENSIONS – THE LENGTHS (L) AND DIAMETERS (ϕ) OF THE TUBING SEGMENTS ARE IN MILLIMETRES
– THE TRANSDUCER CAVITY VOLUMES (V) ARE IN CUBIC MILLIMETRES

COMBUSTION CHAMBER PRESSURE TRANSDUCER

COMBUSTION CHAMBER	L = 15 ϕ = 4	L = 20 ϕ = 3	L = 200 ϕ = 1.6	L = 16 ϕ = 3	L = 6 ϕ = 1.6	TRANSDUCER CAVITY V = 500

FLAT PLATE PRESSURE TRANSDUCER(S)

SURFACE OF FLAT PLATE	L = 1 ϕ = 0.35	L = 25 ϕ = 1	L = 200 ϕ = 1.6	L = 25 ϕ = 1	L = 30 ϕ = 5	TRANSDUCER CAVITY V = 200

PITOT PROBE PRESSURE TRANSDUCER

TIP OF PITOT PROBE	L = 60 ϕ = 0.46	L = 300 ϕ = 1.6	L = 25 ϕ = 1	L = 35 ϕ = 1.6	TRANSDUCER CAVITY V = 40

FIGURE 4.25 SCHEMATIC DIAGRAM OF THE PRESSURE TRANSDUCER CONNECTING TUBE GEOMETRIES

NOTE – PLEASE REFER TO TEXT FOR COMMENTS ON THE VALUES OF RESISTORS Rt, Rb & Rs

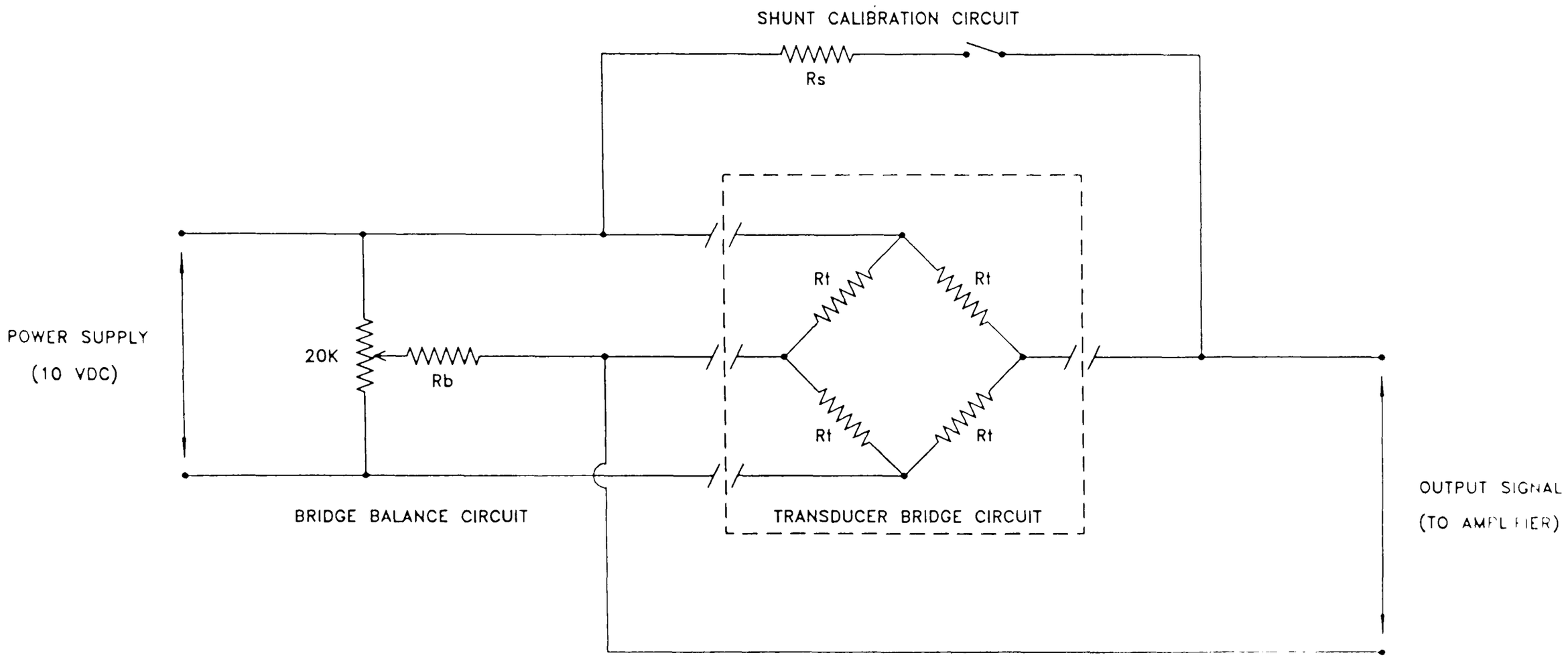

FIGURE 4.26 · SCHEMATIC DIAGRAM OF THE ELECTRICAL CONNECTIONS TO A PRESSURE TRANSDUCER

NOTES – THIS DIAGRAM SHOWS THE ARRANGEMENT FOR A SINGLE AMPLIFIER 'CHANNEL' ; EVERY TRANSDUCER REQUIRED A SEPARATE CHANNEL

– THE POWER SUPPLY, NULL ADJUST & FREQUENCY COMPENSATION CIRCUITS OF EACH OP AMP HAVE BEEN OMITTED FOR DIAGRAM CLARITY

– EACH AMPLIFIER WAS BUILT WITH R1=R2 & R3=R4=R5=R6 AND HENCE IT CAN BE SHOWN (REF) THAT $VO = (V1-V2)\left(1 + \frac{2\,R1}{RV}\right)\left(\frac{R5}{R3}\right)$

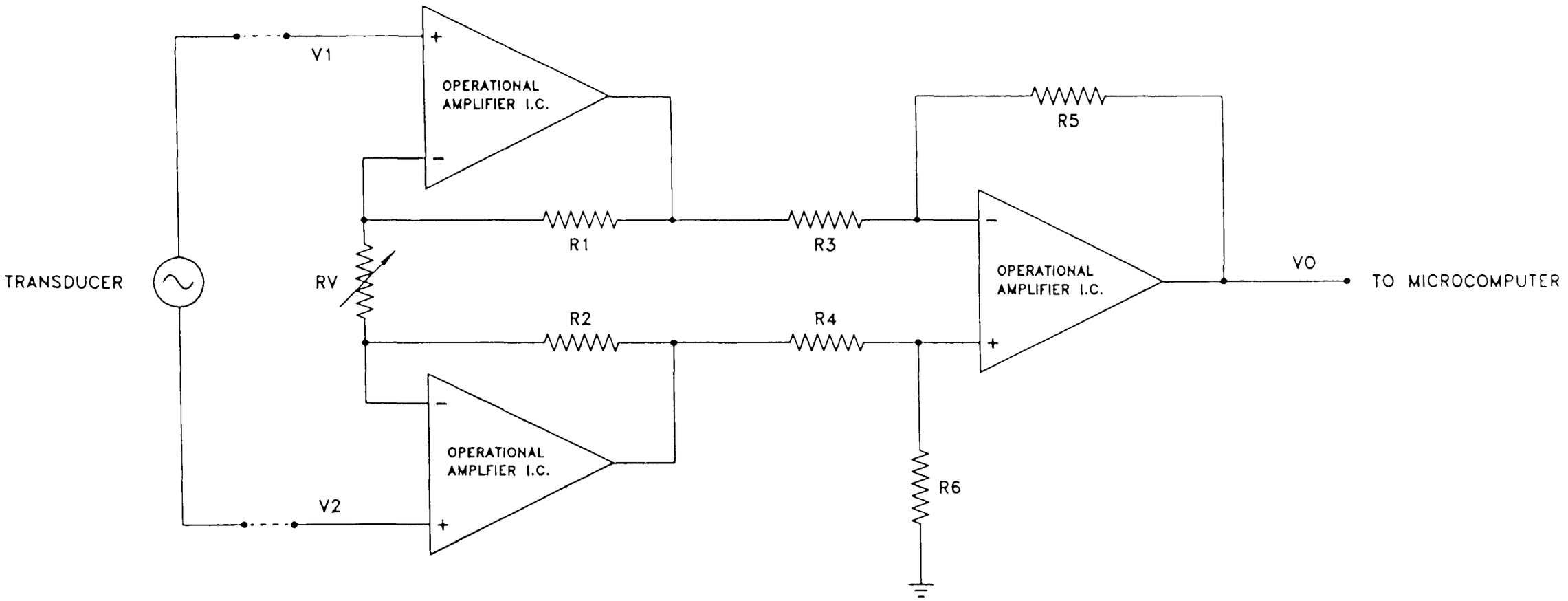

FIGURE 4.27 SIMPLIFIED SCHEMATIC CIRCUIT DIAGRAM OF A DIFFERENTIAL AMPLIFIER

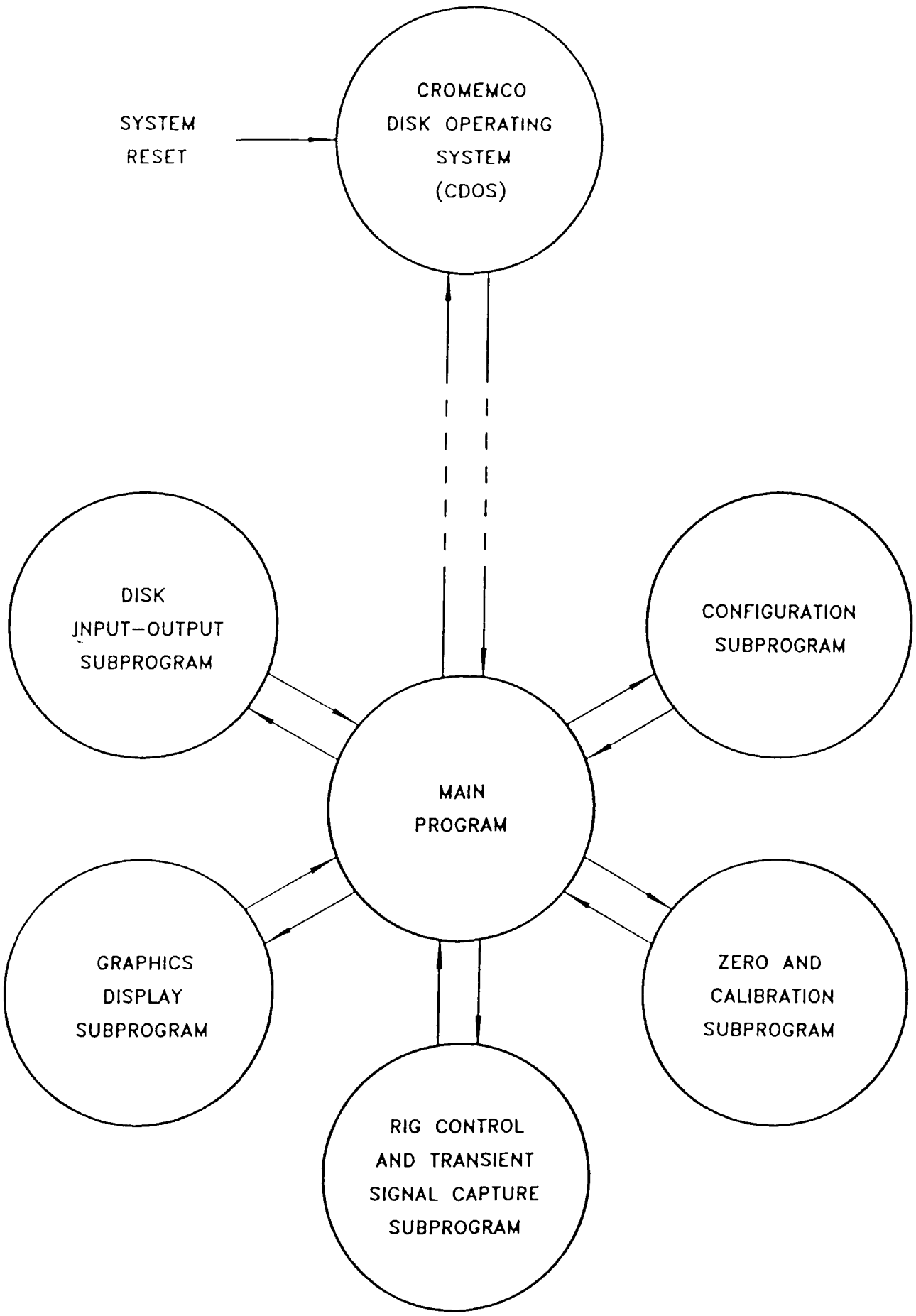

FIGURE 4.28 SIMPLIFIED STATE DIAGRAM OF THE TRANSIENT SIGNAL CAPTURE PROGRAM

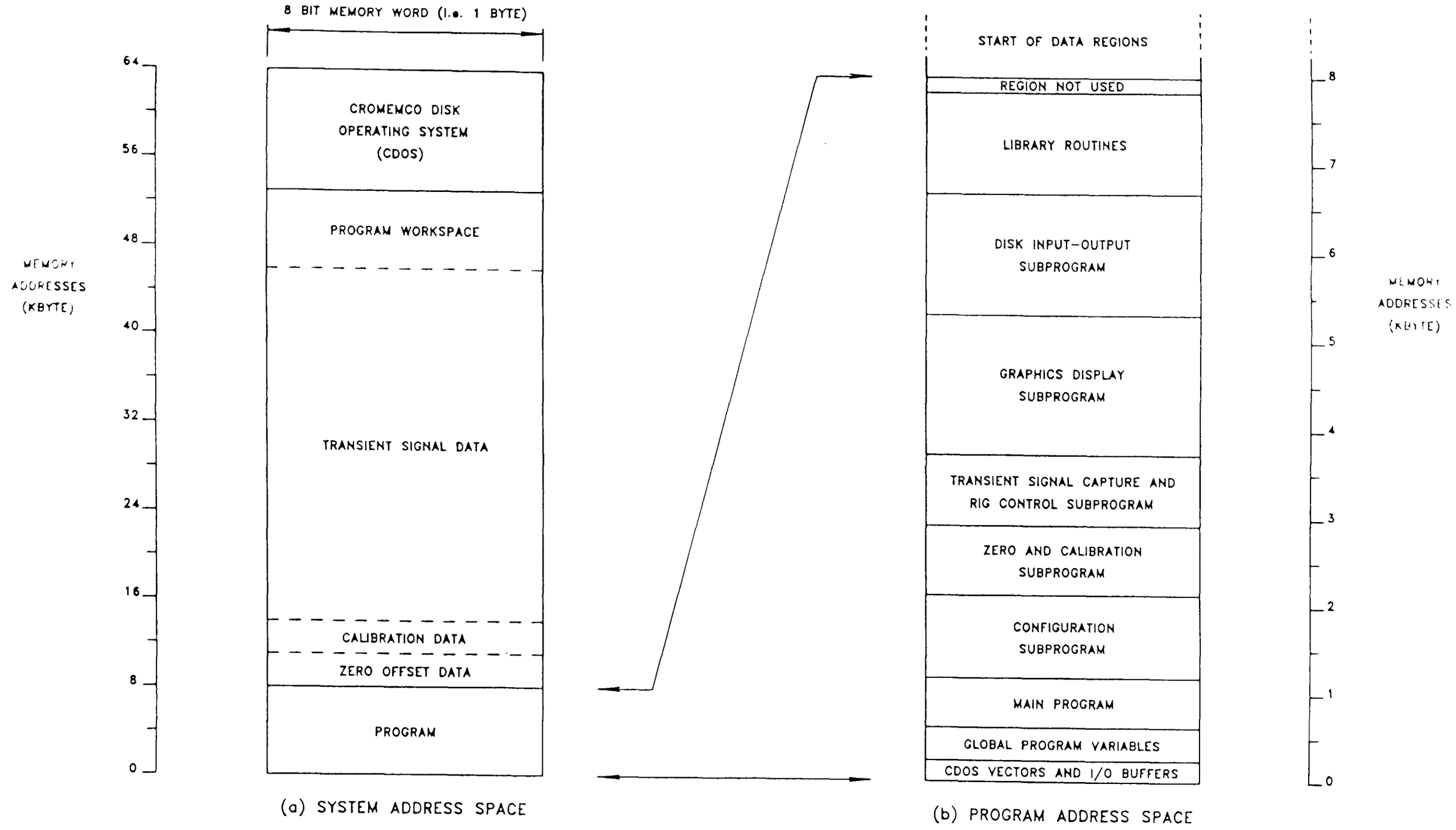

FIGURE 4.29 MEMORY MAPS FOR THE TRANSIENT SIGNAL DATA CAPTURE PROGRAM

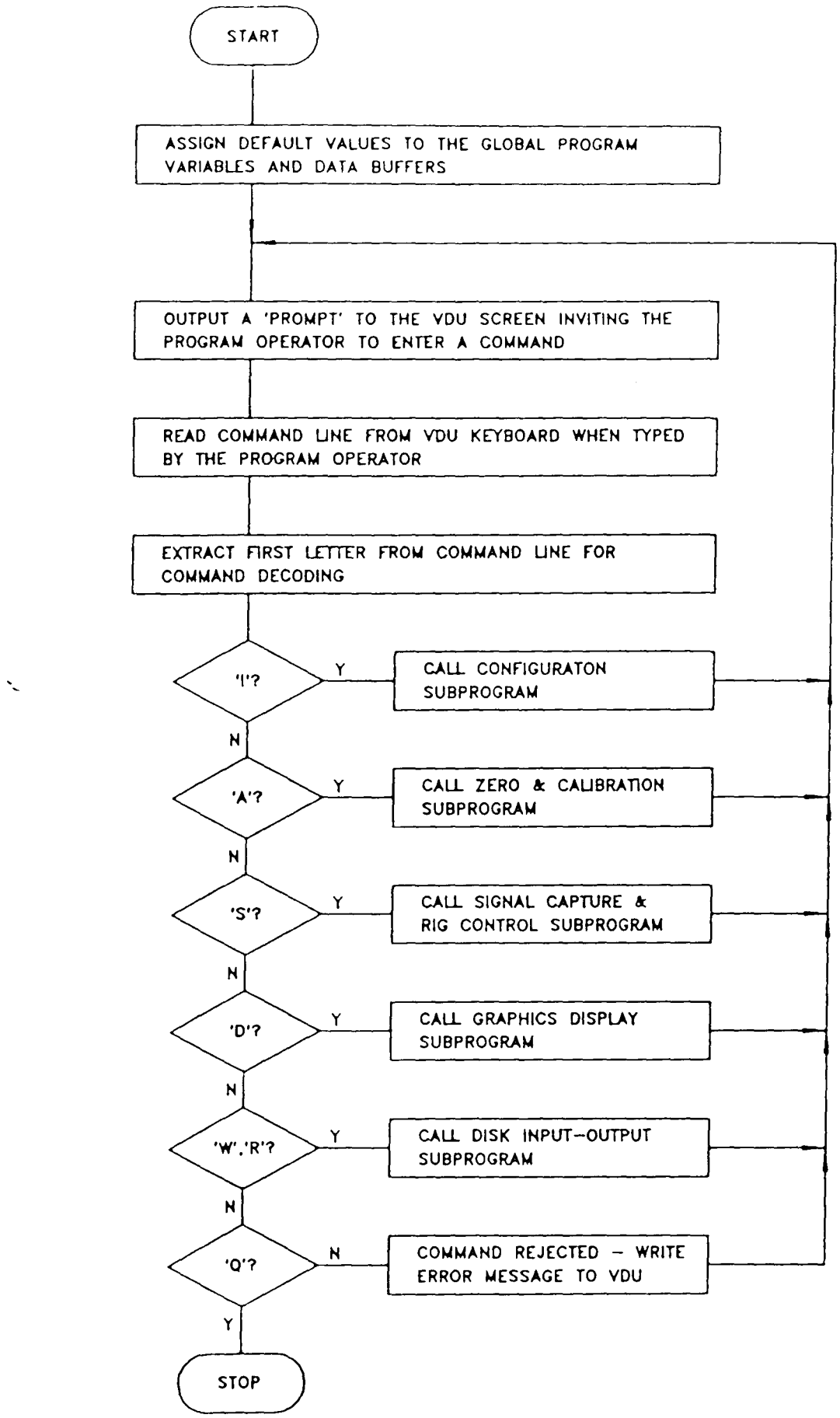

FIGURE 4.30 FLOWCHART OF THE MAIN PROGRAM IN THE MICROCOMPUTER DATA CAPTURE PROGRAM

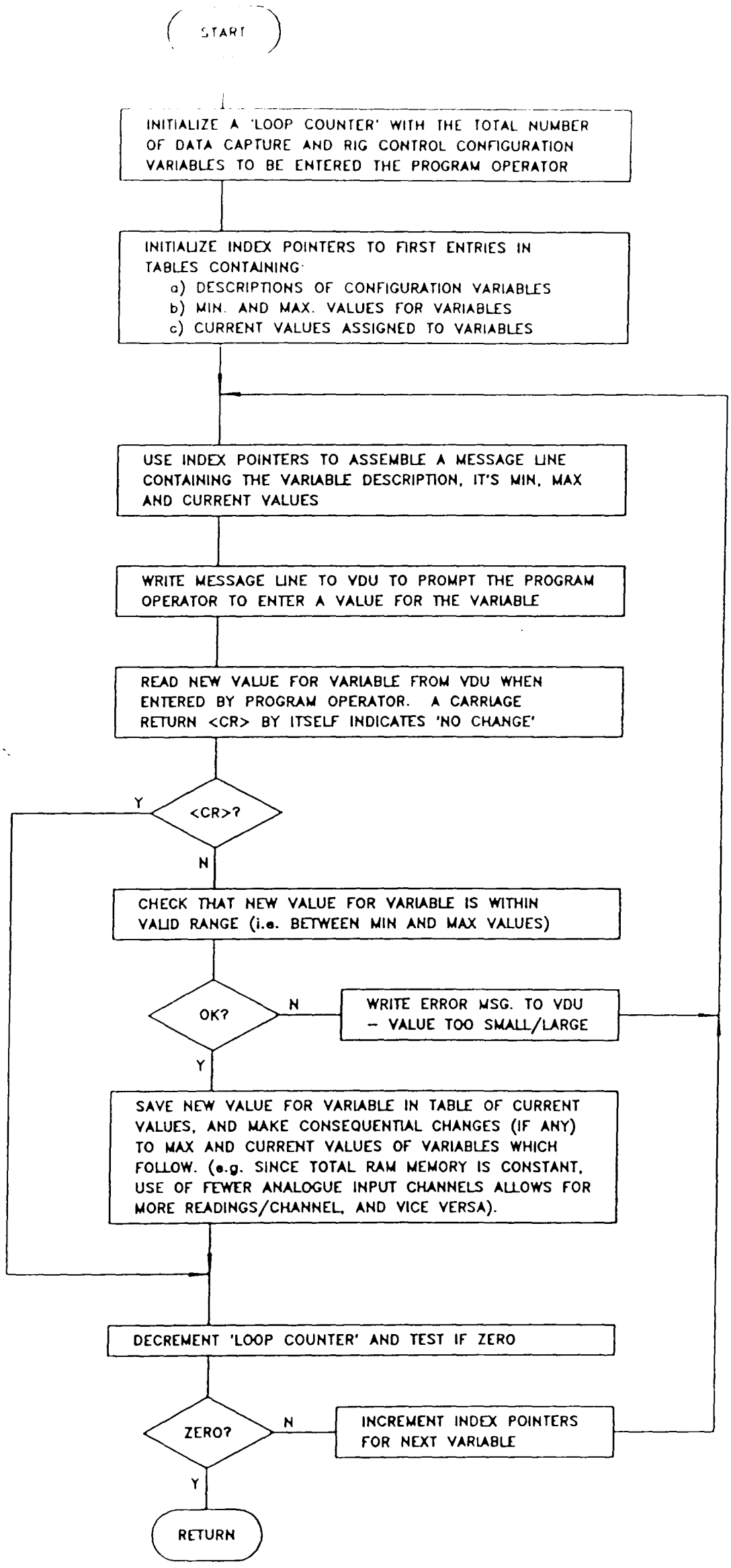

FIGURE 4.31 FLOWCHART OF CONFIGURATION SUBPROGRAM IN MICROCOMPUTER DATA CAPTURE PROGRAM

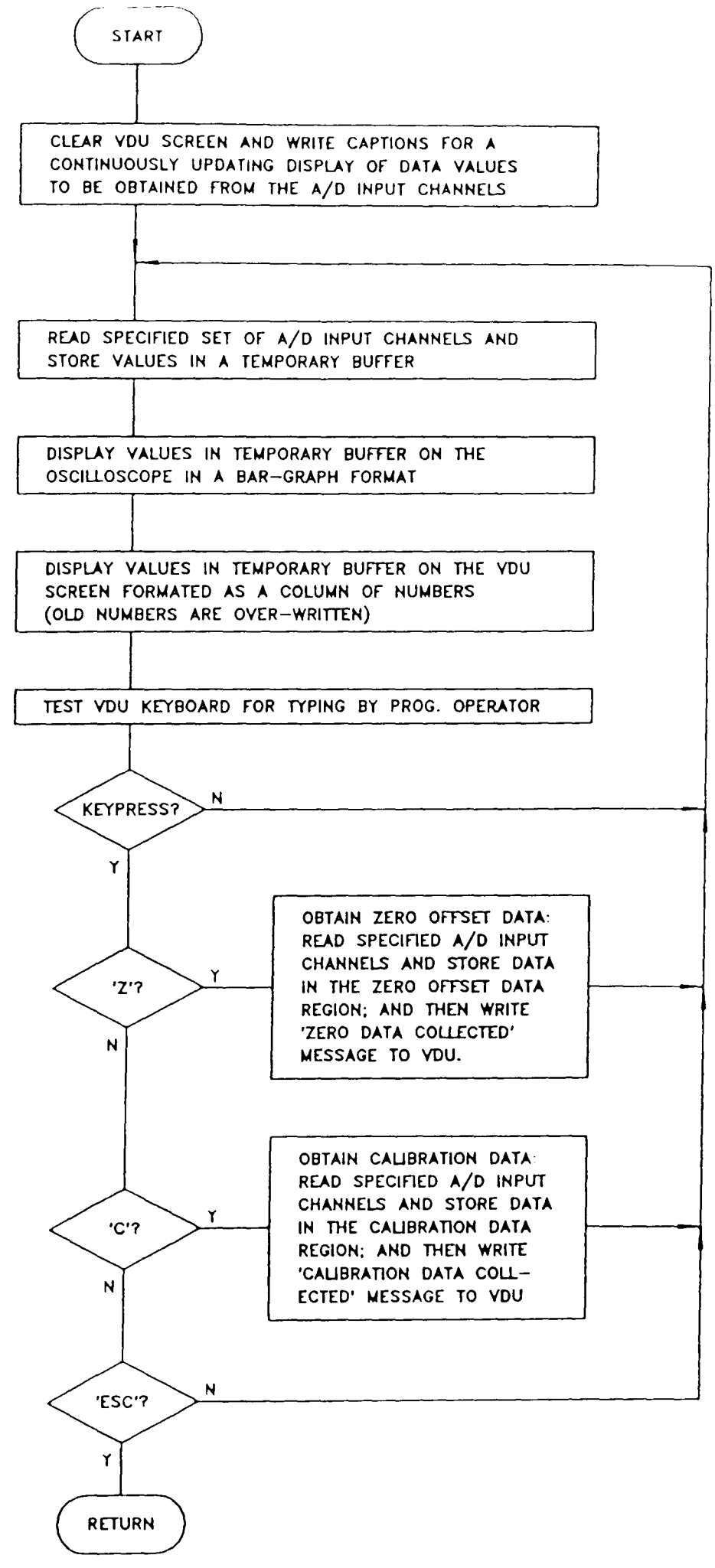

FIGURE 4.32 FLOWCHART OF ZERO AND CAL SUBPROGRAM IN MICROCOMPUTER DATA CAPTURE PROGRAM

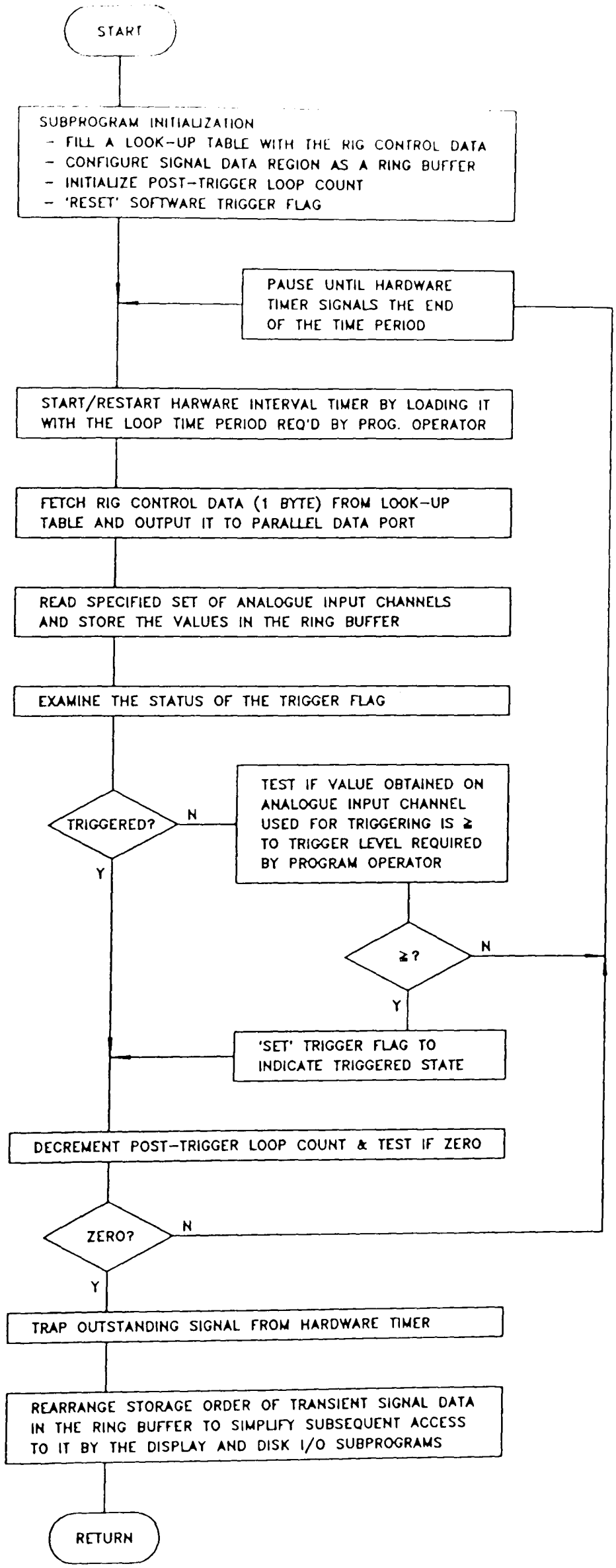

FIGURE 4.33 FLOWCHART OF SIGNAL CAPTURE SUBPROGRAM IN MICROCOMPUTER DATA CAPTURE PROGRAM

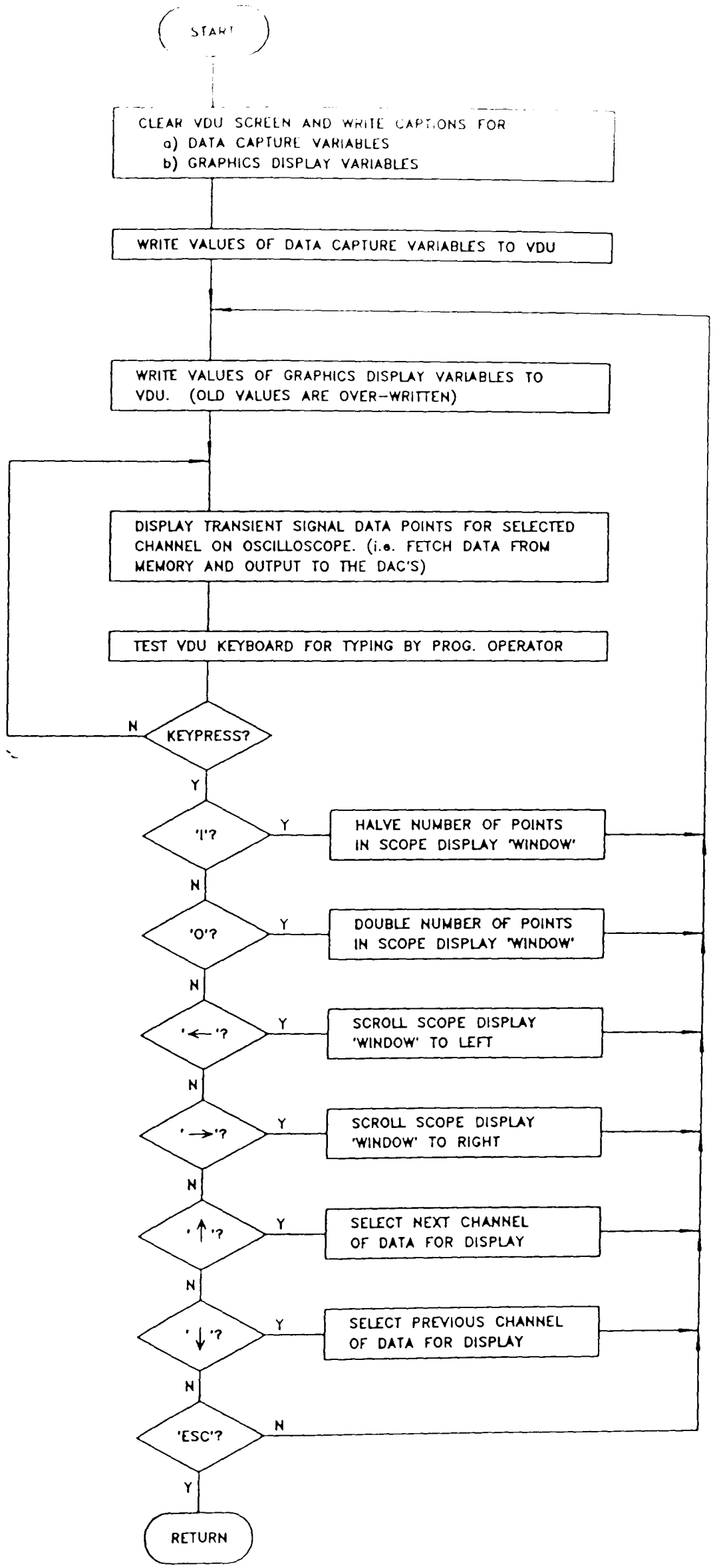

FIGURE 4.34 FLOWCHART OF GRAPHIC DISPLAY SUBPROGRAM IN MICROCOMPUTER DATA CAPTURE PROGRAM

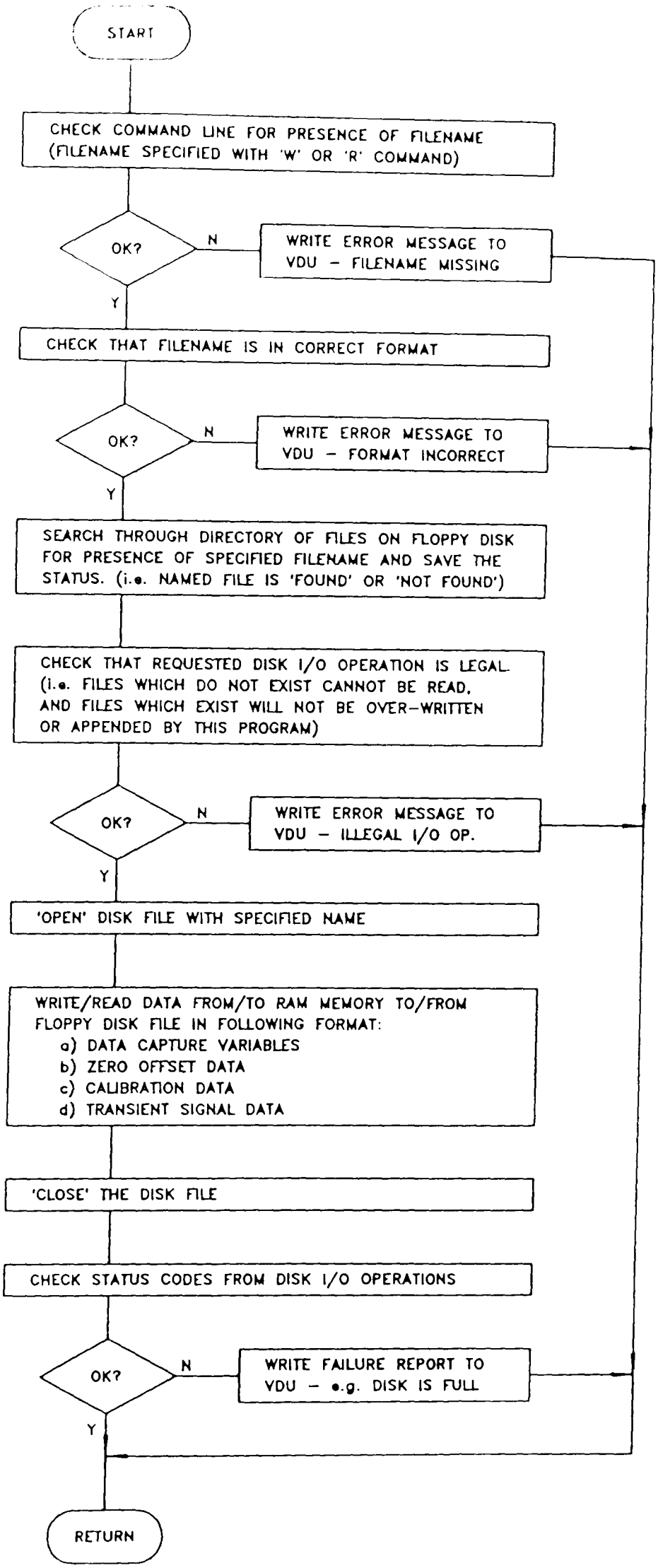

FIGURE 4.35 FLOWCHART OF DISK I/O SUBPROGRAM IN MICROCOMPUTER DATA CAPTURE PROGRAM

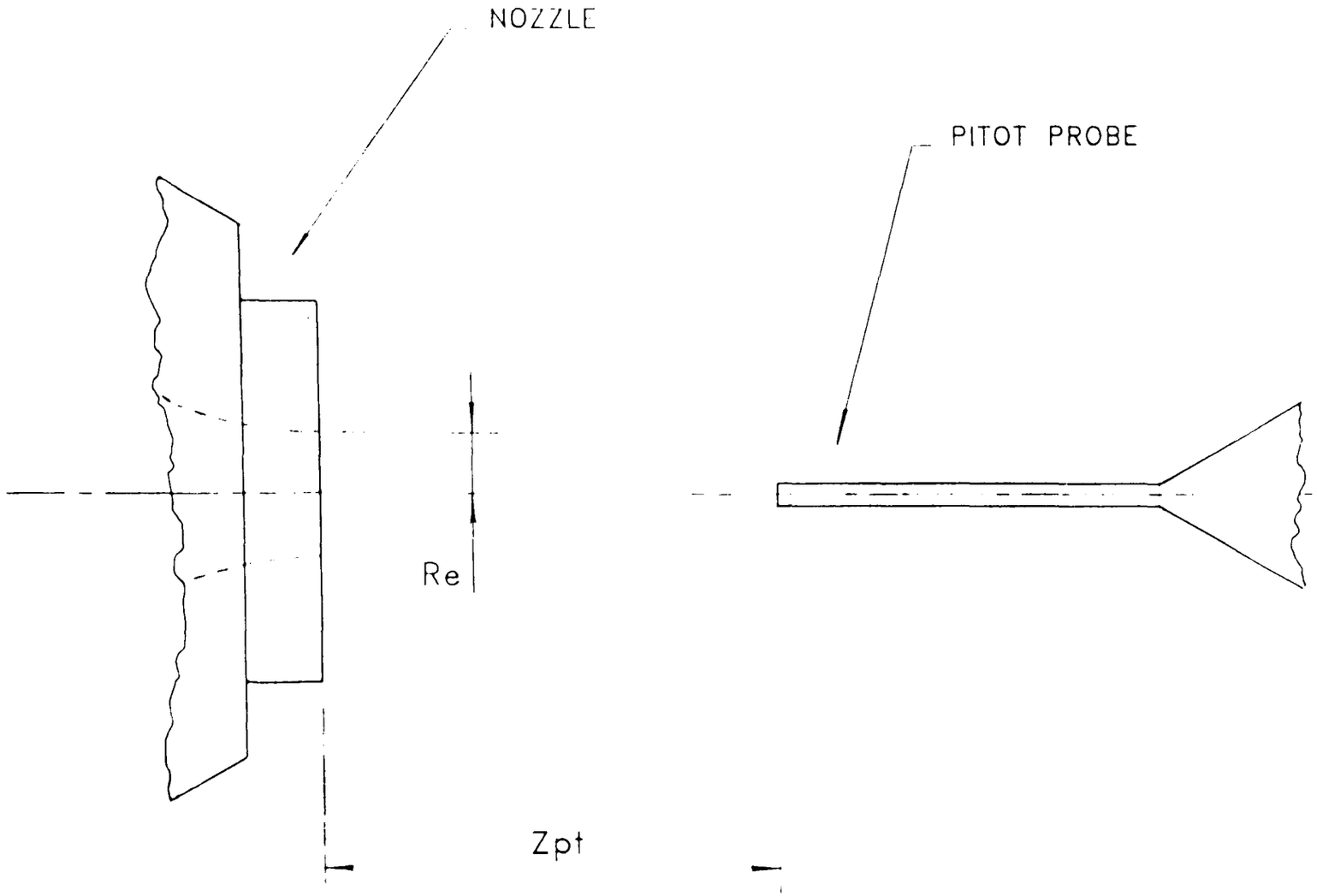

FIGURE 5.1 NOMENCLATURE FOR FREE JET TEST CONFIGURATIONS

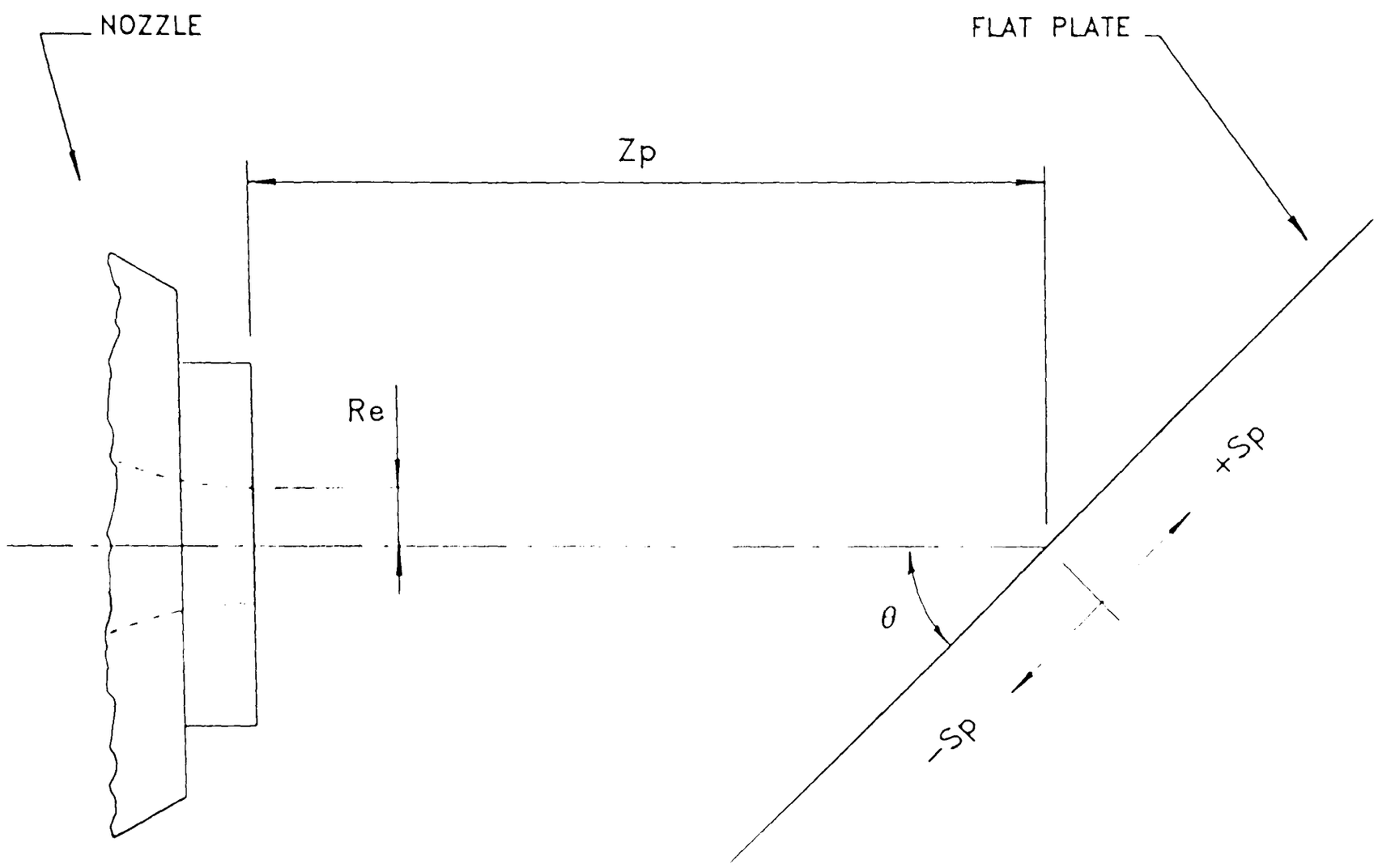

FIGURE 5.2 NOMENCLATURE FOR IMPINGING JET TEST CONFIGURATIONS

a) NOZZLE AXIS ALIGNMENT

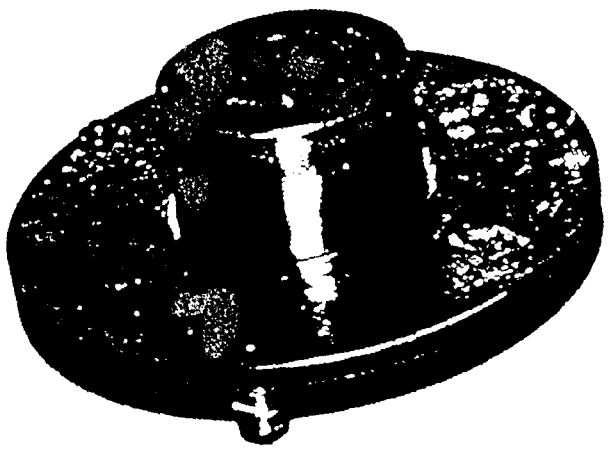

b) PLATE AND PROBE HOLDER MOUNTING BRACKET ALIGNMENT

c) PLATE TAPPING AND PITOT PROBE ORIFICE ALIGNMENT

FIGURE 5.3 TEST RIG ALIGNMENT DEVICES

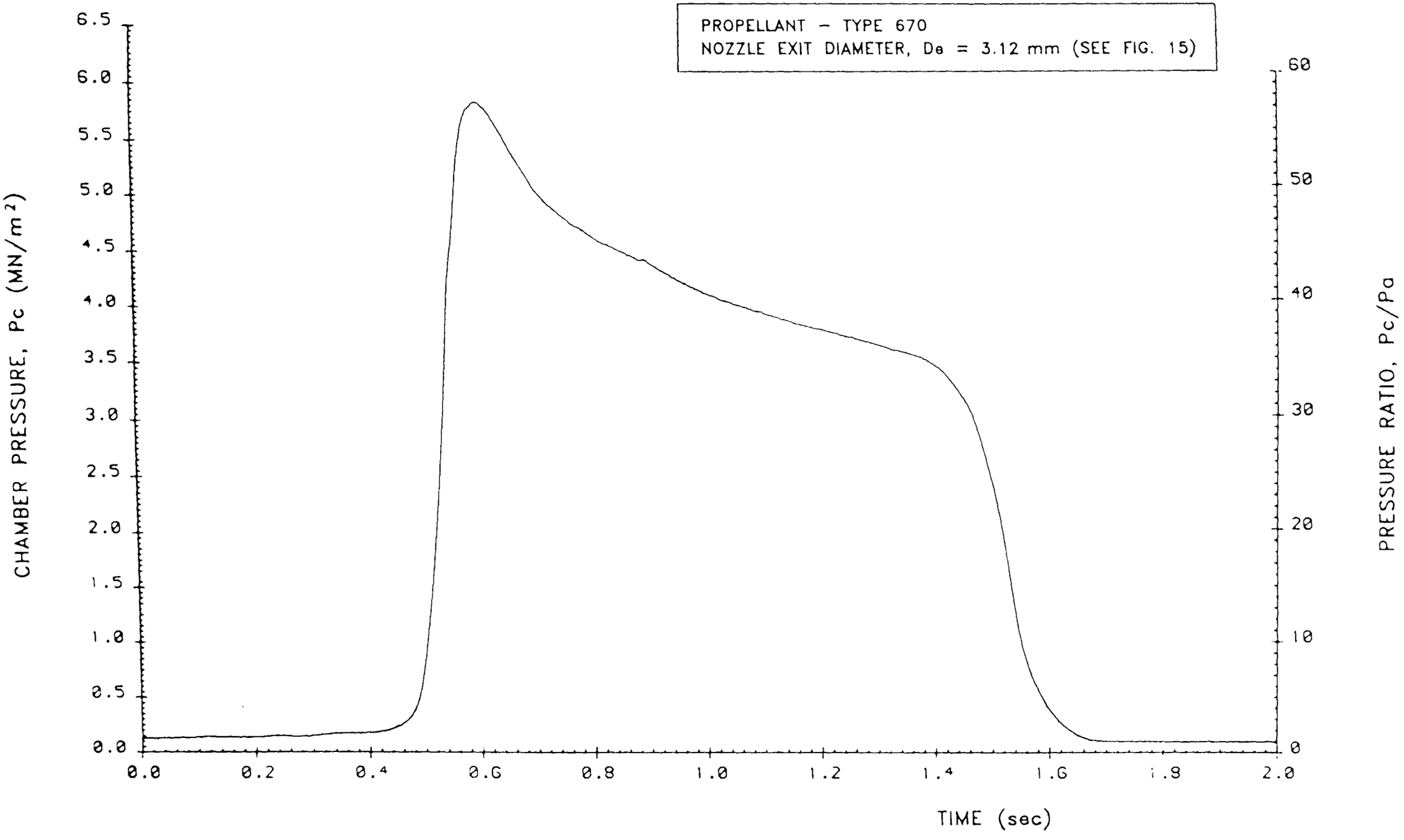

FIGURE 5.4 SAMPLE RECORDING OF THE ROCKET MOTOR COMBUSTION CHAMBER PRESSURE

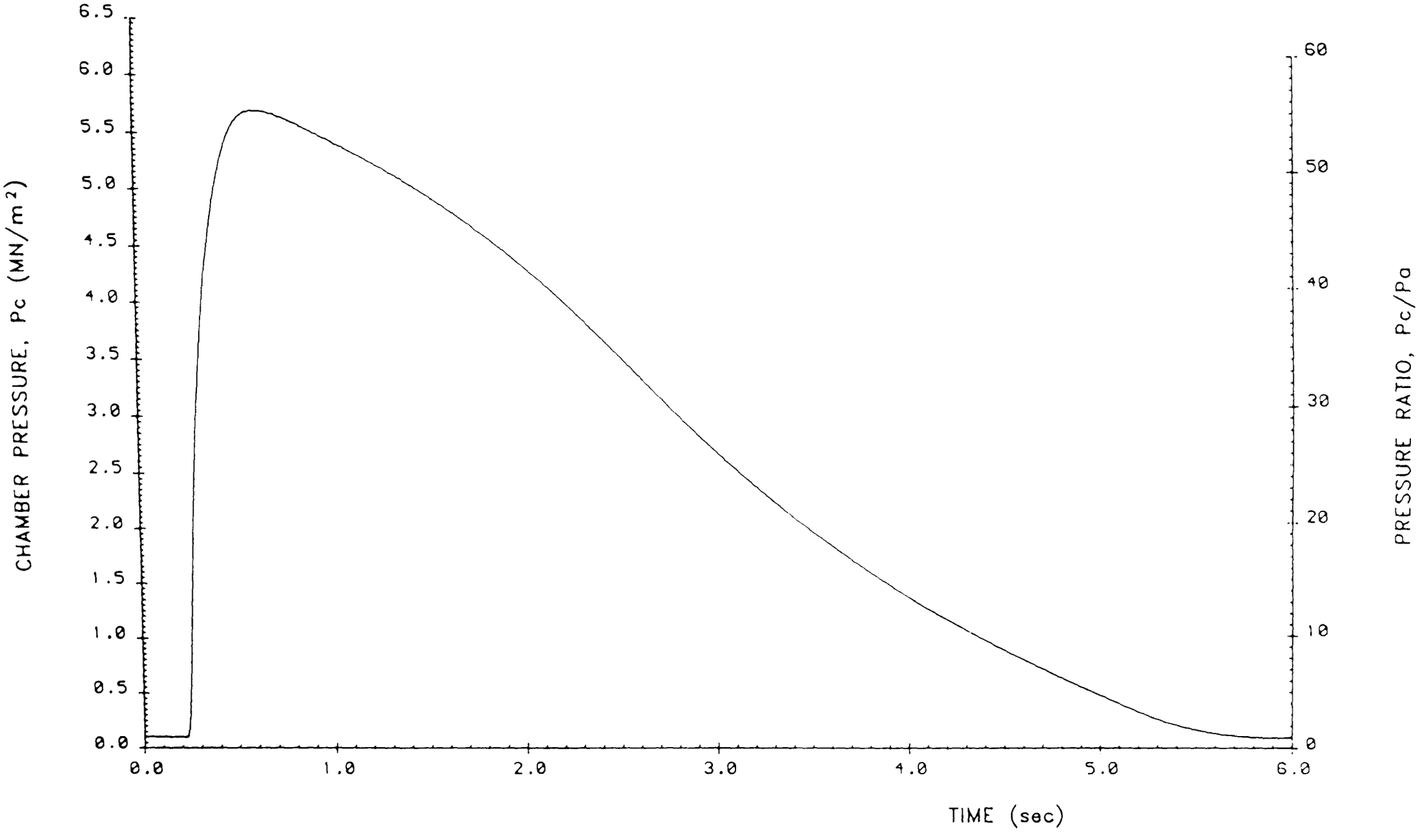

FIGURE 5.5 SAMPLE RECORDING OF THE NITROGEN JET SETTLING CHAMBER PRESSURE

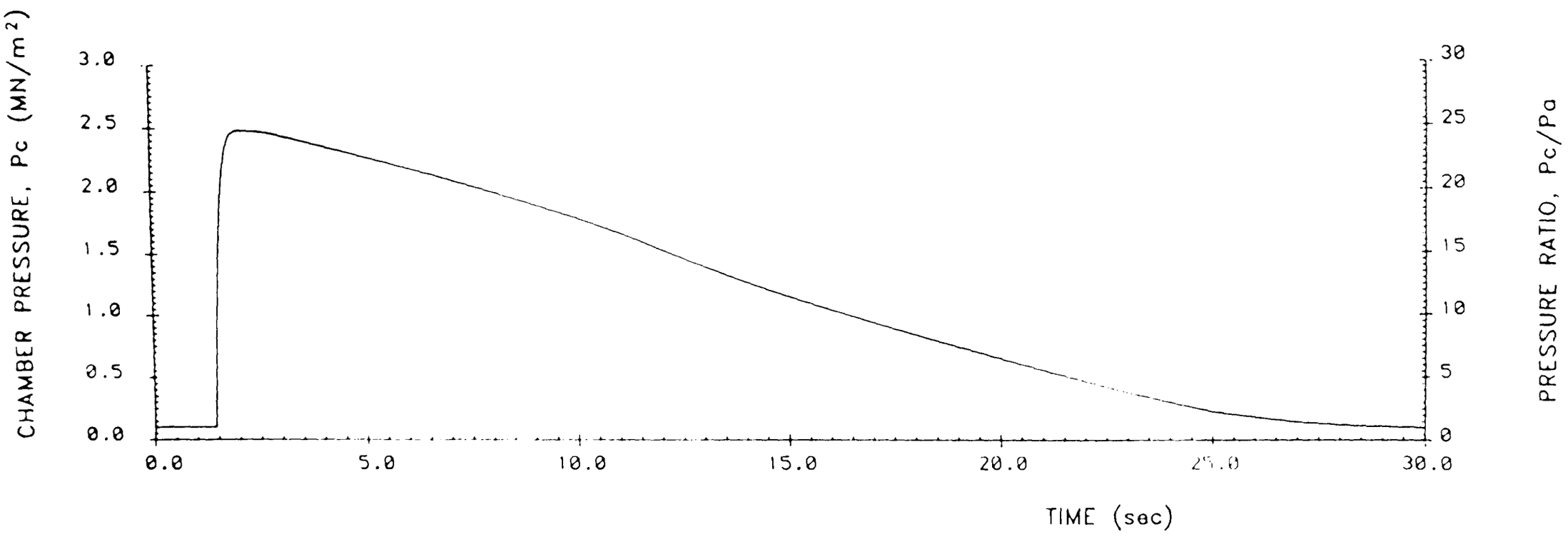

FIGURE 5.6 SAMPLE RECORDING OF THE AIR JET SETTLING CHAMBER PRESSURE

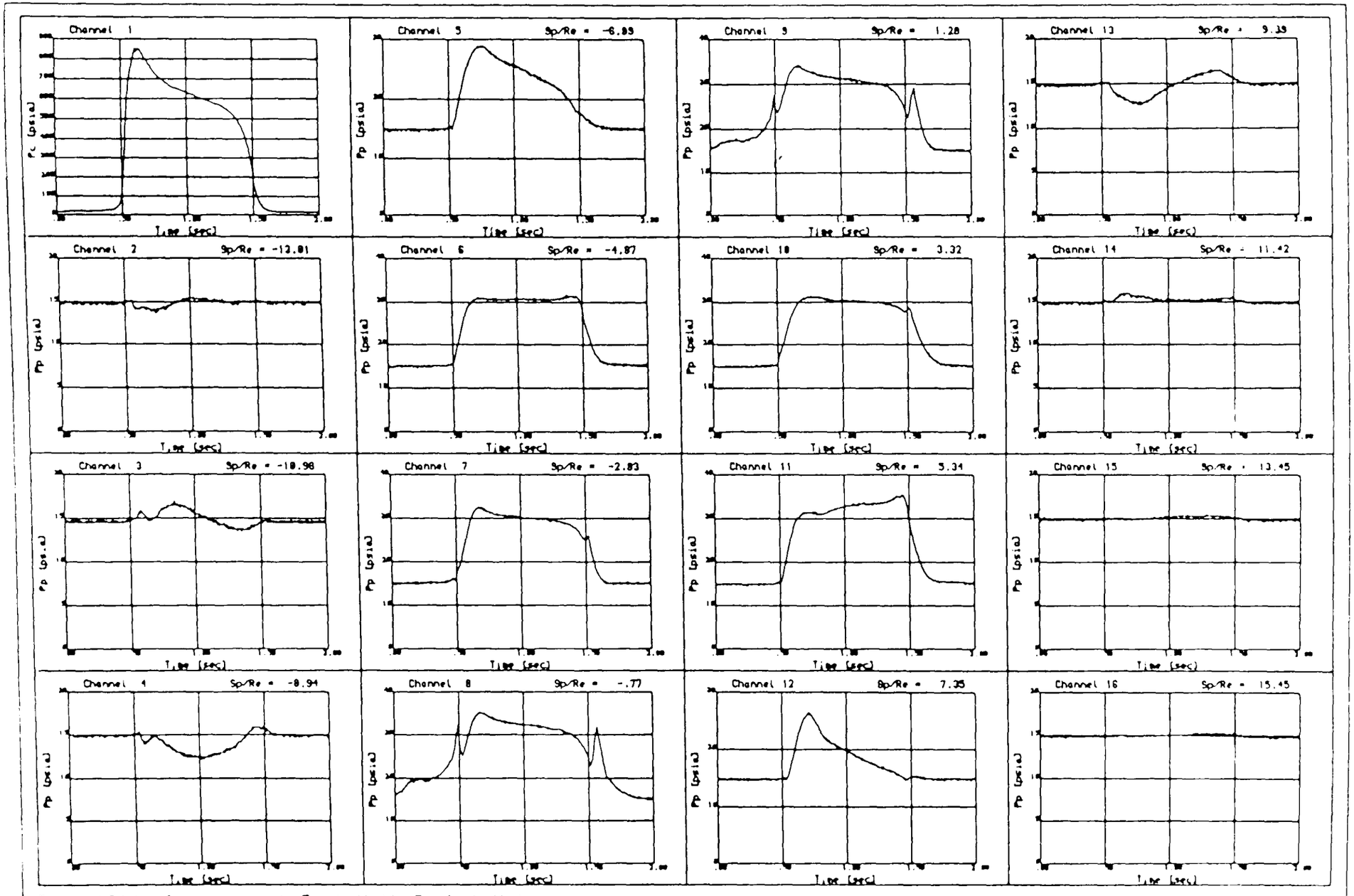

FIGURE 5.7 SAMPLE OF A GRAPHICAL PRESSURE–TIME RECORD FROM AN IMPINGEMENT TEST

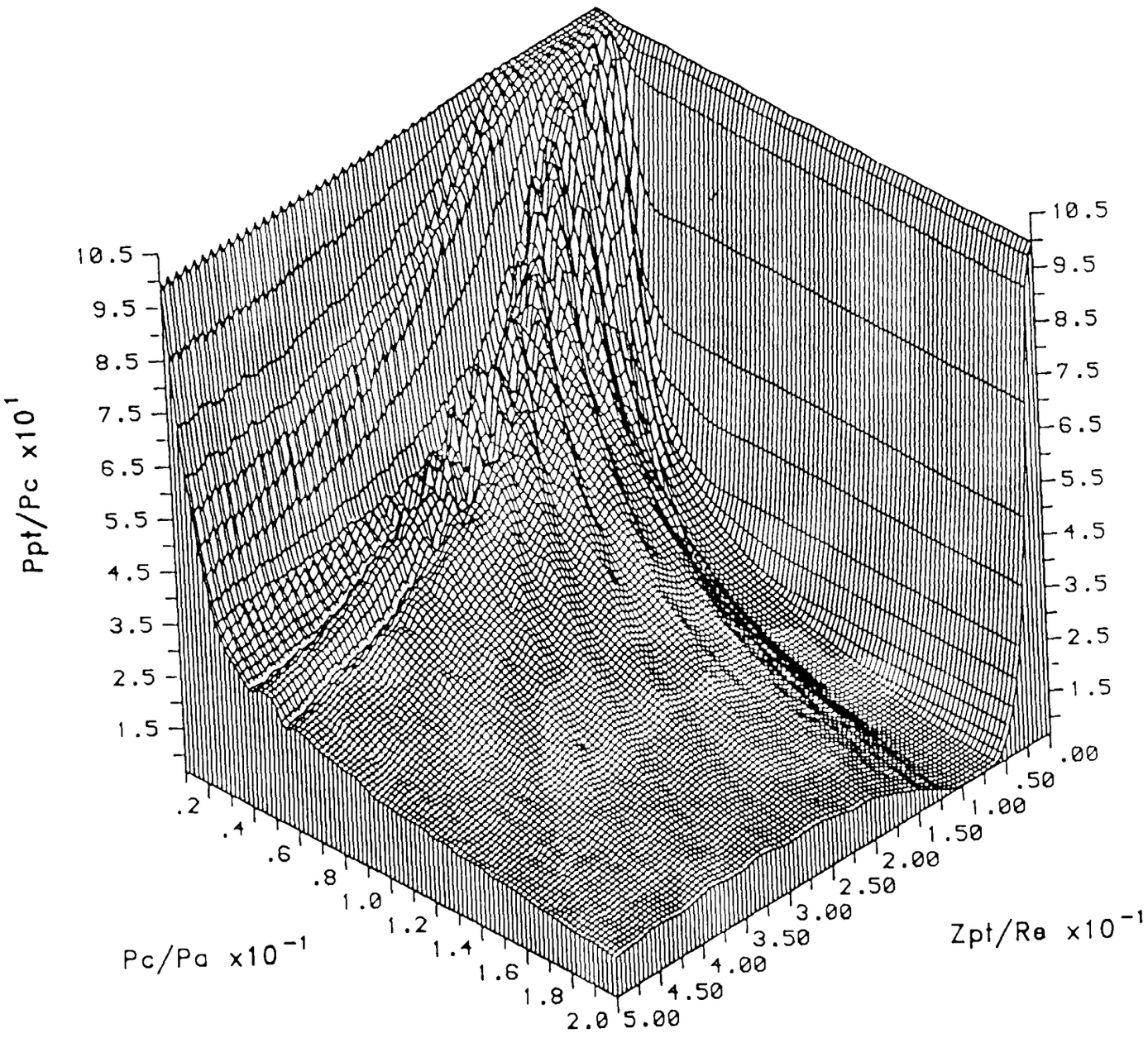

FIGURE 6.1 FREE AIR JET – ISOMETRIC PLOT OF VARIATION OF JET CENTRELINE PITOT PRESSURE DISTRIBUTION WITH JET PRESSURE RATIO FOR: Me=1.0

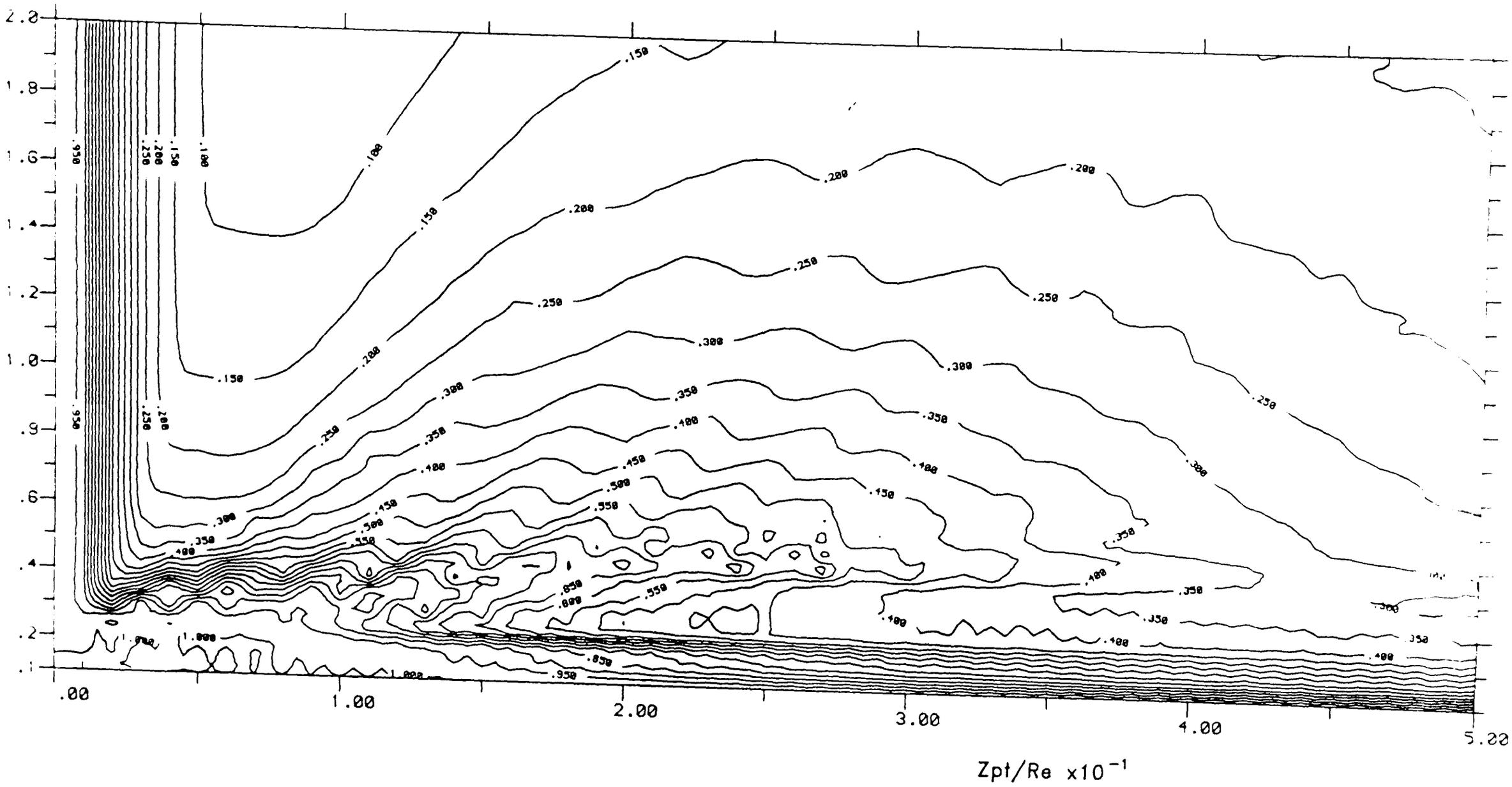

FIGURE 6.2 FREE AIR JET – CONTOUR PLOT OF VARIATION OF JET CENTRELINE PITOT PRESSURE DISTRIBUTION WITH JET PRESSURE RATIO FOR: Me=1.0

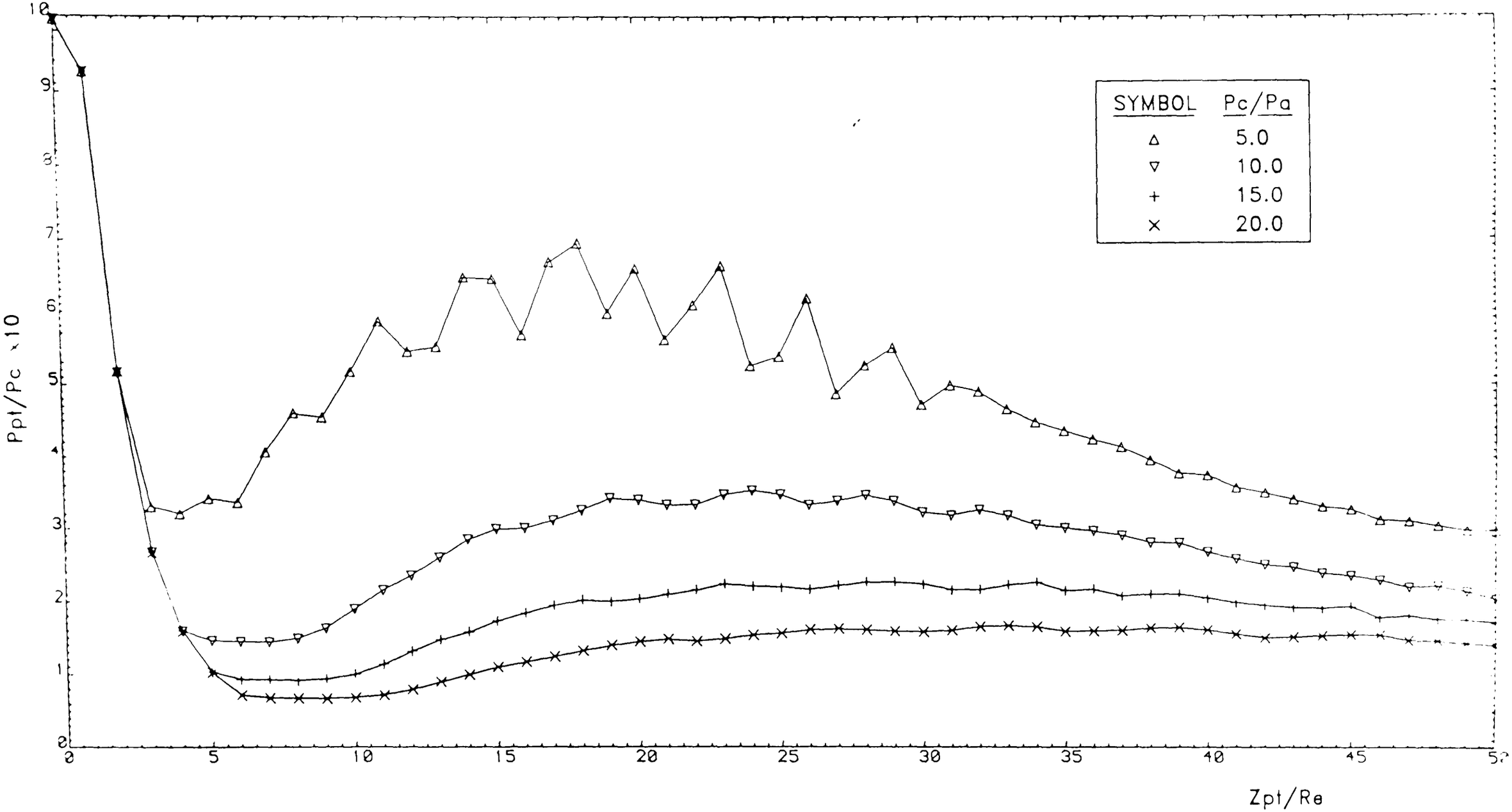

FIGURE 6.3 PITOT PRESSURE DISTRIBUTIONS ALONG AXIS OF FREE AIR JET FOR: Me=1.0; Pc/Pa=5.0, 10.0, 15.0, 20.0

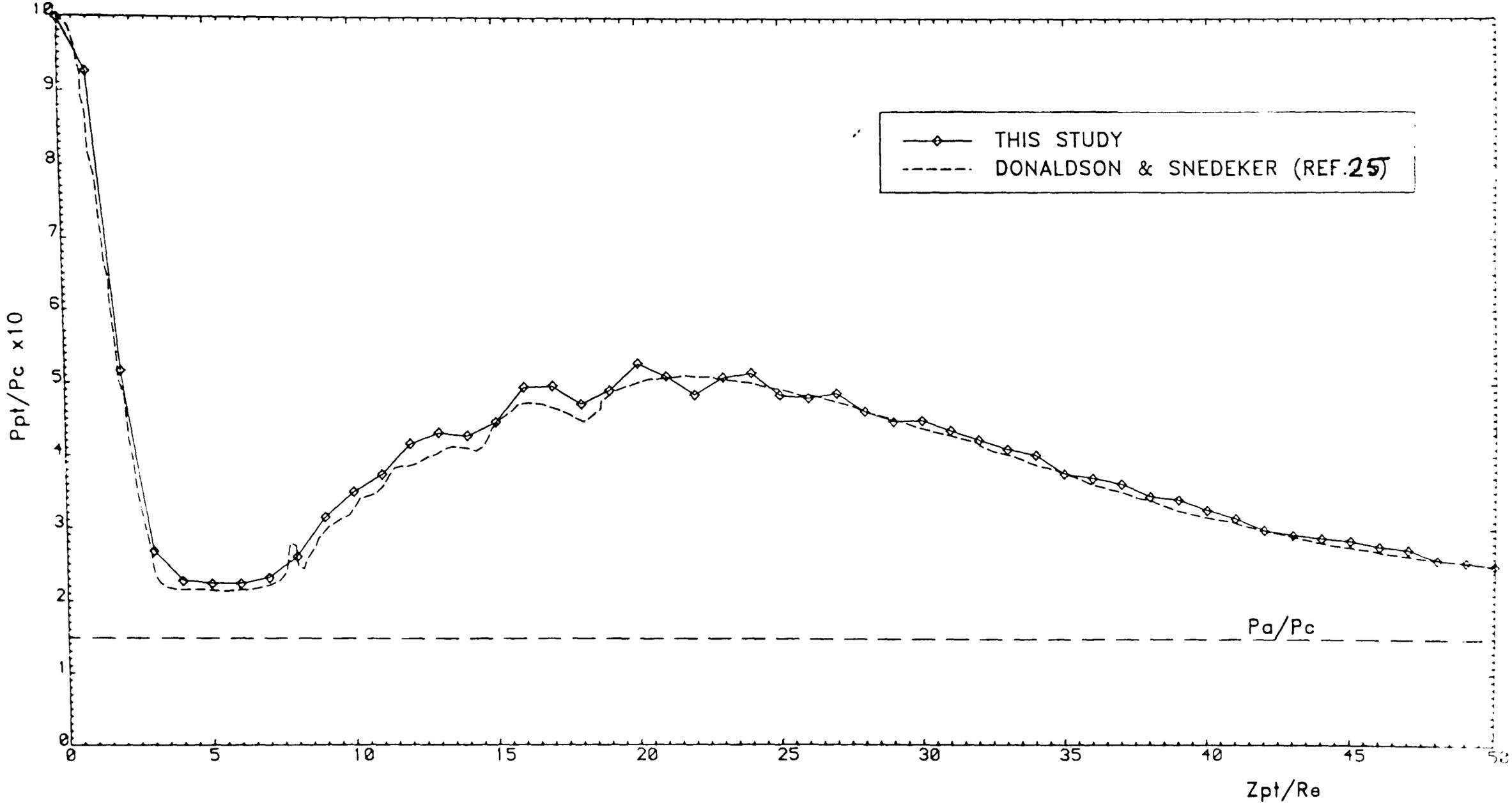

FIGURE 6.4 COMPARISON OF PITOT PRESSURE DISTRIBUTIONS ALONG AXES OF FREE AIR JETS OBTAINED IN THIS STUDY AND BY DONALDSON & SNEDEKER FOR: Me=1.0, Pc/Pa=6.758

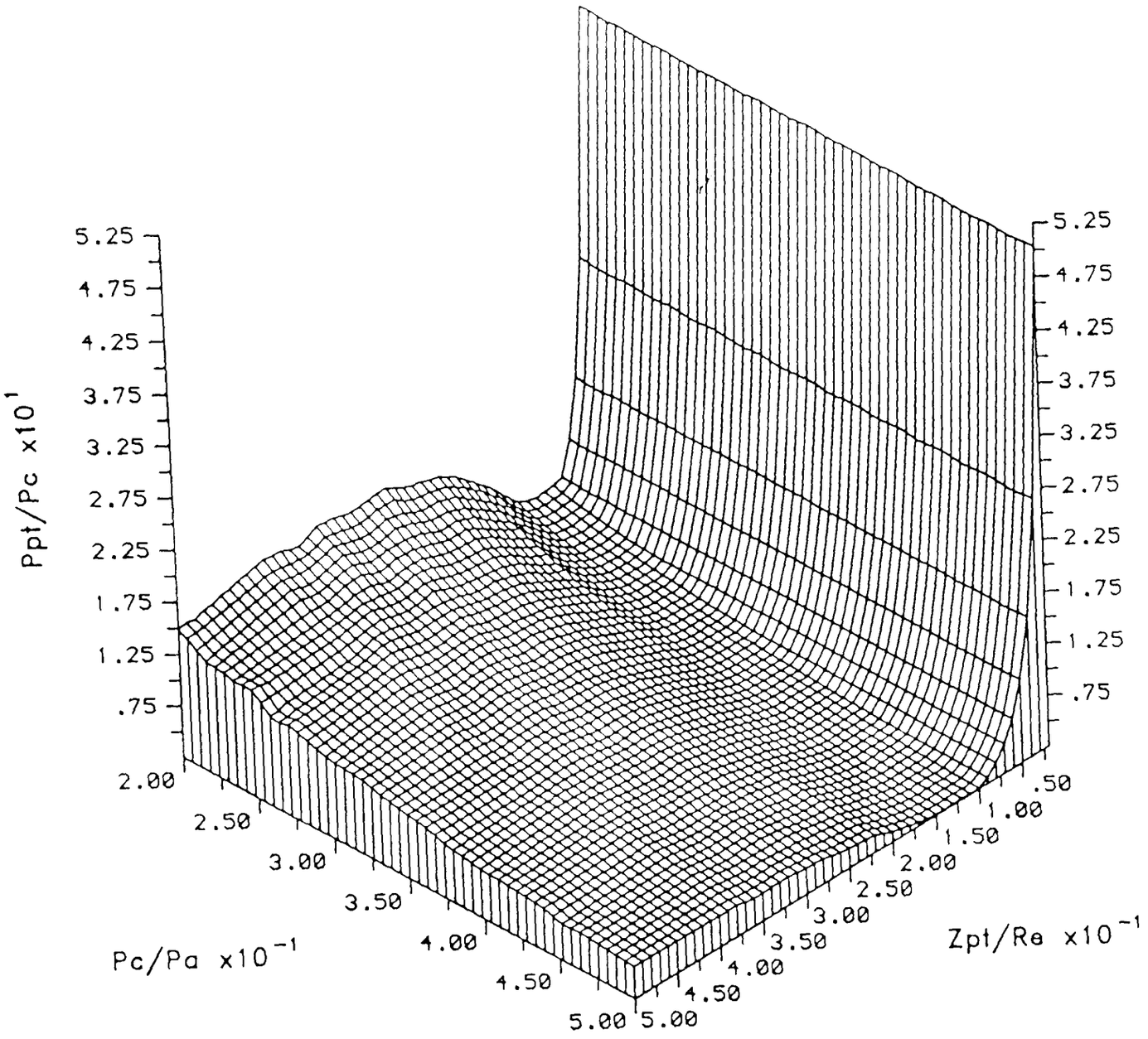

FIGURE 6.5 FREE NITROGEN JET – ISOMETRIC PLOT OF VARIATION OF JET CENTRELINE PITOT PRESSURE DISTRIBUTION WITH JET PRESSURE RATIO FOR: Me=1.0

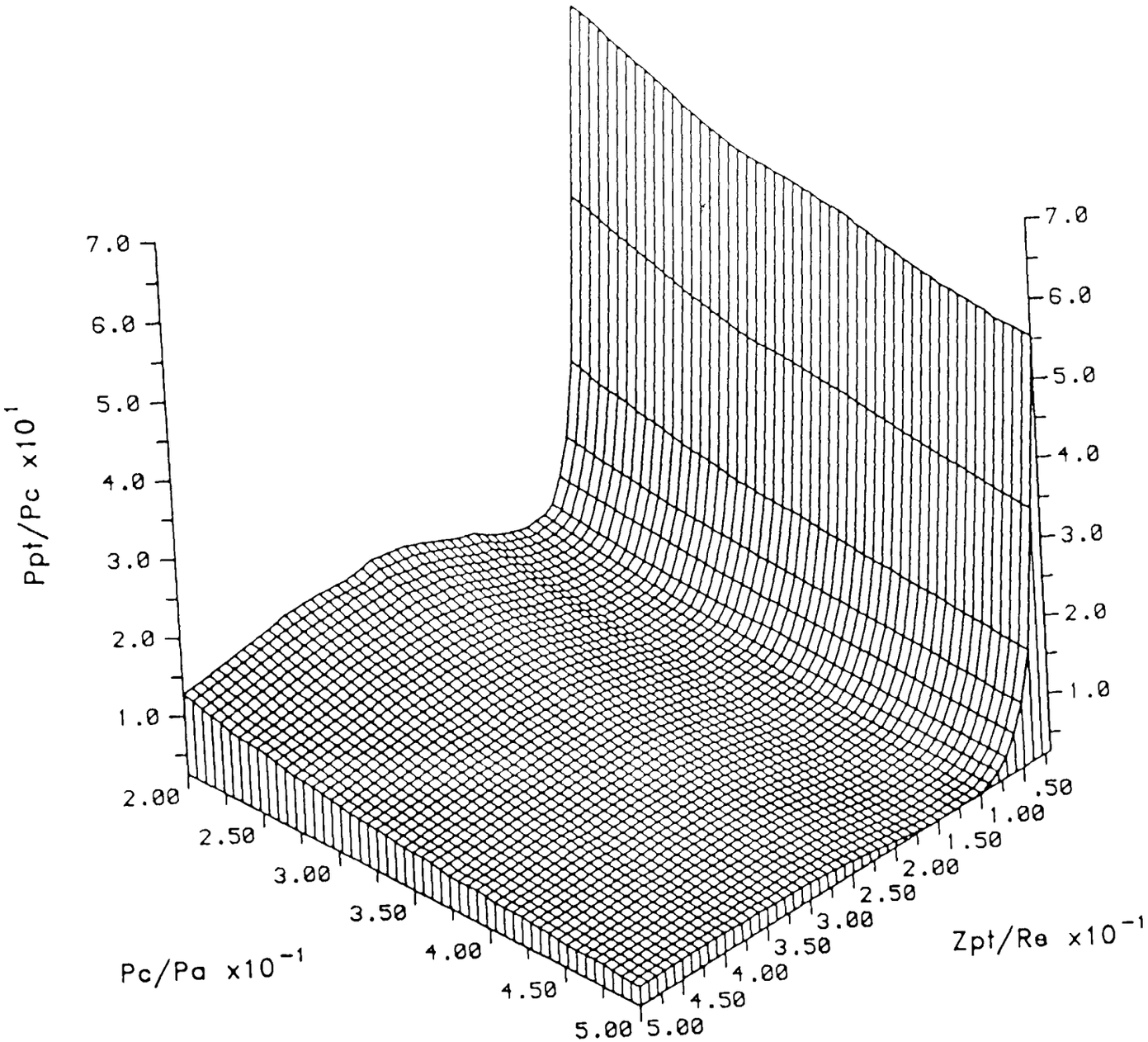

FIGURE 6.6 FREE ROCKET JET – ISOMETRIC PLOT OF VARIATION OF JET CENTRELINE PITOT PRESSURE DISTRIBUTION WITH JET PRESSURE RATIO FOR: Me=1.0

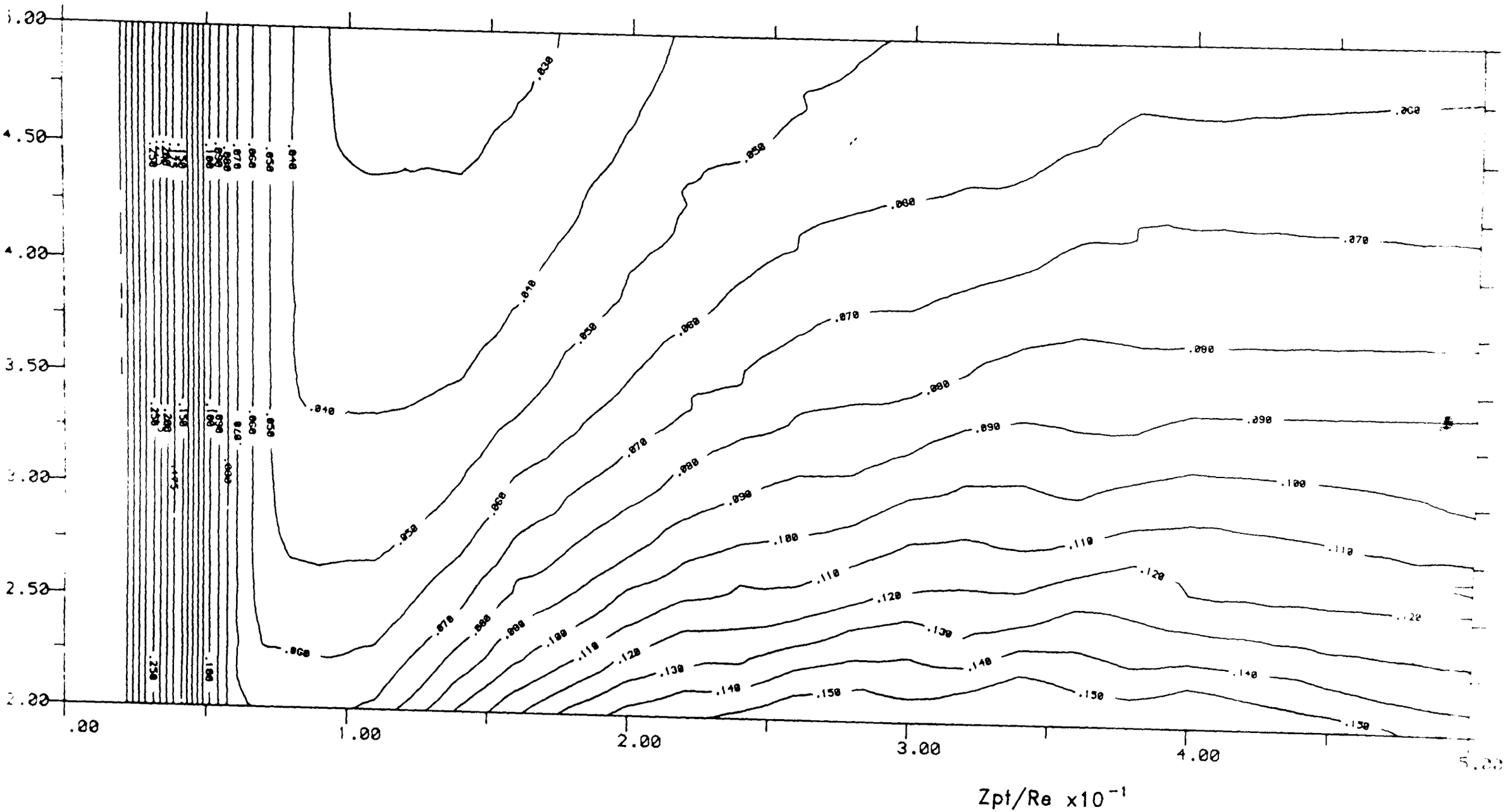

FIGURE 6.7 FREE NITROGEN JET – CONTOUR PLOT OF VARIATION OF JET CENTRELINE PITOT PRESSURE DISTRIBUTION WITH JET PRESSURE RATIO FOR: Me=1.0

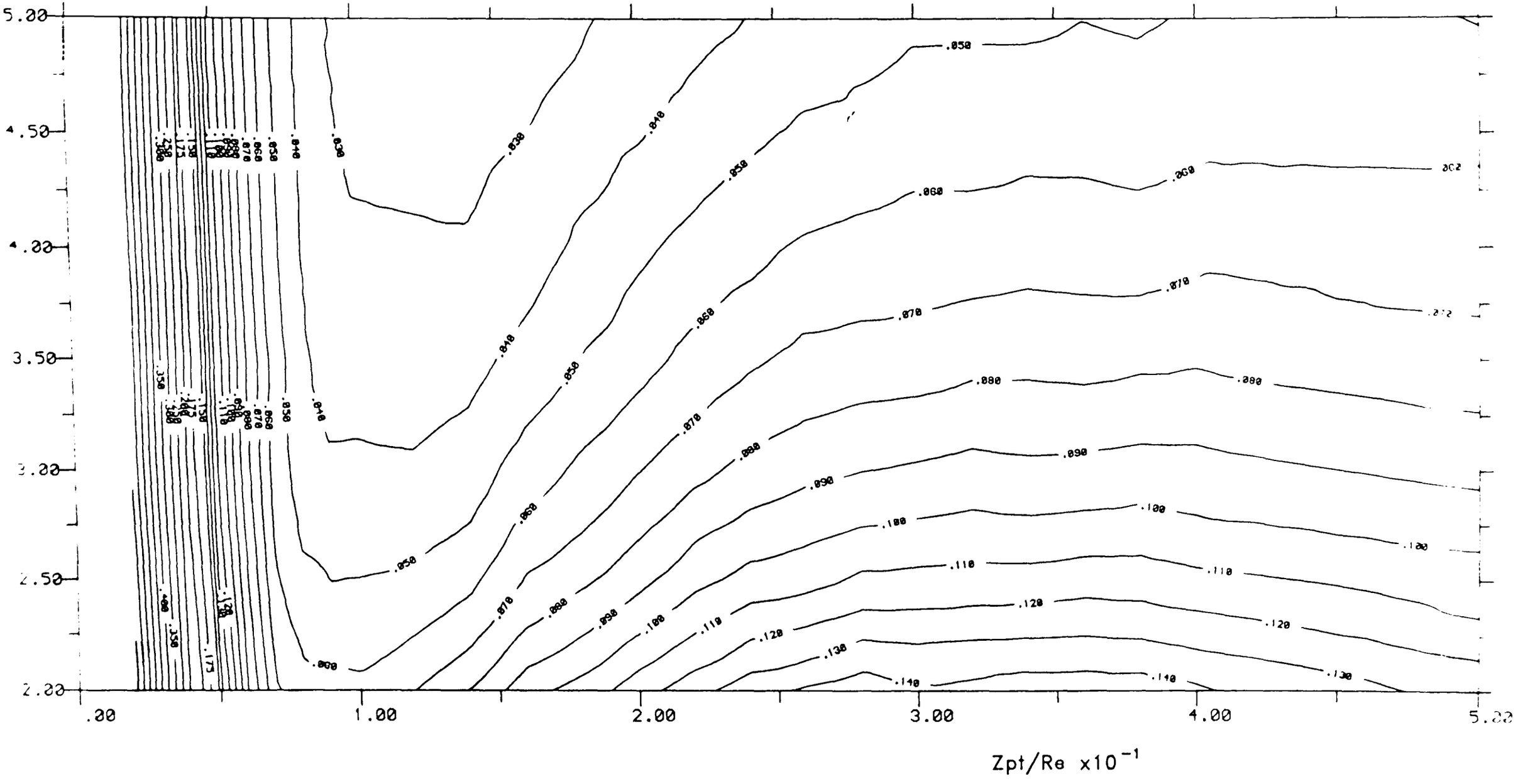

FIGURE 6.8 FREE ROCKET JET – CONTOUR PLOT OF VARIATION OF JET CENTRELINE PITOT PRESSURE DISTRIBUTION WITH JET PRESSURE RATIO FOR: Me=1.0

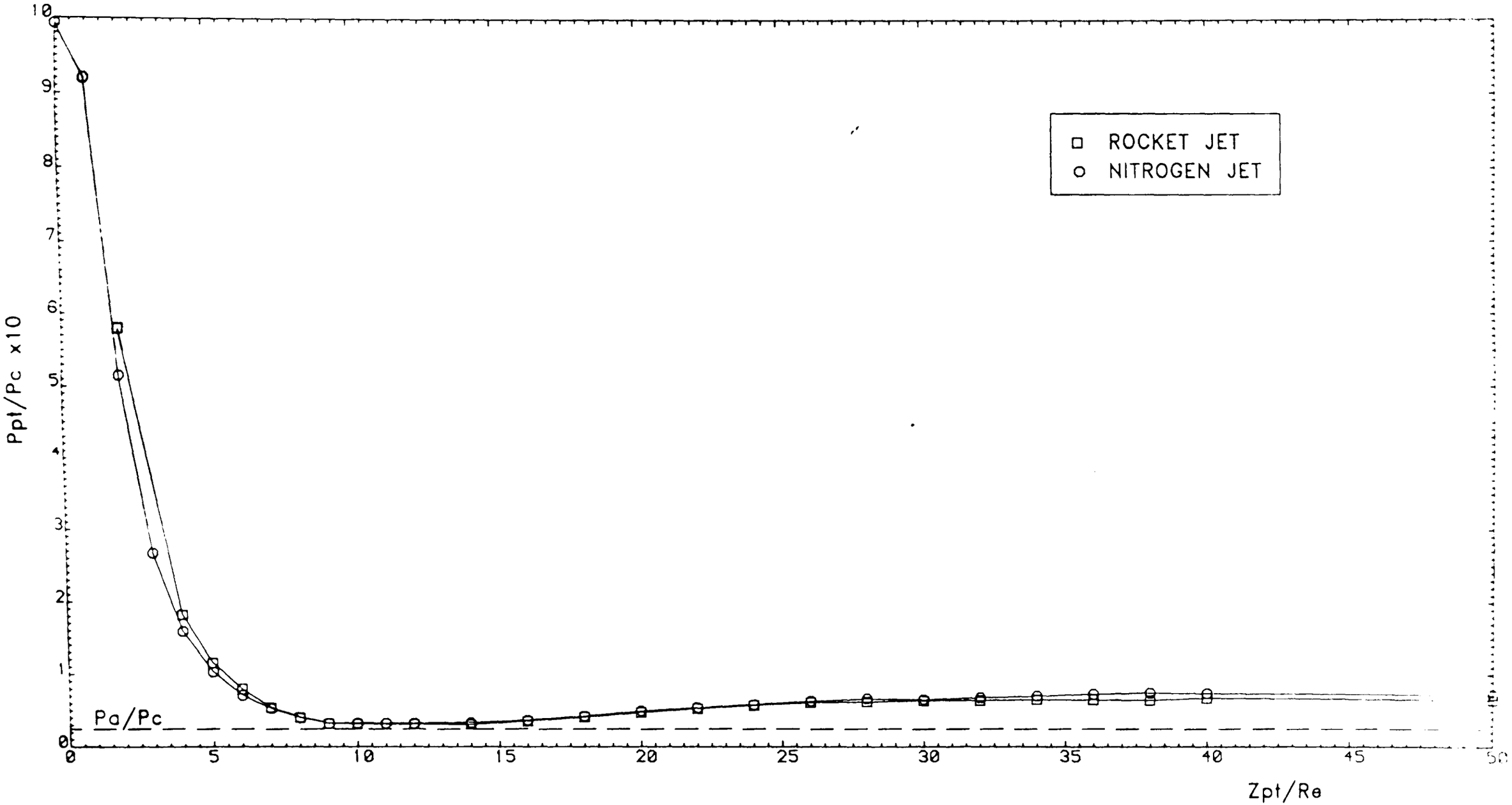

FIGURE 6.9 COMPARISON OF PITOT PRESSURE DISTRIBUTIONS ALONG AXES OF FREE ROCKET AND NITROGEN JETS FOR: Me=1.0, Pc/Pa=40.0

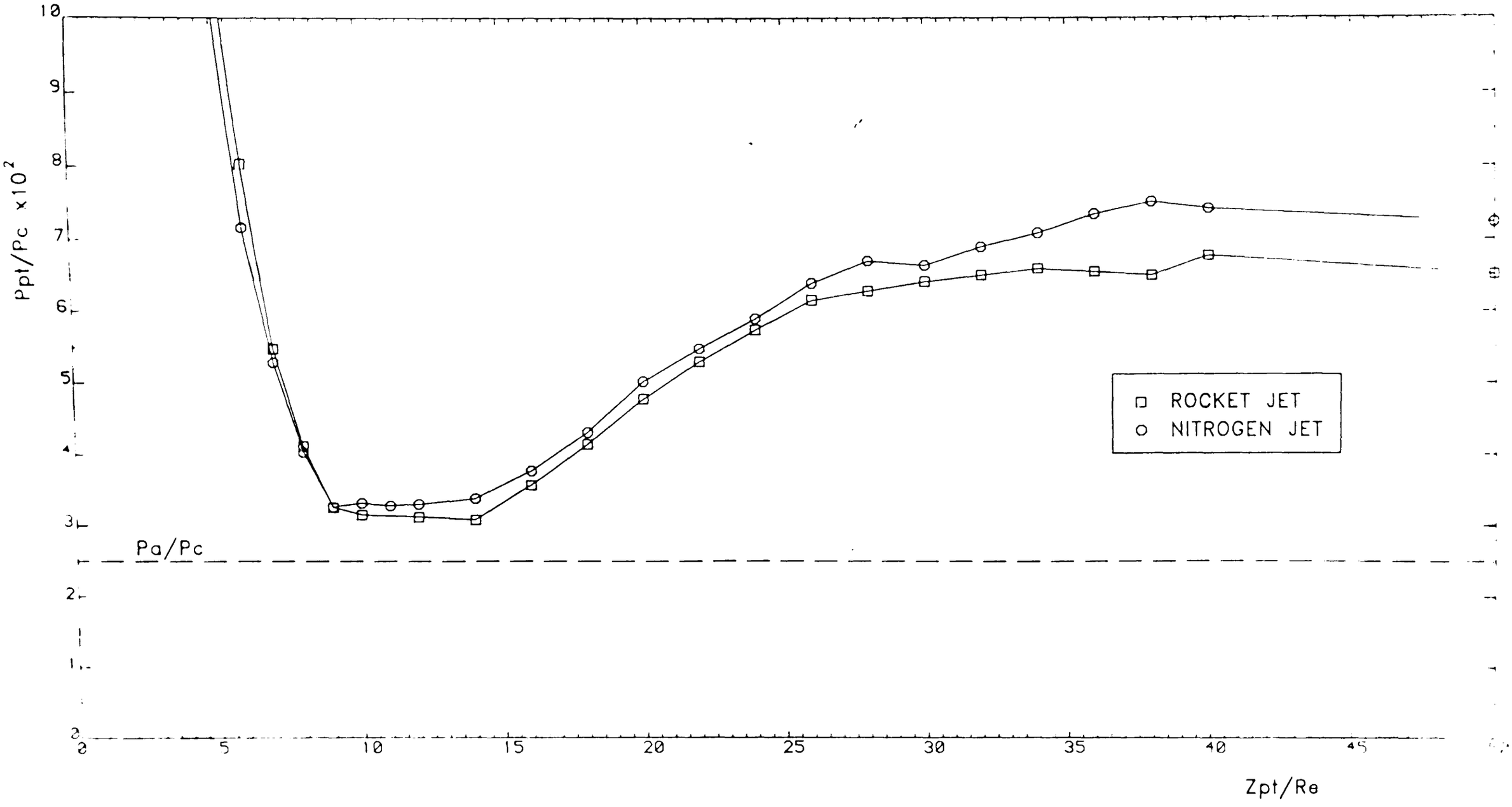

FIGURE 6.10 COMPARISON OF PITOT PRESSURE DISTRIBUTIONS ALONG AXES OF FREE ROCKET AND NITROGEN JETS FOR: Me=1.0, Pc/Pa=40.0

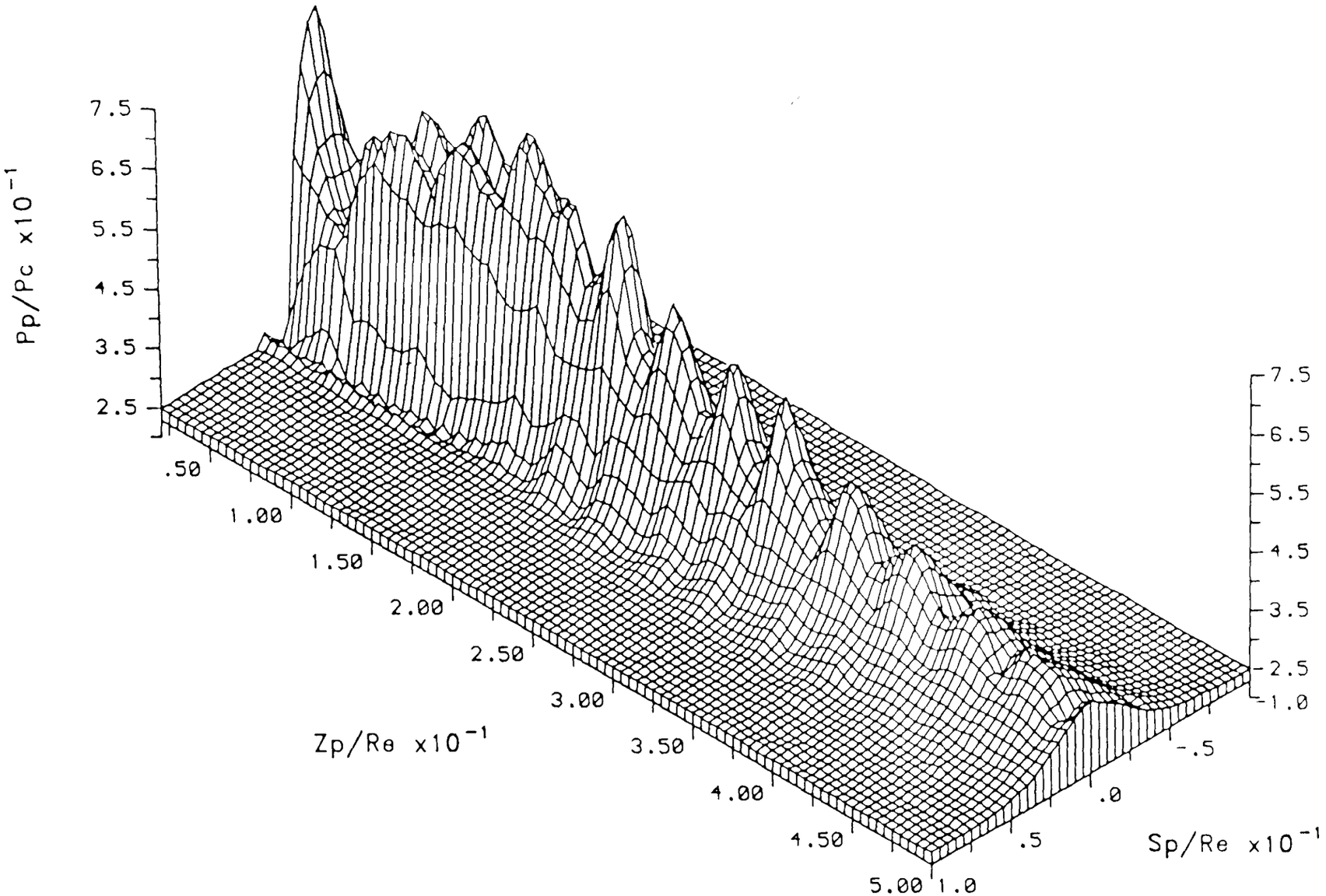

FIGURE 6.11 AIR JET IMPINGEMENT – ISOMETRIC PLOT OF VARIATION OF FLAT PLATE PRESSURE DISTRIBUTION WITH PLATE POSITION FOR: Me=1.0, Pc/Pa=5.0, θ=90.0°

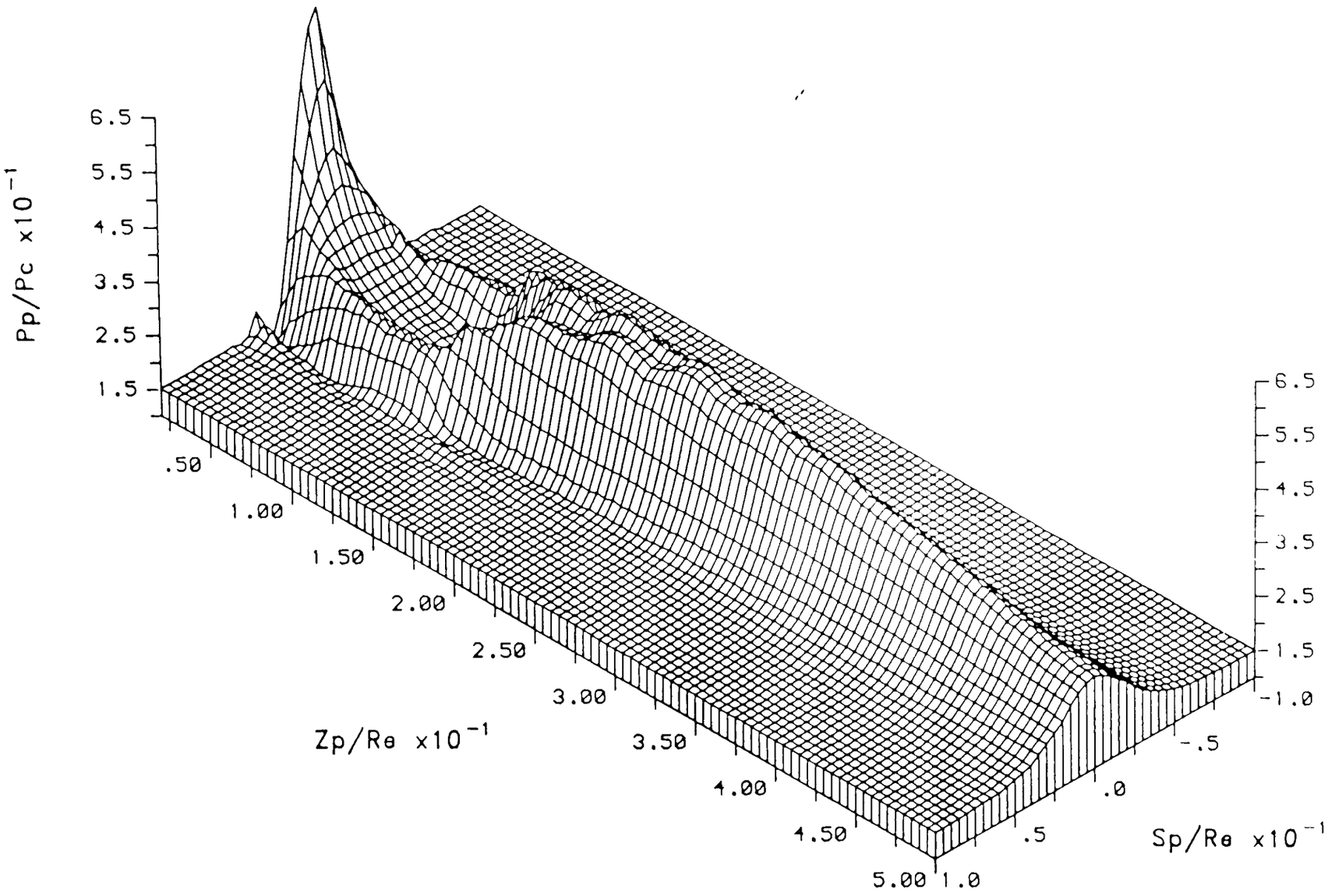

FIGURE 6.12 AIR JET IMPINGEMENT – ISOMETRIC PLOT OF VARIATION OF FLAT PLATE PRESSURE DISTRIBUTION WITH PLATE POSITION FOR: Me=1.0, Pc/Pa=10.0, θ=90.0°

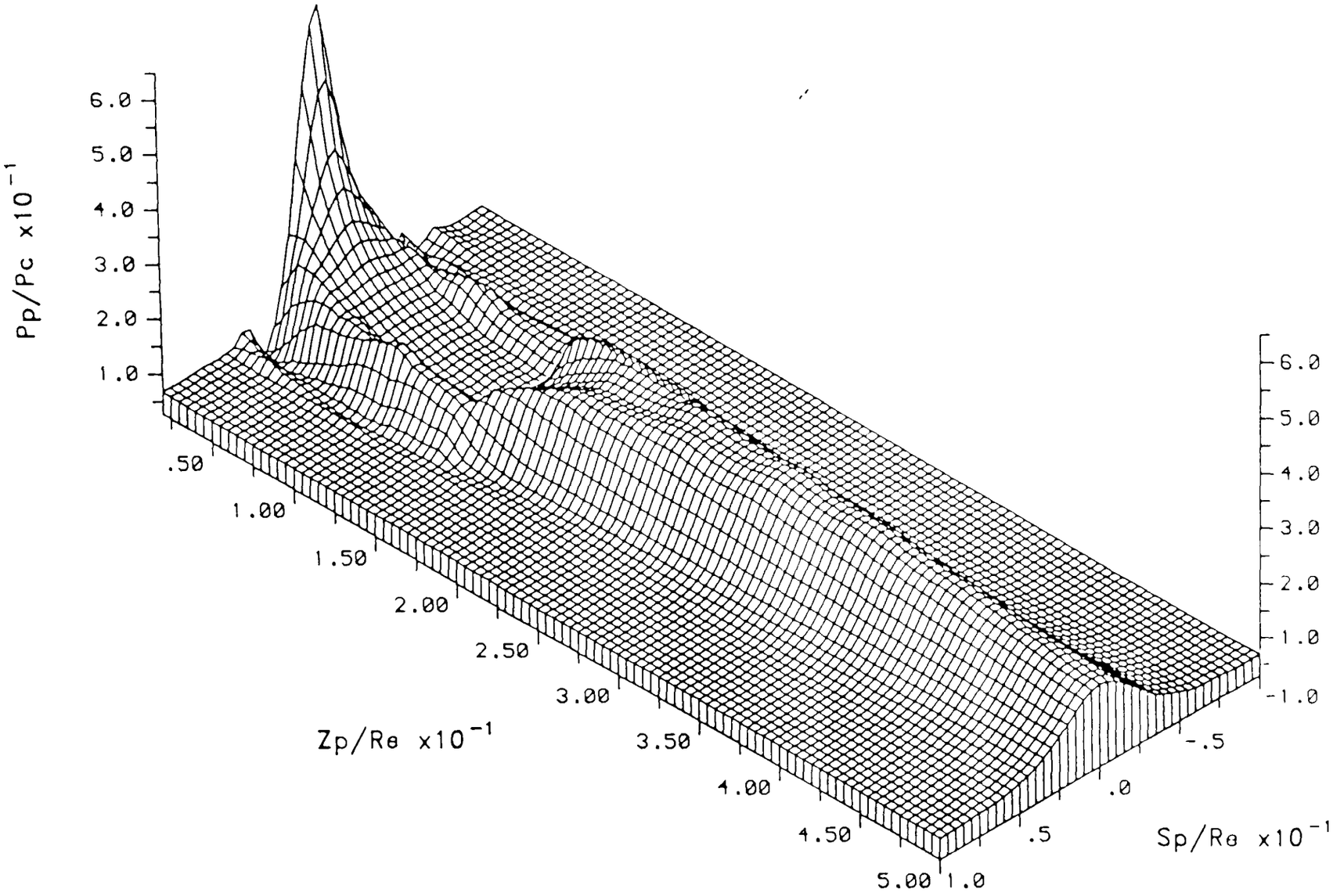

FIGURE 6.13 AIR JET IMPINGEMENT – ISOMETRIC PLOT OF VARIATION OF FLAT PLATE PRESSURE DISTRIBUTION WITH PLATE POSITION FOR: Me=1.0, Pc/Pa=15.0, θ=90.0°

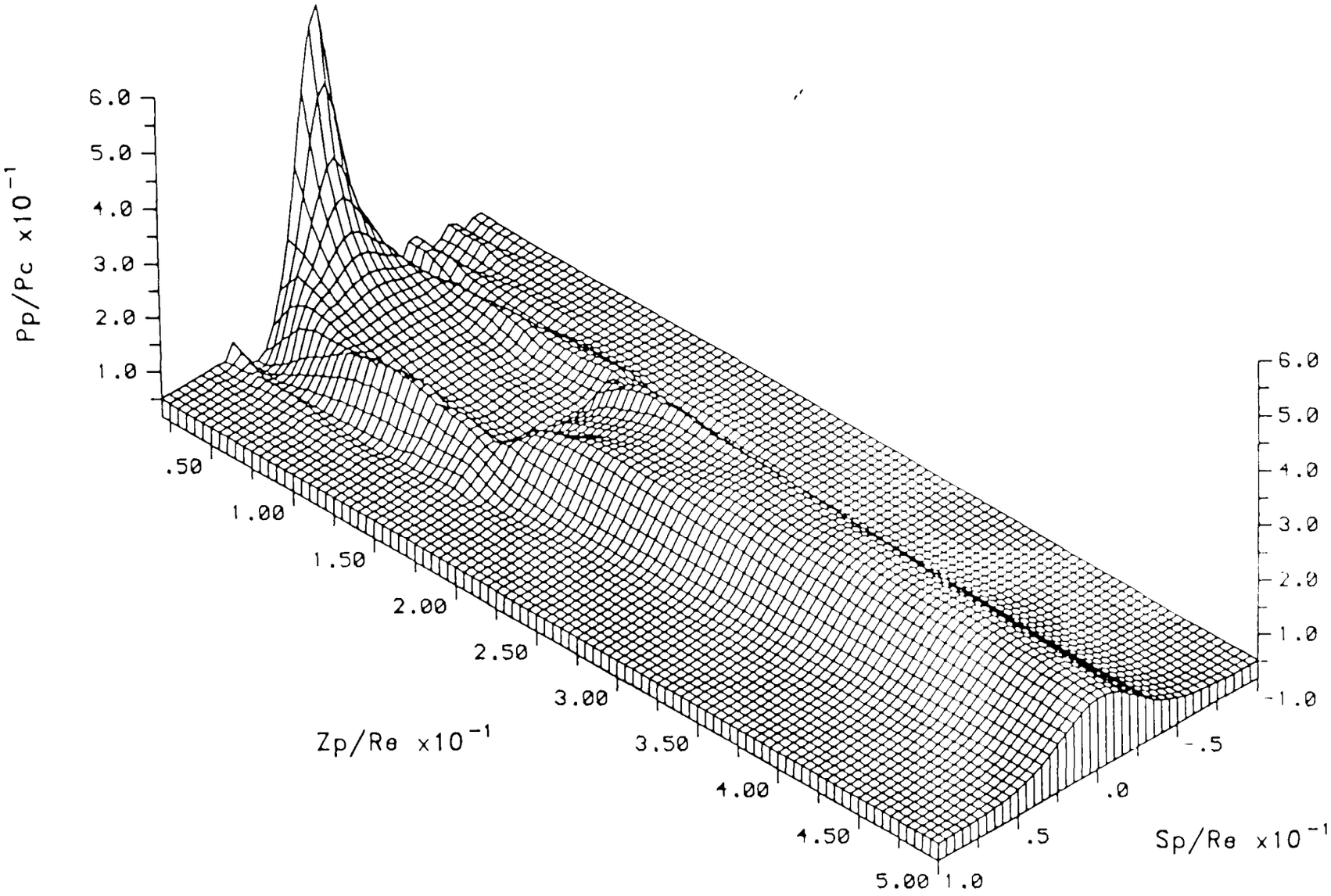

FIGURE 6.14 AIR JET IMPINGEMENT – ISOMETRIC PLOT OF VARIATION OF FLAT PLATE PRESSURE DISTRIBUTION WITH PLATE POSITION FOR: Me=1.0, Pc/Pa=20.0, θ=90.0°

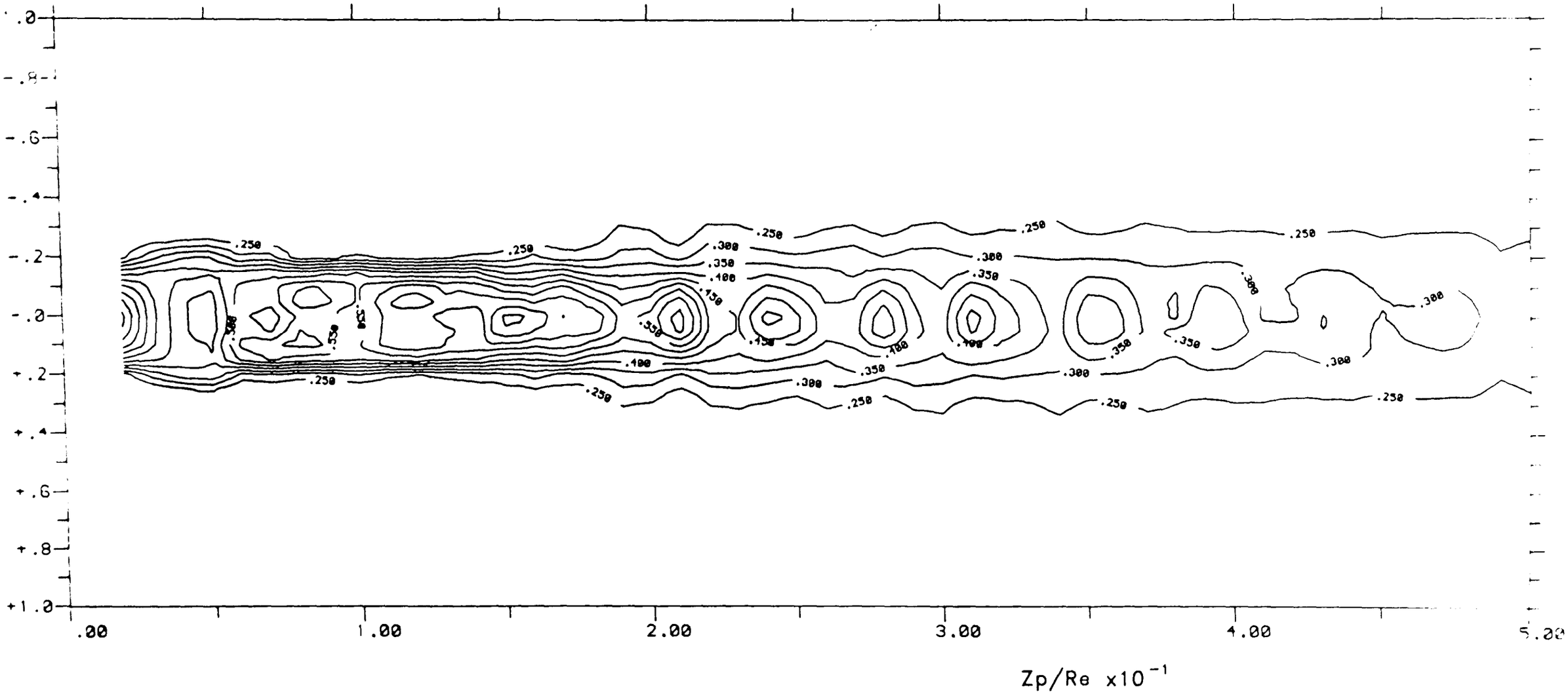

FIGURE 6.15 AIR JET IMPINGEMENT – CONTOUR PLOT OF VARIATION OF FLAT PLATE PRESSURE DISTRIBUTION WITH PLATE POSITION FOR: Me=1.0, Pc/Pa=5.0, θ=90.0°

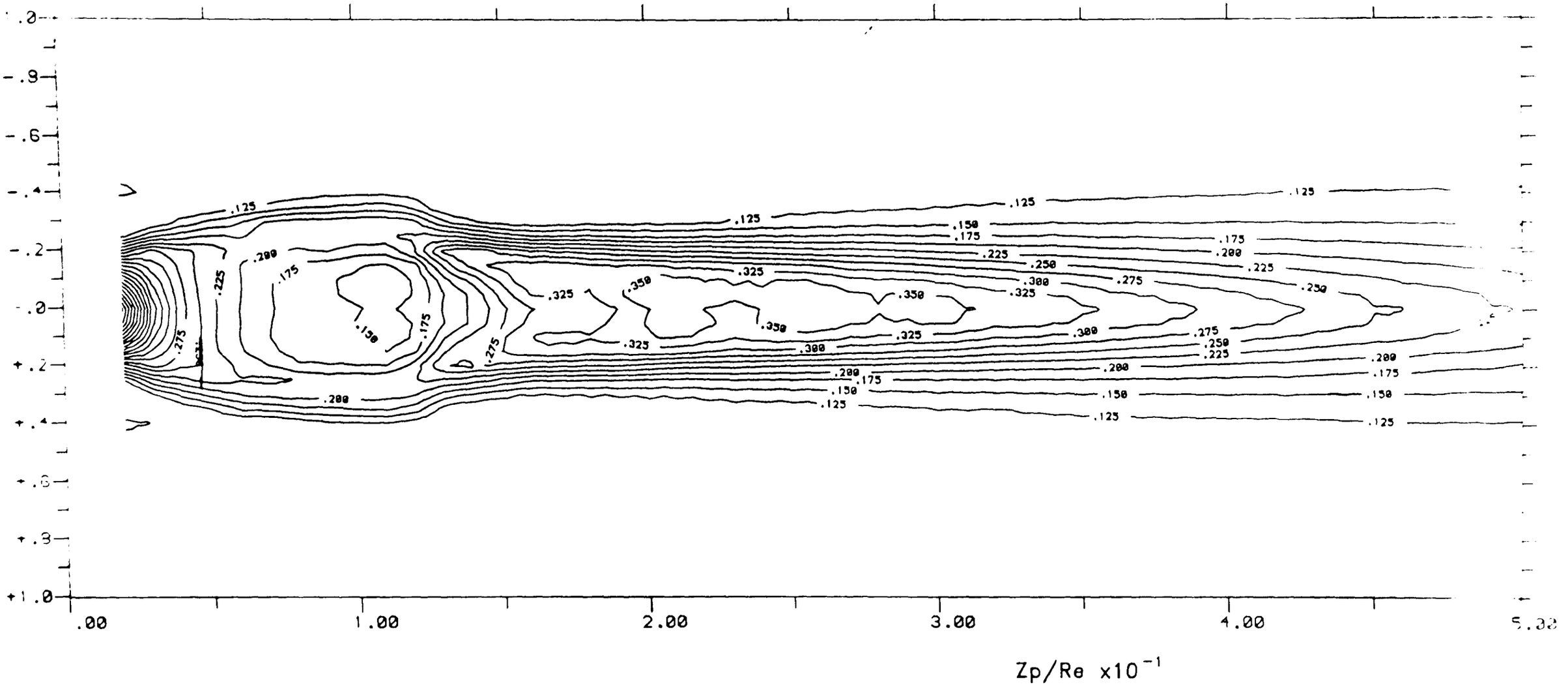

FIGURE 6.16 AIR JET IMPINGEMENT – CONTOUR PLOT OF VARIATION OF FLAT PLATE PRESSURE DISTRIBUTION WITH PLATE POSITION FOR: Me=1.0, Pc/Pa=10.0, θ=90.0°

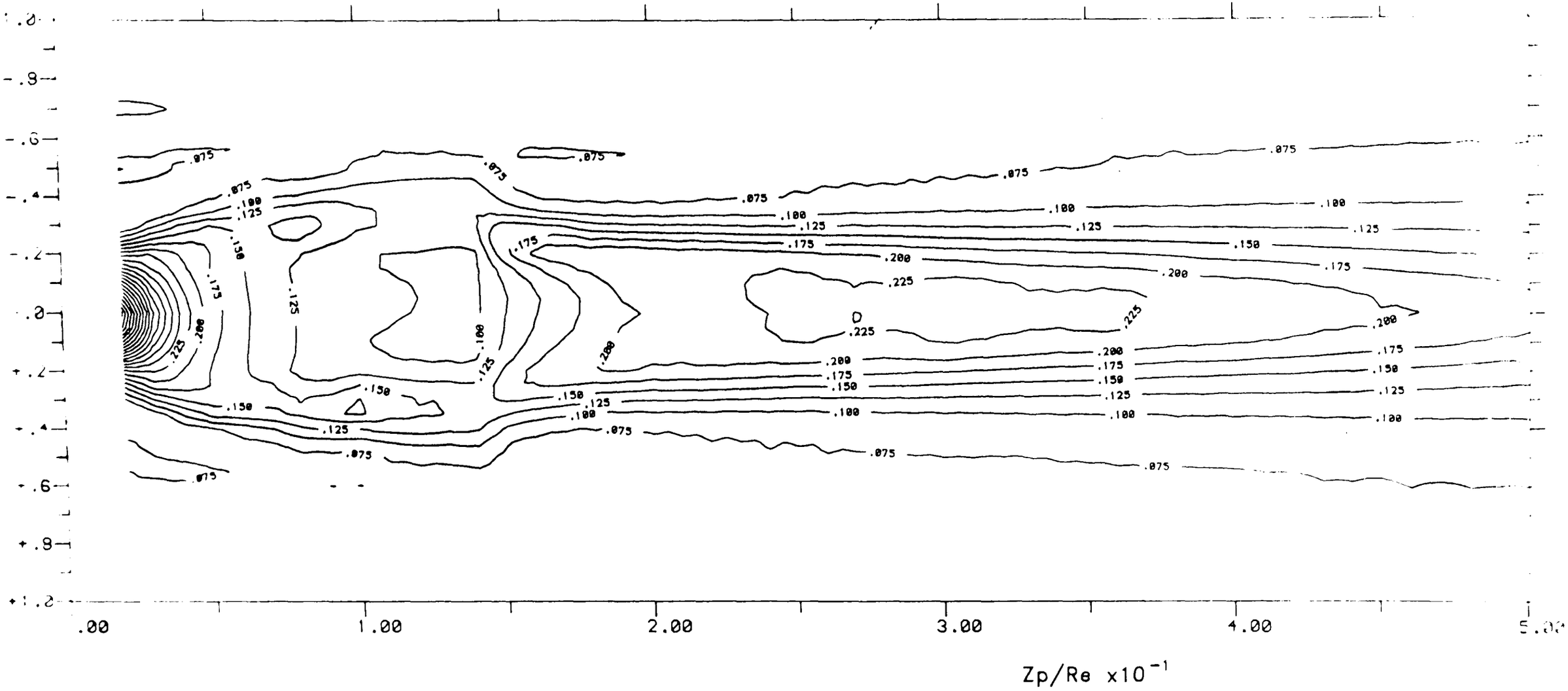

FIGURE 6.17 AIR JET IMPINGEMENT – CONTOUR PLOT OF VARIATION OF FLAT PLATE PRESSURE DISTRIBUTION WITH PLATE POSITION FOR: Me=1.0, Pc/Pa=15.0, θ=90.0°

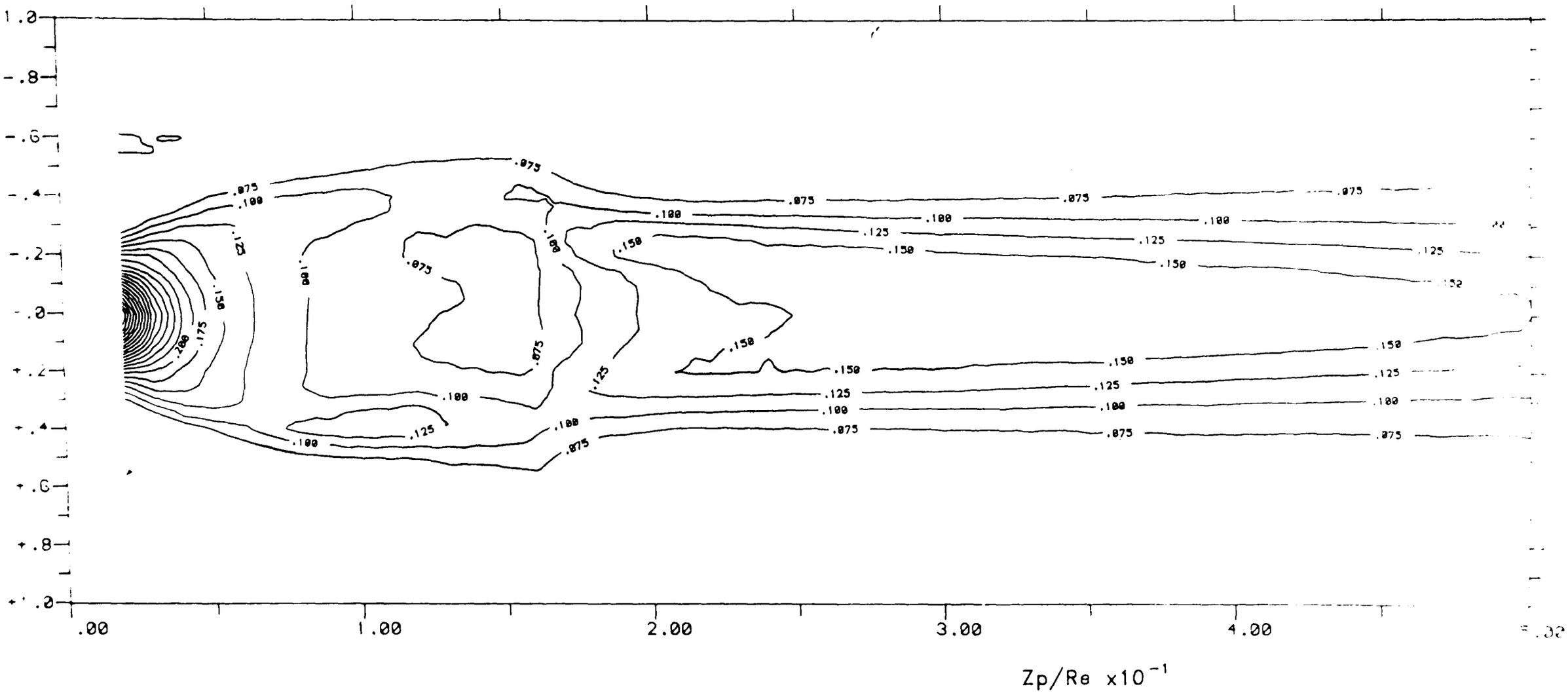

FIGURE 6.18 AIR JET IMPINGEMENT – CONTOUR PLOT OF VARIATION OF FLAT PLATE PRESSURE DISTRIBUTION WITH PLATE POSITION FOR: Me=1.0, Pc/Pa=20.0, θ=90.0°

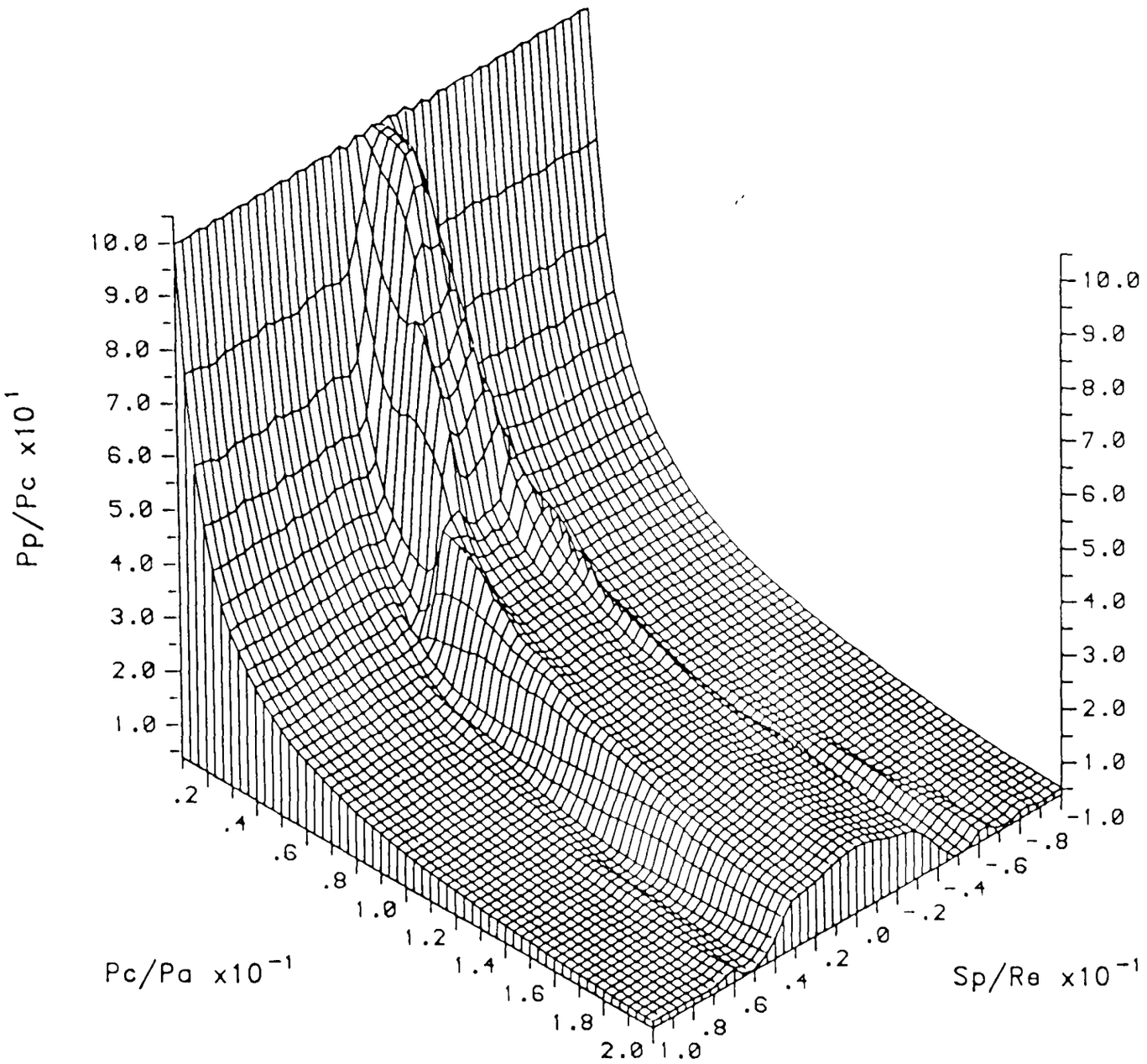

FIGURE 6.19 AIR JET IMPINGEMENT – ISOMETRIC PLOT OF VARIATION OF FLAT PLATE PRESSURE DISTRIBUTION WITH JET PRESSURE RATIO FOR: Me=1.0, Zp/Re=5.0, θ=90.0°

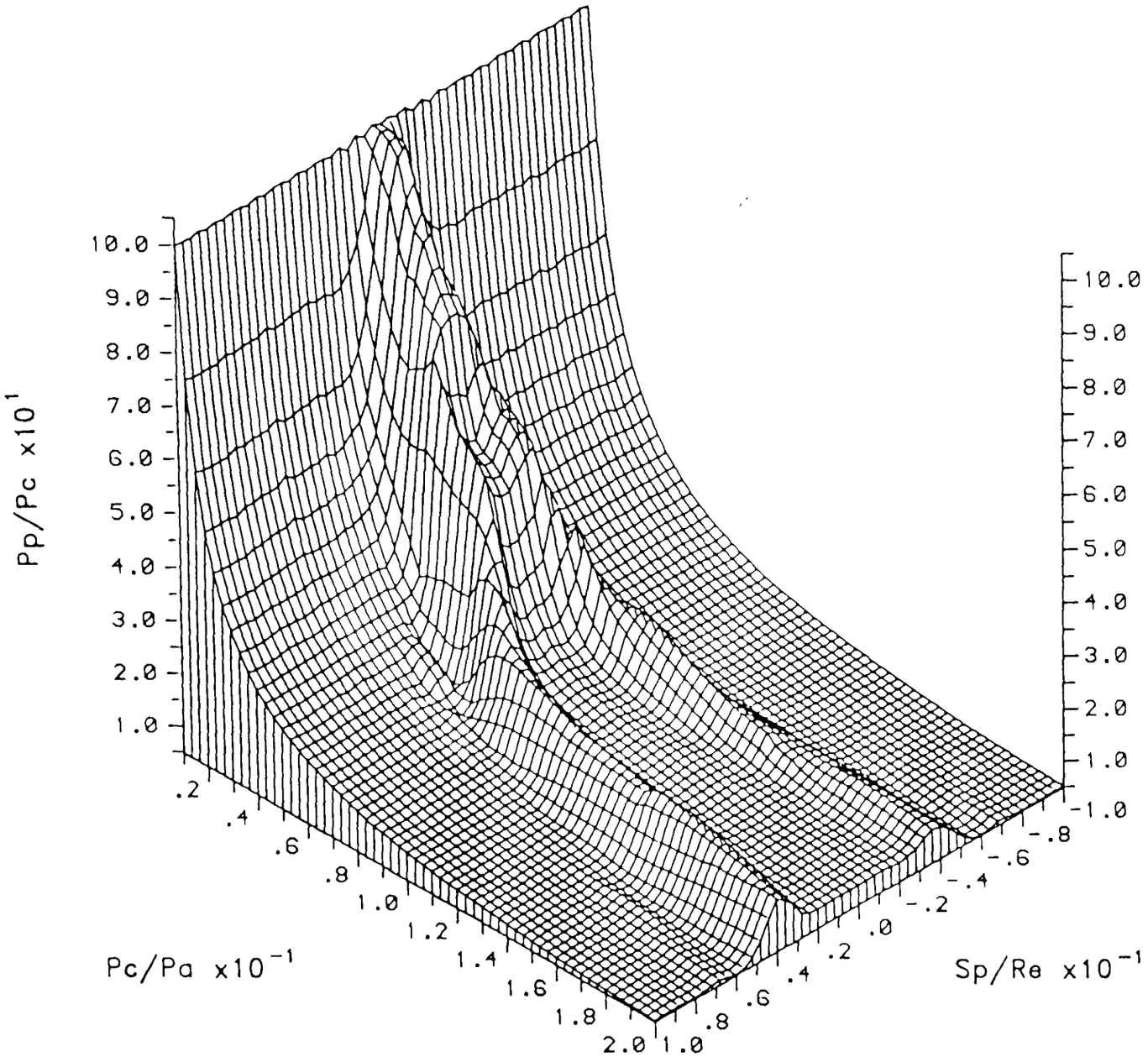

FIGURE 6.20 AIR JET IMPINGEMENT – ISOMETRIC PLOT OF VARIATION OF FLAT PLATE PRESSURE DISTRIBUTION WITH JET PRESSURE RATIO FOR: Me=1.0, Zp/Re=10.0, θ=90.0°

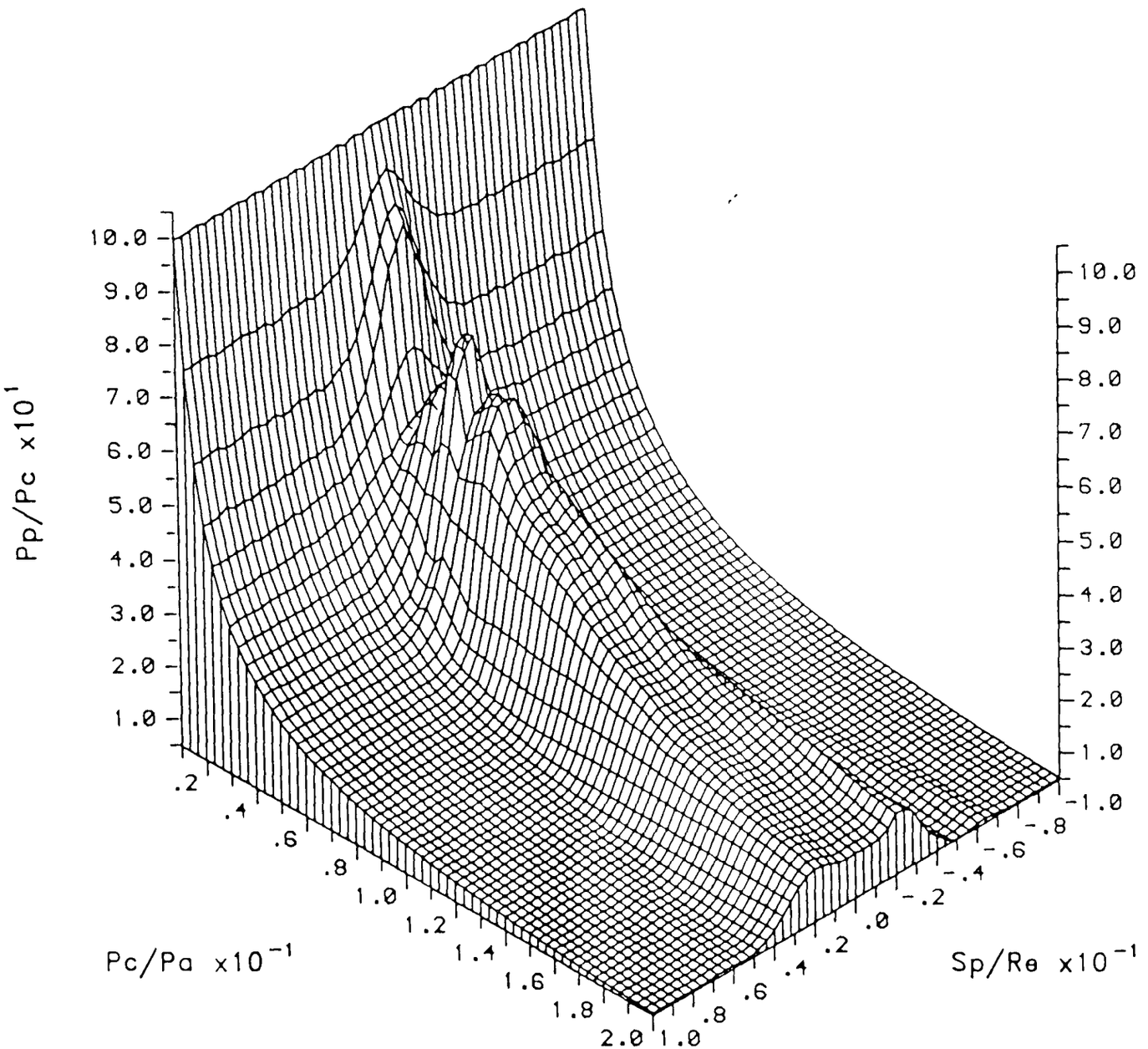

FIGURE 6.21 AIR JET IMPINGEMENT – ISOMETRIC PLOT OF VARIATION OF FLAT PLATE PRESSURE DISTRIBUTION WITH JET PRESSURE RATIO FOR: Me=1.0, Zp/Re=20.0, θ=90.0°

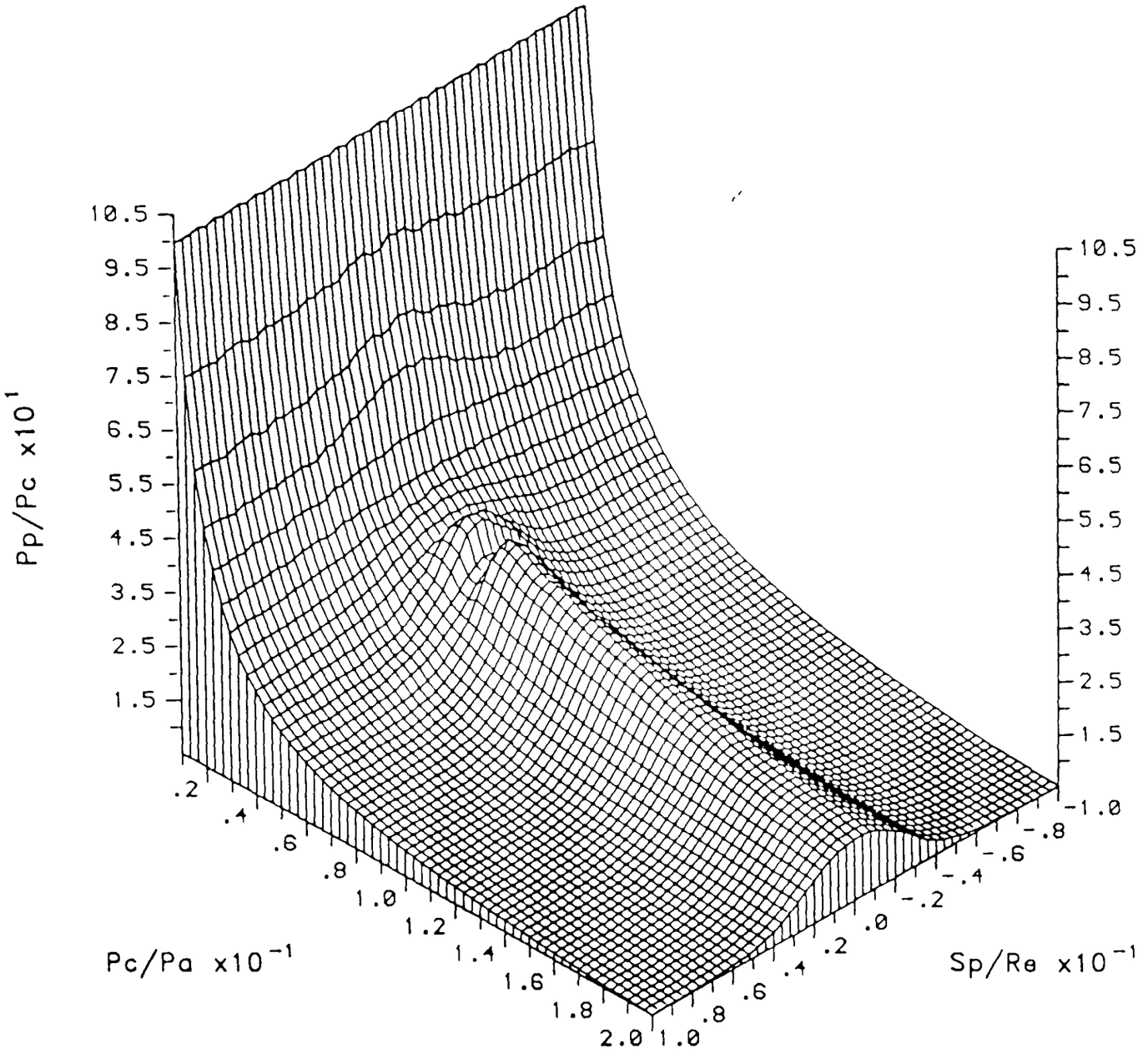

FIGURE 6.22 AIR JET IMPINGEMENT – ISOMETRIC PLOT OF VARIATION OF FLAT PLATE PRESSURE DISTRIBUTION WITH JET PRESSURE RATIO FOR: Me=1.0, Zp/Re=40.0, θ=90.0°

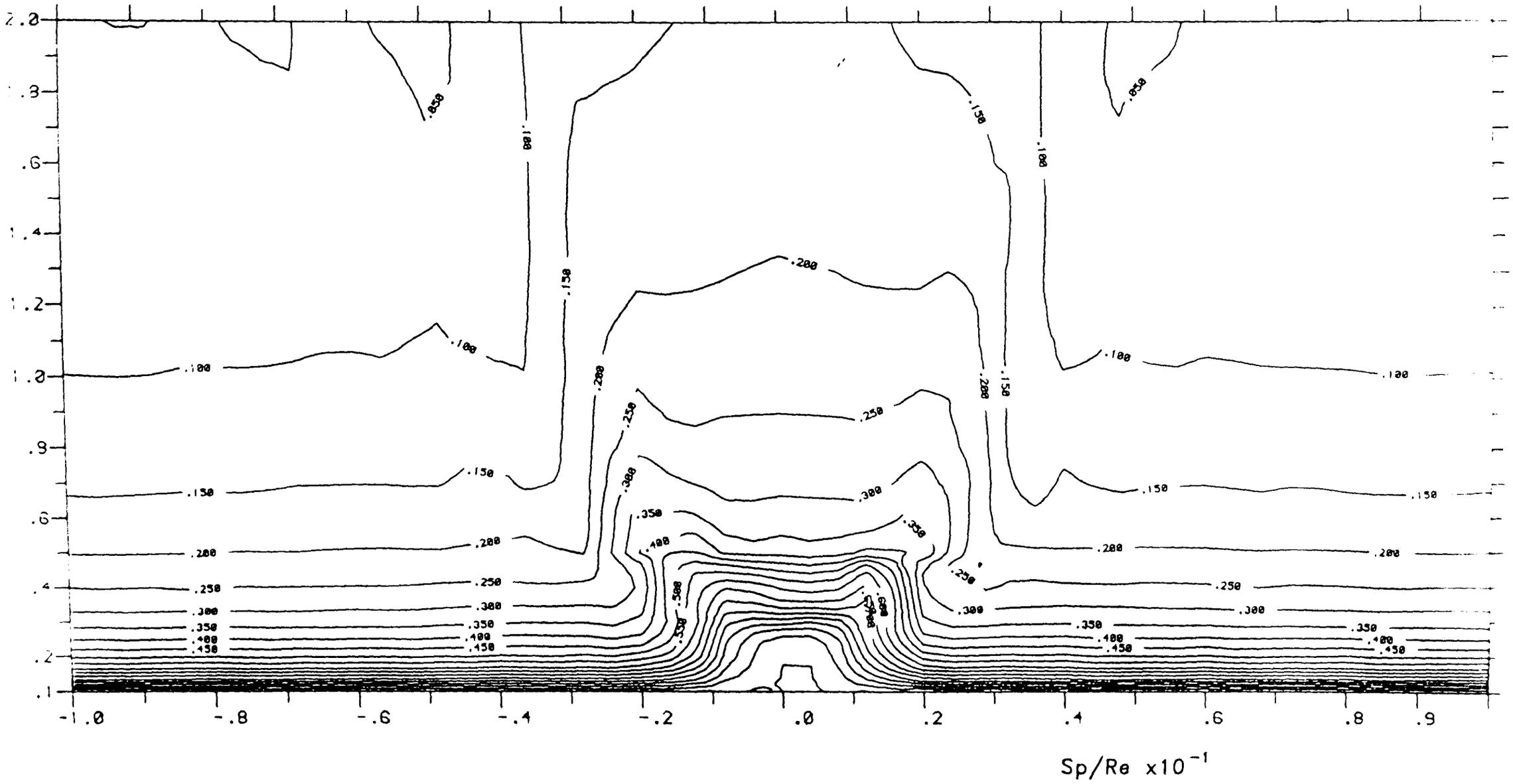

FIGURE 6.23 AIR JET IMPINGEMENT – CONTOUR PLOT OF VARIATION OF FLAT PLATE PRESSURE DISTRIBUTION WITH JET PRESSURE RATIO FOR: Me=1.0, Zp/Re=5.0, θ=90.0°

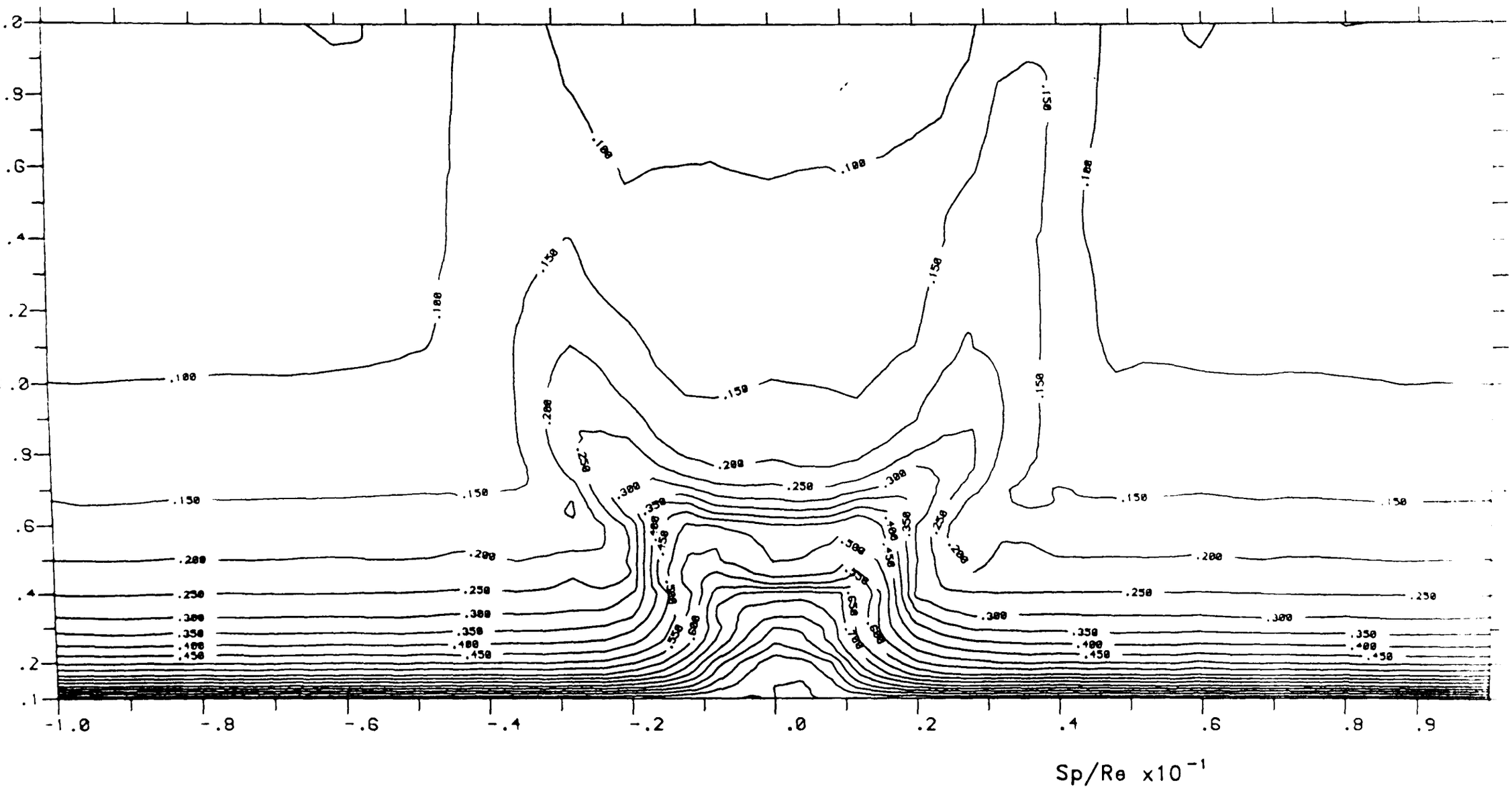

FIGURE 6.24 AIR JET IMPINGEMENT – CONTOUR PLOT OF VARIATION OF FLAT PLATE PRESSURE DISTRIBUTION WITH JET PRESSURE RATIO FOR: Me=1.0, Zp/Re=10.0, θ=90.0°

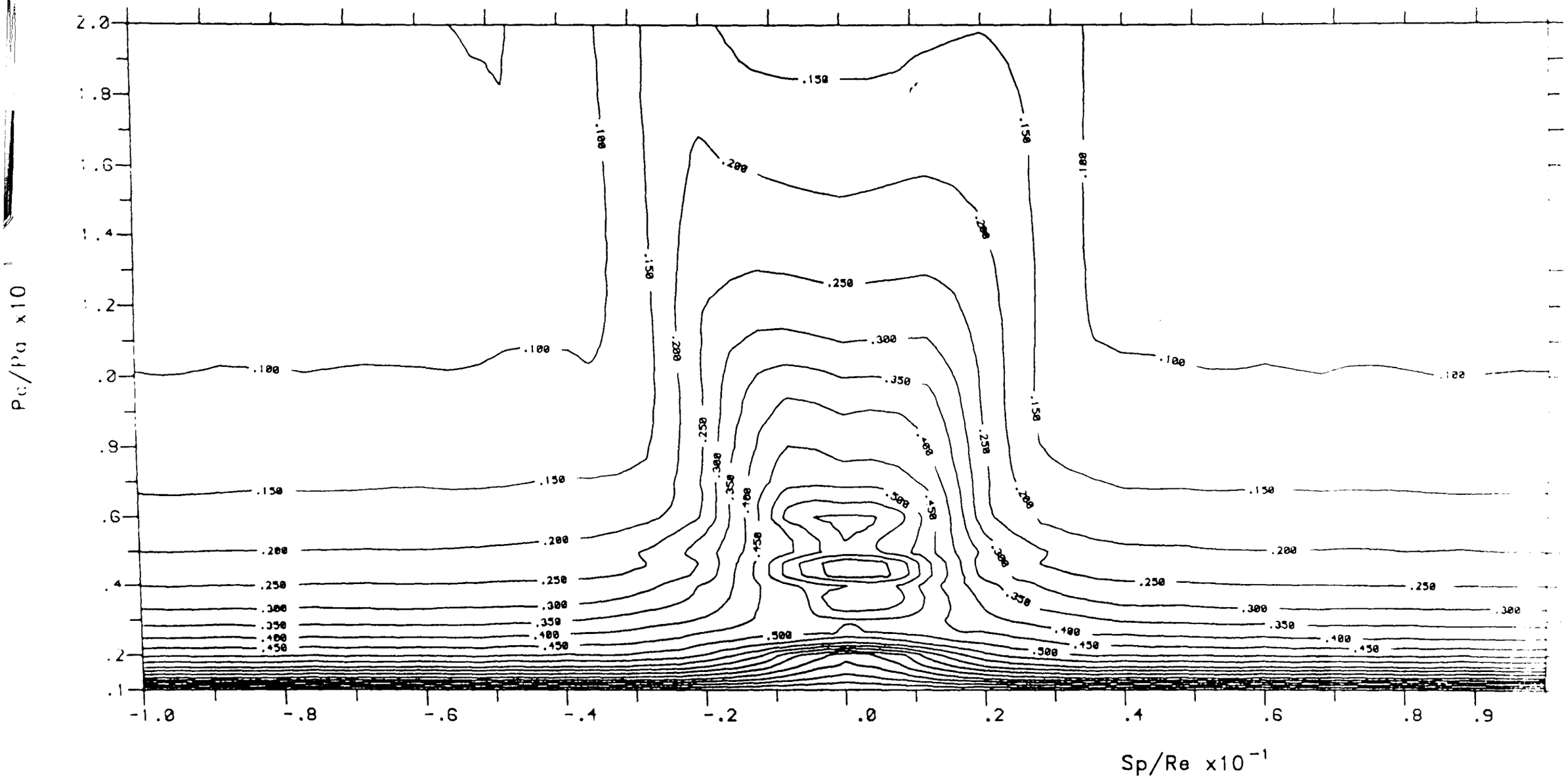

FIGURE 6.25 AIR JET IMPINGEMENT – CONTOUR PLOT OF VARIATION OF FLAT PLATE PRESSURE DISTRIBUTION WITH JET PRESSURE RATIO FOR: Me=1.0, Zp/Re=20.0, θ=90.0°

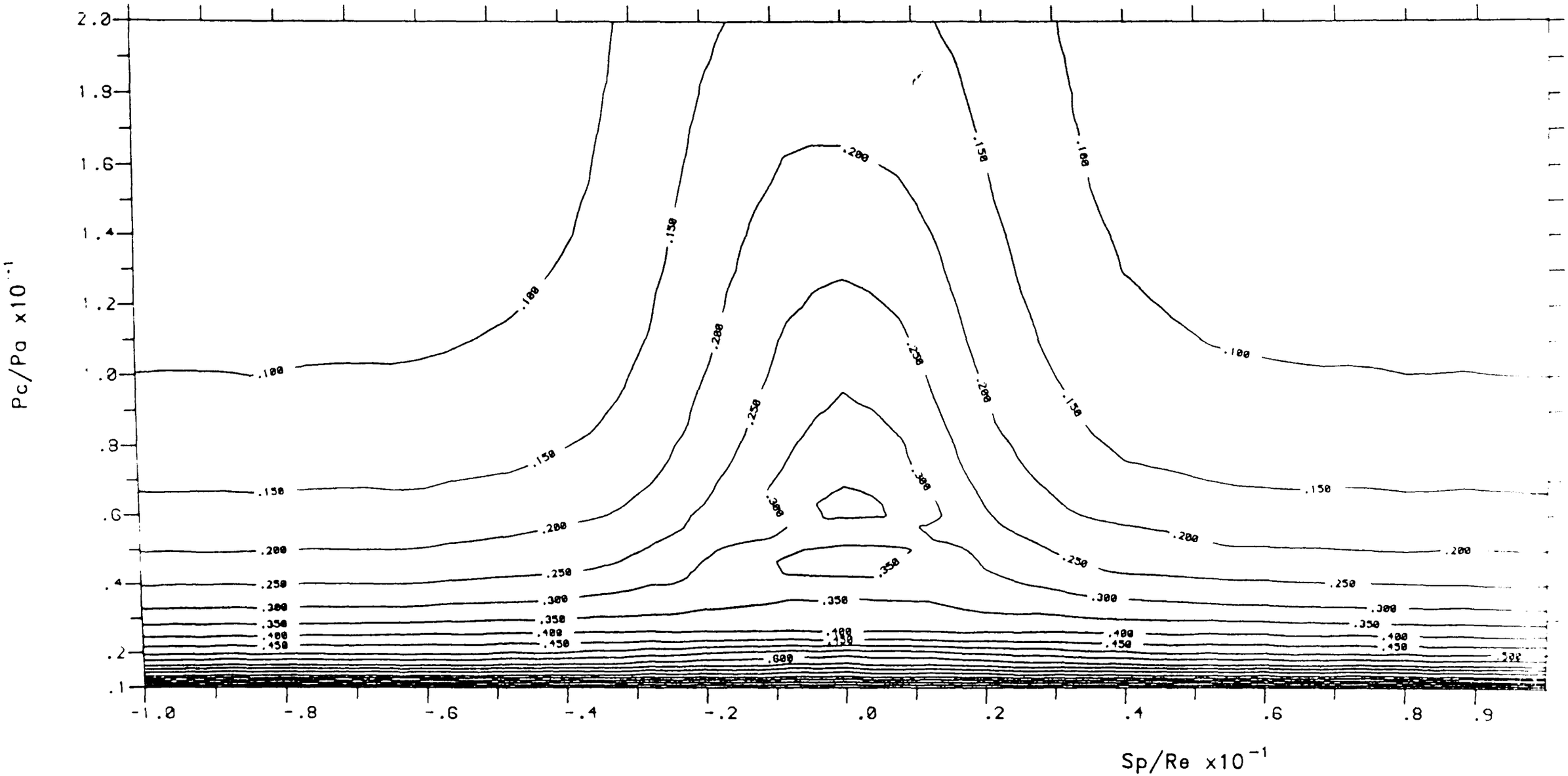

FIGURE 6.26 AIR JET IMPINGEMENT – CONTOUR PLOT OF VARIATION OF FLAT PLATE PRESSURE DISTRIBUTION WITH JET PRESSURE RATIO FOR: Me=1.0, Zp/Re=40.0, θ=90.0°

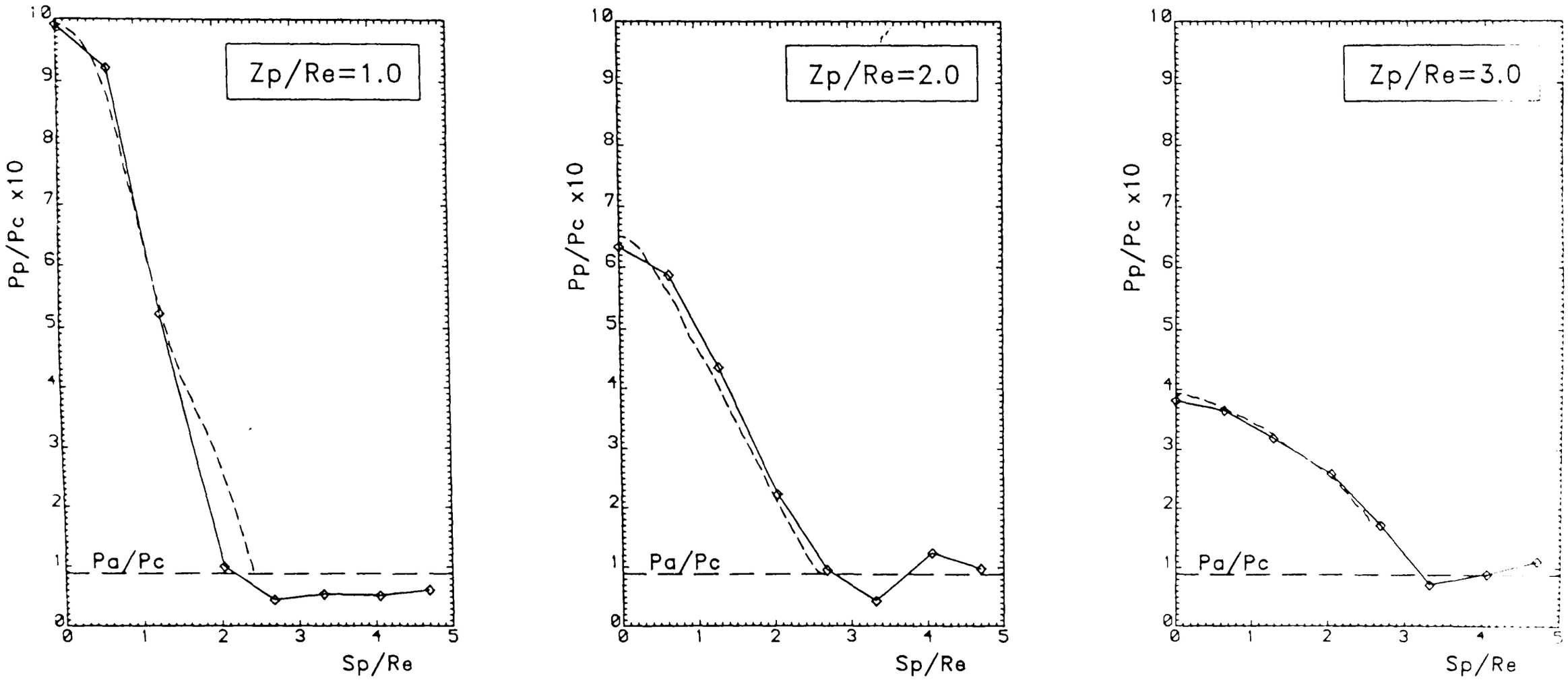

FIGURE 6.27 COMPARISON OF AIR JET IMPINGEMENT PLATE PRESSURE DISTRIBUTIONS OBTAINED IN THIS STUDY WITH THOSE OBTAINED BY GUMMER & HUNT FOR: Me=1.0; Pc/Pa=11.357; θ=90.0°; Zp/Re=1.0, 2.0, 3.0

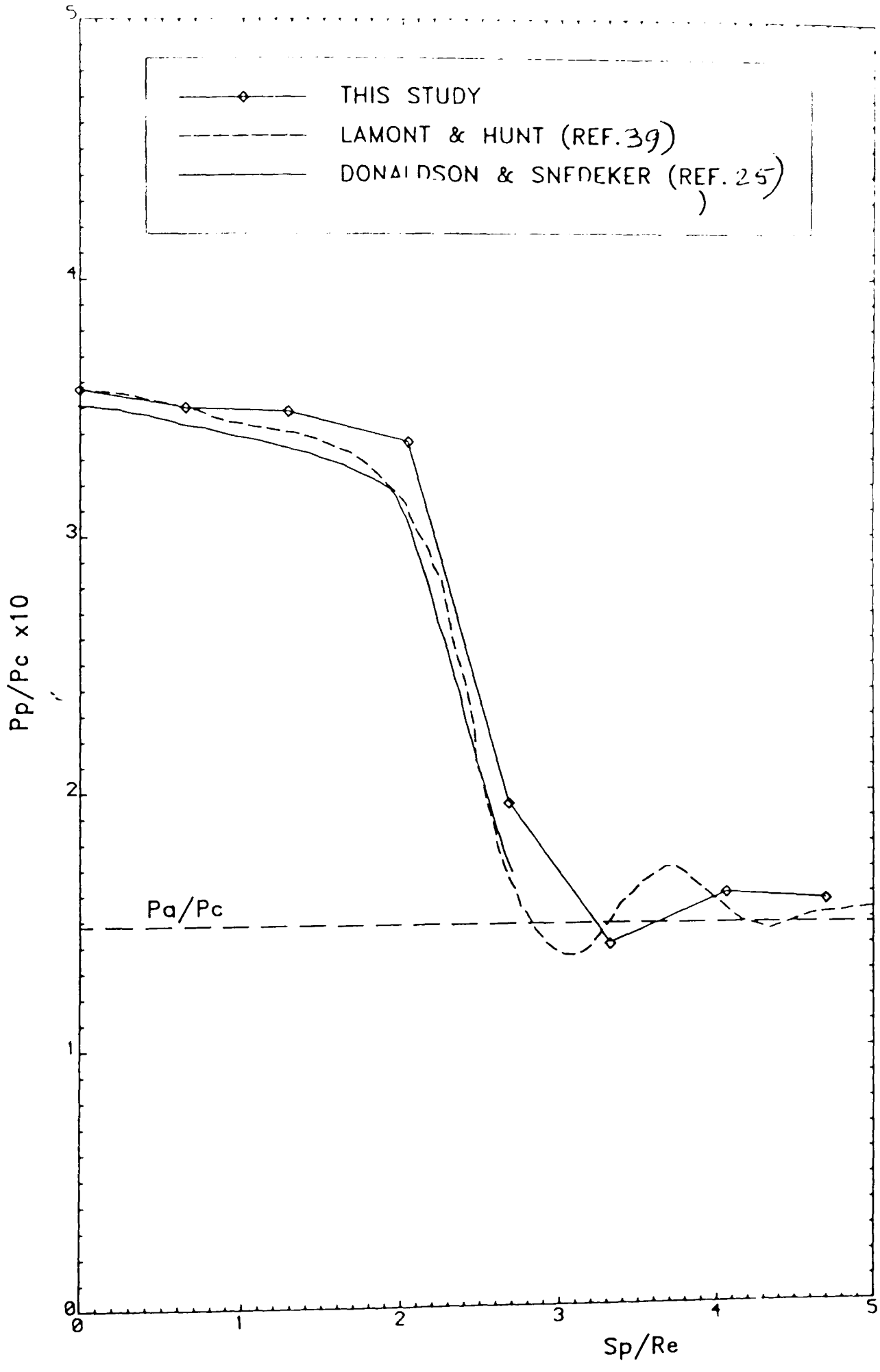

FIGURE 6.28 COMPARISON OF AIR JET IMPINGEMENT FLAT PLATE PRESSURES OBTAINED IN THIS STUDY WITH THOSE OBTAINED BY LAMONT & HUNT AND BY DONALDSON & SNEDEKER FOR : Pc/Pa=6.758, Zp/Re=3.92, θ =90.0°

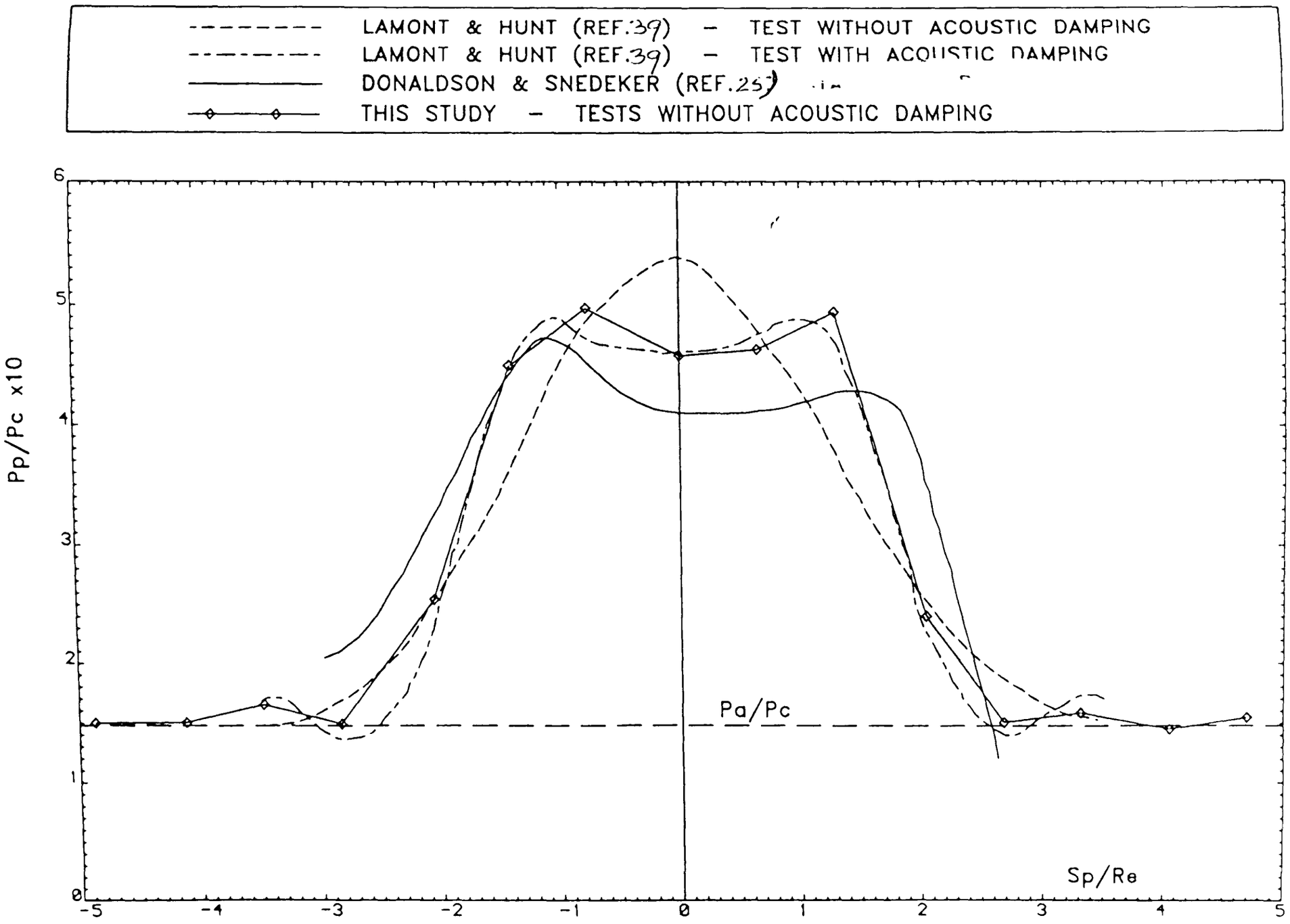

FIGURE 6.29 COMPARISON OF AIR JET IMPINGEMENT FLAT PLATE PRESSURES OBTAINED IN THIS STUDY WITH THOSE OBTAINED BY DONALDSON & SNEDEKER AND LAMONT & HUNT FOR: Me=1.0, Pc/Pa=6.758, Zp/Re=14.64, θ =90.0°

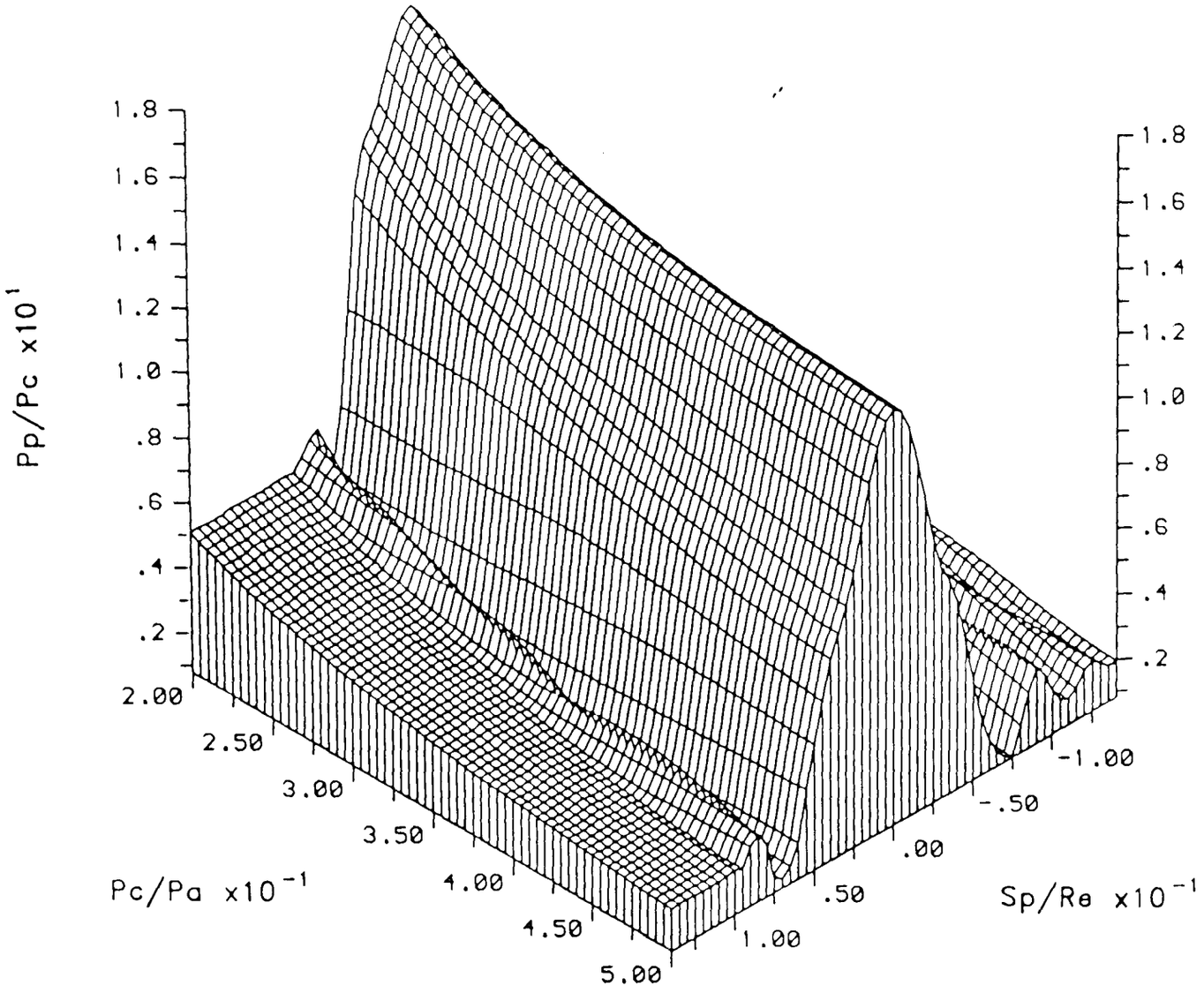

FIGURE 6.30 NITROGEN JET IMPINGEMENT – ISOMETRIC PLOT OF VARIATION OF FLAT PLATE PRESSURE DISTRIBUTION WITH JET PRESSURE RATIO FOR: Me=1.0, Zp/Re=5.0, θ=90.0°

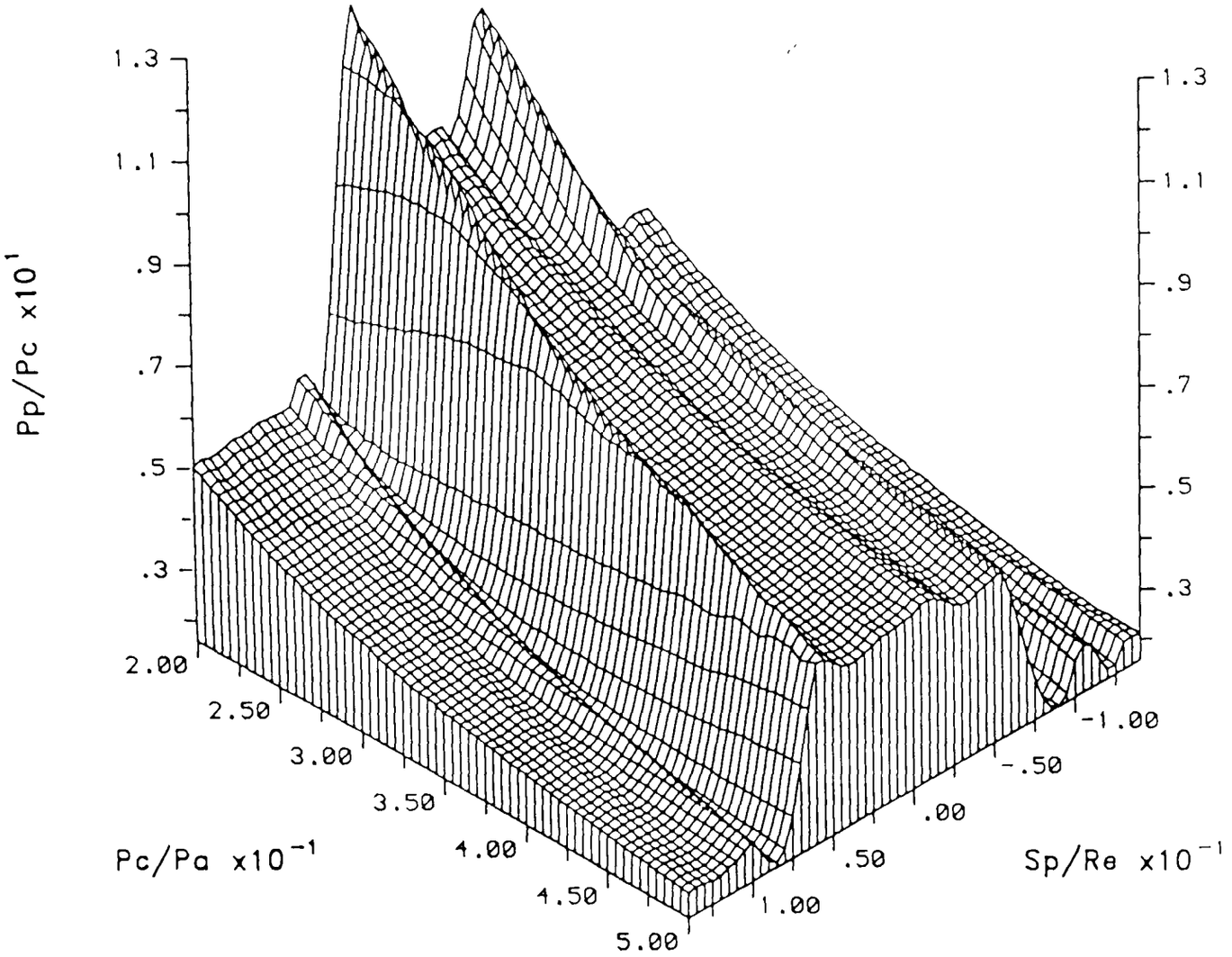

FIGURE 6.31 NITROGEN JET IMPINGEMENT – ISOMETRIC PLOT OF VARIATION OF FLAT PLATE PRESSURE DISTRIBUTION WITH JET PRESSURE RATIO FOR: Me=1.0, Zp/Re=10.0, θ=90.0°

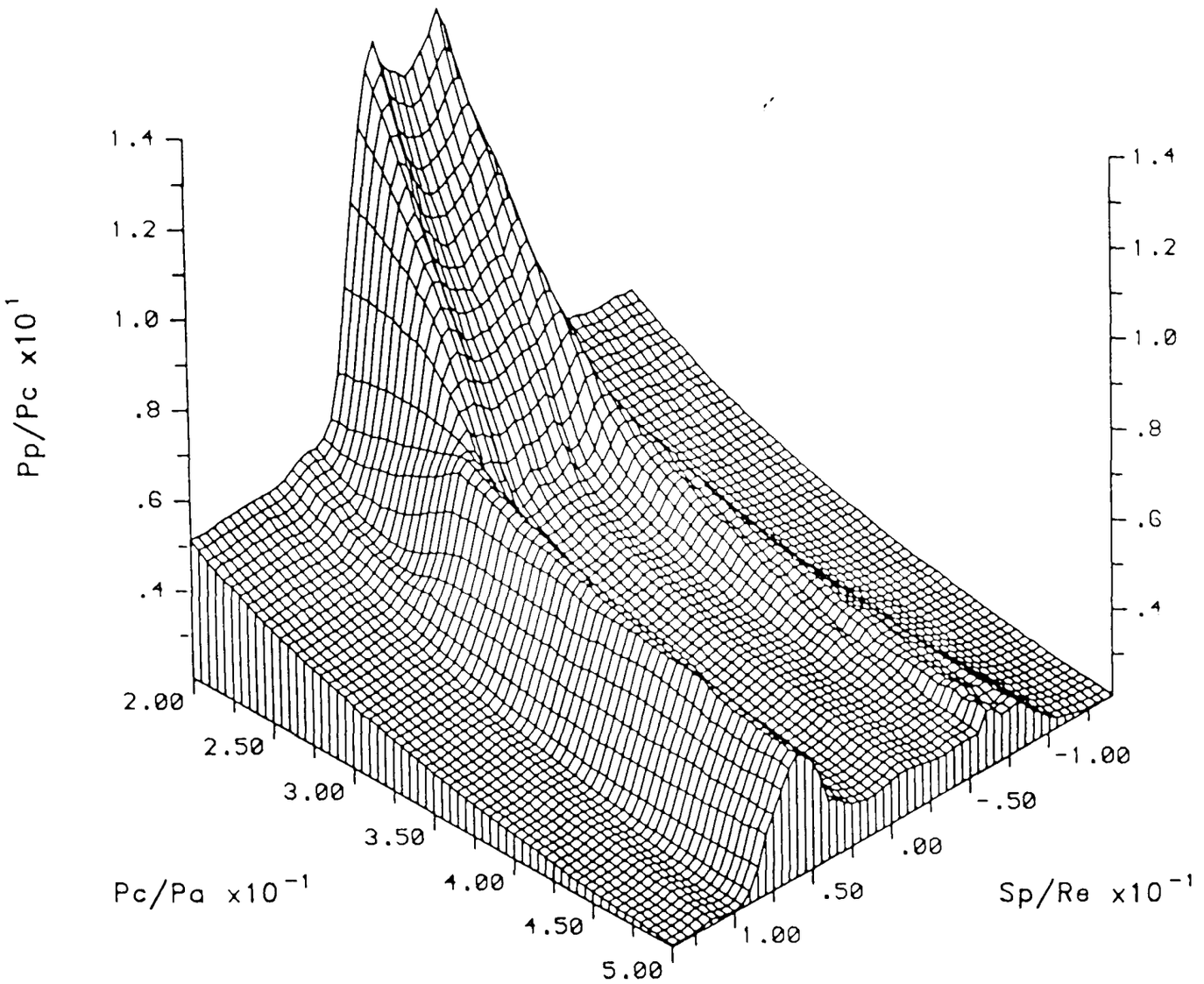

FIGURE 6.32 NITROGEN JET IMPINGEMENT – ISOMETRIC PLOT OF VARIATION OF FLAT PLATE PRESSURE DISTRIBUTION WITH JET PRESSURE RATIO FOR: Me=1.0, Zp/Re=20.0, θ=90.0°

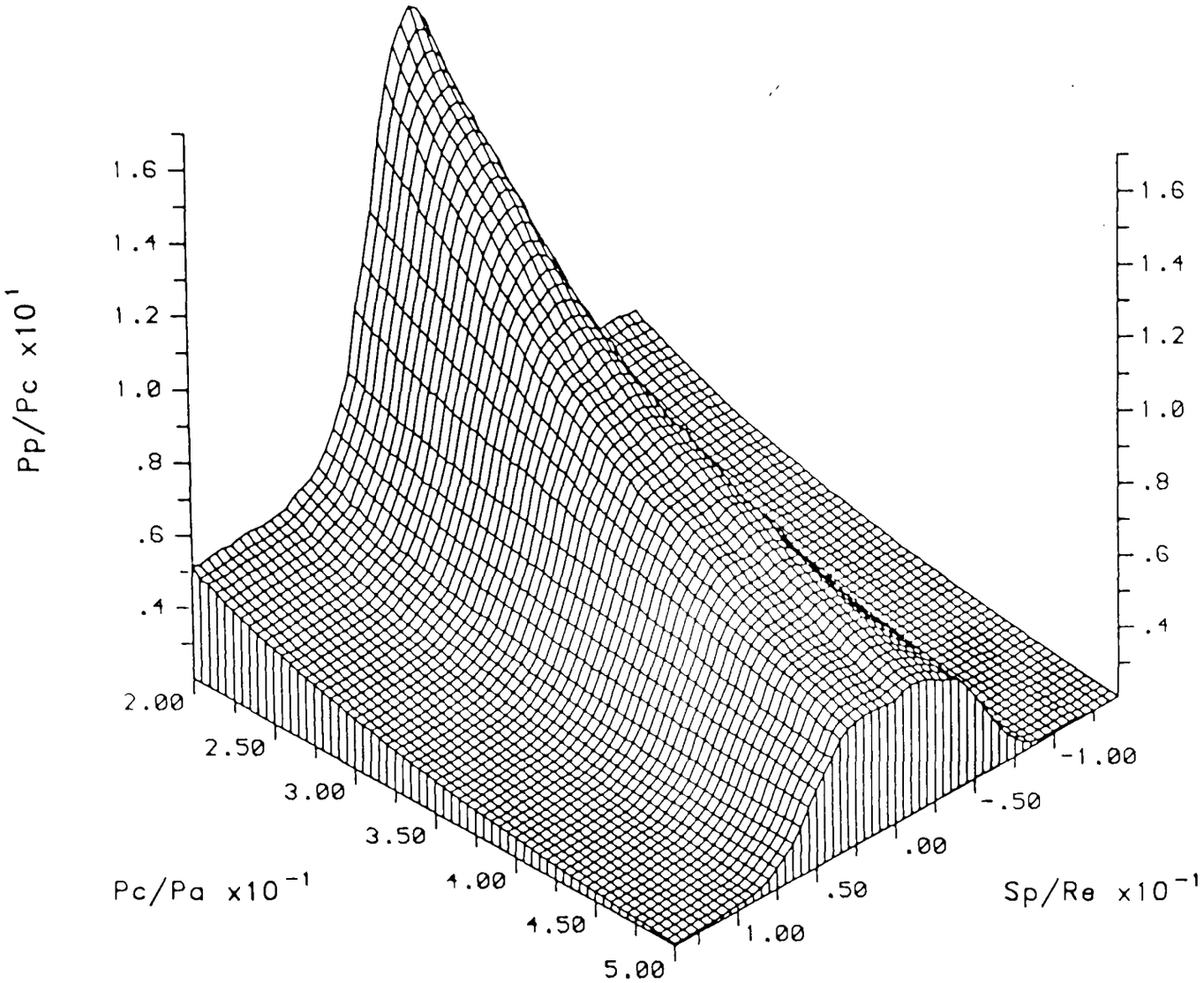

FIGURE 6.33 NITROGEN JET IMPINGEMENT – ISOMETRIC PLOT OF VARIATION OF FLAT PLATE PRESSURE DISTRIBUTION WITH JET PRESSURE RATIO FOR: Me=1.0, Zp/Re=40.0, θ=90.0°

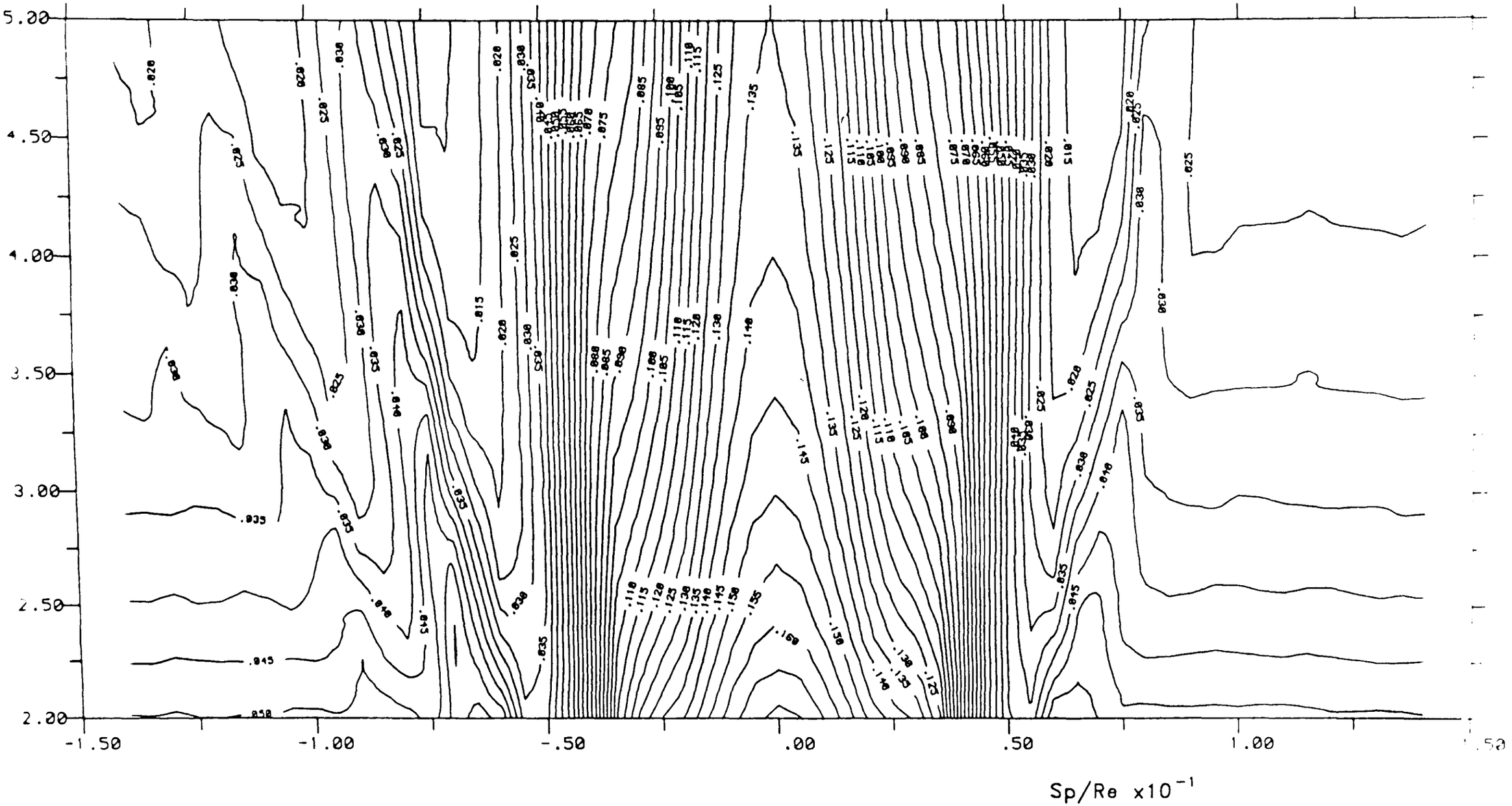

FIGURE 6.34 NITROGEN JET IMPINGEMENT – CONTOUR PLOT OF VARIATION OF FLAT PLATE PRESSURE DISTRIBUTION WITH JET PRESSURE RATIO FOR: Me=1.0, Zp/Re=5.0, θ=90.0°

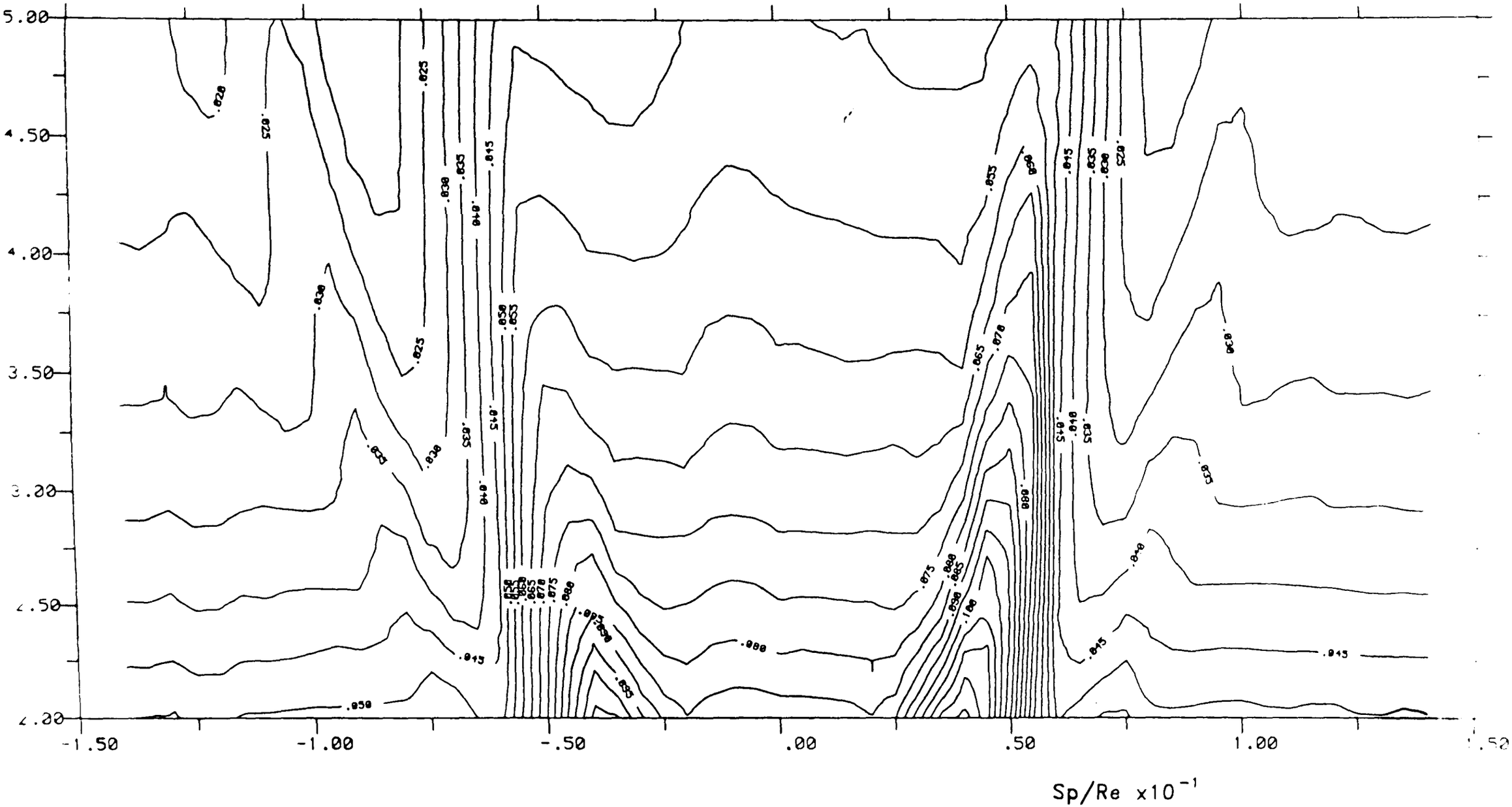

FIGURE 6.35 NITROGEN JET IMPINGEMENT – CONTOUR PLOT OF VARIATION OF FLAT PLATE PRESSURE DISTRIBUTION WITH JET PRESSURE RATIO FOR: Me=1.0, Zp/Re=10.0, θ=90.0°

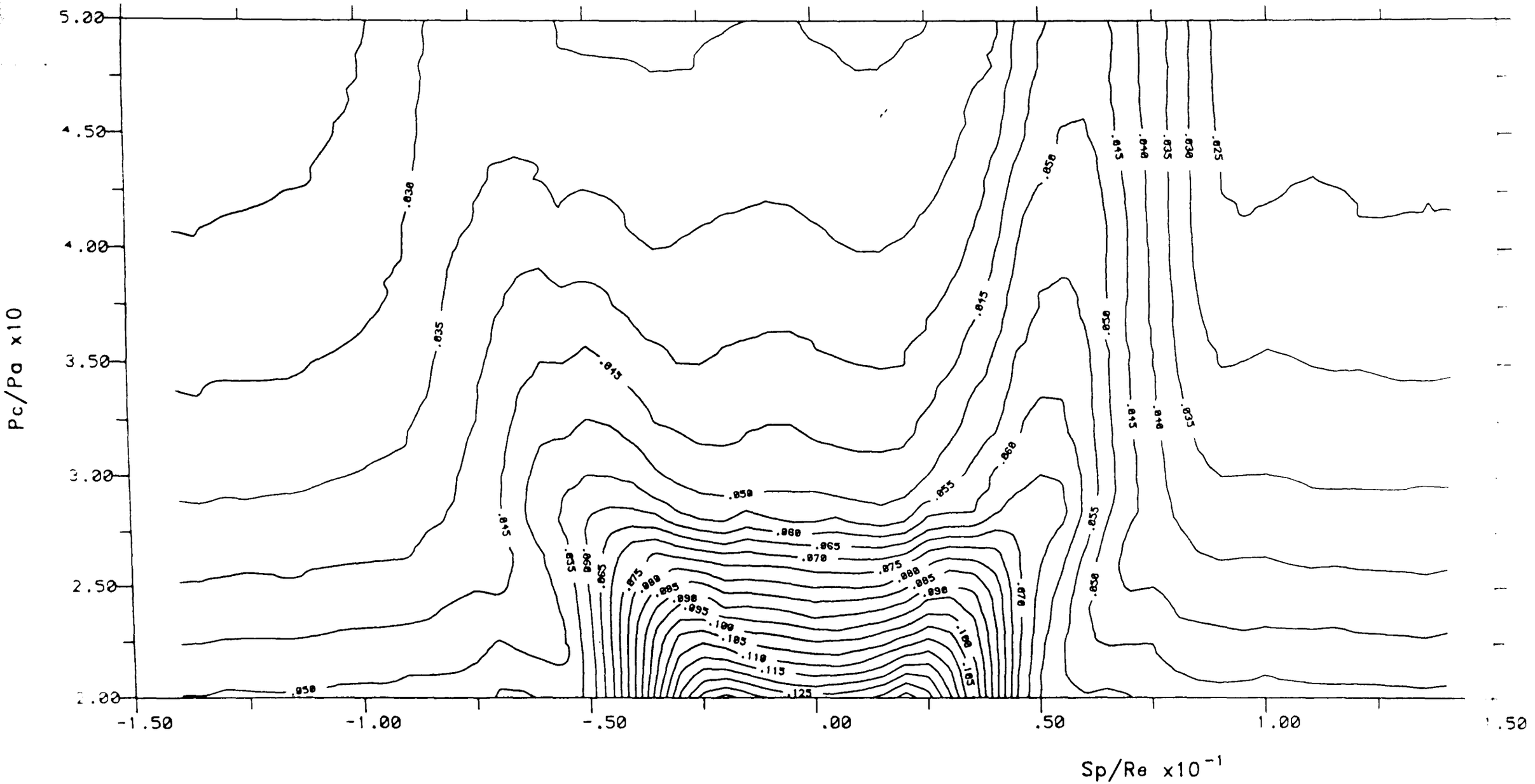

FIGURE 6.36 NITROGEN JET IMPINGEMENT – CONTOUR PLOT OF VARIATION OF FLAT PLATE PRESSURE DISTRIBUTION WITH JET PRESSURE RATIO FOR: Me=1.0, Zp/Re=20.0, θ=90.0°

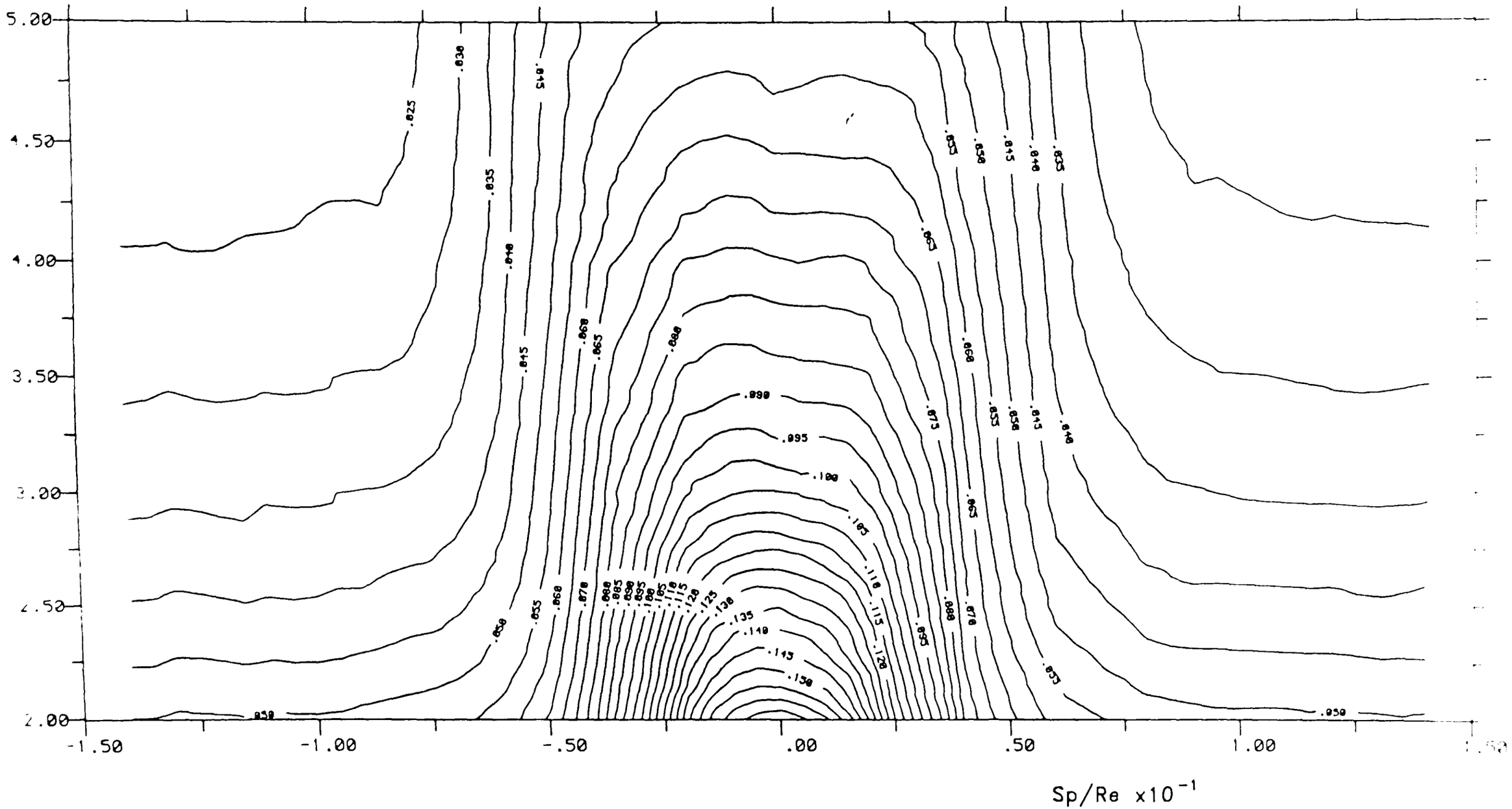

FIGURE 6.37 NITROGEN JET IMPINGEMENT – CONTOUR PLOT OF VARIATION OF FLAT PLATE PRESSURE DISTRIBUTION WITH JET PRESSURE RATIO FOR: Me=1.0, Zp/Re=40.0, θ=90.0°

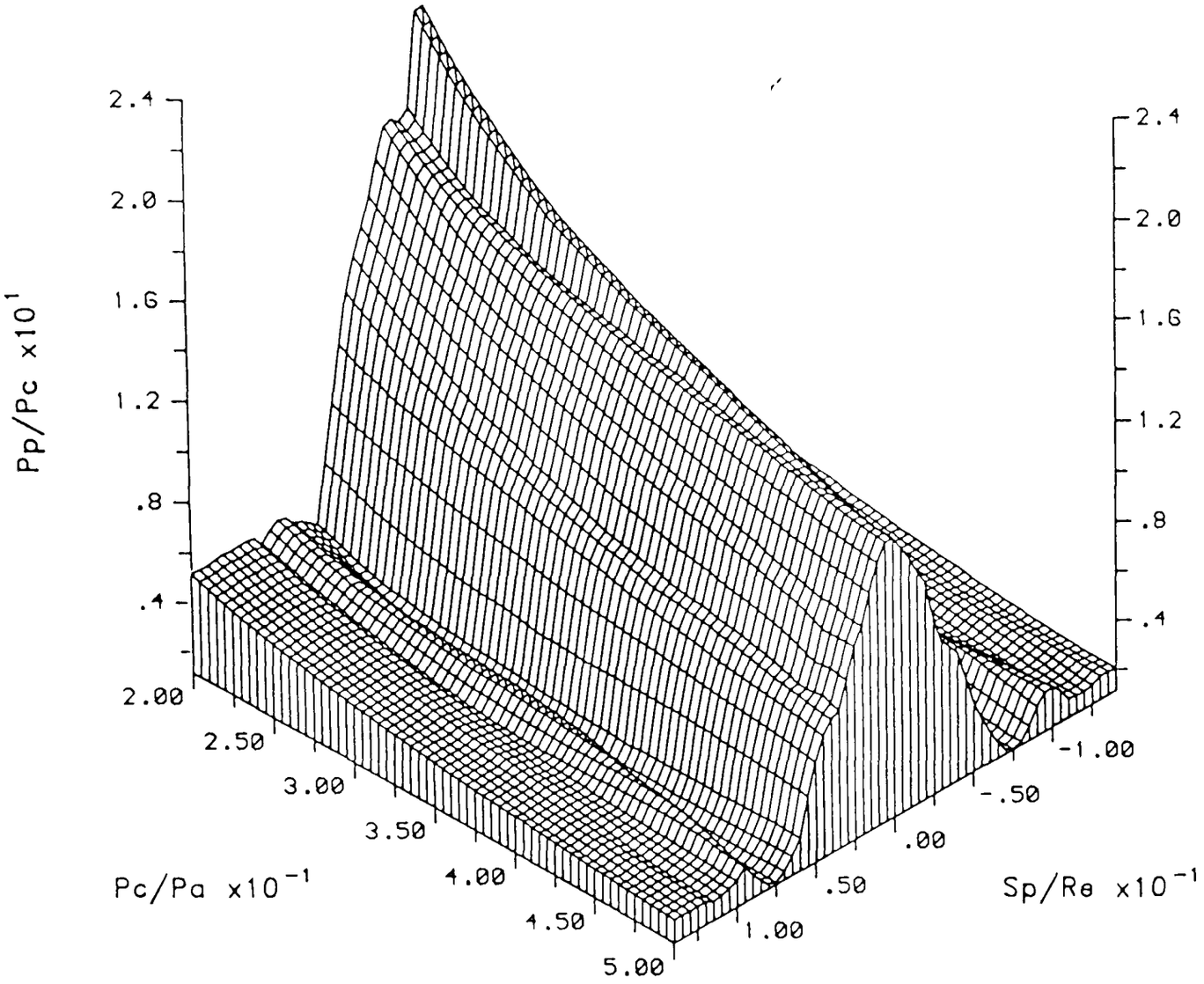

FIGURE 6.38 ROCKET JET IMPINGEMENT – ISOMETRIC PLOT OF VARIATION OF FLAT PLATE PRESSURE DISTRIBUTION WITH JET PRESSURE RATIO FOR: Me=1.0, Zp/Re=5.0, θ=90.0°

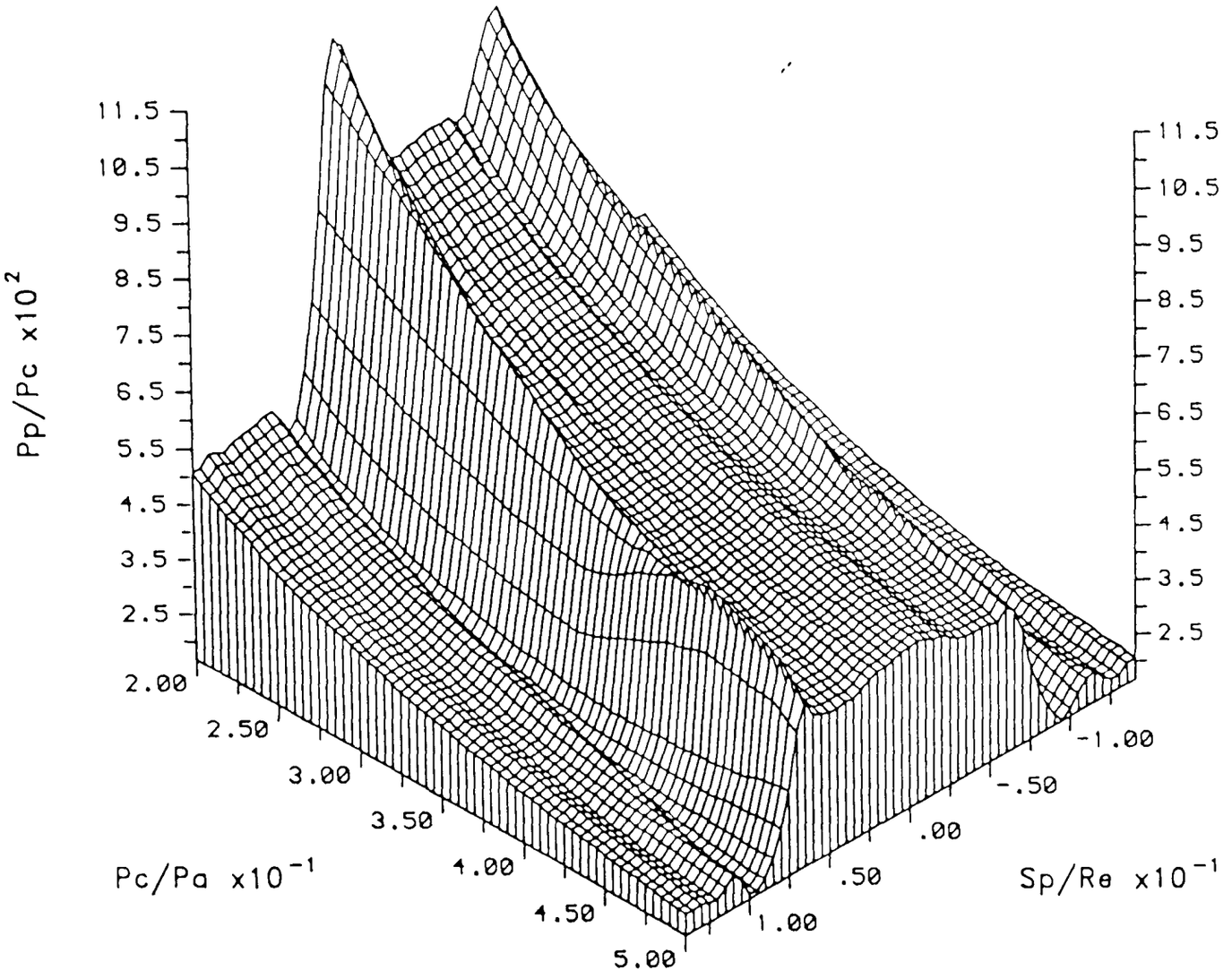

FIGURE 6.39 ROCKET JET IMPINGEMENT – ISOMETRIC PLOT OF VARIATION OF FLAT PLATE PRESSURE DISTRIBUTION WITH JET PRESSURE RATIO FOR: Me=1.0, Zp/Re=10.0, θ=90.0°

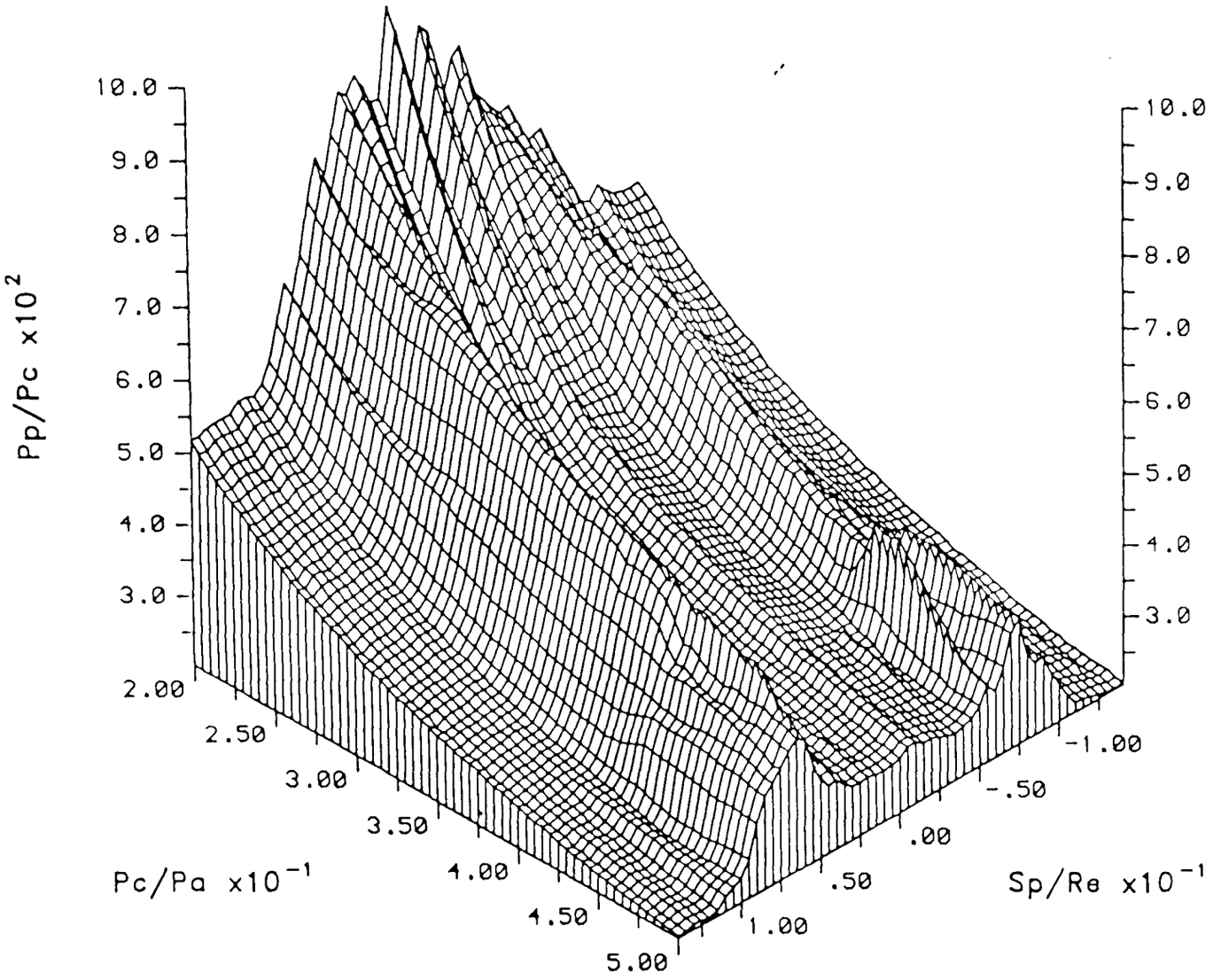

FIGURE 6.40 ROCKET JET IMPINGEMENT – ISOMETRIC PLOT OF VARIATION OF FLAT PLATE PRESSURE DISTRIBUTION WITH JET PRESSURE RATIO FOR: Me=1.0, Zp/Re=20.0, θ=90.0°

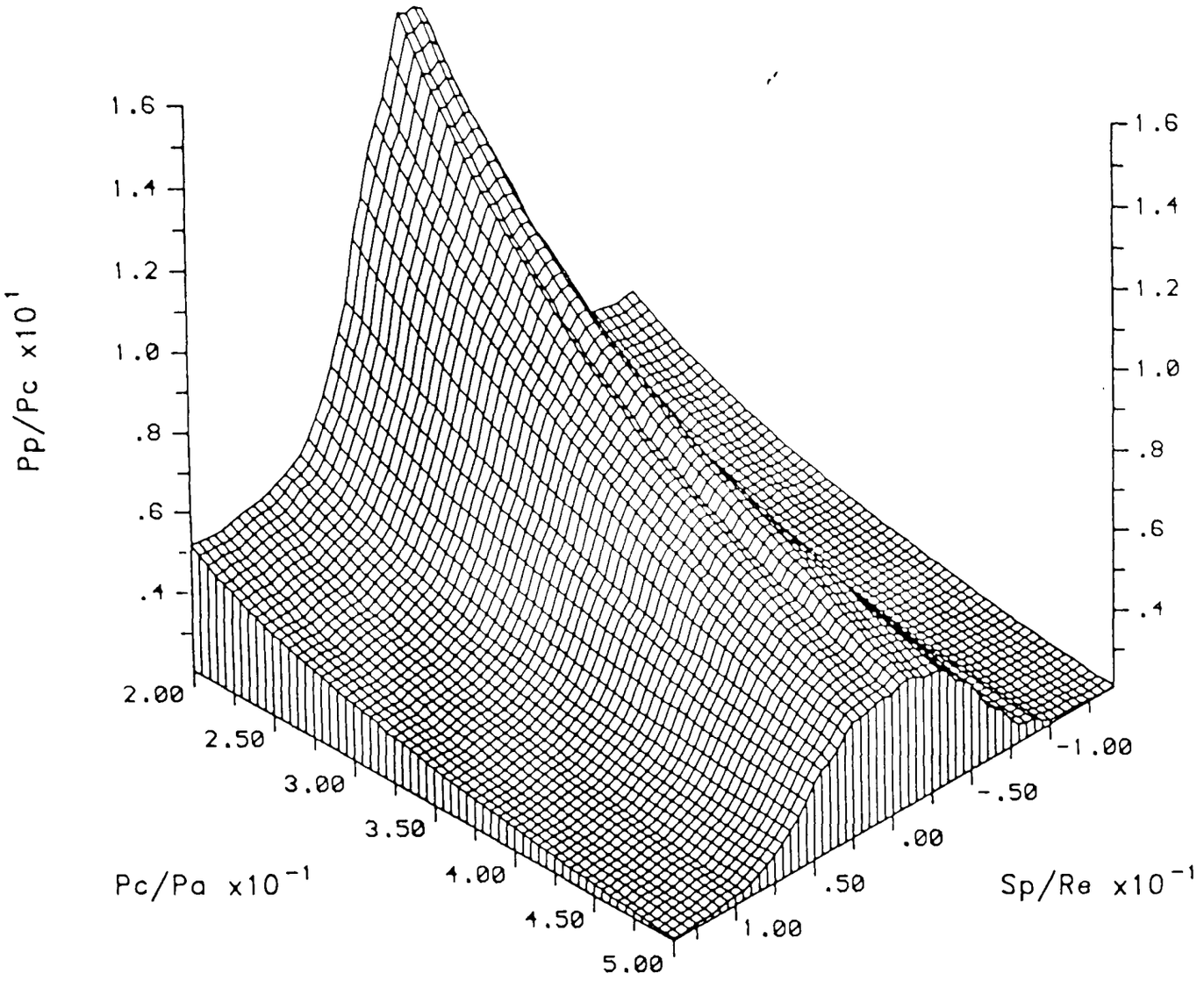

FIGURE 6.41 ROCKET JET IMPINGEMENT – ISOMETRIC PLOT OF VARIATION OF FLAT PLATE PRESSURE DISTRIBUTION WITH JET PRESSURE RATIO FOR: Me=1.0, Zp/Re=40.0, θ=90.0°

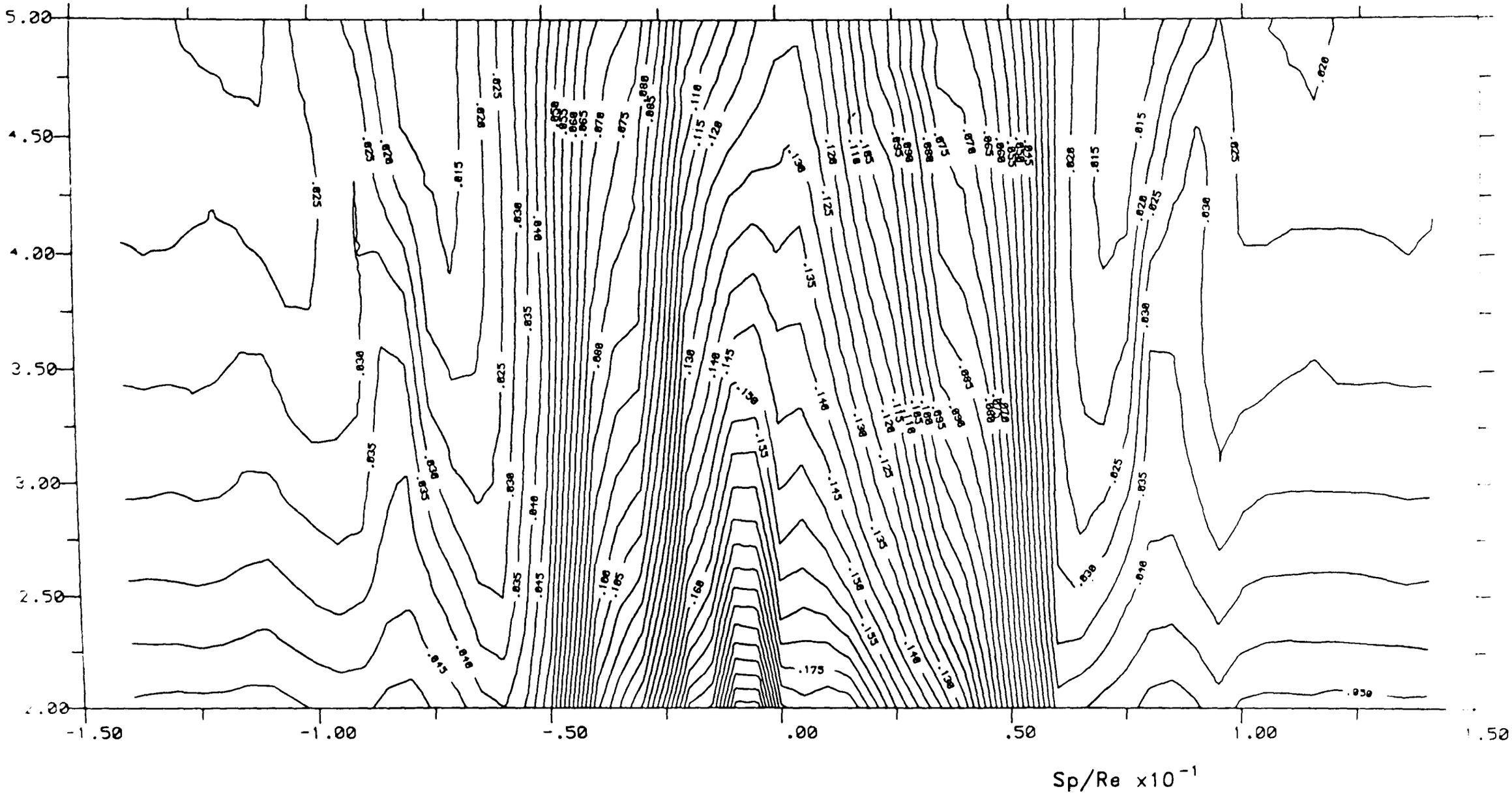

FIGURE 6.42 ROCKET JET IMPINGEMENT – CONTOUR PLOT OF VARIATION OF FLAT PLATE PRESSURE DISTRIBUTION WITH JET PRESSURE RATIO FOR: Me=1.0, Zp/Re=5.0, θ=90.0°

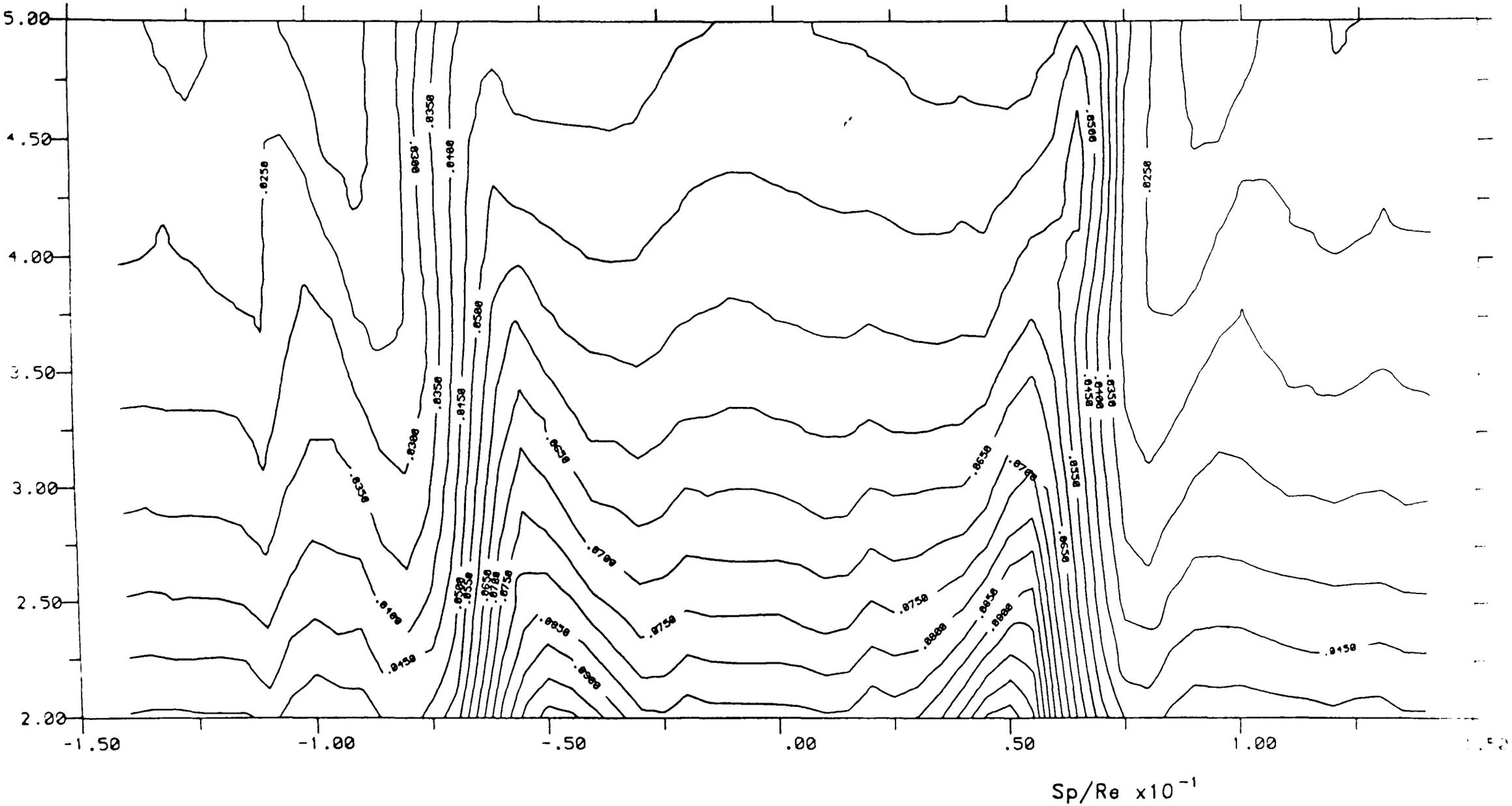

FIGURE 6.43 ROCKET JET IMPINGEMENT – CONTOUR PLOT OF VARIATION OF FLAT PLATE PRESSURE DISTRIBUTION WITH JET PRESSURE RATIO FOR: Me=1.0, Zp/Re=10.0, θ=90.0°

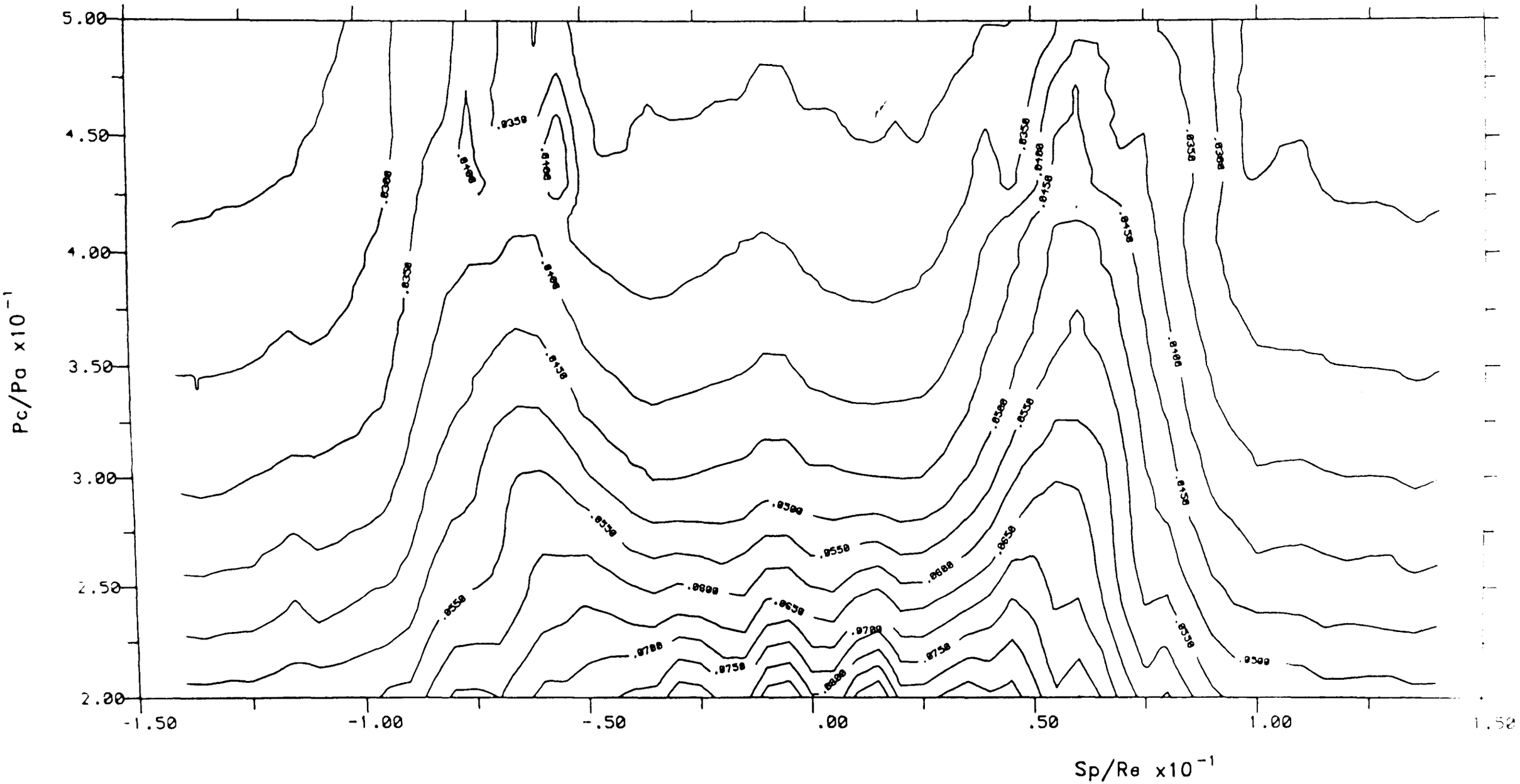

FIGURE 6.44 ROCKET JET IMPINGEMENT – CONTOUR PLOT OF VARIATION OF FLAT PLATE PRESSURE DISTRIBUTION WITH JET PRESSURE RATIO FOR: Me=1.0, Zp/Re=20.0, θ=90.0°

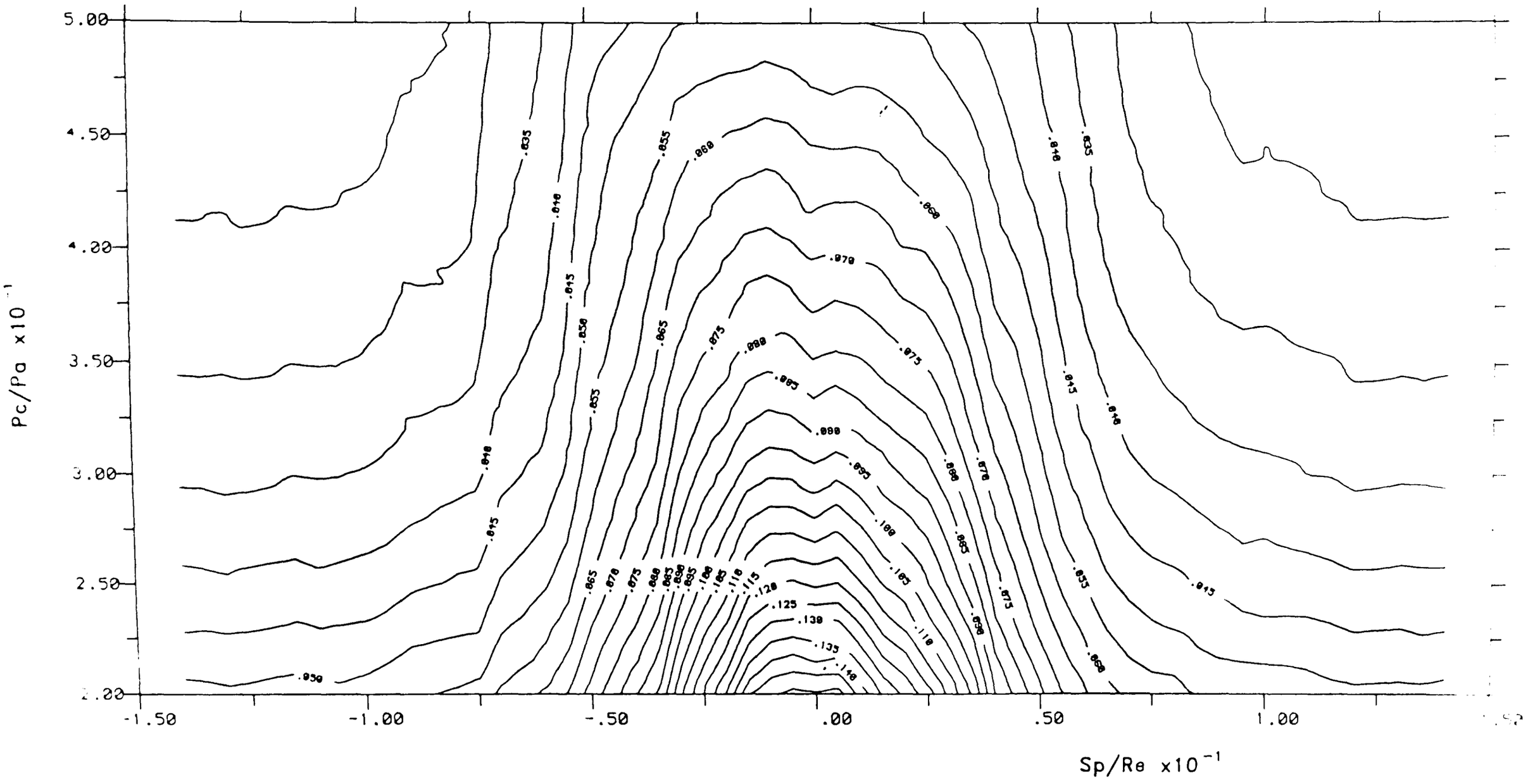

FIGURE 6.45 ROCKET JET IMPINGEMENT – CONTOUR PLOT OF VARIATION OF FLAT PLATE PRESSURE DISTRIBUTION WITH JET PRESSURE RATIO FOR: Me=1.0, Zp/Re=40.0, θ=90.0°

(a) COMPLETE PLATE, $\alpha = 3°$

(b) COMPLETE PLATE, $\alpha = 45°$

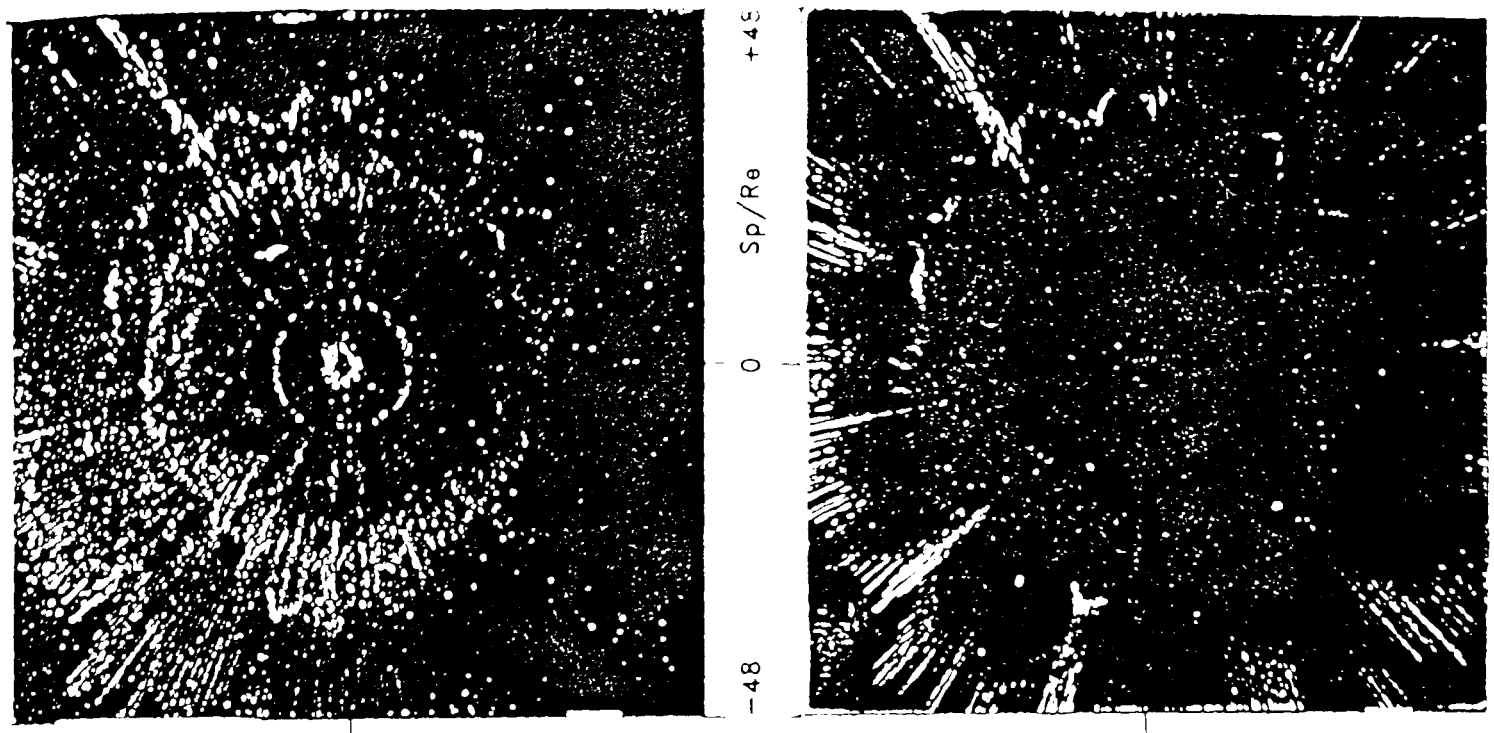

THESE PHOTOGRAPHS HAVE BEEN ARRANGED SO THAT THE ARRAYS OF PRESSURE TAPPINGS ARE CO-LINEAR WITH THE LINES ADJACENT TO THIS TEXT

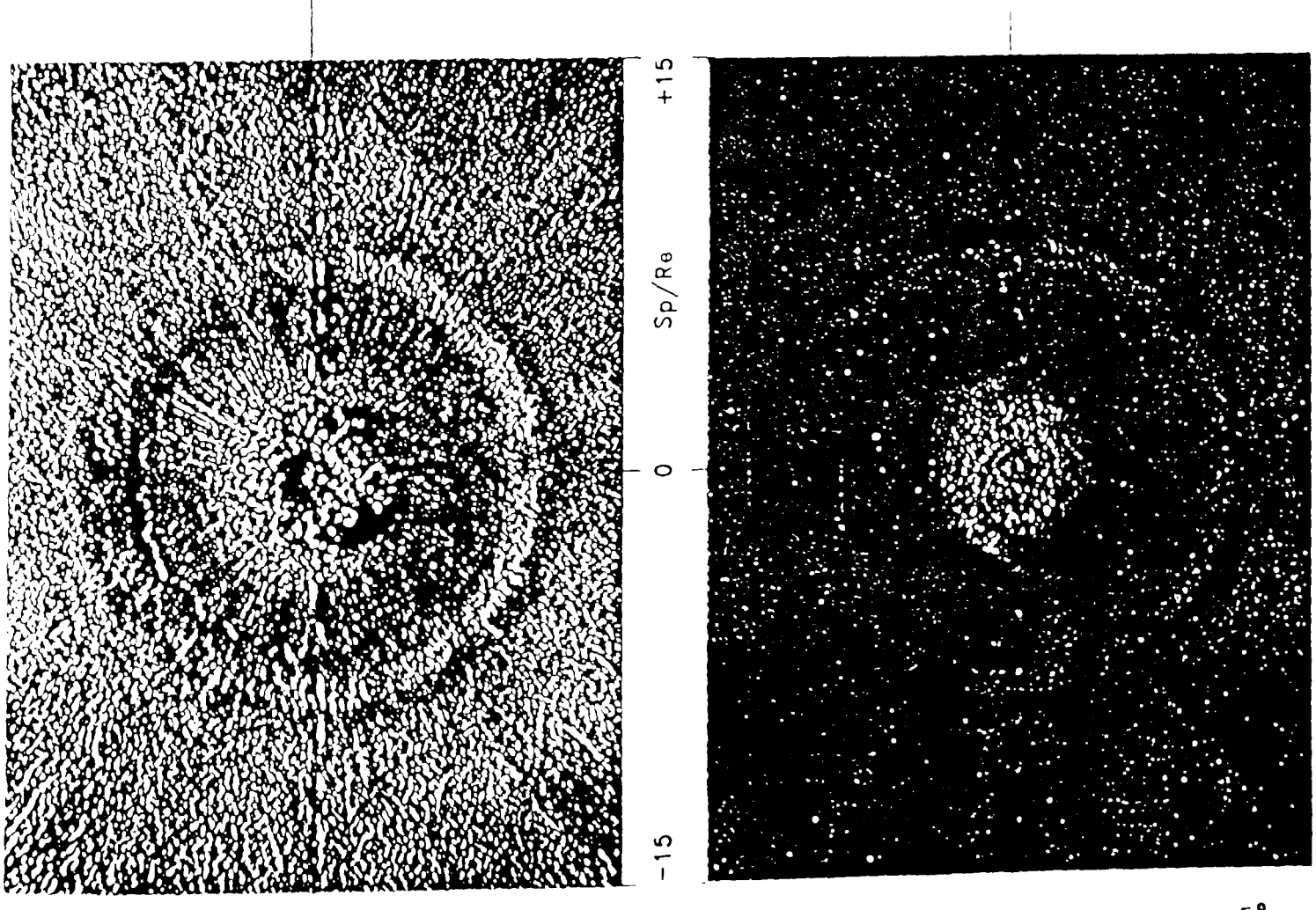

(c) TAPPING REGION, $\alpha = 3°$

(d) TAPPING REGION, $\alpha = 45°$

FIGURE 6.46 ROCKET JET IMPINGEMENT FLAT PLATE HEAT DEPOSITION FOR: Z_p, R_e 5.0, α 90.0°

(a) COMPLETE PLATE, α = 3°

(b) COMPLETE PLATE, α = 45°

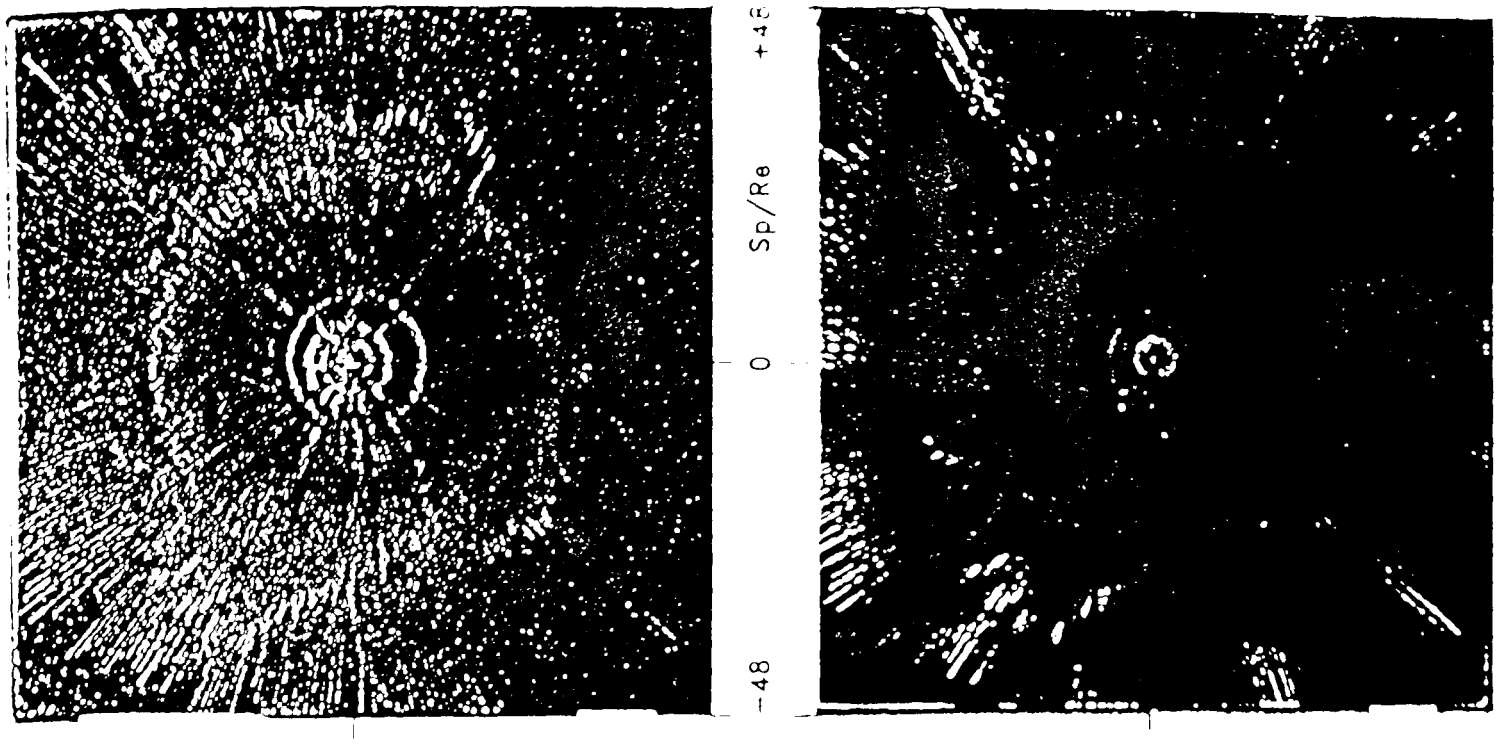

THESE PHOTOGRAPHS HAVE BEEN ARRANGED SO THAT THE ARRAYS OF PRESSURE TAPPINGS ARE CO-LINEAR WITH THE LINES ADJACENT TO THIS TEXT

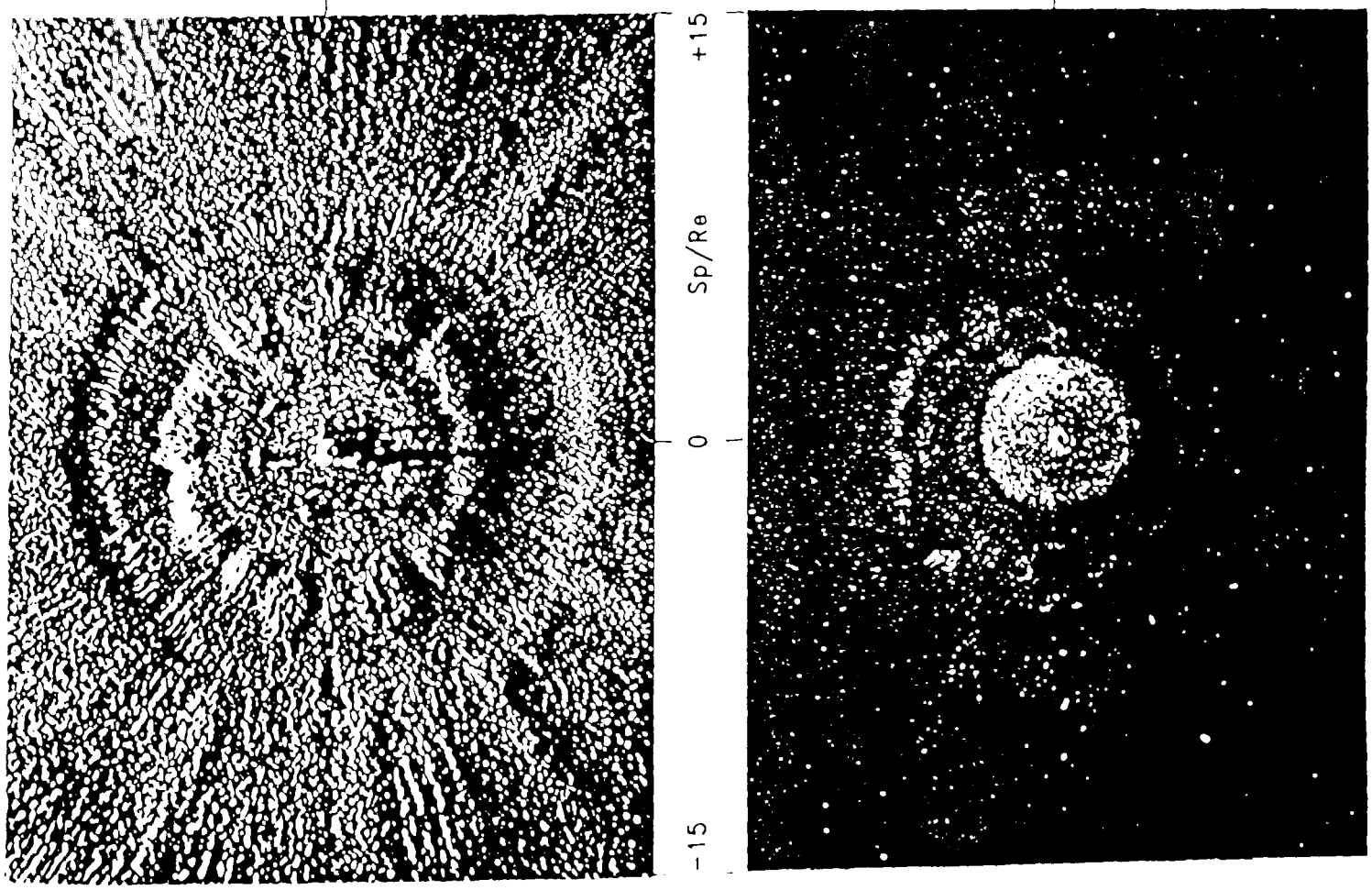

(c) TAPPING REGION, α = 3°

(d) TAPPING REGION, α = 45°

FIGURE 6.47 ROCKET JET IMPINGEMENT FLAT PLATE SOOT DEPOSITION FOR: Jp/Re 10.0, θ 90.0°

(a) COMPLETE PLATE, α = 3

(b) COMPLETE PLATE, α = 45

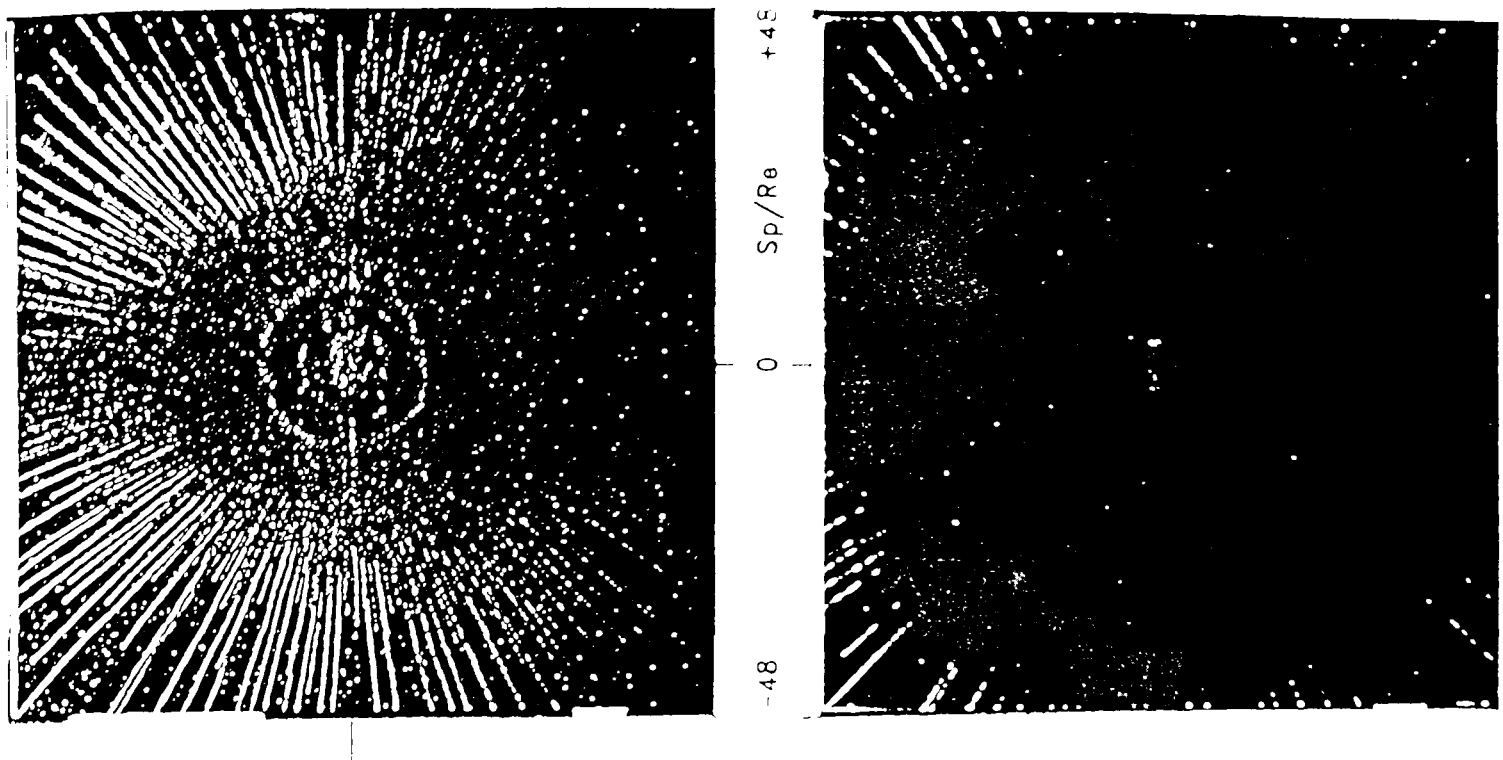

THESE PHOTOGRAPHS HAVE BEEN ARRANGED SO THAT THE ARRAYS OF PRESSURE TAPPINGS ARE CO-LINEAR WITH THE LINES ADJACENT TO THIS TEXT

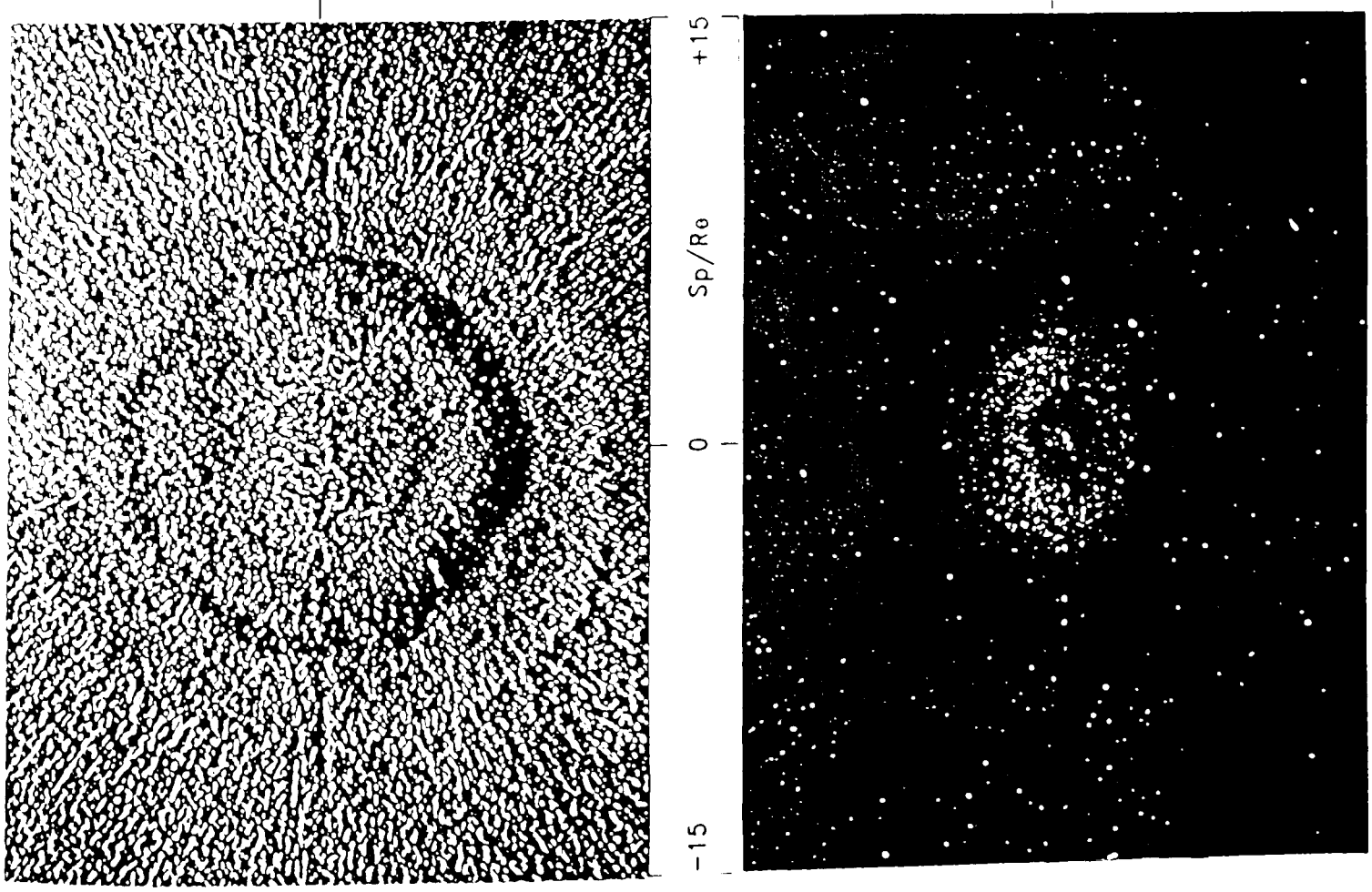

(c) TAPPING REGION, α = 3°

(d) TAPPING REGION, α = 45°

FIGURE 6.46 ROCKET JET IMPINGEMENT FLAT PLATE SOOT DEPOSITION FOR θ = 90.0°

(a) COMPLETE PLATE, $\alpha = 3°$

(b) COMPLETE PLATE, $\alpha = 45°$

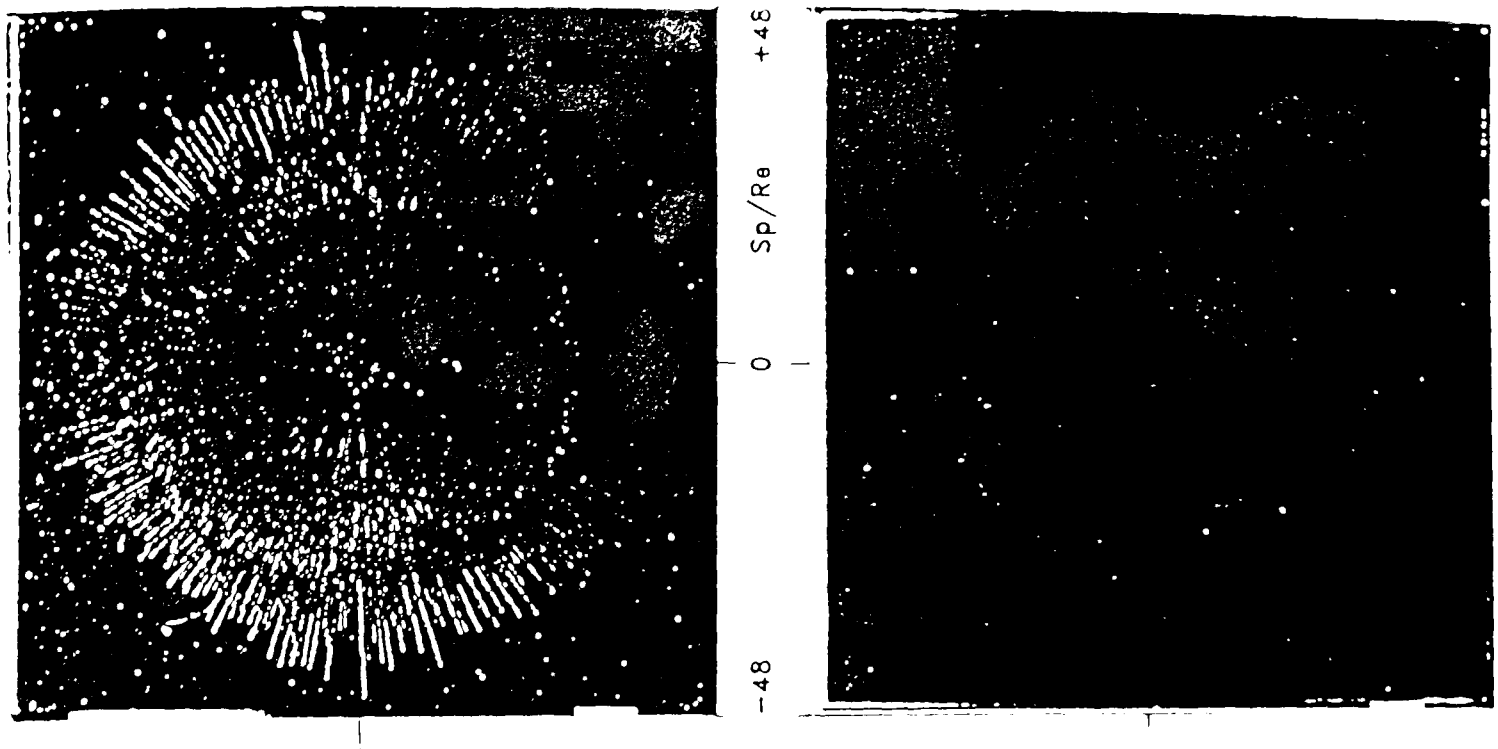

THESE PHOTOGRAPHS HAVE BEEN ARRANGED SO THAT THE ARRAYS OF PRESSURE TAPPINGS ARE CO-LINEAR WITH THE LINES ADJACENT TO THIS TEXT

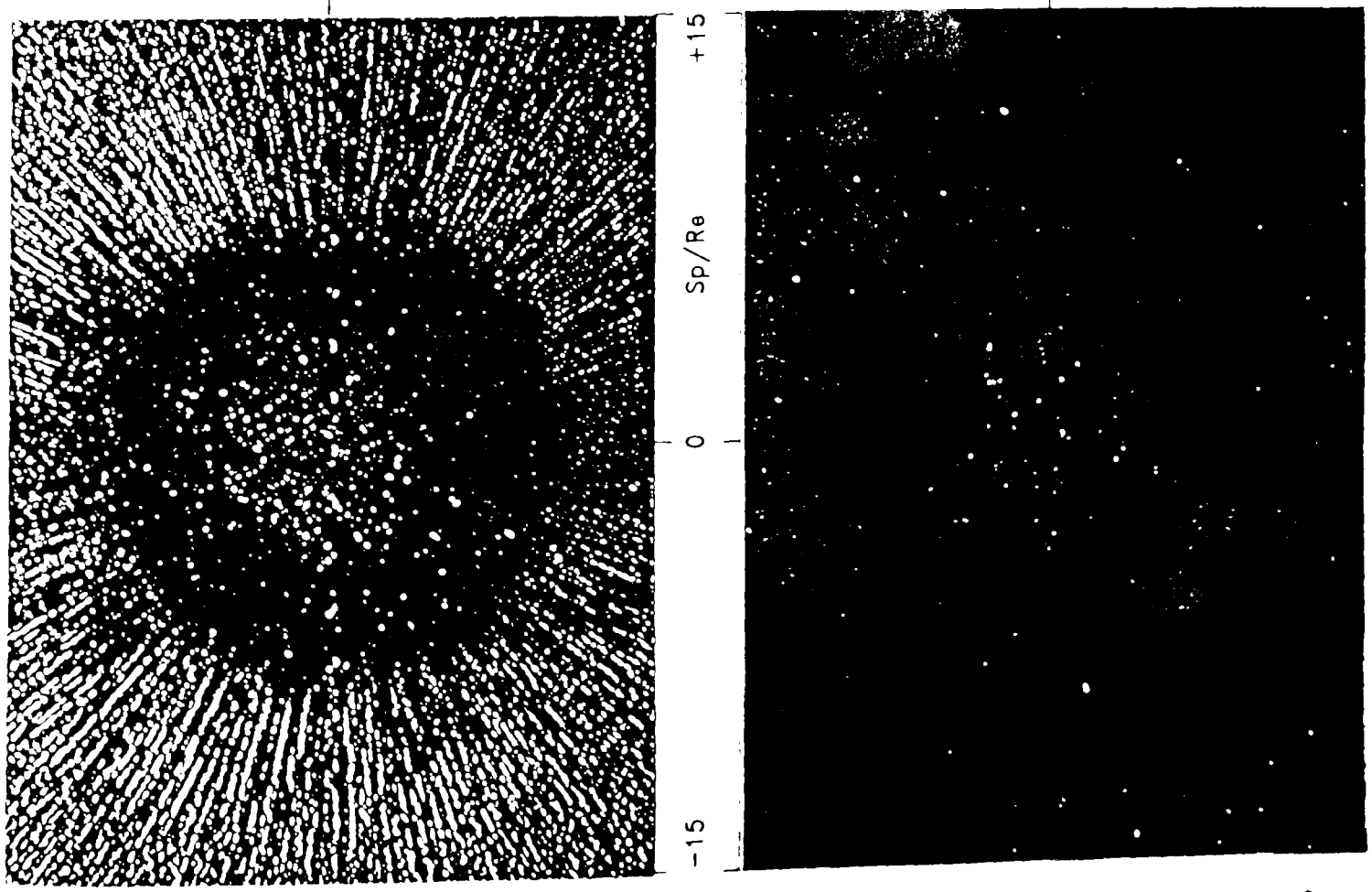

(c) TAPPING REGION, $\alpha = 3°$

(d) TAPPING REGION, $\alpha = 45°$

FIGURE C.49 ROCKET JET IMPINGEMENT FLAT PLATE SOOT DEPOSITION FOR: $Sp/R\theta = 40.0$, $\theta = 90.0°$

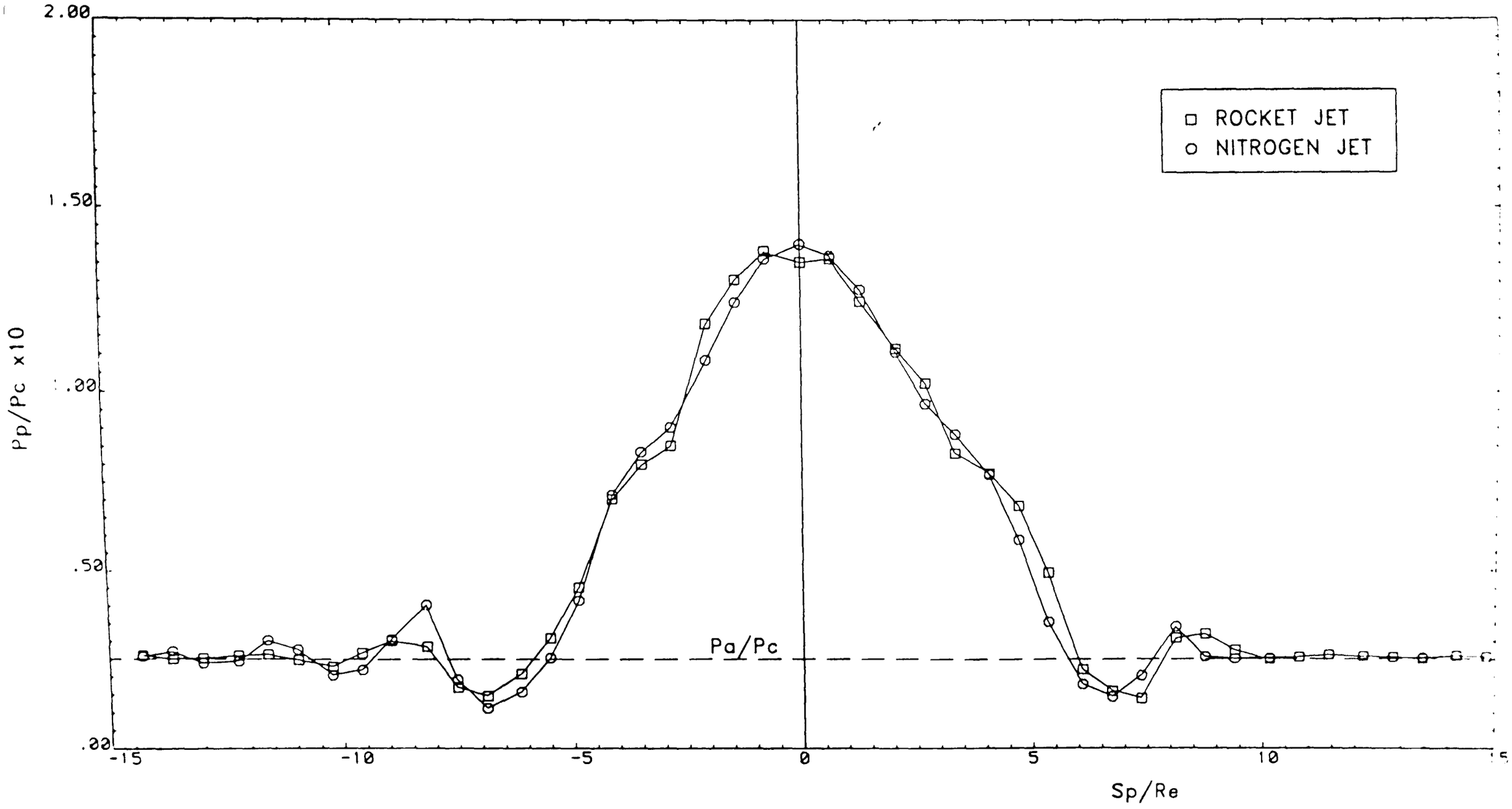

FIGURE 6.50 COMPARISON OF FLAT PLATE PRESSURE DISTRIBUTIONS GENERATED BY IMPINGING ROCKET AND NITROGEN JETS WHEN: Me=1.0, Pc/Pa=40.0, Zp/Re=5.0, θ=90.0°

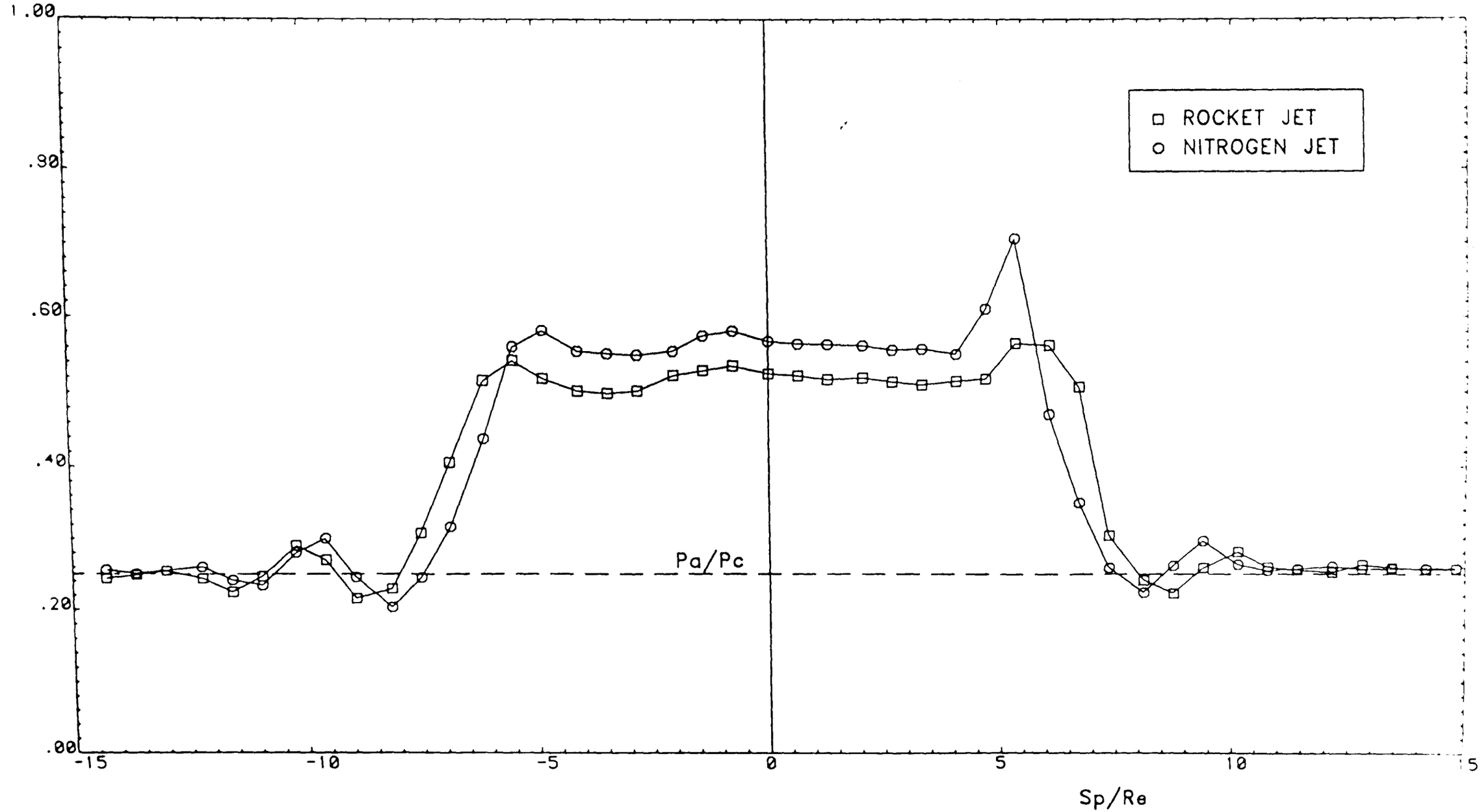

FIGURE 6.51 COMPARISON OF FLAT PLATE PRESSURE DISTRIBUTIONS GENERATED BY IMPINGING ROCKET AND NITROGEN JETS WHEN: Me=1.0, Pc/Pa=40.0, Zp/Re=10.0, θ=90.0

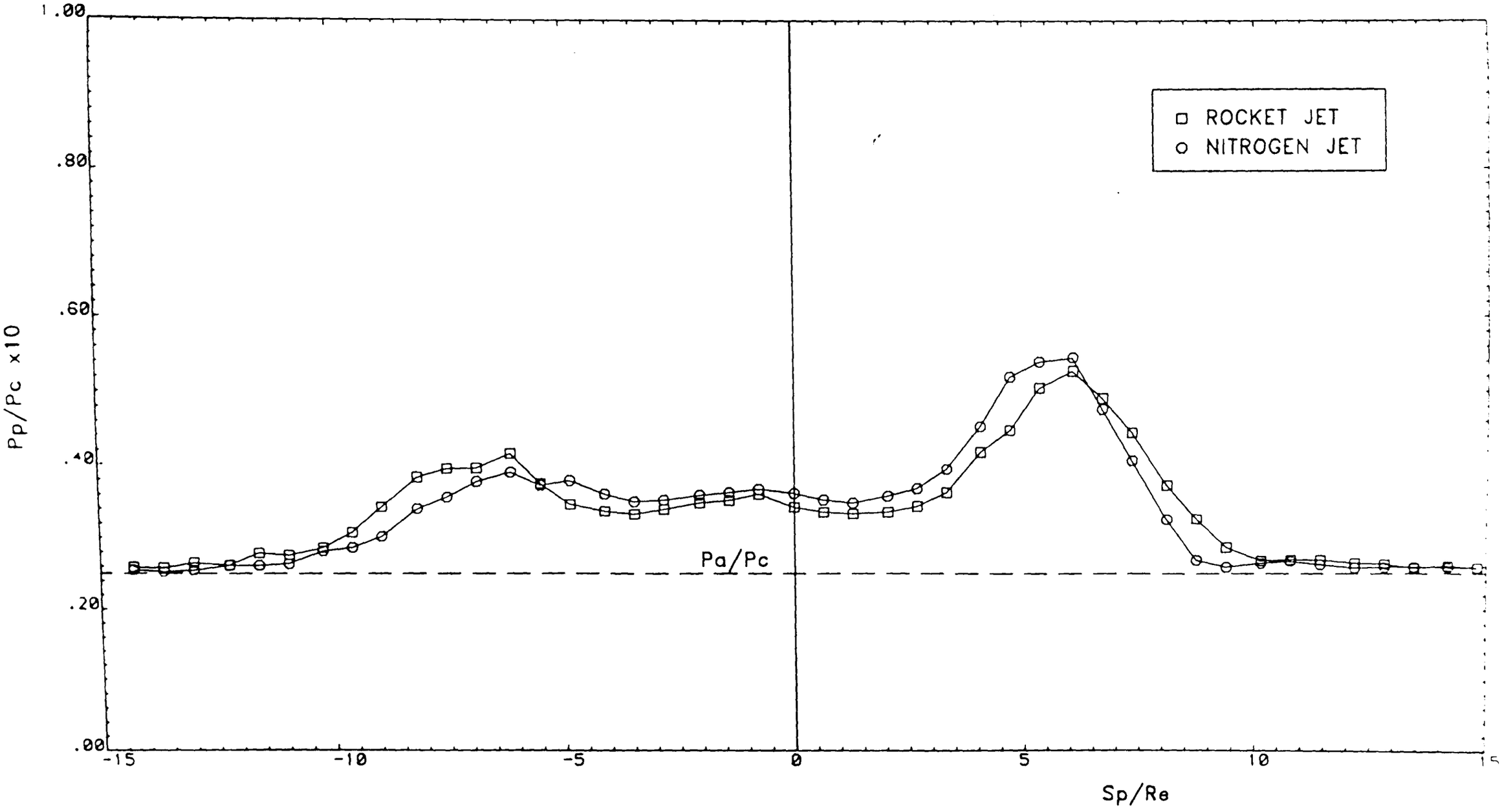

FIGURE 6.52 COMPARISON OF FLAT PLATE PRESSURE DISTRIBUTIONS GENERATED BY IMPINGING ROCKET AND NITROGEN JETS WHEN: Me=1.0, Pc/Pa=40.0, Zp/Re=20.0, θ=90.0°

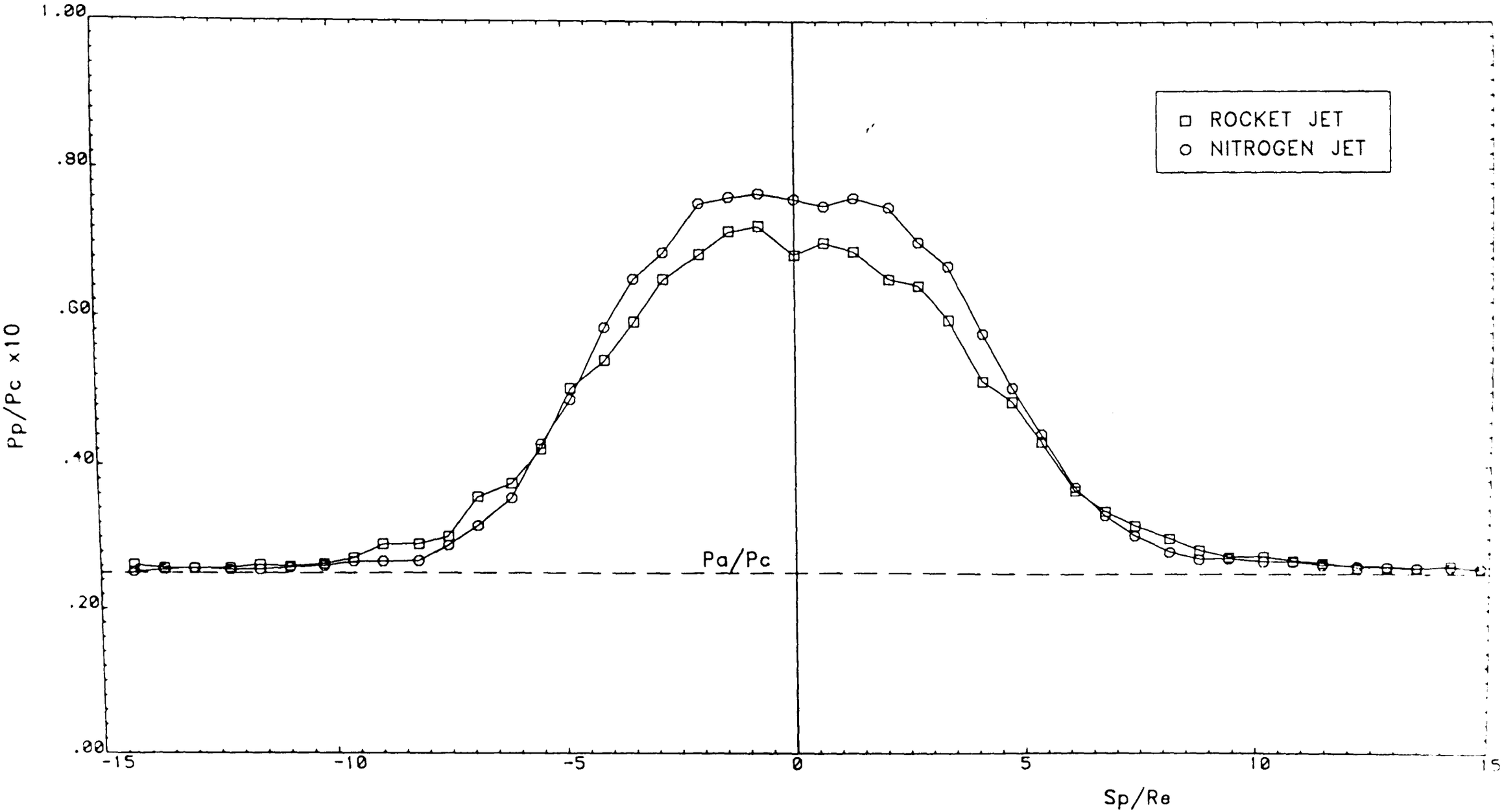

FIGURE 6.53 COMPARISON OF FLAT PLATE PRESSURE DISTRIBUTIONS GENERATED BY IMPINGING ROCKET AND NITROGEN JETS WHEN: Me=1.0, Pc/Pa=40.0, Zp/Re=40.0, θ=90.0°

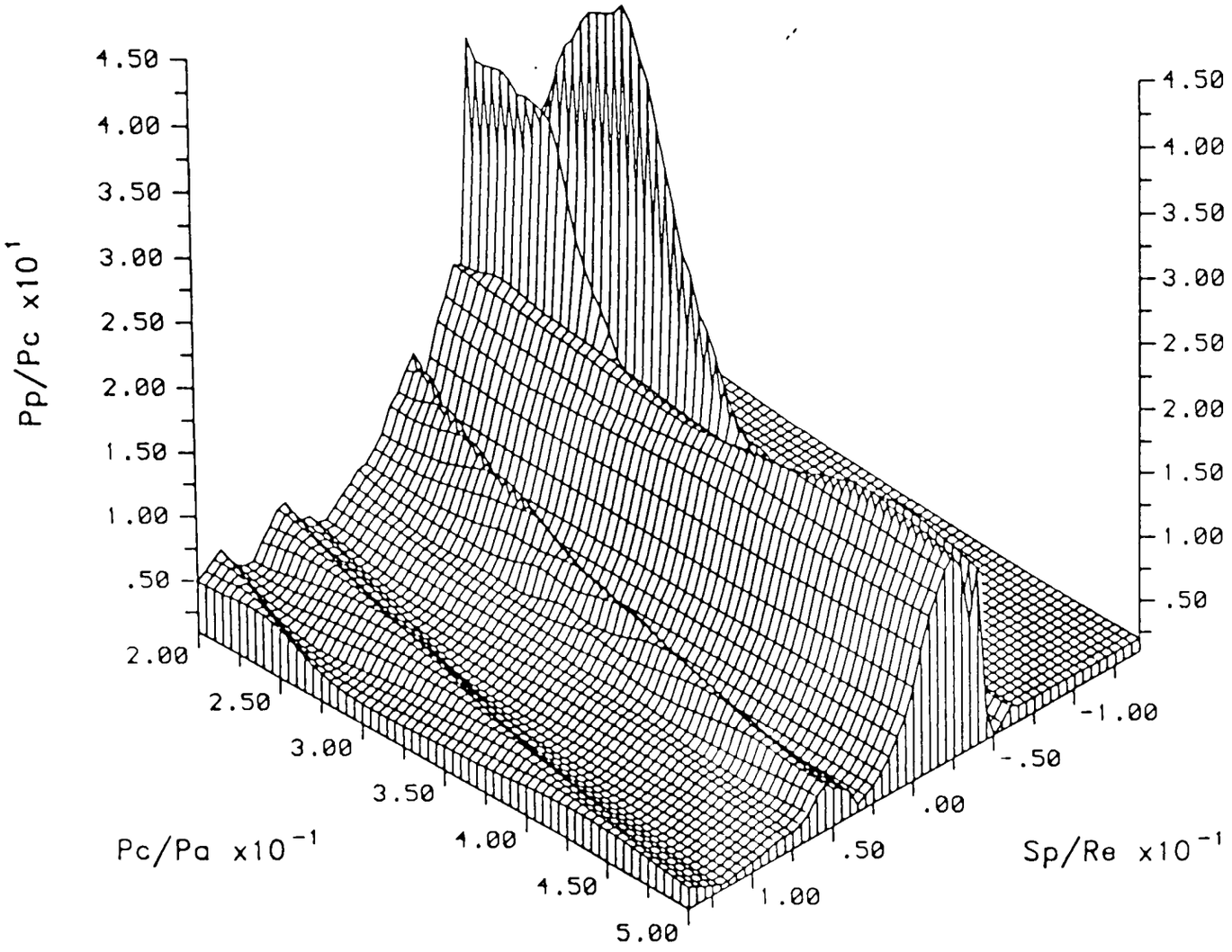

FIGURE 6.54 NITROGEN JET IMPINGEMENT – ISOMETRIC PLOT OF VARIATION OF FLAT PLATE PRESSURE DISTRIBUTION WITH JET PRESSURE RATIO FOR: Me=1.0, Zp/Re=5.0, θ=45.0°

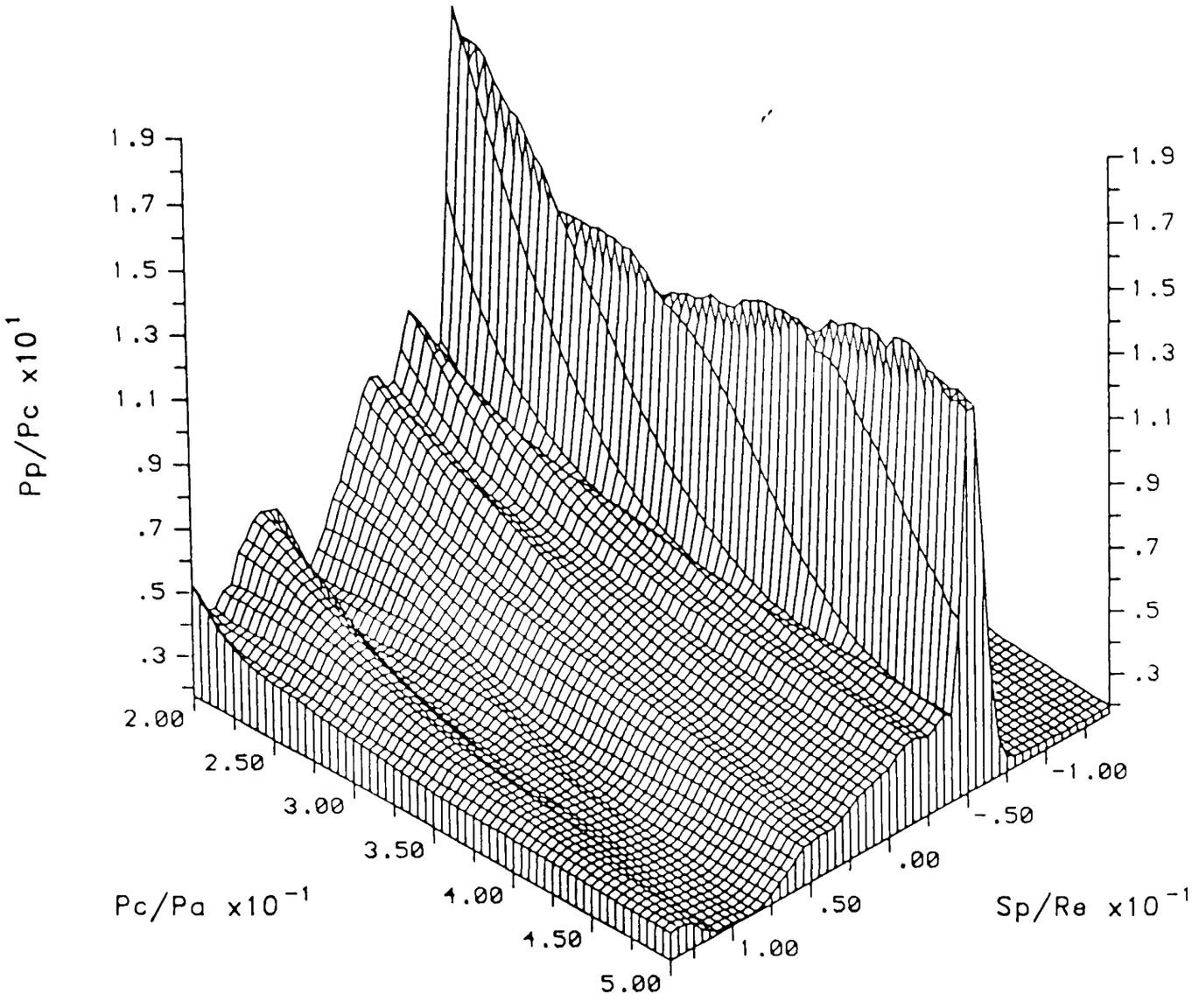

FIGURE 6.55 NITROGEN JET IMPINGEMENT – ISOMETRIC PLOT OF VARIATION OF FLAT PLATE PRESSURE DISTRIBUTION WITH JET PRESSURE RATIO FOR: Me=1.0, Zp/Re=10.0, θ=45.0°

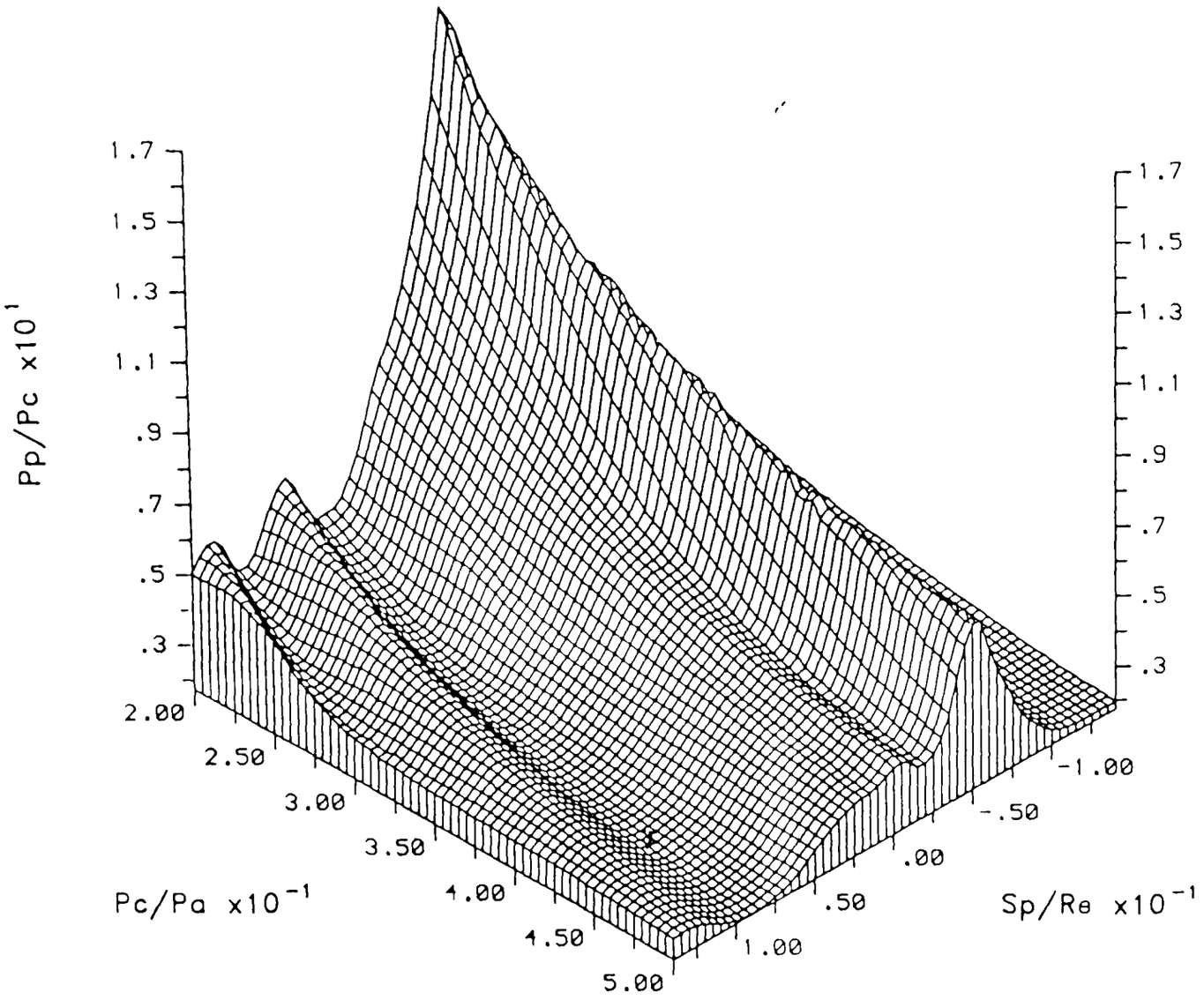

FIGURE 6.56 NITROGEN JET IMPINGEMENT – ISOMETRIC PLOT OF VARIATION OF FLAT PLATE PRESSURE DISTRIBUTION WITH JET PRESSURE RATIO FOR: M_e=1.0, Z_p/R_e=20.0, θ=45.0°

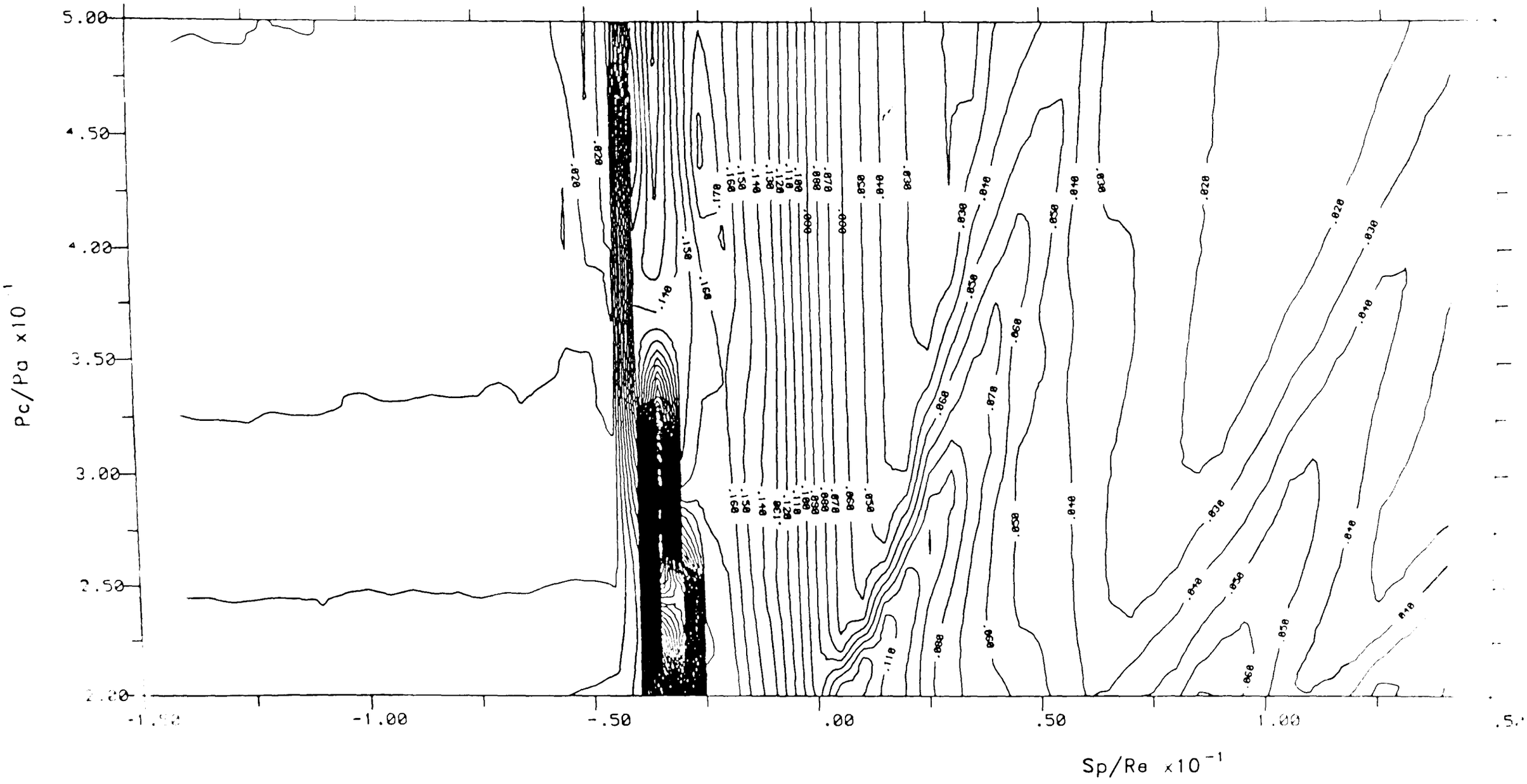

FIGURE 6.58 NITROGEN JET IMPINGEMENT – CONTOUR PLOT OF VARIATION OF FLAT PLATE PRESSURE DISTRIBUTION WITH JET PRESSURE RATIO FOR: Me=1.0, Zp/Re=5.0, θ=45.0°

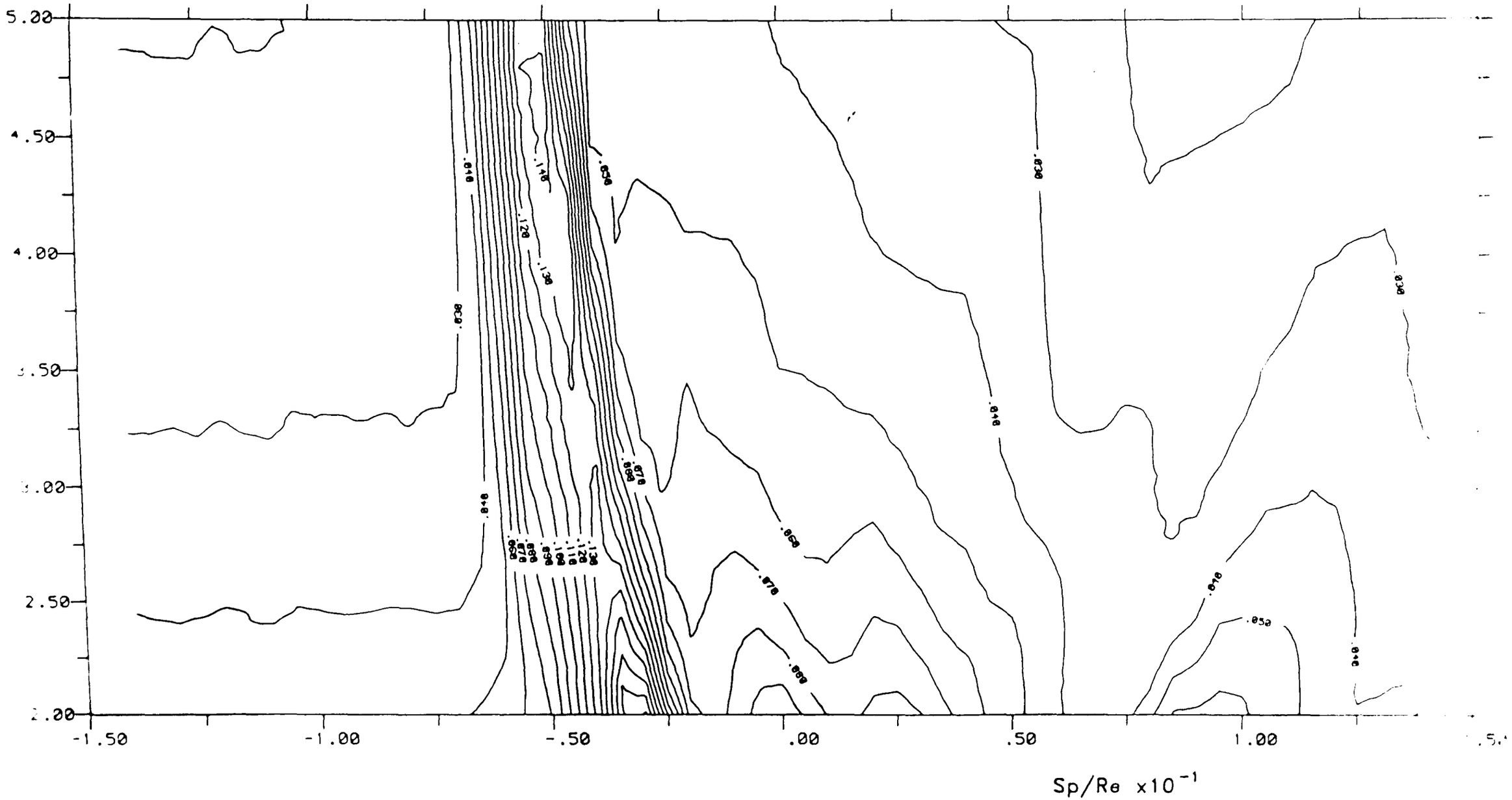

FIGURE 6.59 NITROGEN JET IMPINGEMENT – CONTOUR PLOT OF VARIATION OF FLAT PLATE PRESSURE DISTRIBUTION WITH JET PRESSURE RATIO FOR: Me=1.0, Zp/Re=10.0, θ=45.0°

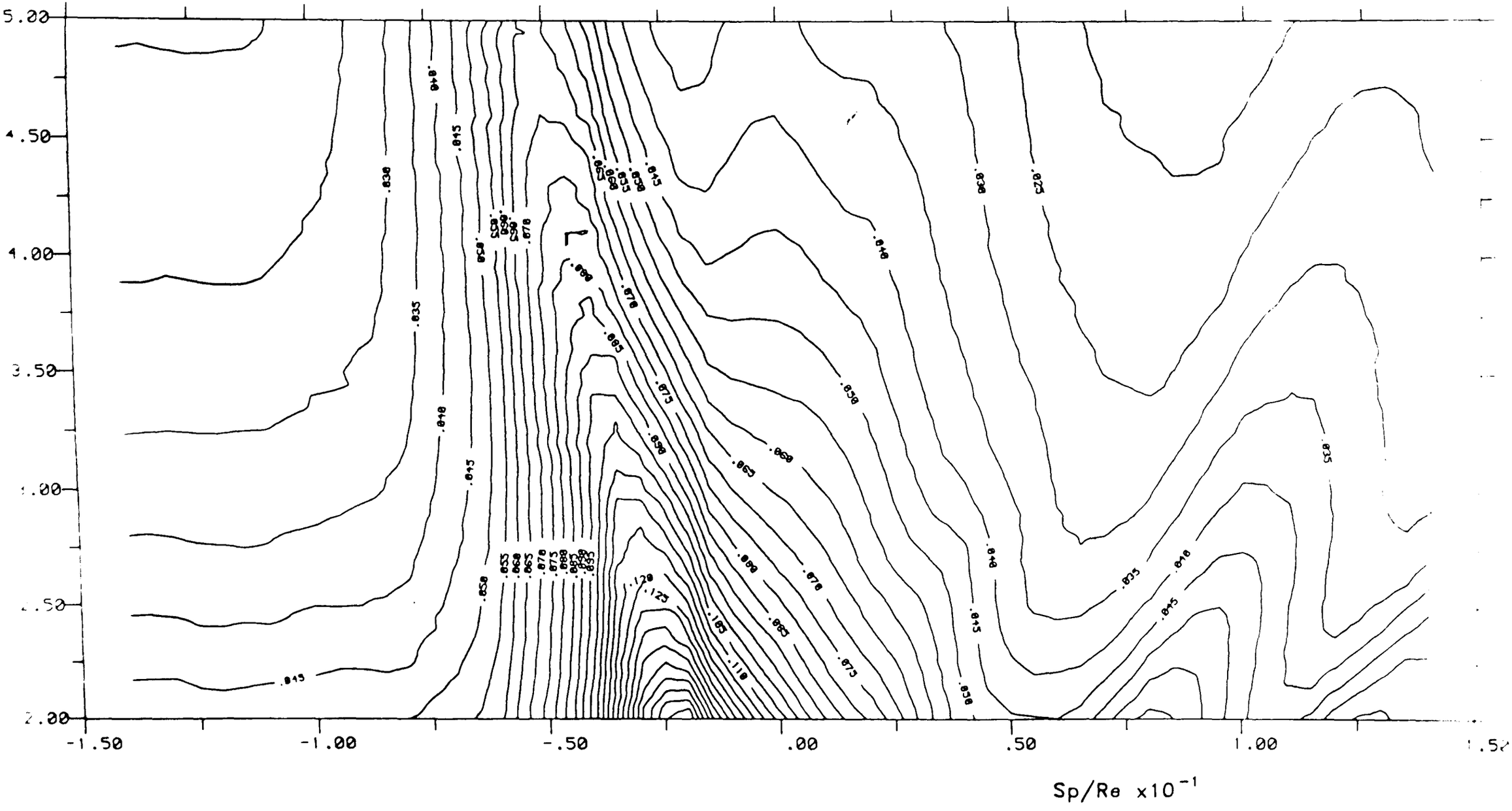

FIGURE 6.60 NITROGEN JET IMPINGEMENT – CONTOUR PLOT OF VARIATION OF FLAT PLATE PRESSURE DISTRIBUTION WITH JET PRESSURE RATIO FOR: Me=1.0, Zp/Re=20.0, θ=45.0°

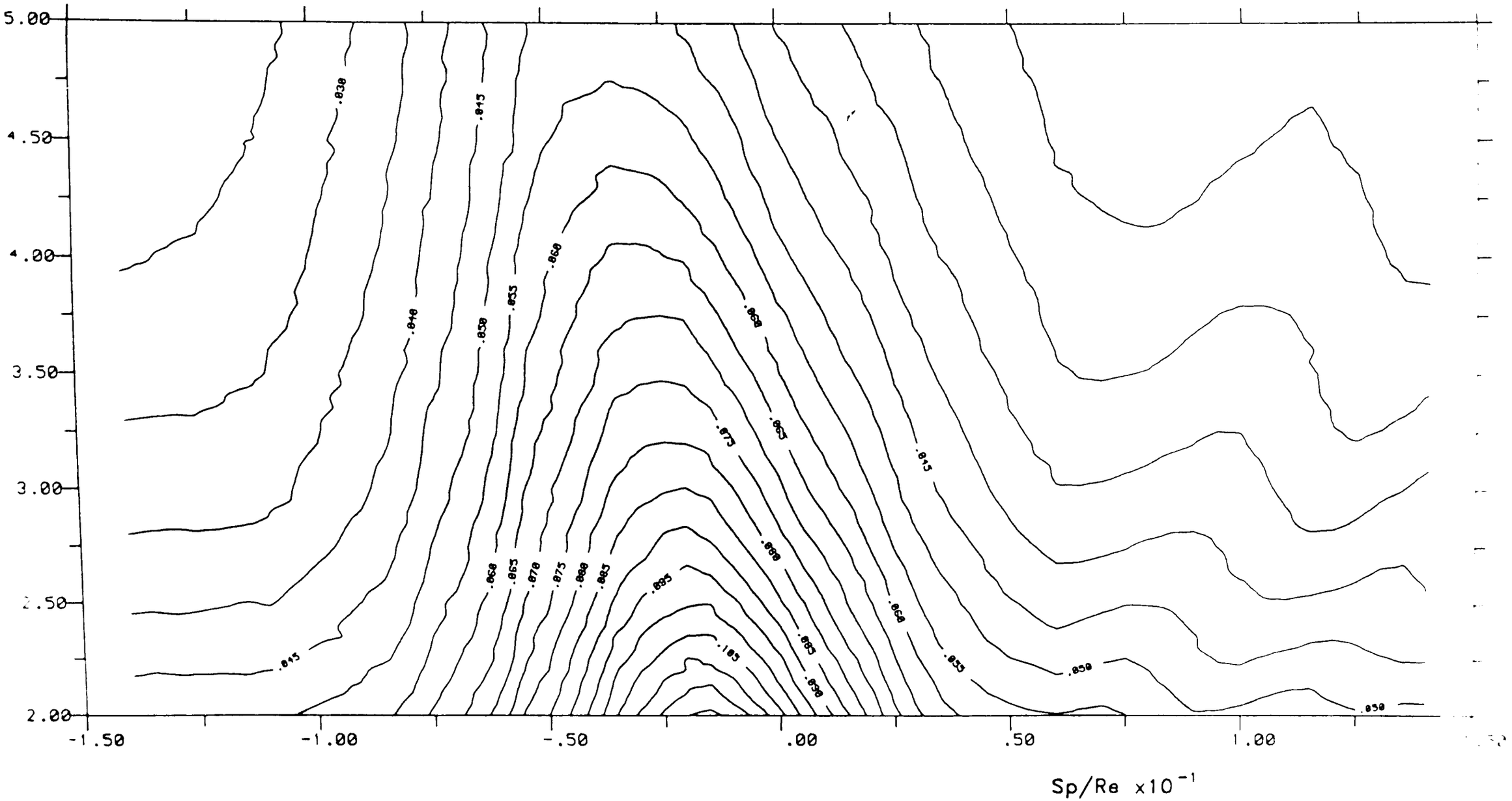

FIGURE 6.61 NITROGEN JET IMPINGEMENT – CONTOUR PLOT OF VARIATION OF FLAT PLATE PRESSURE DISTRIBUTION WITH JET PRESSURE RATIO FOR: Me=1.0, Zp/Re=40.0, θ=45.0°

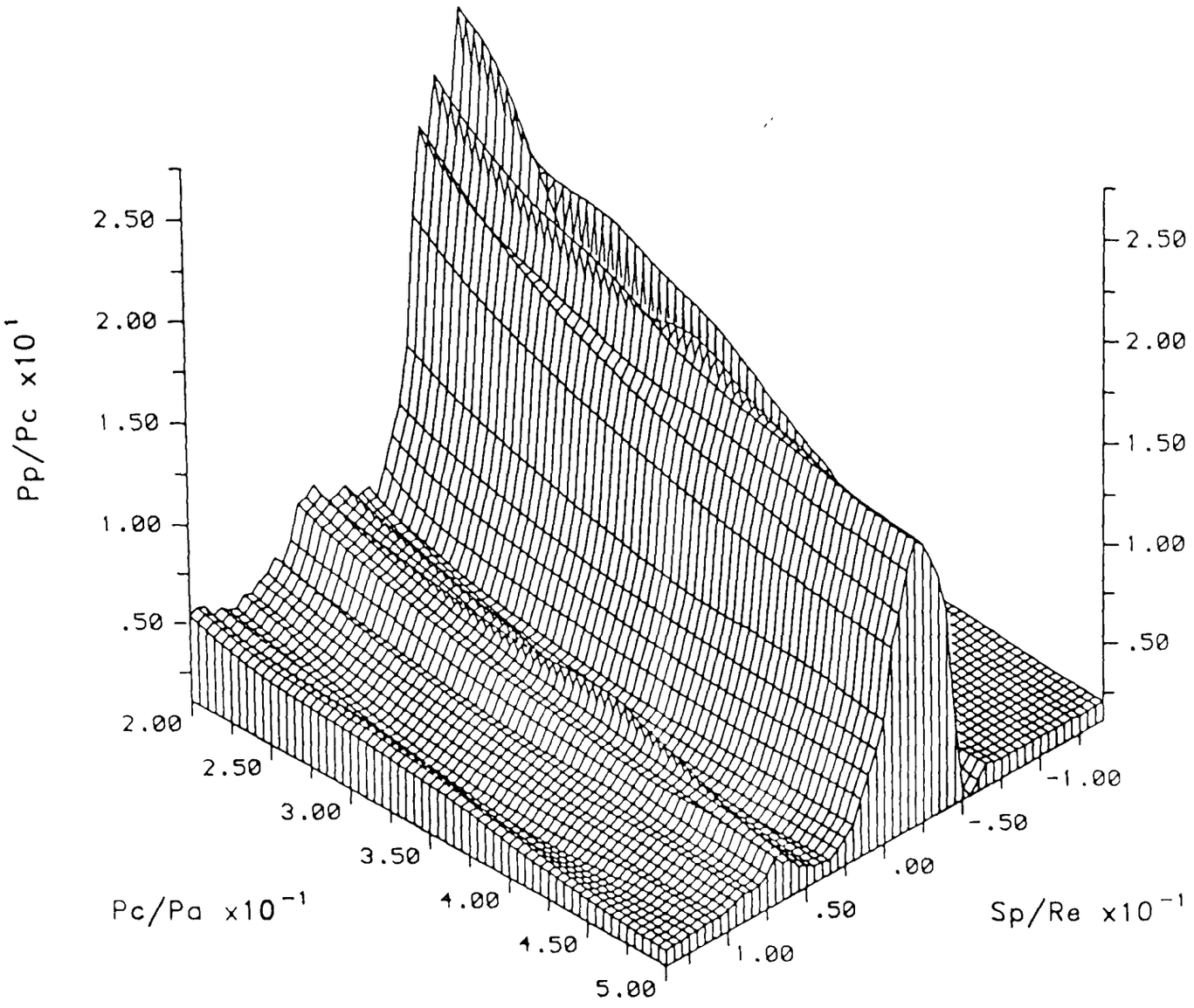

FIGURE 4.62 ROCKET JET IMPINGEMENT – ISOMETRIC PLOT OF VARIATION OF FLAT PLATE PRESSURE DISTRIBUTION WITH JET PRESSURE RATIO FOR: Me=1.0, Zp/Re=5.0, θ=45.0°

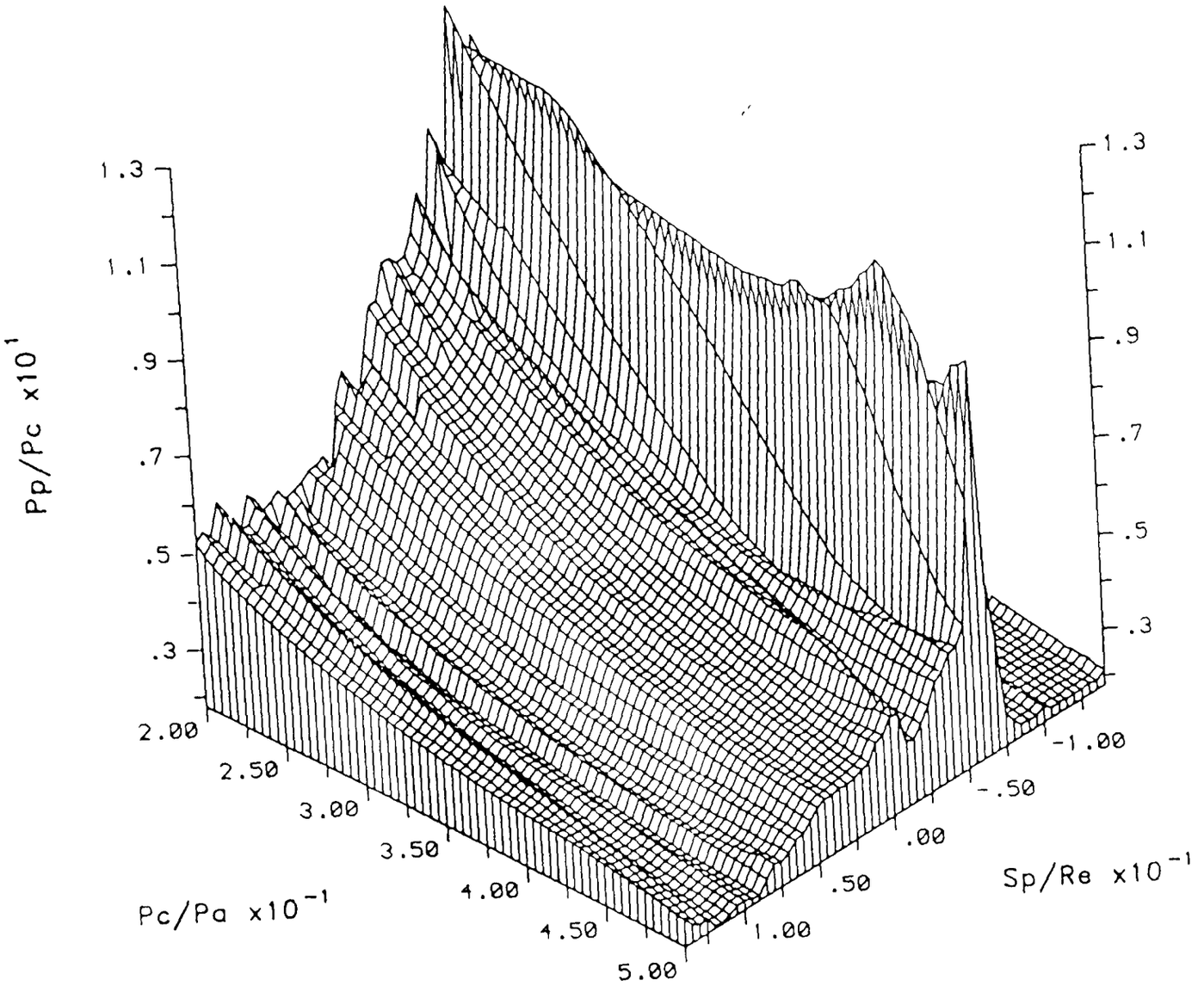

FIGURE 6.63 ROCKET JET IMPINGEMENT – ISOMETRIC PLOT OF VARIATION OF FLAT PLATE PRESSURE DISTRIBUTION WITH JET PRESSURE RATIO FOR: Me=1.0, Zp/Re=10.0, θ=45.0°

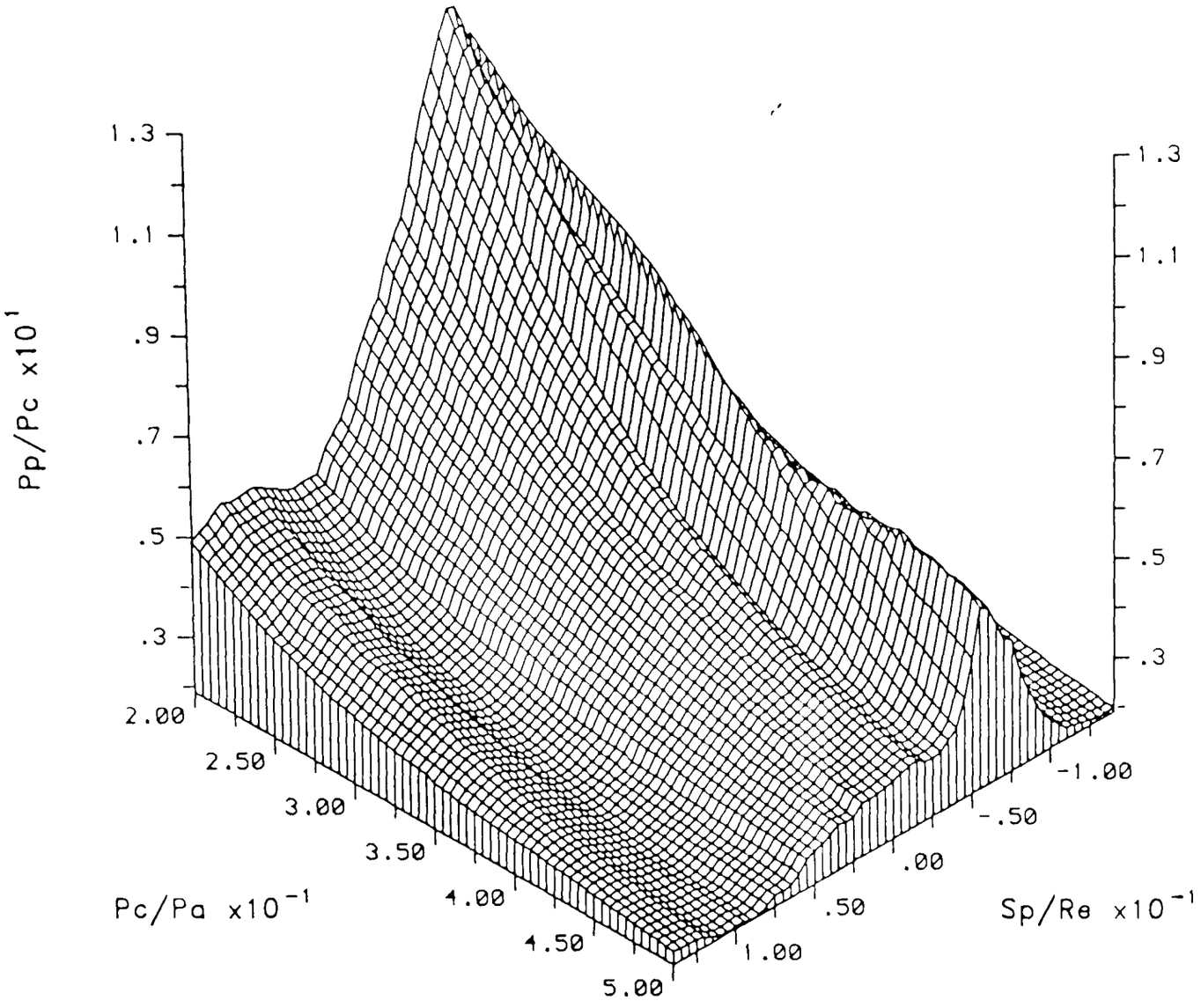

FIGURE 6.64 ROCKET JET IMPINGEMENT – ISOMETRIC PLOT OF VARIATION OF FLAT PLATE PRESSURE DISTRIBUTION WITH JET PRESSURE RATIO FOR: Me=1.0, Zp/Re=20.0, θ=45.0°

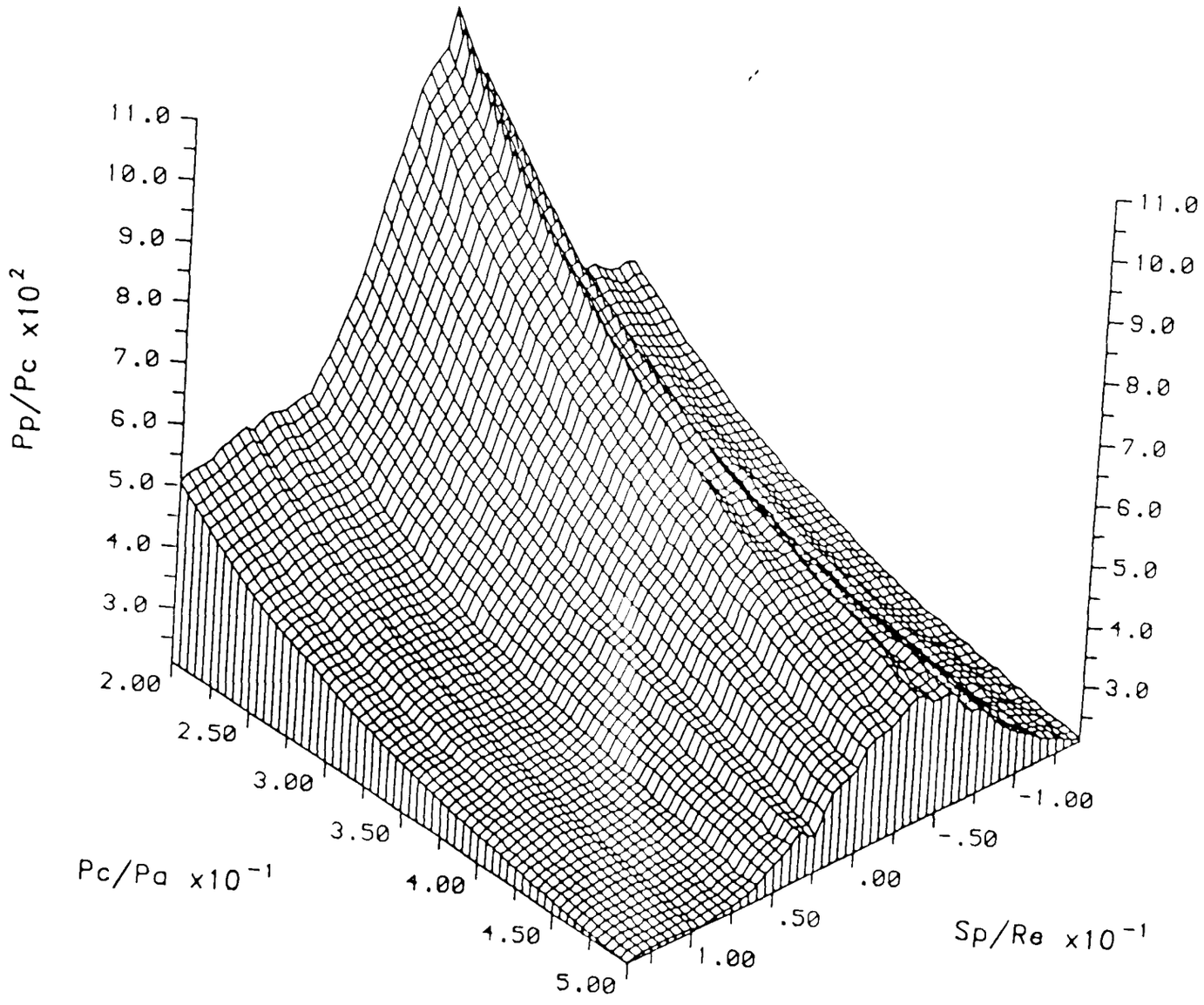

FIGURE 6.65 ROCKET JET IMPINGEMENT – ISOMETRIC PLOT OF VARIATION OF FLAT PLATE PRESSURE DISTRIBUTION WITH JET PRESSURE RATIO FOR: Me=1.0, Z_p/R_e = 10.0, $\theta = 45^\circ$

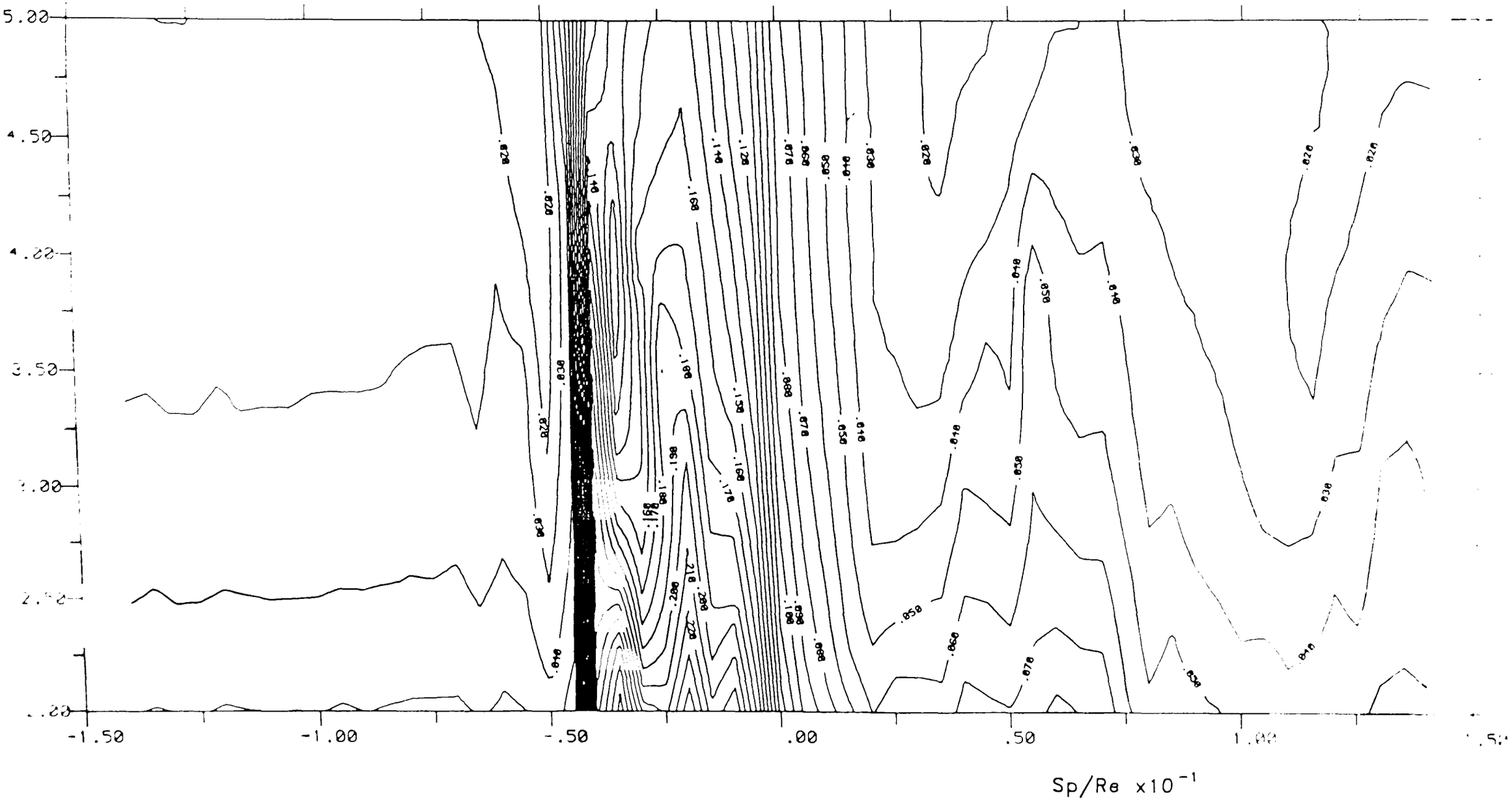

FIGURE 6.66 ROCKET JET IMPINGEMENT – CONTOUR PLOT OF VARIATION OF FLAT PLATE PRESSURE DISTRIBUTION WITH JET PRESSURE RATIO FOR: Me=1.0, Zp/Re=5.0, θ=45.0°

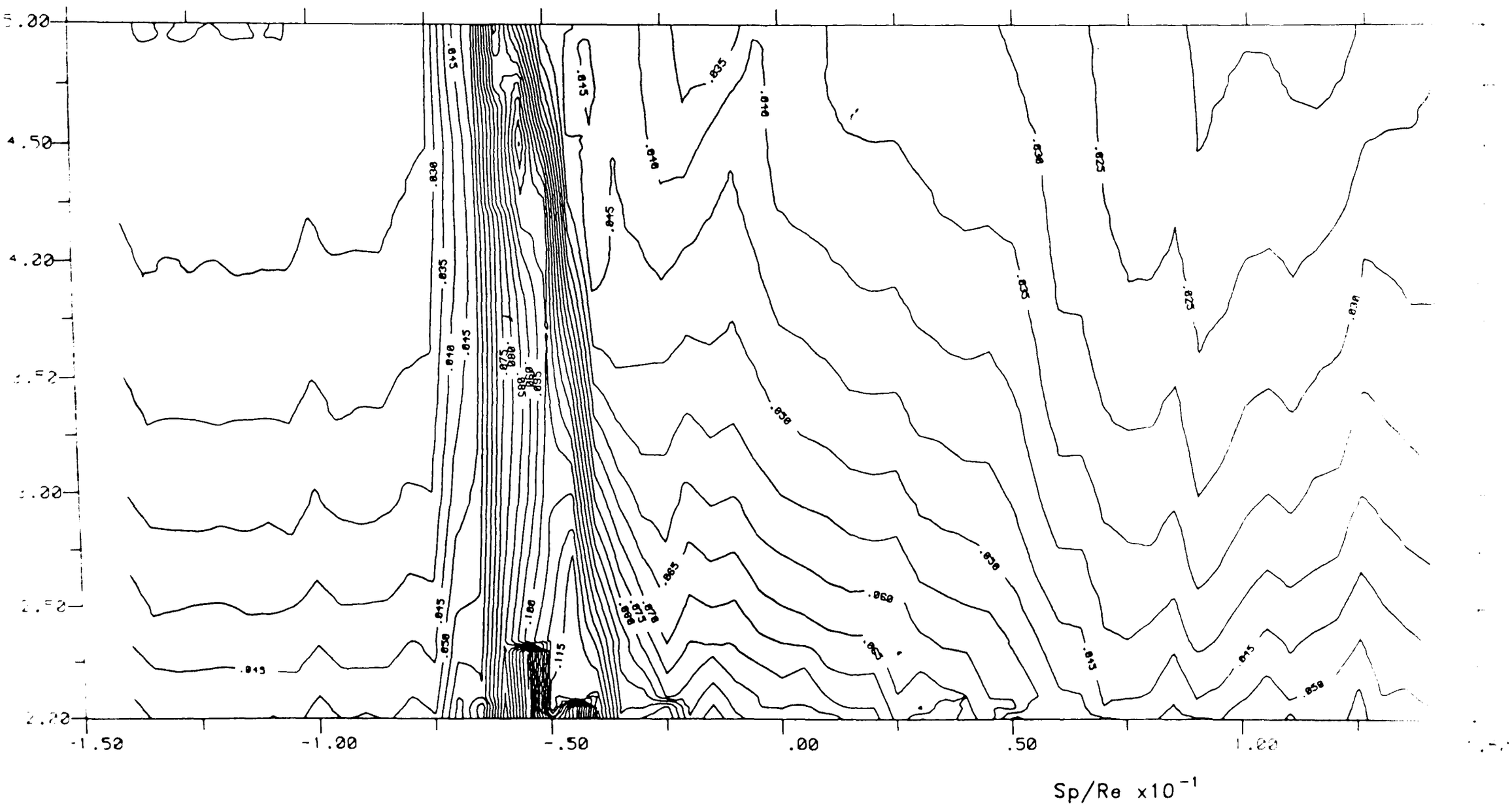

FIGURE 6.67 ROCKET JET IMPINGEMENT – CONTOUR PLOT OF VARIATION OF FLAT PLATE PRESSURE DISTRIBUTION WITH JET PRESSURE RATIO FOR: Me=1.0, Zp/Re=10.0, θ=45.0°

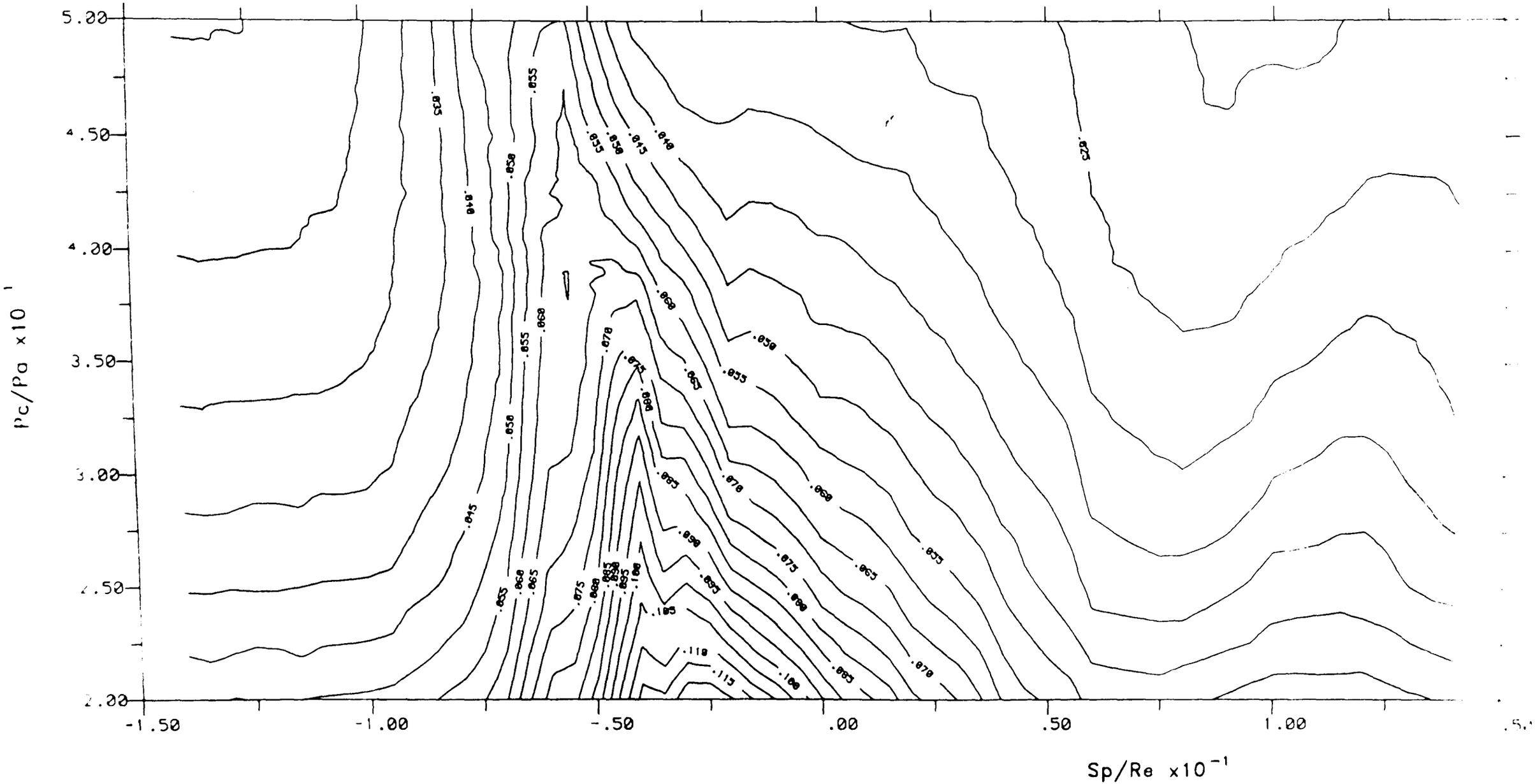

FIGURE 6.68 ROCKET JET IMPINGEMENT – CONTOUR PLOT OF VARIATION OF FLAT PLATE PRESSURE DISTRIBUTION WITH JET PRESSURE RATIO FOR: Me=1.0, Zp/Re=20.0, θ=45.0°

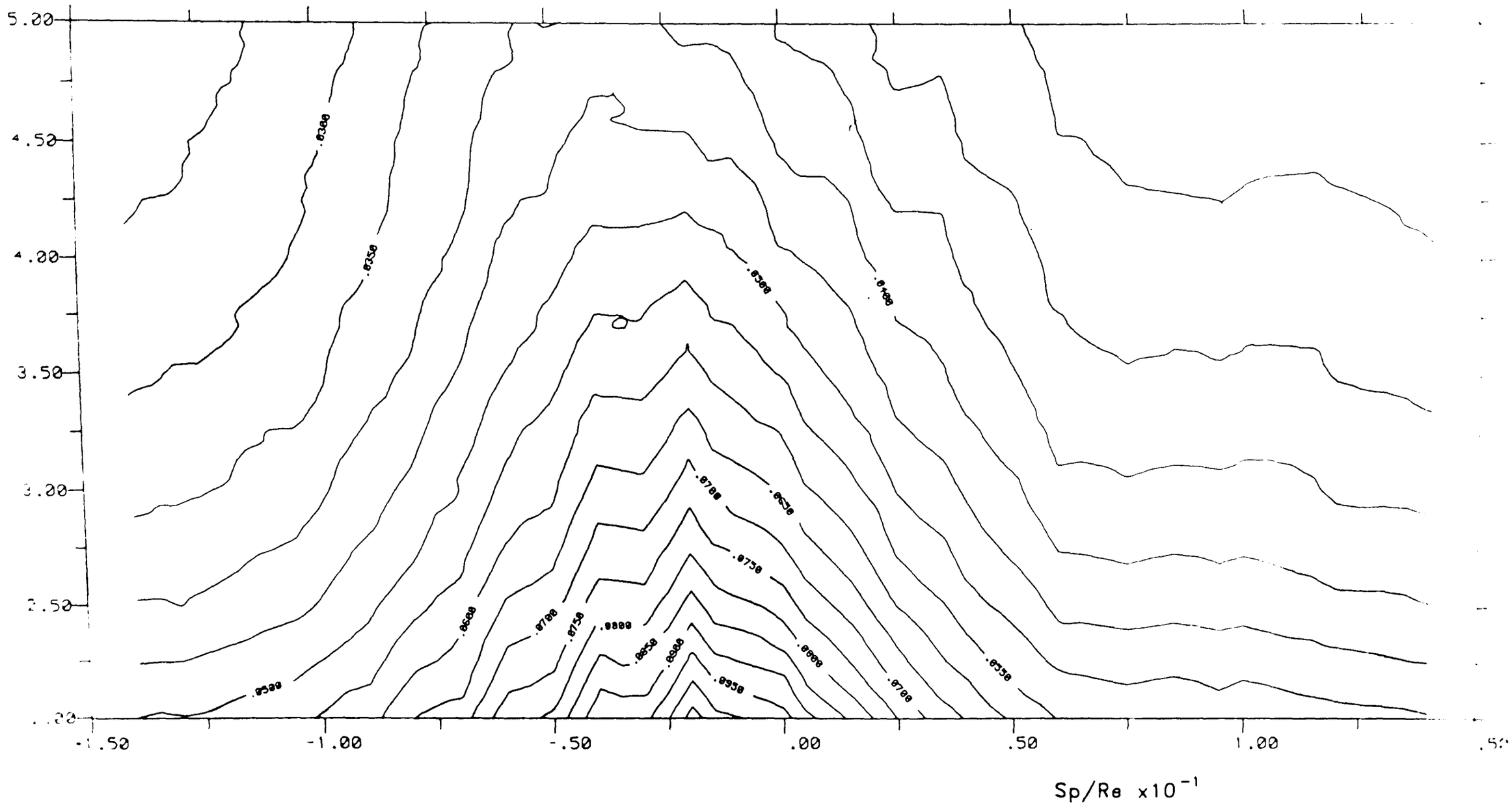

FIGURE 6.69 ROCKET JET IMPINGEMENT – CONTOUR PLOT OF VARIATION OF FLAT PLATE PRESSURE DISTRIBUTION WITH JET PRESSURE RATIO FOR: Me=1.0, Zp/Re=40.0, θ=45.0°

(a) COMPLETE PLATE, α = 3°

(b) COMPLETE PLATE, [illegible]

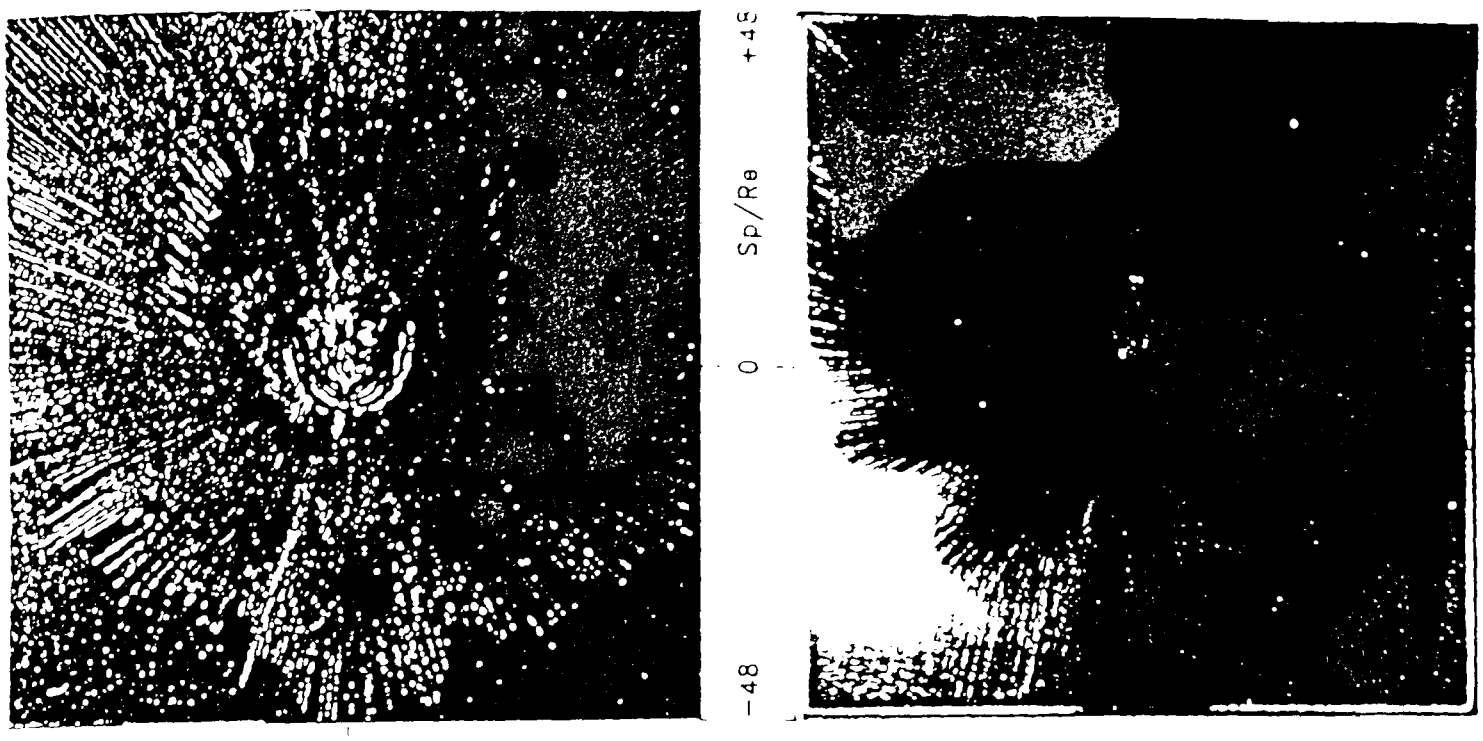

THESE PHOTOGRAPHS HAVE BEEN ARRANGED SO THAT
THE ARRAYS OF PRESSURE TAPPINGS ARE CO-LINEAR
WITH THE LINES ADJACENT TO THIS TEXT

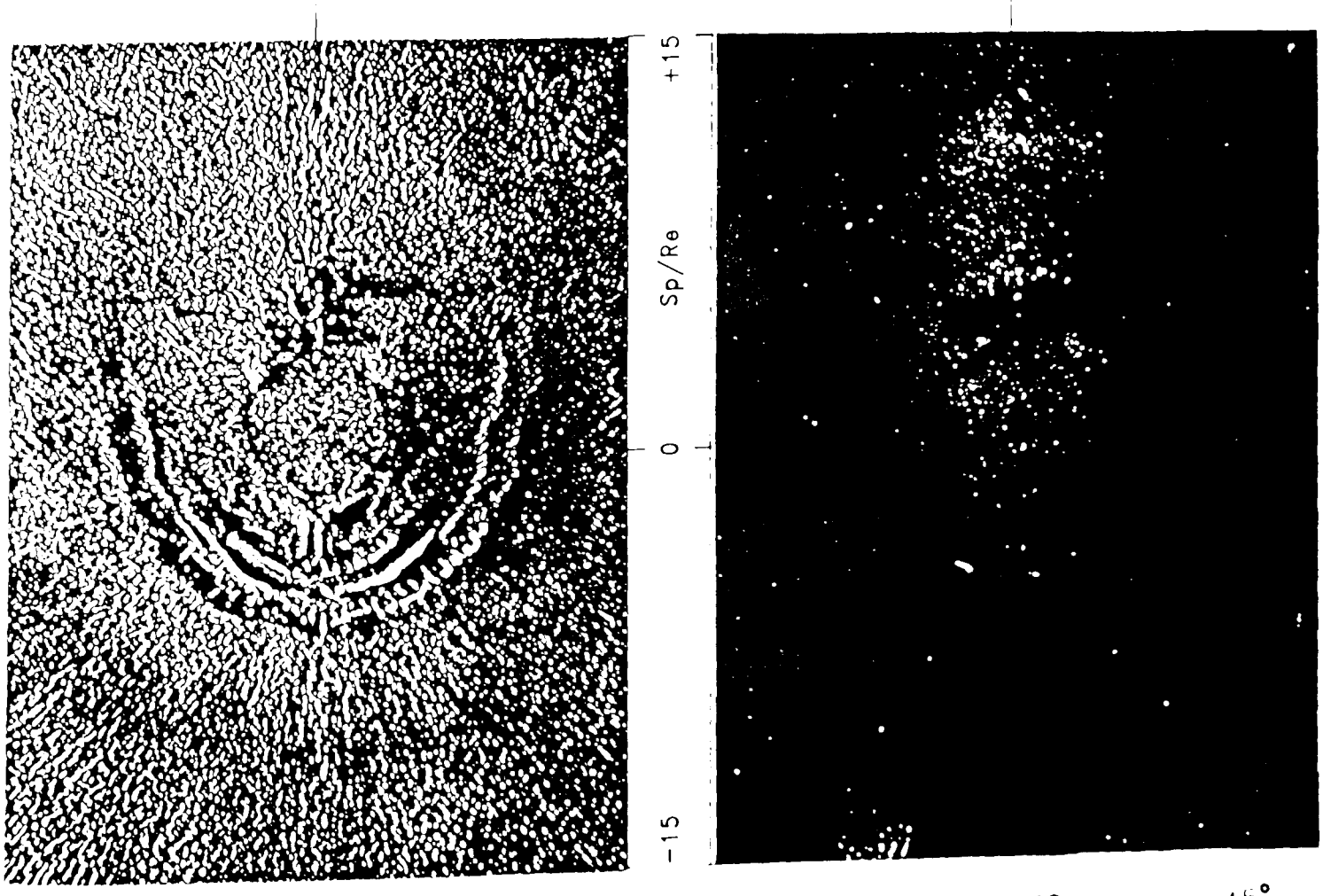

(c) TAPPING REGION, α = 3°

(d) TAPPING REGION, [illegible] 45°

FIGURE 6.7c ROCKET JET IMPINGEMENT [illegible]
COOL DEPOSITION FOR Z_p/R_θ [illegible]

(c) COMPLETE PLATE, α = 3°

(d) COMPLETE PLATE, α = 45°

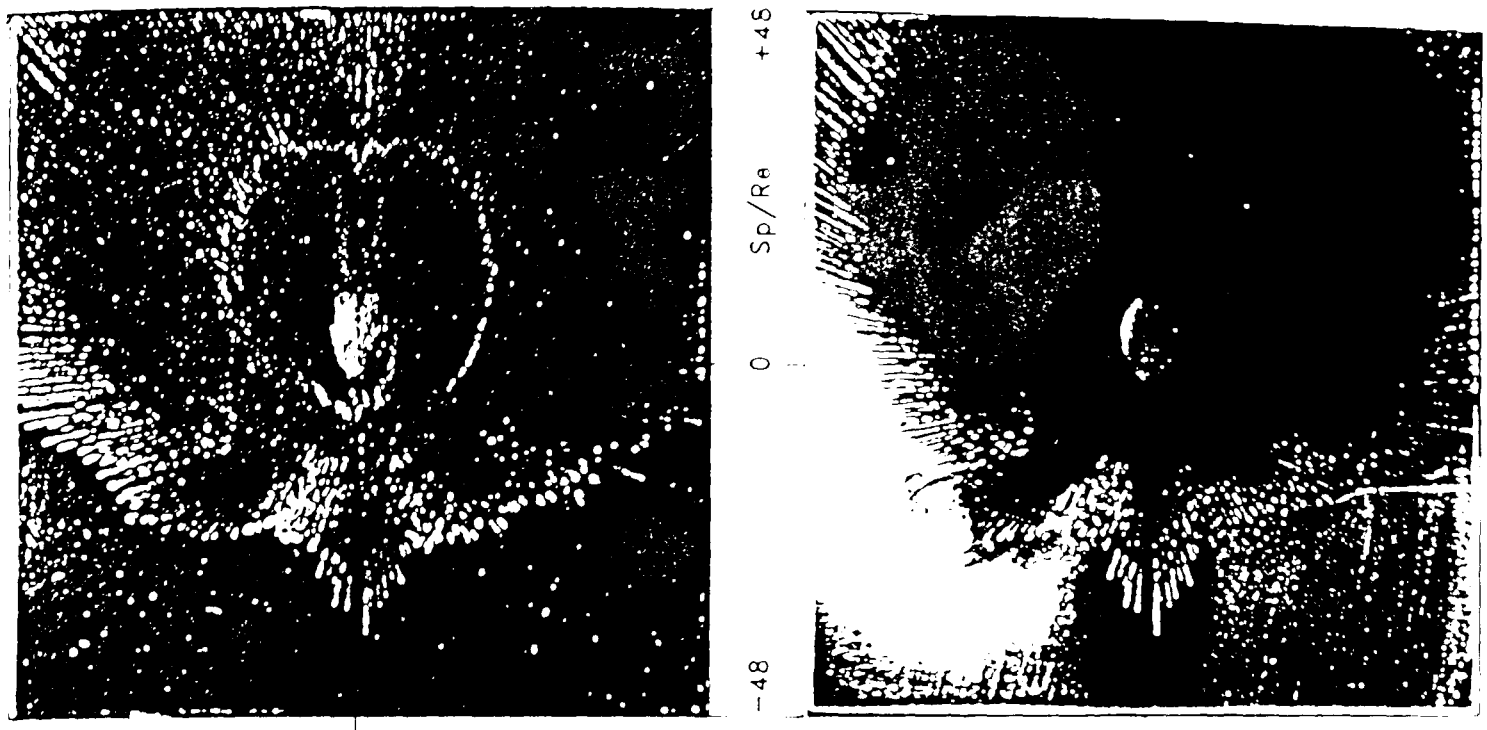

THESE PHOTOGRAPHS HAVE BEEN ARRANGED SO THAT
THE ARRAYS OF PRESSURE TAPPINGS ARE CO-LINEAR
WITH THE LINES ADJACENT TO THIS TEXT

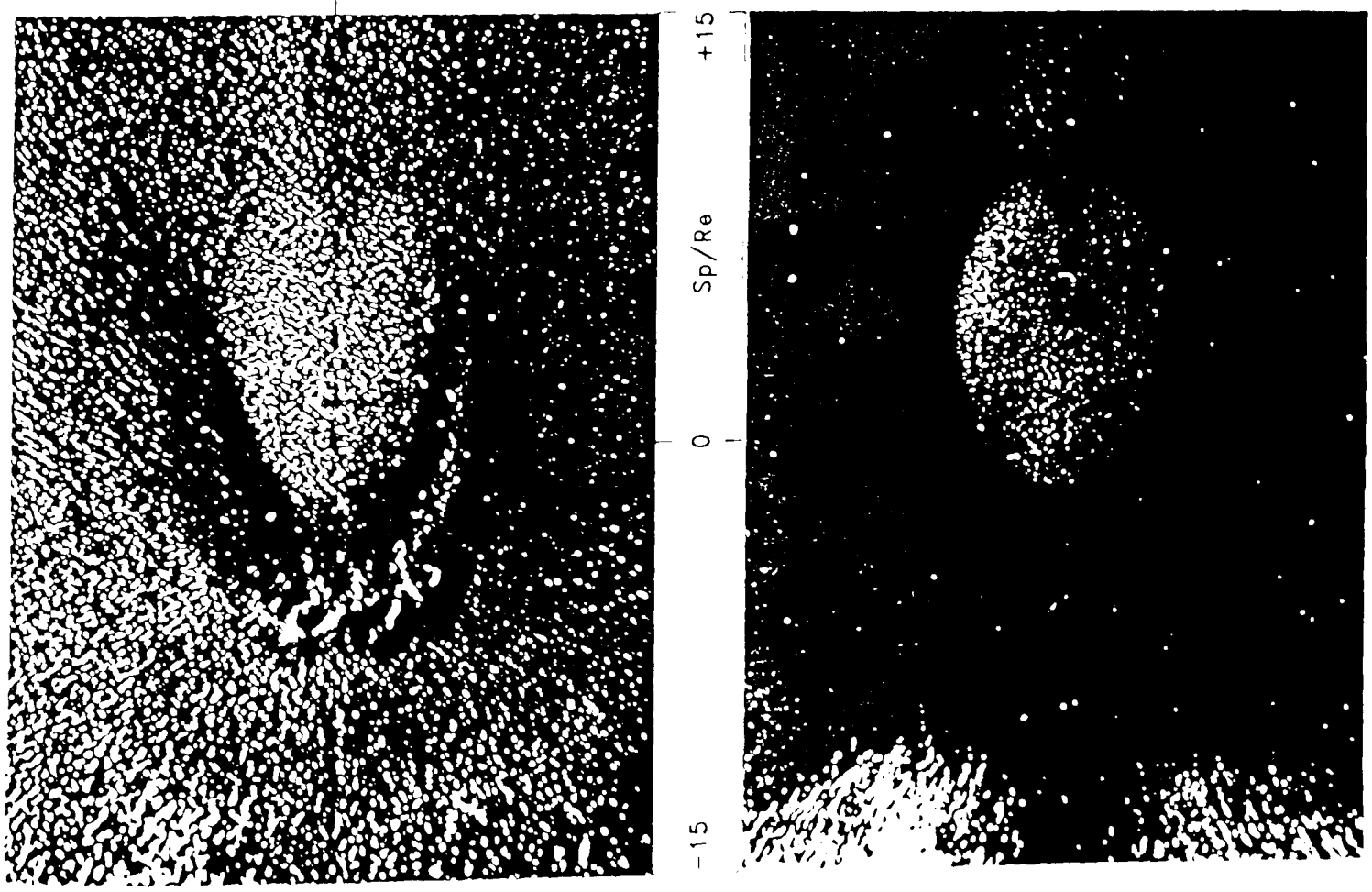

(c) TAPPING REGION, α = 3°

(d) TAPPING REGION, α = 45°

FIGURE 6.7 ROCKET JET IMPINGEMENT FLAT PLATE
COOL DEPOSITION LOSS, Z/D = 10.0, θ = 45°

(a) COMPLETE PLATE, α = 3°

(b) COMPLETE PLATE, α = 45°

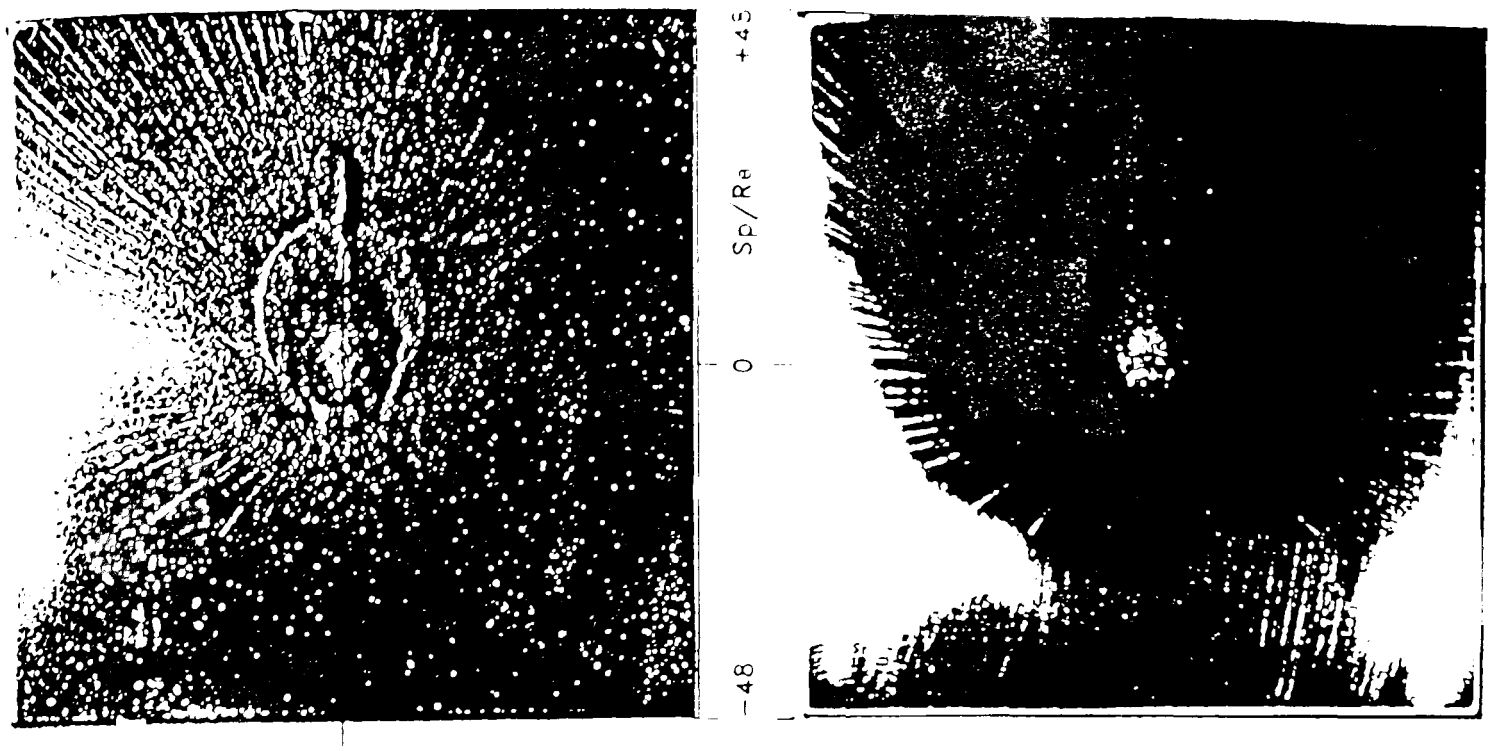

THESE PHOTOGRAPHS HAVE BEEN ARRANGED SO THAT
THE ARRAYS OF PRESSURE TAPPINGS ARE SO LINEAR
WITH THE LINES ADJACENT TO THE TEXT

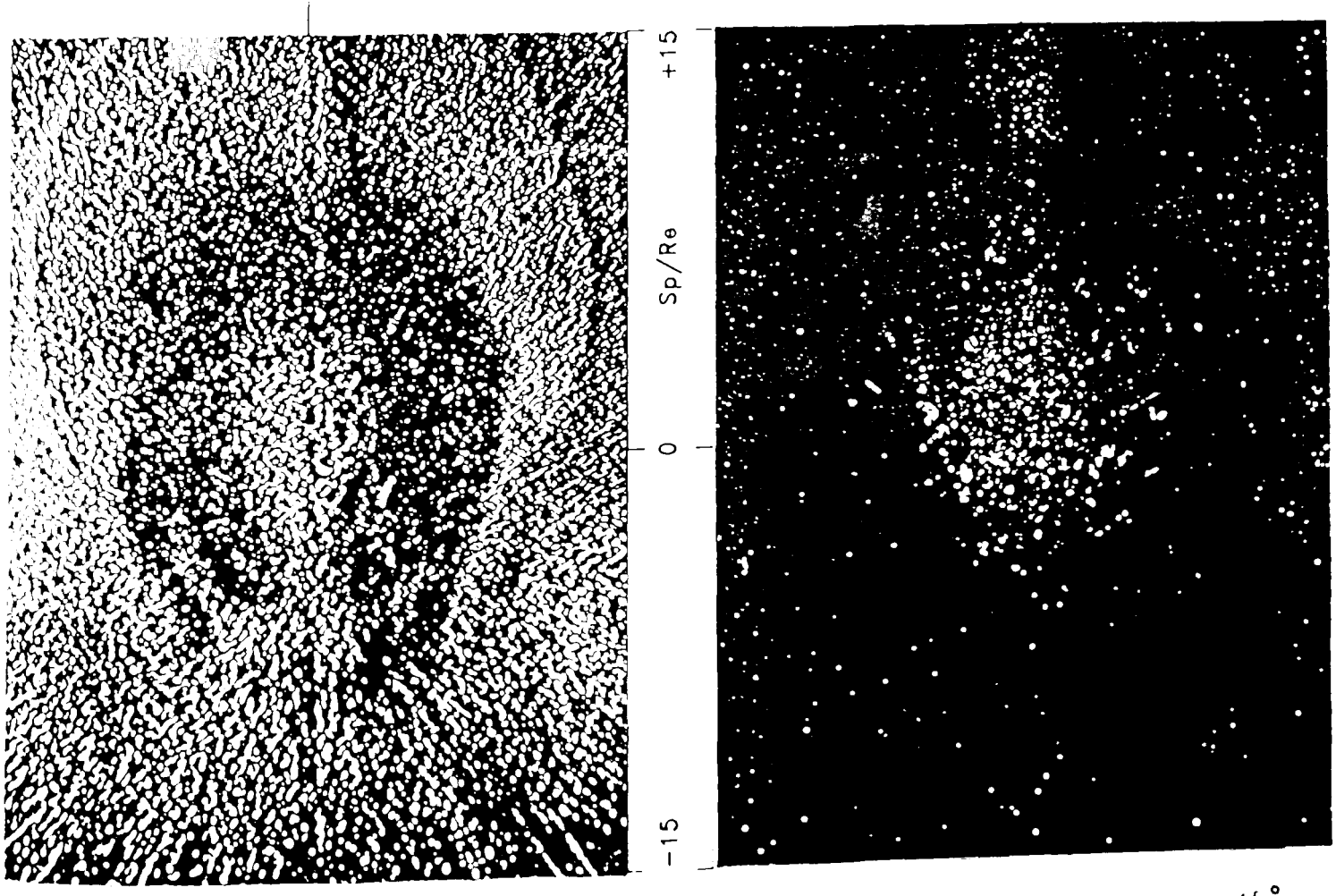

(c) TAPPING REGION, α = 3°

(d) TAPPING REGION, α = 45°

FIGURE 6.72 ROCKET JET IMPINGEMENT ON FLAT PLATE
SOOT DEPOSITION FOR θ = 20.0, θ = 45.0°

(a) COMPLETE PLATE, α = 3

(b) COMPLETE PLATE, α = 45

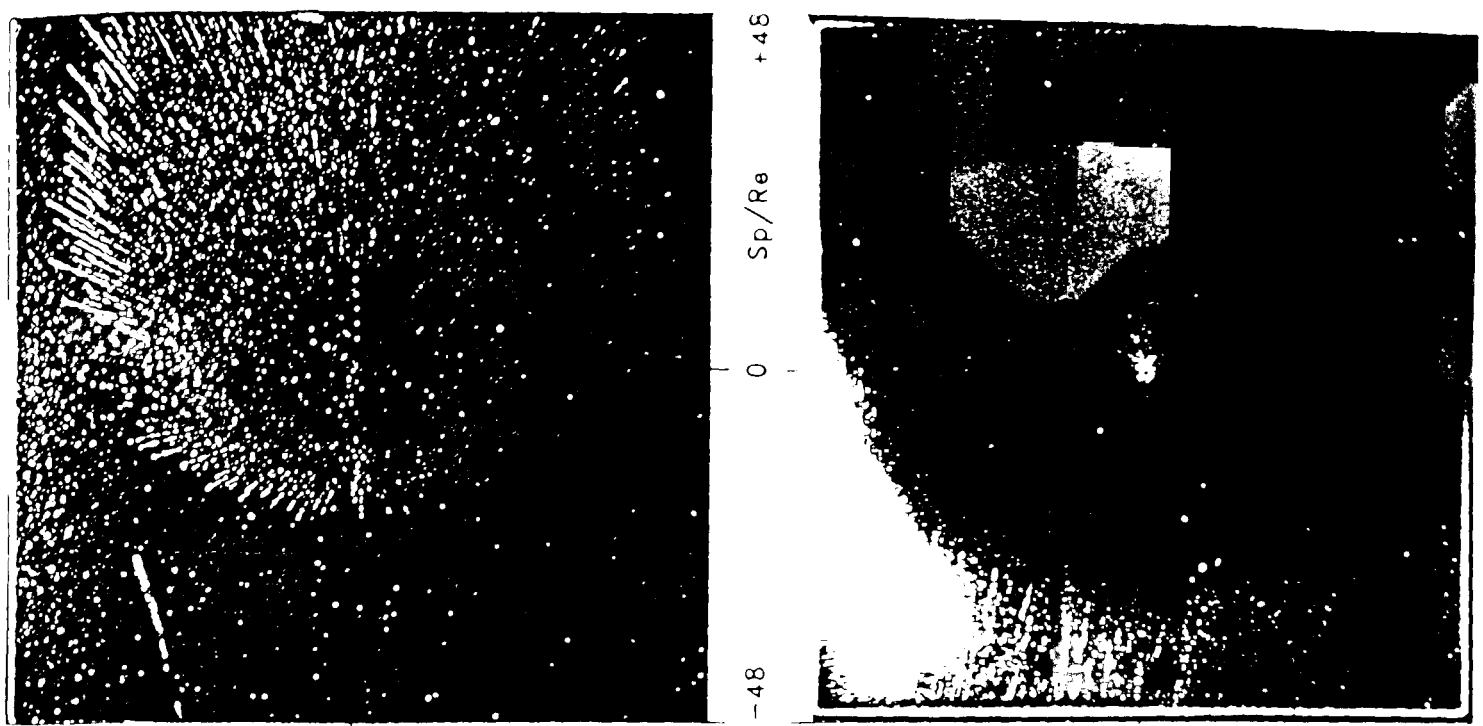

THESE PHOTOGRAPHS HAVE BEEN ARRANGED SO THAT THE ARRAYS OF PRESSURE TAPPINGS ARE CO-LINEAR WITH THE LINES ADJACENT TO THIS TEXT

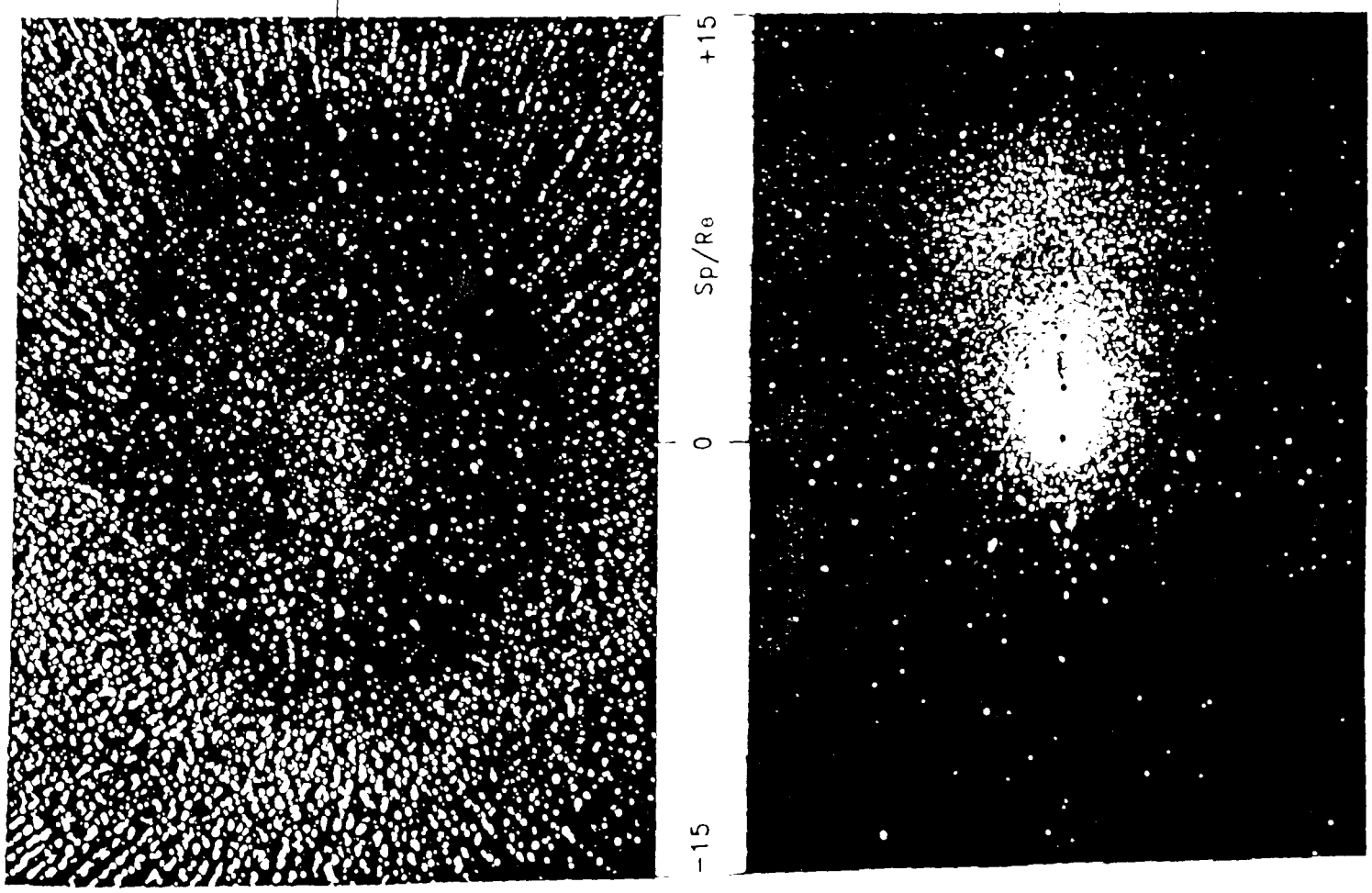

(c) TAPPING REGION, α = 3°

(d) TAPPING REGION, α = 45°

FIGURE 6.73 ROCKET JET IMPINGEMENT FLAT PLATE SOOT DEPOSITION FOR [illegible]

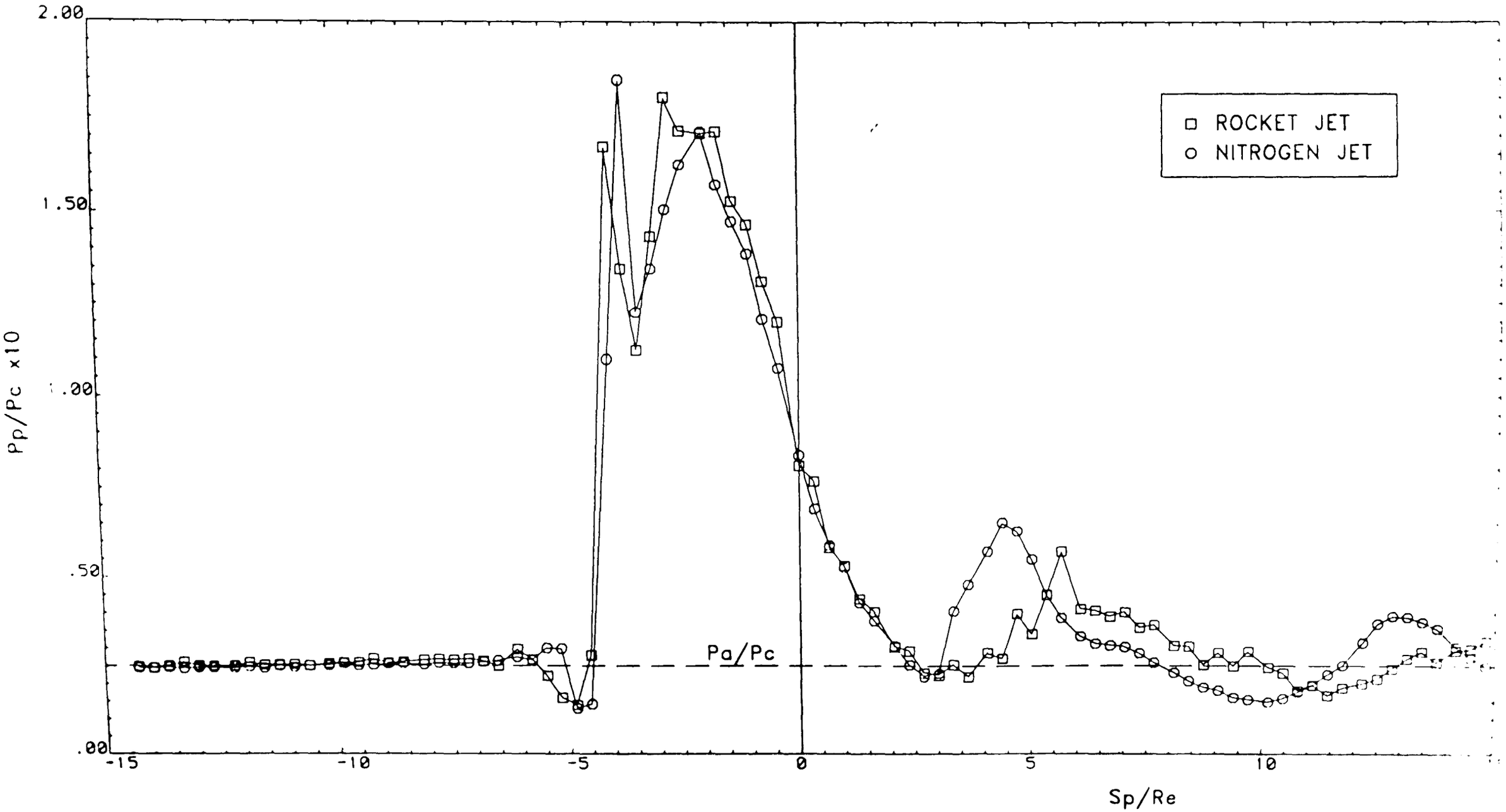

FIGURE 6.74 COMPARISON OF FLAT PLATE PRESSURE DISTRIBUTIONS GENERATED BY IMPINGING ROCKET AND NITROGEN JETS WHEN: Me=1.0, Pc/Pa=40.0, Zp/Re=5.0, θ=45.0

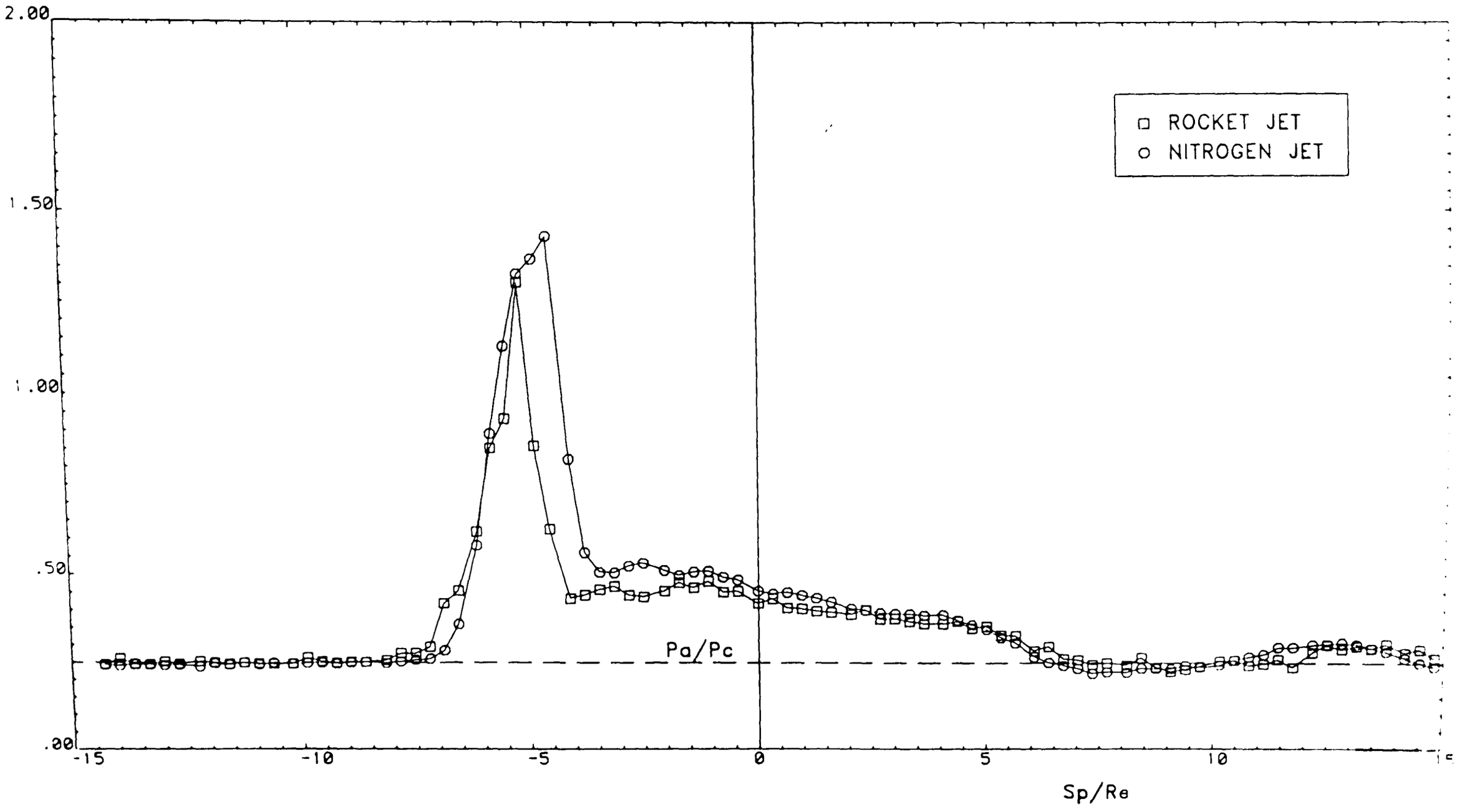

FIGURE 6.75 COMPARISON OF FLAT PLATE PRESSURE DISTRIBUTIONS GENERATED BY IMPINGING ROCKET AND NITROGEN JETS WHEN: Me=1.0, Pc/Pa=40.0, Zp/Re=10.0, θ=45.0°

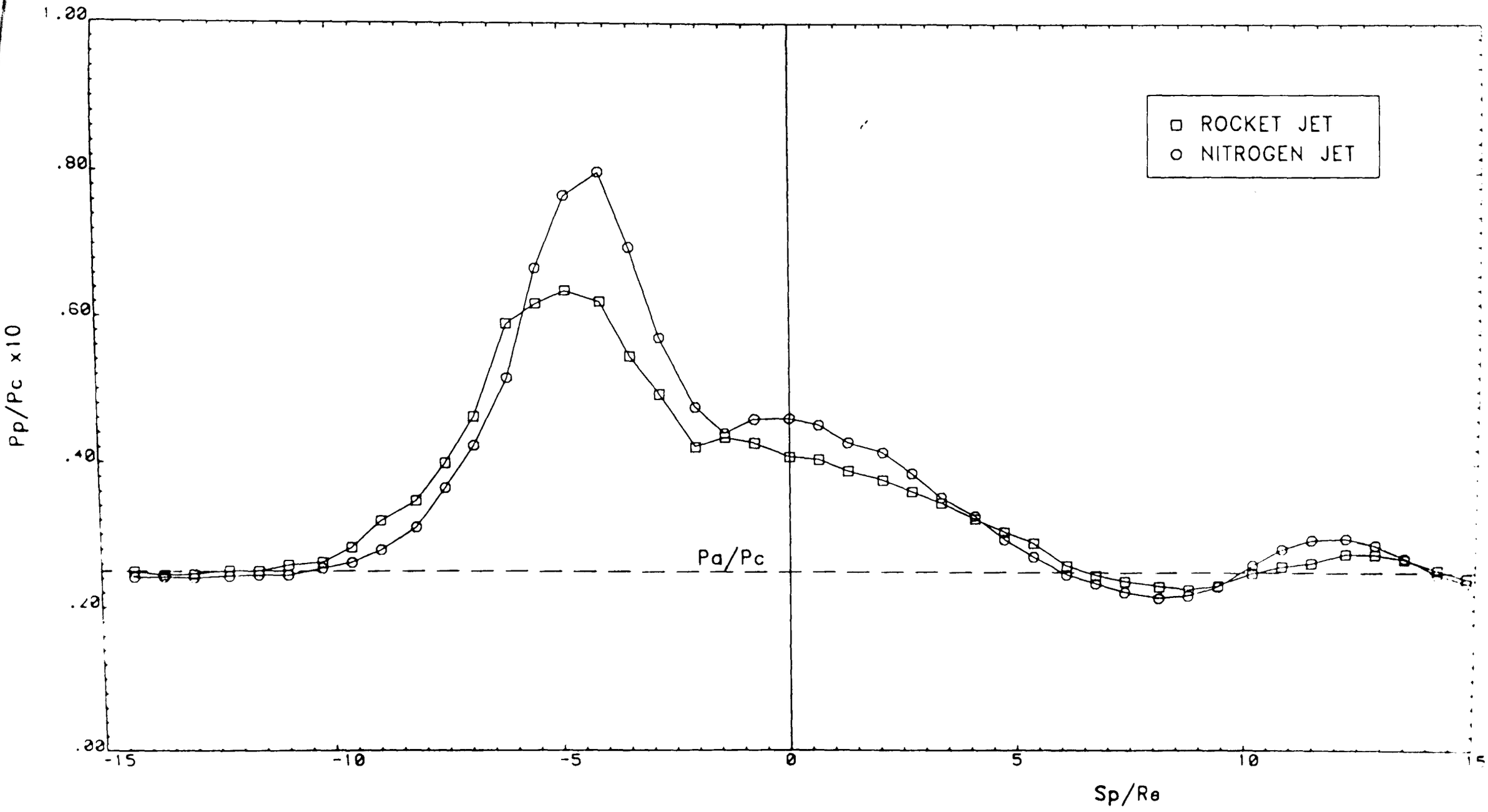

FIGURE 6.76 COMPARISON OF FLAT PLATE PRESSURE DISTRIBUTIONS GENERATED BY IMPINGING ROCKET AND NITROGEN JETS WHEN: Me=1.0, Pc/Pa=40.0, Zp/Re=20.0, θ=45.0°

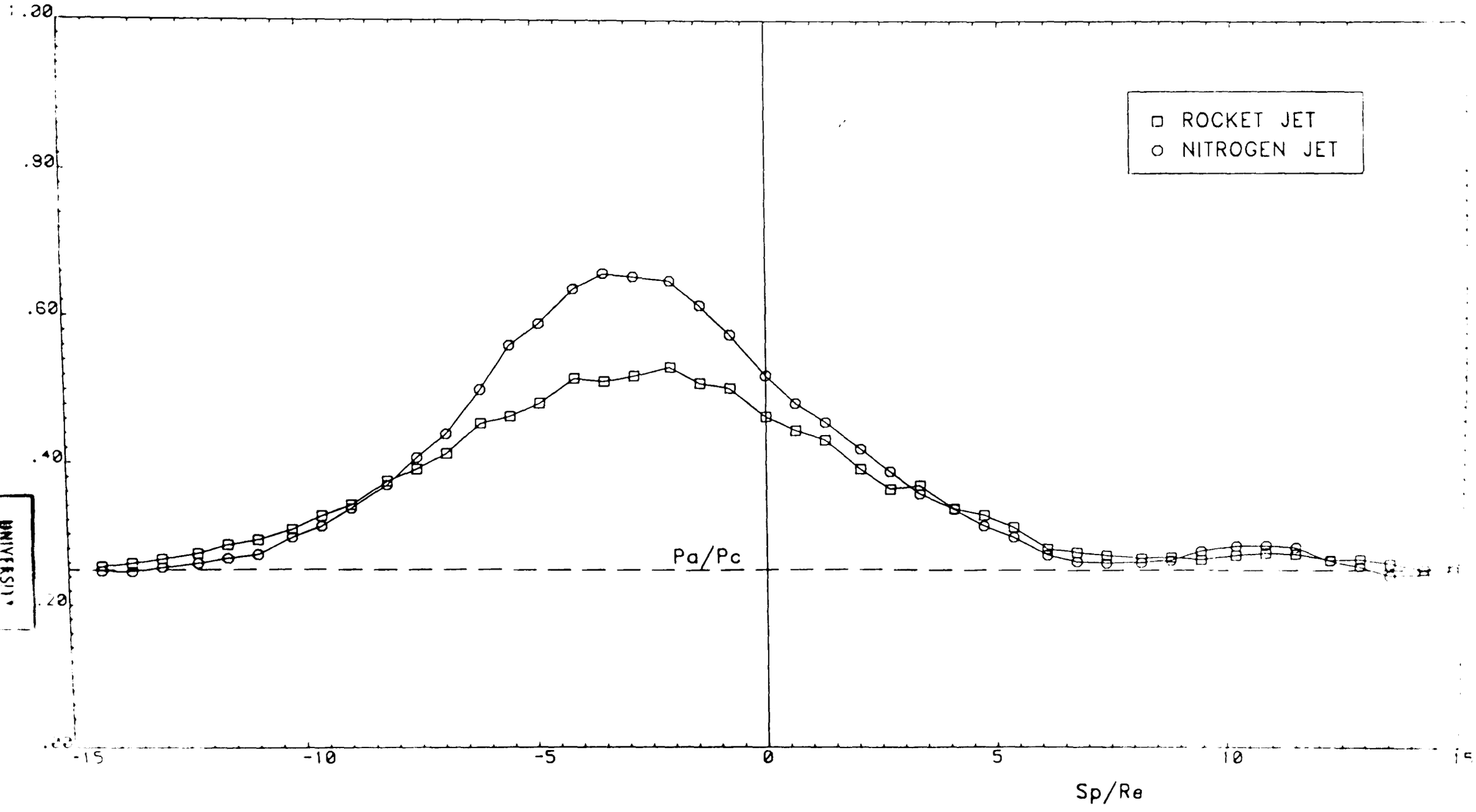

FIGURE 6.77 COMPARISON OF FLAT PLATE PRESSURE DISTRIBUTIONS GENERATED BY IMPINGING ROCKET AND NITROGEN JETS WHEN: Me=1.0, Pc/Pa=40.0, Zp/Re=40.0, θ=45.0